# Dissecting peripheral $CD8^+$ T cell responses and immune interactions during immune checkpoint blockade for metastatic melanoma

**Orion Tong**

A thesis presented for the degree of Doctor of Philosophy

Supervisor: Dr Benjamin Fairfax
Co-supervisor Prof Mark Middleton




March 2023

**Thank you to all my friends, colleagues and family who never stopped believing in and encouraging me. This is for you.**

A big new journey,
Findings and growth on the way,
Proudly completed

# Abstract

Immune checkpoint blockade has provided a revolution in solid cancer treatment particularly in the metastatic setting. Although many patients demonstrate clinical responses upon receiving checkpoint therapy, a considerable number of individuals fail to benefit from treatment and continue to progress from their cancers. It is therefore important to establish the immunological contributors that mediate treatment success and identify easily accessible biomarkers that can be used to monitor this process. Here, I utilised bulk and single-cell RNA sequencing, and flow cytometry, to characterise early peripheral immunity across immune checkpoint blockade in an Oxford-based cohort of metastatic melanoma patients.

Firstly, I focus on peripheral $CD8^+$ T cells as central mediators of anti-tumour responses. I demonstrate that a central tenet of the immune response to immune checkpoint blockade is mitosis, which is accompanied by type I interferon and interferon-ɣ signalling and other immune activation pathways. I then employ single-cell RNA sequencing to dissect the $CD8^+$ T cell compartment, finding that mitotically active cells are under-represented amongst clonal expansion. Instead, cytotoxic effector cells and expanding effector memory cells dominate the clonal pool and demonstrate phenotypic and clonal stability across immune checkpoint treatment. Immune checkpoint blockade shifts T cell subsets towards increased differentiation and has particularly stimulatory effects on effector $CD8^+$ T cells.

Next, I describe how these aspects of peripheral $CD8^+$ immunity contribute to clinical patient responses and survival. Individuals with greater levels of CD8 clonal expansion and effector responses show improved treatment outcomes, whilst mitosis and interferon activity have limited patient benefit. I describe how a simple, tractable measure of clinical lymphocyte count predicts long-term survival benefit for patients.

Lastly, I dissect how $CD8^+$ T cell responses interact with other immune subsets, such as monocytes, B cells and $CD4^+$ T cells to create expression and subset composition networks that reflect enhanced T cell activity and homeostasis, or dysregulated inflammation and suppressed T cell immunity. Intersecting these responses with genetic variation provides

further insight into the factors influencing immunotherapy responses. Altogether, these results generate multiple blood-based biomarkers to predict therapy success, and provide novel angles for therapeutic adjuvants to support immune checkpoint blockade, spanning potential cellular, cytokine and metabolic mechanisms.

# Acknowledgements

This work would not have been possible without the people that make up the Fairfax group. Firstly, to my supervisors Ben and Mark, thank you for your support over the years. It's been an honour to work with you. To the current and past members of the group; Chelsea, Alba, Surya, Christina, Flavia, Rob, Bo, Piyush, Ros, James, Esther, Elsi, Isar, Victoria - it's been such a great ride working and teaming up with you all, learning alongside and from you, and laughing and smiling all the way. I've really treasured all the moments spent together. The hours and late days would not have been the same without you.

The results of this thesis also would not be possible without the patients who have been so kind to donate samples for research, without knowing the exact process we go through but still placing their faith that their contributions will go on to help future patients. We are all indebted to you and hope to improve the treatment process.

Moving away from the WIMM, thank you to the team at Infinitopes for putting up with me and for offering me advice, extra intellectual stimulation and a lot of fun company; particularly Jonathan, Joana, Lian Ni, Senthil, Dan, Ava, Chloe, Masy and Annemieke. I've cherished my time with all of you so far.

To my friends - I'm not sure which of you would actually want to read this but I've been lucky to have your support, countenance and humour. It would have been a much tougher journey without you alongside me and I'm always grateful for our friendship, and count myself lucky to have you by my side. It's been great to celebrate the ups and commiserate the downs of a PhD with you.

Lastly, but not the least, to my family - I think you would want to read this even less but to say thank you feels even more inadequate. I'm honoured by your love.

# Contents


**1 Introduction** **1**

1.1 Overview of ICB in metastatic melanoma . . . . . 1

1.1.1 Incidence and immunogenicity of melanoma . . . . . 1

1.1.2 Clinical management and response rates of melanoma to ICB . . . . . 3

1.2 Cellular sensitivity and resistance to ICB . . . . . 5

1.2.1 T-cell mediated anti-tumour immunity . . . . . 5

1.2.2 Overview of immune responses to ICB . . . . . 6

1.2.2.1 α-CTLA-4 . . . . . 6

1.2.2.2 α-PD-1 . . . . . 8

1.2.3 Beneficial immune cell activity in ICB across cell subsets . . . . . 10

1.2.3.1 $CD8^+$ T cells . . . . . 10

1.2.3.2 $CD4^+$ T cells . . . . . 11

1.2.3.3 Monocytes . . . . . 12

1.2.3.4 B cells . . . . . 14

1.2.3.5 NK cells . . . . . 15

1.2.3.6 DCs . . . . . 15

1.3 Genetic sensitivity and resistance to ICB . . . . . 17

1.4 Key aims . . . . . 21

**2 Methods** **22**

2.1 Patient and clinical cohort . . . . . 22

2.2 Sample collection and preparation . . . . . 22

2.3 Genotyping . . . . . 23

2.4 Bulk RNAseq . . . . . 25

2.5 Single-cell RNAseq . . . . . 26

2.6 Flow cytometry . . . . . 29

2.7 General statistical analysis . . . . . 30

**3 $CD8^+$ T cell transcriptomic responses to ICB** **31**

3.1 Summary and Aims . . . 31
3.2 Bulk RNAseq-based characterisation of the CD8+ T cell response . . . 32
3.3 Single-cell RNAseq characterisation of the CD8+ T cell response . . . 38
3.3.1 Describing single-cell peripheral CD8+ T cell subsets . . . 38
3.3.2 Describing the clonal dynamics of CD8+ T cell subsets following ICB at single-cell resolution . . . 42
3.3.3 Assessing CD8+ T cell subset changes during ICB . . . 48
3.4 Conclusions and Discussion . . . 53

**4 Examining CD8+ T cell heuristics associated with clinical response 55**
4.1 Summary and Aims . . . 55
4.2 Clonal expansion of CD8+ T cells . . . 56
4.3 Subset-associated signatures . . . 58
4.4 Clinical lymphocyte stability . . . 61
4.5 Pre-existing CD8+ T cell IFN responses . . . 66
4.6 Conclusions and Discussion . . . 69

**5 Assessing related changes across PBMC subsets during ICB 72**
5.1 Summary and Aims . . . 72
5.2 Changes associated with differential ICB binding across cell subsets . . . 73
5.3 Global transcriptomic correlates across peripheral immune subsets . . . 76
5.4 Changes in monocytes and B cells according to T cell factors . . . 78
5.4.1 T cell mitotic and interferon signatures . . . 78
5.4.2 T cell clonality and effector score . . . 80
5.4.3 Lymphocyte stability . . . 82
5.5 Changes in T cells based on B cell chain usage . . . 86
5.6 Overall associations of cross-subset heuristics . . . 88
5.7 Conclusions and Discussion . . . 90

**6 Identifying subset interactions in single-cell RNAseq analysis of PBMCs 93**
6.1 Summary and Aims . . . 93
6.2 Annotating subsets in single-cell RNAseq of melanoma and healthy PBMCs . 94
6.3 Using single-cell RNAseq to uncover B cell dynamics associated with IL7 . . 97
6.4 Correlating cell type proportions across single-cell RNAseq PBMCs . . . 99
6.5 Exploring cell-cell interactions in the context of lymphocyte stability . . . 101
6.6 Understanding specific CD4+ and CD8+ subset interactions with other cell types 104
6.7 Interactions between regulatory T cells and conventional CD8+ and CD4+ T cells 105

6.8 Describing T cell interaction networks associated with clinical response to ICB 110
6.9 Conclusions and Discussion . . . . . 112

**7 Summary and future work** **115**
7.1 Overall summary . . . . . 115
7.2 Clonal expansion, effector cells and long-lived effector phenotypes . . . . . 115
7.3 ICB binding, downstream signalling and effects on various T cell types . . . . 117
7.4 Lymphocyte stability as a clinical marker and relation with B cell *IL7* . . . . . 118
7.5 Developing an understanding of genetic determinants of ICB immunity . . . 120

**8 Appendix** **122**

# List of Figures


1.1 Immune checkpoint blockade . . . . . 2
1.2 Patient survival with ICB . . . . . 4
1.3 Conventional $CD8^+$ T cell subsets . . . . . 5
1.4 Signalling pathways downstream of CTLA-4 and PD-1 . . . . . 8
1.5 Quantitative analysis of genetic variation . . . . . 18
1.6 GWAS analysis of irAE development in ICB . . . . . 20

2.1 Patient blood sample collection . . . . . 23
2.2 Downstream assays for processed patient PBMCs . . . . . 24

3.1 Bulk RNAseq analysis of DEGs and pathways modulated by ICB . . . . . 33
3.2 Correlations between responses induced by ICB in $CD8^+$ T cells . . . . . 35
3.3 Associations between IgG4 staining and $CD8^+$ T cell responses to ICB . . . . . 37
3.4 Single-cell RNAseq of $CD8^+$ T cells . . . . . 39
3.5 Expression and pathway characterisation of $CD8^+$ T cell subsets . . . . . 41
3.6 Clonal characteristics and dynamics of $CD8^+$ T cell subsets during ICB . . . . 44
3.7 Characterisation of long-lived effector cells . . . . . 45
3.8 Characterisation of the mitotic response at a clonal level . . . . . 47
3.9 Changes in $CD8^+$ T cell subset proportion during ICB . . . . . 49
3.10 Gene expression changes within $CD8^+$ T cell subsets during ICB . . . . . 51

4.1 Clinical and transcriptomic associations of $CD8^+$ T cell clonal expansion . . . 57
4.2 Subset score associations with clonality, clinical outcome and transcriptomics 59
4.3 Stability of hospital lymphocyte counts associates with long-term ICB survival 62
4.4 Phenotypic, clonal and subset associations with lymphocyte stability . . . . . 64
4.5 Transcriptomic differentiators between stable and falling lymphocyte stability 65
4.6 Distinct patient responses underlying lymphocyte stability and immune-related adverse events . . . . . 67
4.7 Pre-treatment type I IFN responses associate with clinical outcome . . . . . 68

5.1 Transcriptomic associations of monocytes and B cells with IgG4 binding . . . 74
5.2 Gene correlation heatmaps across subset pairs . . . 78
5.3 Monocyte and B cell associations with $CD8^+$ T cell mitosis, IFN-I and IFNg signatures . . . 79
5.4 Monocyte and B cell associations with $CD8^+$ T cell clonality . . . 81
5.5 Monocyte and B cell transcriptomic associations with lymphocyte stability . . . 83
5.6 Immunological associations with the *IL7* SNP rs16906115 . . . 85
5.7 $CD8^+$ T cell transcriptomic associations with B cell chain usage . . . 87
5.8 Pan-subset heuristic correlation network . . . 89

6.1 Single-cell RNAseq workflow for sample batching, PBMC clustering and subset annotation . . . 95
6.2 GOBP pathway characterisation of PBMC pathways . . . 96
6.3 Single-cell characterisation of B cell *IL7* expression . . . 98
6.4 Correlations of subset proportion across cell types . . . 100
6.5 Ligand-receptor interaction analysis across cell types in the context of LS . . . 102
6.6 Analysis of monocyte and T cell subsets enriched for CD244-CD48 interactions 103
6.7 Analysis of $CD8^+$, $CD4^+$ and B cell subset interactions . . . 106
6.8 Regulatory $CD4^+$ T cell dynamics during ICB . . . 107
6.9 Regulatory $CD4^+$ T cell phenotype . . . 108
6.10 T cell interaction network enriched in progressing individuals . . . 112

8.1 Subset gene expression in B cells and NK cells . . . 123
8.2 Subset gene expression in DCs and monocytes . . . 124
8.3 Subset gene expression in T cells . . . 125
8.4 UMAP and B cell subsets for combined single-cell RNAseq dataset . . . 126

# Chapter 1

# Introduction

## 1.1 Overview of ICB in metastatic melanoma

### 1.1.1 Incidence and immunogenicity of melanoma

Melanoma skin cancer is the fifth most prevalent cancer type in the UK[1] and occurs from the development of malignant melanocytes. Whilst non-melanoma skin cancers such as basal and squamous cell carcinomas are more common, cutaneous melanoma is the most aggressive form of skin cancer. Localised melanomas (Stages 0-II) and some cases of regionally spread melanoma (Stage III) are typically treated by surgical excision of the tumour[2]. However, alternative approaches are needed for unresectable and metastatic (Stage IV) melanoma (MM), which also have high resistance to radiotherapy and chemotherapy. Globally, the incidence of melanoma has been increasing, possibly due to greater rates of ultraviolet (UV) exposure[3].

Melanoma predominantly arises from chronic skin exposure to UV, which leads to mutagenic DNA lesions in driver genes involved in cell cycle and proliferation, including *BRAF*, *NRAS* and *NF1*[4]. In line with this pathophysiology, increased melanoma susceptibility occurs in individuals with germline genetic mutations in *MC1R*[5], which is involved in skin pigmentation and melanin production, and *CDKN2A*[6], which is involved in cell cycle regulation. Despite its predominant UV basis, melanoma can develop in both frequent and less sun-exposed areas although the former carries a greater number of mutations and occurs in older populations. Overall, melanoma is considered a highly mutated tumour type and has the highest average tumour mutational burden (TMB) across all cancer types[7,8]. The high mutation rate of melanoma has historically been associated with its increased

immunogenicity[9] and thus survival, in part due to greater presence of neo-antigens; mutated tumour-specific epitopes that trigger immunity[10,11]. This is evidenced through observations of spontaneous regression of melanomas in approximately 5% of metastatic patients, in which metastatic lesions have disappeared or the primary cutaneous tumour is no longer identifiable[12]. Development of auto-immune vitiligo has also been associated with improved Stage III-IV melanoma survival[13], suggestive of beneficial cross-reactivity between normal and transformed melanocytes[14]. Lastly, melanomas are often infiltrated by lymphocytes, with the degree of immune infiltration in the primary tumour generally corresponding with improved survival[15–17]. As such, the constant immunosurveillance and elimination of early, mutated tumours is an important aspect of anti-melanoma control and may explain the relative prevalence of melanoma in older individuals, at which time immune output is reduced.

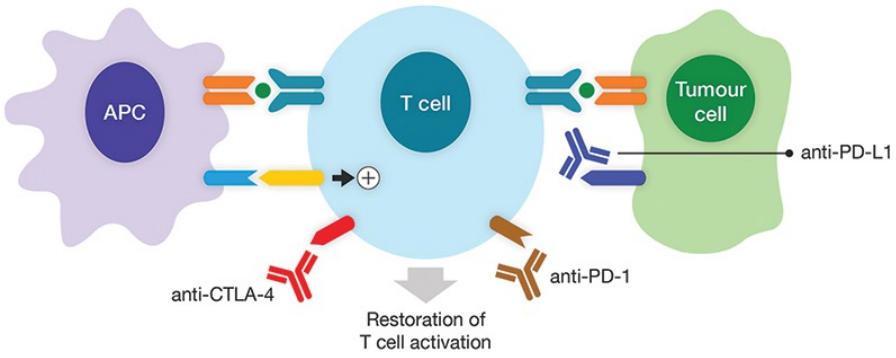



**Figure 1.1 Immune checkpoint blockade.** Neutralising antibodies used in immune checkpoint blockade for metastatic melanoma. Adapted from Bourke et al[18].

However, melanoma can adeptly hamper and evade effective anti-tumour immune responses, typified by roughly 30% of patients developing metastases following excision of the primary tumour[19]. For melanoma and other tumour types, immune evasion is recognised as a key hallmark of cancer[20] and is encoded by multiple immunosuppressive mechanisms. To circumvent this, pioneering work by Leach et al.[21] in James Allison's group showed that delivery of neutralising antibodies against the inhibitory receptor CTLA-4 (cytotoxic T-lymphocyte-associated protein 4) led to tumour rejection in mice. Subsequent human trials showed α-CTLA-4 (ipilimumab) significantly prolonged survival in MM patients[22,23]. Likewise, programmed cell death protein 1 or PD-1 was identified as an immune regulatory receptor by Tasuka Honjo's group[24,25] and found to suppress tumour immunity[26]. Blocking PD-1 using α-PD-1 antibodies (nivolumab and pembrolizumab) resulted in improved survival

for metastatic melanoma even when compared to ipilimumab[27–29], and is now standard of care for MM treatment. Collectively, the use of monoclonal antibodies targeting PD-1, its ligand PD-L1, and CTLA-4 is referred to as immune checkpoint blockade (ICB) (Figure 1.1), and its clinical use will be discussed next.

### 1.1.2 Clinical management and response rates of melanoma to ICB

ICB was first approved in the UK in 2012 for advanced melanoma (unresectable Stage III or metastatic) using ipilimumab as a second-line treatment, replacing standard-of-care chemotherapeutic agents such as dacarbazine[30]. This was superceded in 2015 by α-PD-1 agents for ipilimumab-naive advanced melanoma[31], with nivolumab and pembrolizumab approved as first-line therapy in 2016[32]. Trials combining ipilimumab and nivolumab as a combination treatment (cICB) showed superior efficacy in advanced melanoma compared to single agent α-PD-1 (sICB)[33], and this was approved in the UK as an additional first-line treatment for advanced melanoma in 2016[34]. In 2021, single-agent α-PD-1 was also approved for resectable Stage III melanoma as a post-excision adjuvant treatment[35] associated with increased recurrence-free survival[36]. Although monoclonal antibodies targeting other checkpoint molecules have shown preliminary indications of survival benefit in advanced melanoma, such as LAG-3 (relatlimab)[37], they have not reached widespread adoption. Clinically, the decision to treat advanced melanoma with sICB or cICB is based on patient fitness and preference, particularly factoring in potential side effects. There is a slant towards cICB for younger, fitter individuals and those requiring aggressive treatment i.e. brain and central nervous system metastases[2].

ICB has dramatically changed treatment outcomes for MM. Prior to the adoption of ICB, MM had a 5-year survival rate ranging from 5-19% and median overall survival of 5.3 months[38]. At 5 year follow-up, nivolumab was associated with a 39% overall survival (OS) rate and 28% progression-free survival (PFS) rate, with a median survival time of 37.3 months, compared to 11.2 months for dacarbazine[39]. Similarly, pembrolizumab treatment had a 34% OS rate and median survival rate of 23.8 months[40]. Combination treatment with nivolumab and ipilimumab resulted in a 52% OS rate and a median overall survival of 60 months[41], as represented in Figure 1.2. Use of α-PD-1 or α-PDL-1 antibodies (durvalumab, atezolizumab and avelumab) has also extended to other cancer types including non-small cell lung cancer (NSCLC), Merkel cell carcinoma, urothelial carcinoma, renal cell carcinoma (RCC), hepatocellular carcinoma (HCC), cervical cancer and Hodgkin's lymphoma (reviewed in Wang et al.[42]).

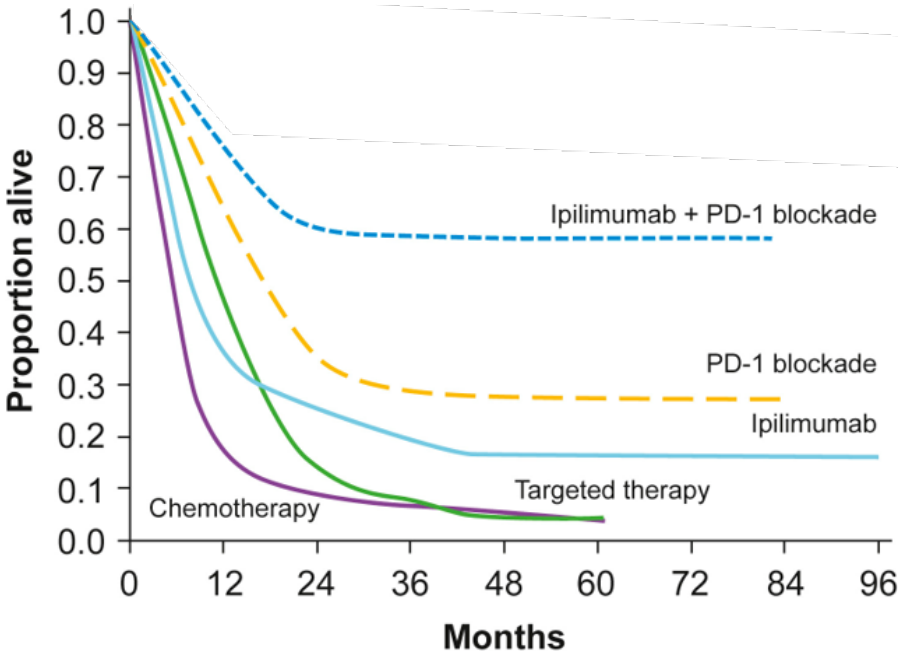



**Figure 1.2 Patient survival with ICB.** Kaplan Meier curve comparing approximate survival rates of different treatment modalities for metastatic melanoma. Adapted from Emens et al[43].

Despite this, complete response rates for MM are only 20% for nivolumab[39], 16% for pembrolizumab[40] and 22% for combination ipilimumab and nivolumab[41]. Furthermore, treatment with ICB often leads to autoimmune side effects, referred to as immune-related adverse events (irAEs), such as autoimmune dermatitis, colitis, arthritis and hepatitis. Severe irAEs (clinical grade 3 or 4) often require steroids for symptom management and are observed in 16% of patients receiving nivolumab but for 55% on combination treatment. Although irAE development is associated with improved responses to ICB[44], they can cause considerable morbidity and necessitate ICB interruption or discontinuation. Prolonged steroidal or $\alpha$-tumour necrosis factor (TNF) therapy to treat irAEs also increases the risk of serious infection[45] and may potentially be linked to reduced survival benefit from ICB[46–48]. This indicates ICB in its current form may not be suitable for all MM patients; treatment success may require finer clinical stratification and/or escalation of additional combination therapies.

## 1.2 Cellular sensitivity and resistance to ICB

### 1.2.1 T-cell mediated anti-tumour immunity

$CD8^+$ T cells are a key mediator of cytotoxic activity but encompass a variety of subsets. T cells can be classically grouped by their differentiation status from naive T cells that are antigen-inexperienced, to effector T cells following cognate antigen recognition, and central and effector memory T cells (CM, EM) responsible for antigen recall[49,50] (Figure 1.3). CM have an increased capacity for self-renewal with putative differentiation potential to EM which responds most rapidly to antigen re-exposure but has the shortest lifespan. A population of stem cell memory cells (SCM) has also been described[51], representing a subset that may replenish the memory and effector pools, having the greatest self-renewal and differentiation capacity. Further tissue-specificity across $CD8^+$ T cells has also been described, in particular, resident memory cells (Trm) which express markers of retention and downregulate markers of lymphocyte egress[52,53]. Canonically, effector and EM subsets have greatest cytotoxic activity and are able to lyse foreign pathogens most effectively[54].

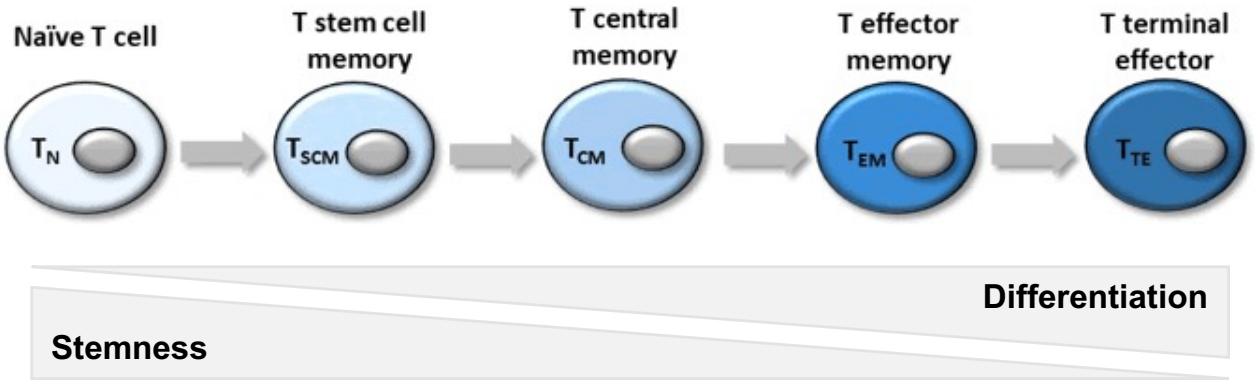



**Figure 1.3 Conventional $CD8^+$ T cell subsets.** Five subsets of $CD8^+$ T cells have been described with increasing differentiation and decreasing stemness going from left to right. Adapted from https://cellculturedish.com/t-cell-media-comprehensive-guide-key-components/.

$CD8^+$ T cells can directly recognise tumour antigens to deliver cytolytic perforins and granzymes to recognised cells, leading to loss of cell membrane potential and caspase and mitochondrial apoptotic pathways. Alternatively, cytokines such as interferon(IFN)-$\gamma$ and TNF-$\alpha$ can induce apoptosis in neighbouring tumour cells in a paracrine manner by binding to their respective receptors and triggering downstream caspase expression[55,56]. IFN-$\gamma$ has further well-recognised effects to allow improved antigen-directed cytolysis including

upregulating HLA antigen presentation and enhancing T cell cytotoxicity[57,58] whilst TNF-α has been identified as a crucial mediator of cancer killing based on loss-of-function CRISPR screens in tumour cells[59]. Lastly, $CD8^+$ T cells can ligate Fas expressed on the tumour, leading to caspase-mediated cell death.

There is also increasing recognition for the cytotoxic potential of $CD4^+$ T cells. Although they are traditionally recognised as 'helper' T cells, $CD4^+$ T cells are recognised to directly kill tumour cells expressing tumour peptides on major histocompatability complex (MHC)-II molecules[60–62]. They also provide help to $CD8^+$ T cells via IL-2 production and enhance licensing of DCs and B cells via CD40L interactions to improve adaptive immune functions.

However, cancer encodes multiple forms of immune evasion and dysfunction to prevent its direct and indirect lysis. Firstly, tumours can develop loss-of-function mutations in antigen presentation machinery which precludes antigenic recognition and killing (reviewed in Dhatchinamoorthy et al.[63]). Secondly, the local tumour microenvironment (TME) can be highly immunosuppressive, with increased fibroblast content, infiltration from Tregs and tumour-associated macrophages, attenuating T cell activity. Thirdly, tumours can limit tumour-infiltrating lymphocyte (TIL) recruitment in so-called 'immune-cold' or 'barren' tumours. This collectively results in a battle between immune activation and suppression that ICB seeks to overcome.

### 1.2.2 Overview of immune responses to ICB

#### *1.2.2.1 α-CTLA-4*

As a regulatory immune receptor, CTLA-4 can be expressed on a variety of immune cells including T and B cells, monocytes and dendritic cells (DCs)[64–66] but is predominantly associated with its immunosuppressive functions in T cells. CTLA-4 is upregulated in T cells following T cell receptor (TCR) engagement, peaking in surface expression across the following 48 hours[67], and acts a negative feedback regulator of T cell activation. Specifically, CTLA-4 is trafficked from intracellular stores to the immunological synapse following TCR engagement. Stronger TCR signalling leads to greater synaptic accumulation of CTLA-4[68]. Expression of CTLA-4 on T cells prevents engagement of the co-stimulatory receptor CD28 with its ligands CD80 and CD86 expressed on antigen-presenting cells (APCs) through competitive binding[69]. In particular, CTLA-4 binds CD80/6 with rapid kinetics and greater affinity and avidity than CD28[70,71], thus preventing the secondary signals required for complete TCR activation. Furthermore, engagement of CTLA-4 leads to the recruitment of phosphatases targeting immunoreceptor tyrosine-based activation motifs

(ITAMs) downstream particularly of CD28[72], thereby preventing AP-1, NFκB and NFAT signalling required for T cell activation[73] (Figure 1.4). Lastly, CD80 and CD86 expressed by APCs undergo endocytosis following interaction with CTLA-4[74], which limits further co-stimulatory activity. Upon global CTLA-4 ablation in mice, early and fatal autoimmune multi-organ tissue destruction occurs[75,76], thus demonstrating the importance of CTLA-4 for immune regulation.

CTLA-4 is also constitutively expressed on regulatory T cells (Tregs), which develop from cells strongly recognising self-peptides during thymic selection. Treg-associated CTLA-4 plays a similar role in preventing engagement of CD80/6 with CD28 on effector T cells and its expression is indispensible for their immunosuppressive function[77]. Recent CRISPR (clustered regularly-interspaced short palindromic repeats) screens have identified that FOXP3 activity is essential for stable CTLA-4 expression, indicating CTLA-4 is a key feature of the Treg phenotype[78]. Therefore, CTLA-4 acts as an immune checkpoint on both conventional and regulatory T cells to constrain T cell immune activation. Whilst its role in maintaining peripheral tolerance is paramount, CTLA-4 serves as a block to tumour eradication in contexts like cancer where sustained anti-tumour responses are required.

Ipilimumab binds directly to the CD80/6-interacting domain of CTLA-4[79]. This permits unrestrained CD28 co-stimulation between APCs and T cells and thus reverses T cell exhaustion for anti-tumour activity. In particular, CTLA-4 blockade leads to *in vivo* upregulation of the co-stimulatory molecule ICOS in $CD4^+$ T cells and to a lesser extent $CD8^+$ T cells across peripheral blood, tumour and adjacent tissue[80–82]. An increase in exhausted $CD8^+$ T cells and an effector PD-$1^+$ $ICOS^+$ Tbet $^+$ population of $CD4^+$ T cells following ipilimumab has also been described[83]. Furthermore, a broadening of the peripheral T cell and anti-tumour $CD8^+$ repertoires has been seen[84,85], with lower affinity TCRs permitted to mature during T cell selection and expand even upon weak antigen recognition without the restriction imposed by CTLA-4[86].

Given tumour cells typically lack expression of CD80/6, the invigorating effect of CTLA-4 blockade is thought to have the greatest action in sites of antigen recognition, such as tumour-draining lymph nodes (tdLN)[86,87]. tdLN APCs can cross-present cancer antigens to prime and activate tumour-reactive T cells effectively. More recently, intratumoural tertiary lymphoid structures (TLS) as additional sites of bolstered α-CTLA-4-mediated activity. These are organised aggregates of immune cells adopting a lymph node-like structure that form under chronic inflammation. TLS-associated APCs may therefore also benefit from α-CTLA-4 activation and understanding where anti-tumour T cell priming occurs will help inform responsivity to ipilimumab.

In addition, ipilimumab binds to CTLA-4$^+$ Tregs and putatively depletes them via antibody dependent cell cytotoxicity (ADCC) given it's high constitutive expression on this population. In particular, ipilimumab has an IgG1 backbone which is recognised through FcγRIII (CD16), expressed highly on non-classical monocytes. Amino acid modifications to the Fc backbone of ipilimumab that mitigate ADCC are described to prevent Treg depletion[88]. Reports of Treg depletion have also been accompanied by greater CD8$^+$ T cell tumour infiltration[88]. However, there remains debate over whether intratumoral Tregs are indeed depleted after α-CTLA-4 and its relative significance compared to CTLA-4 blockade on effector cells[88–90]. Overall, successful responses to ipilimumab may require a latent anti-tumour population of T cells constrained largely by CTLA-4 expressing Tregs, with the ensuing balance of effector to regulatory function tipped in favour of the former following treatment.

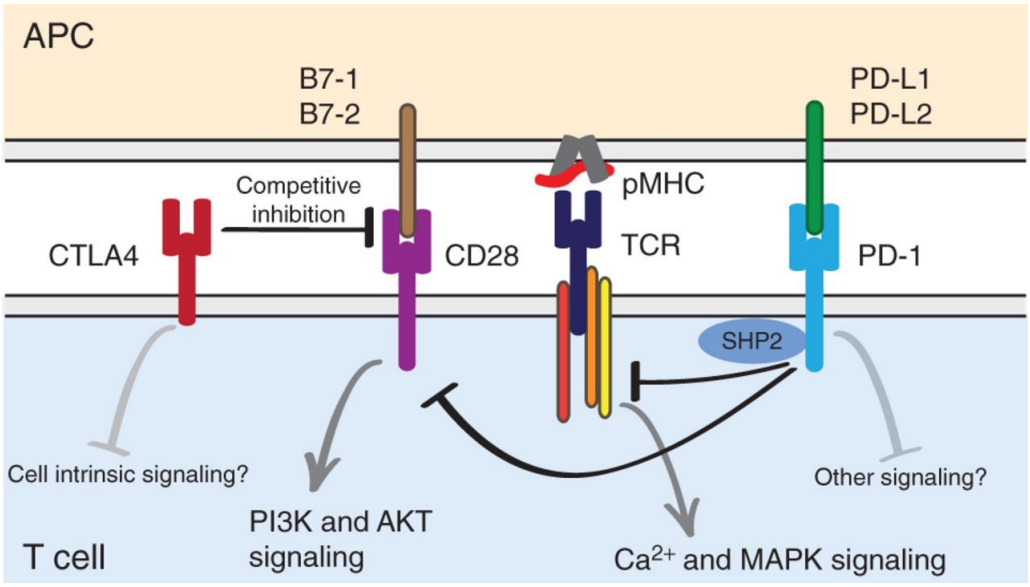



**Figure 1.4 Signalling pathways downstream of CTLA-4 and PD-1.** CTLA-4 competitively inhibits CD28 co-stimulation by CD80 (B7-1) and CD86 (B7-2)-expressing antigen presenting cells (APC) and additionally restricts ITAM signalling downstream of CD28. PD-1 recruits SHP2 and inhibits TCR and CD28 signalling to prevent T cell stimulation. Figure from Wei et al[86].

#### *1.2.2.2 α-PD-1*

Like CTLA-4, PD-1 expression is upregulated following cellular activation as a negative feedback regulator and has become a defining marker of immune exhaustion. PD-1 is expressed predominantly on T and B cells whilst its corresponding ligands PD-L1 and PD-L2 are limited in expression to antigen presenting cells such as DCs, and importantly, tumours and tumour-associated macrophages as well. PD-1 expression is induced after TCR signalling

whilst PD-L1/2 are induced upon exposure to IFN-ɣ[91–93], thus attenuating T cell stimulation and cytotoxicity. Ligation of PD-1 leads to downstream immunoreceptor tyrosine-based inhibitory motif signalling that permits recruitment of SHP-1 and SHP-2 phosphatases[91,94]. Like CTLA-4, these phosphatases target ITAMs associated with CD28, TCR/CD3 complexes, ZAP70, Phosphoinositide 3-kinase and Spleen tyrosine kinase[94,95] (Figure 1.4). This leads to signalling perturbations at multiple stages downstream of the TCR including CD4/CD8 co-receptor accumulation, TCR/peptide-MHC recognition, TCR expression and RAS/ERK signalling[95–97]. Furthermore, PD-1 modulates cellular metabolism by promoting fatty acid oxidation and limiting aerobic glycolysis[98], thus limiting T cell effector function and leading to a metabolically restricted state associated with exhaustion[99,100]. Globally, PD-1 deletion leads to the development of lupus-like autoimmunity[25] like CTLA-4, but is not lethal. PD-1 blockade has been principally described to work at intratumoural sites where exhausted PD-1$^+$ T cells are abundant due to chronic antigenic stimulation[101]. Nivolumab and pembrolizumab bind to different epitopes of PD-1 but both binding sites overlap with the domain responsible for PD-L1/2 interactions[102]. As such, this prevents the aforementioned inhibitory PD-1 signalling on PD-1$^+$ cells, allowing these activated cells to retain their effector functions and an 'invigorated' state. Accordingly, tumours have increased expression of activation and exhaustion markers following α-PD-1, with enrichment for lymphocyte and cell activation pathways[103]. T cells are phenotypically activated and proliferate both intratumourally and peripherally following PD-1 blockade[83,104] and are key mediators of ensuing anti-cancer responses that may result in destruction of the tumour. Increased numbers of CD8$^+$ and CD4$^+$ TILs are also observed after α-PD-1[105], based on a CXCR3-CXCL9/10 chemokine signalling axis[106,107] which is upregulated by IFN-ɣ and TNF-α expression.

Given the increasing body of evidence suggesting chronic T cell exhaustion is epigenetically coded and irreversible, especially in association with anti-tumour responses[108–111], there is renewed focus on the cells that mediate reinvigorated immunity after PD-1 blockade. Paired TCR analyses of blood, normal adjacent tissue, tumour and tdLNs have posited a theory of 'clonal replacement' where on-treatment TILs carry different TCRs to the exhausted pre-treatment TILs and instead originate from peripheral blood and secondary lymphoid organs like tdLNs[112,113]. As such, lymphocyte recruitment may be a key mechanism behind the efficacy of α-PD-1 therapies.

### 1.2.3 Beneficial immune cell activity in ICB across cell subsets

#### *1.2.3.1 CD8⁺ T cells*

As the key recipients of ICB invigoration, baseline and on-treatment $CD8^+$ T cell profiles are crucial determinants of response to checkpoint blockade. Higher degrees of $CD8^+$ TIL infiltration have been associated with clinical benefit from ICB particularly in melanoma[88,103,114,115]. Both tumour-reactive and bystander TILs can be found in the tumour[116]. Due to chronic antigenic exposure and re-programming from the TME, tumour-reactive TILs are often associated with T cell exhaustion[116,117], evidenced by upregulation of markers such as PD-1 and CD39[101,118]. Indeed, increased CD103 and CD39 positivity are found on TILs from ICB responders[119–122]. Intriguingly, tumour-reactivity is rarely associated with a memory phenotype[116] despite an increased memory and Trm phenotype on TILs being tentatively associated with clinical ICB benefit[123–125]. Given exhausted T cells are epigenetically re-wired, preventing their re-activation, TIL exhaustion may serve as a marker of underlying presence of tumour-reactive immunity whilst memory markers may indicate a capacity for immune responsivity. In particular, TCF1 is a transcription factor that promotes memory differentiation[126] that is also associated with beneficial outcomes to immunotherapy[125]. Exhausted progenitor $TCF1^+$ T cells with proliferation potential appear to be required for ICB response[127,128], are enriched for tumour antigens[129] and their proximity to $PD\text{-}L1^+$ DCs in tdLNs is increased in ICB responders[130]. $TCF1^+$ T cells from tdLNs may consistently repopulate the tumour with non-exhausted TILs[129,131–133], thereby enhancing the post-ICB immune response. Indeed, *ex vivo* TCR stimulation of tumour fragments associates with clinical response to PD-1 blockade[134], showing the importance of T cell reactivity to ICB outcome.

In addition to contributions from tdLNs, overlap between TILs and their peripheral counterparts, and the phenotype of the peripheral $CD8^+$ T cell compartment can shape ICB responsivity. Several studies have implicated increased overlap between circulating and tumour T cell clones, and greater numbers of dual-expanded clones as beneficial for ICB outcome[135,136]. Dual-expanded clones carry increased cytotoxicity and reduced exhaustion[135,137], suggesting recent immigration to the tumour. Correspondingly, higher peripheral cytotoxicity correlates with increased TIL cytotoxicity[138] and improved response to ICB[122,139,140]. Added characteristics of peripheral $CD8^+$ T cells associated with ICB benefit include high CX3CR1 expression and a shift towards an effector phenotype[141–143]. On the other hand, CD39 and LAG-3 expression correlate with poor ICB responses[131,144] although these observations are disputed[145]. Notably, long term melanoma immunotherapy responders

with survival past 5 years have T cell clones shared between blood, tumour and neighbouring skin that carry cytotoxic signatures in circulation[146].

In particular, clonal expansion of peripheral $CD8^+$ T cells has been observed in patients with beneficial ICB responses across melanoma[143,147] and RCC[148]. The number of large clones (occupying 0.5% of the repertoire) after 1 cycle of ICB in MM was significantly correlated with longer PFS and OS[147]. Likewise, responders to PD-1 therapy in RCC have significantly increased numbers of expanded T cell clones and a concomittant fall in their peripheral TCR diversity after 1 month of treatment[145]. Expanding T cell clones in peripheral blood following ICB appear to be clonally convergent, particularly in responding patients[143], and share overlap with publicly identified melanoma reactive TCRs[147]. In support of a peripheral anti-tumour response reflecting tumour control, the emergence of neo-antigen reactive peripheral $CD8^+$ T cells associates with improved outcome to ICB[149]. In summary, $CD8^+$ T cell tumour reactivity and cytotoxic potential both appear to be hallmarks of individuals deriving benefit from ICB, both in the tumour and peripheral compartments.

#### *1.2.3.2 $CD4^+$ T cells*

Compared to $CD8^+$ T cells, the characteristics of $CD4^+$ T cells that are beneficial and detrimental to ICB responses remain relatively under-explored. Pro-inflammatory Th1 responses are conventionally considered desirable in chronic infections upon PD-L1 blockade due to restoration of IFN-$\gamma$ and IL-12 cytokine production and cytotoxic killing potential[150]. In particular, an abundance of $CD4^+$ T cells that produce CXCL13 following tumour antigen recognition correlates with $CD8^+$ T cell, B cell and macrophage activation and patient survival in melanoma and following ICB in breast cancer[151]. In parallel, tumour-specific follicular Th cells (Tfh) can produce IL21 and interact with tumour-infiltrating B cells to promote $CD8^+$ T cell effector functions, which can collectively enact tumour control[152]. Increased $CD4^+$ intratumoural cytotoxicty is associated with improved response to ICB in bladder cancer[61]. Accordingly, a MHC-II signature in tumours associates with successful ICB-induced tumour rejection, as driven by $CD4^+$ T cell recognition of tumour antigens[62,153,154]. Interestingly, exhaustion of cytotoxic $CD4^+$ T cells could be induced by both HLA-I and HLA-II restricted tumour antigens[62], suggesting $CD4^+$ T cell-mediated killing plays an important role even in $MHC\text{-}II^-$ tumours[154].

Similar to $CD8^+$ T cells, the circulating $CD4^+$ compartment also appears to be deterministic of ICB response. Expansion of a $CD27^-$ $ICOS^+$ $T\text{-}bet^+$ $CD62L^{low}$ subset of $CD4^+$ T cells following ICB correlates with tumour rejection in mice and melanoma patients[155]. Higher pre-treatment numbers of CM and EM $CD4^+$ T cells are found in ICB responders in NSCLC[156,157]. Only

individuals with an increased memory $CD4^+$ T cell pool had corresponding restoration of $CD8^+$ function following ICB treatment[156]. The circulating memory pool in these individuals resembled proliferating Th1-like cells and functionally enhanced cytolytic $CD8^+$ T cell responses[157]. Parallel results were observed in metastatic melanoma where higher proportions of clonally expanded and activated memory $CD4^+$ T cells at baseline associate with irAE development following ICB, indicative of a systemic immune response to treatment[158].

Finally, the proportion and phenotype of regulatory $CD4^+$ T cells (Treg) is a strong determinant of clinical ICB outcome. Given Tregs have a self-antigen directed repertoire[159], they are highly active within the TME and so exert a strong immunosuppressive phenotype on effector $CD8^+$ and $CD4^+$ T cells. High intratumoural and peripheral Treg counts are observed in individuals deriving poor outcome with ICB[124,160]. In the TME, depleting Tregs via ADCC or inhibiting their function enhances sensitivity to $\alpha$-PD-1 treatment[161,162]. Phenotypically, PD-1 can also be expressed on Tregs which ironically constrains their suppressive capacity[163]. However, inhibition of this via PD-1/L1 blockade allows for Treg proliferation and suppressor function to be restored[164], which can lead to hyper-progressive cancer[165]. As such, the ratio of PD-1 expression on Tregs and effector T cells is deterministic of ICB responsivity[163]. ICB response is primed by higher PD-1 burden on effector $CD8^+$ T cells, reflecting a greater degree of anti-tumour potential. Similarly, expression of the activation marker CD38 on Tregs associates with poor ICB responses as it denotes a highly suppressive Treg phenotype[166]. Ultimately, there is increasing appreciation for the role of cytotoxic and helper $CD4^+$ T cells derived from a 'conventional' lineage in supporting ICB responses whilst Tregs have consistently been associated with poor treatment sensitivity.

#### *1.2.3.3 Monocytes*

Cells of monocytic lineage can be broadly grouped into three subsets with cancer relevance; tumour-associated macrophages (TAMs), circulating monocytes and myeloid-derived suppressor cells (MDSCs) found across both compartments. In general, these cells are associated with inhibited tumour immunity and poor response to ICB. TAMs can exist across both pro-inflammatory and suppressive phenotypes which are commonly referred to as M1 or M2, as reviewed in Chen et al[167]. Each macrophage population is demarcated by distinct markers; CD80, CD68 and MHC-II are M1 markers whilst CD163, Arg1 and CD206 are expressed by M2 macrophages. Most TAMs are polarised toward an M2-like state by Th2 cytokines including IL-4, IL-10 and IL-13. M2 TAMs exert pro-tumourogenic effects such as angiogenesis, tissue remodelling, tumour cell invasion and metastasis. They also produce immuno-suppressive cytokines namely TGF-$\beta$, prostaglandins, arginase, IL-10 and IL-13,

which stimulate immune checkpoint expression and Treg responses. A minority of TAMs also exhibit a M1 phenotype following Th1 cytokine polarisation via IFN-γ and IL-12. M1 TAMs can contribute to anti-tumour immunity by producing reactive oxygen and nitrogen species to kill tumour cells as well as pro-inflammatory cytokines including IL-1β, IL-6 and TNF-α. M1 macrophages are also potent sources of CXCR3 ligands for the recruitment of TILs[107,168]. Overall, TAMs have been strongly associated with TIL exhaustion; both in terms of density and spatiotemporal position within the tumour[169–172]. Both PD-L1 and PD-1 are upregulated on TAMs with PD-L1 being enriched on M2 TAMs, contributing to their immunosuppressive potency[173]. PD-1 on TAMs also associates with decreased macrophage phagocytosis of tumour cells[174]. In the context of ICB responses, an abundance of TAMs, particularly of a M2 phenotype, typically corresponds with treatment resistance. A fall in macrophage signatures following α-PD-1 associates with improved outcome in melanoma[103]. A lower ratio of M2 to M1 signatures is associated with pan-cancer immune enriched tumours responding to ICB[175]. Similarly, an increased density of M2 macrophages associates with an immune-ignored state that has low sensitivity to ICB[176]. Lastly, higher baseline frequency of M1 macrophages associates with response to α-PD-L1 therapy[168].

MDSCs represent a stalled immature myeloid population that accumulates in advanced cancers[177,178], and are marked by reduced HLA-DR compared to monocytes whilst displaying lower levels of IRF8 and higher $CD11b^+$ and S100A9 than TAMs[179,180]. In particular, IRF8 is a marker of terminal macrophage differentiation[181,182]. How MDSCs arise is incompletely understood but it's suggested that chronic inflammation associated with cancer, such as IL-1 signalling, leads to increased myelopoiesis and a conversion of myeloid progenitors and mature monocytes to functionally active MDSCs[183,184]. MDSCs have well-characterised immunosuppressive functions including suppressing TCR and CD28-driven T cell proliferation and IFN-γ production. MDSCs are also potent producers of IL-10 which suppresses T cell activity and stimulates Treg development[120]. Globally across advanced tumours, higher MDSC count is associated with poor cancer prognosis[177] and correspondingly worse responses to ICB[120,178]. Indeed, prevention of MDSC recruitment and polarisation leads to increased TIL infiltration and activation, and enhanced survival following ICB[183,185].

Lastly, the circulating monocyte compartment has important ramifications for ICB responses. Baseline monocyte count has been shown to predict poor ICB responses in MM patients treated with ICB[44,186,187]. Both $CD14^+$ classical and $CD16^+$ non-classical monocytes have been implicated in poor responses to pembrolizumab in HCC[140]. Classical monocyte and MDSC populations associate with poor ICB outcomes in a pan-cancer study[142]. The exact nature of

the contribution of circulating monocytes to ICB-mediated immunity is unclear. A greater monocyte pool may relate to a potentially expanded source of MDSCs and TAMs associated with development of an immunosuppressive TME. Collectively, an abundance of M2 TAMs and MDSCs reflects an immune landscape where immunosuppression is too severe for ICB to have a restorative effect on anti-tumour immunity.

#### *1.2.3.4 B cells*

Increasingly the contribution of B cells to immunotherapy efficacy has been recognised, where high B cell tumour infiltration is associated with clinical response across melanoma and a multitude of other cancer types[188–193]. B cells are predominantly found in local immune aggregates in the tumour such as TLS[190,191]. Within TLS, melanoma antigen presentation from follicular DCs and germinal centre reactions drive B maturation including class switching, somatic hypermutation and differentiation into antibody-producing plasma cells[193,194].

B cells can produce antibodies that directly recognise melanoma antigens leading to tumour killing through ADCC, with the amount of local tumour IgG labelling being predictive of immunotherapy response[194]. Increased titres of switched antibodies and melanoma-specific antibodies within tumours are also associated with clinical response implicating a direct role of antibody production in anti-tumour ICB responses[195,196]. Further, the clinical benefit associated with TLS appears to also be dependent on activation-induced cytidine de-aminase (AID) expression[197] required for somatic hypermutation and increased antibody affinity. Consistent with this, increased plasma cell, switched memory and CD86$^+$ phenotype of intratumoural B cells is associated with clinical response[190]. In addition, B cells are essential for recruiting T cells and inducing their activation within TLS. B cells express high levels of CCL3, CCL4 and CCL5, which recruit CCR5$^+$ T cells and are associated with increased intratumoural *CD8A* expression, CD8$^+$ TIL infiltration, and IFN-ɣ and T cell effector signatures[192,198]. Tumours with increased B cell infiltration are accompanied by increased TCF7$^+$ T cells[191]. B cells from ICB responders express increased levels of antigen presentation, IFN-ɣ and T cell activation genes[199]. Canonically, CCR7$^+$ T cells may be recruited to TLS which leads to antigen presentation from follicular DCs and B cells and subsequent effector differentiation.

Following ICB, an increase in tumour TLS formation has been described, possibly stemming from CXCL13 upregulation accompanied by the recruitment of CXCR5$^+$ B cells[172,200]. In particular, PD-1$^+$ and tumour-specific CD8$^+$ T cells express high levels of CXCL13[101], as well as cancer-associated fibroblasts[200]. Indeed, CXCL13 expression is one of the strongest predictors of immunotherapy response across cancer types[201].

In tandem with the intratumoural environment, peripheral B cell signatures have also been associated with clinical ICB prognosis. Higher pre-treatment B cell counts are prognostic for immunotherapy response as well as increased IgM+ memory B cells[202,203]. A drop in B cell count following ICB accompanied by B cell clonal expansion is associated with irAE development[204], and persistence of peripheral plasma cells exhibiting class switch recombination is tentatively favourable in ICB[205]. These characteristics may reflect an increase in CXCL13-driven migration and maturation associated with TLS formation and recirculation. Overall, increasing evidence suggests that B cell presence and function supports an immune-enriched TME conducive to ICB treatment.

#### *1.2.3.5 NK cells*

NK cells are key players in anti-tumour immunity via multiple mechanisms. Based on their array of activating and inhibitory receptors, NK cells can recognise tumour cells with downregulated MHC-I expression which would otherwise escape $CD8^+$ T cell surveillance. NK cells can also express FCGR3A (CD16) and other Fc receptors to recognise antibody and complement-coated tumour cells via ADCC, and express cytotoxic cytokines and chemokines such as IFN-ɣ, CCL5 and XCL1 to recruit T cells and DCs. Much like T cells, PD-1 can be expressed on NK cells through activating cytokines such as IL-2, IL-15 or IL-18[206–208]. $PD\text{-}1^+$ NK cells display a similarly inhibited function with decreased expression of granzymes, perforins and IFN-ɣ and reduced degranulation activity[206,209] although PD-1 expression appears to be more transiently modulated in NK cells than T cells[210]. However, studies investigating *ex vivo* PD-1 expression in mouse cancer models and from human patients have differed on whether NK-associated PD-1 is physiologically relevant[209,211]. Furthermore, NK infiltration of melanoma appears to be minimal[212,213]. This means the capacity for NK cells to directly respond to α-PD-1 ICB is unclear. However, several lines of evidence suggest NK cells are still required for effective ICB responses, such as reduced ICB efficacy in NK-depleted murine tumour models[209], functional immunity of PD-1/L1 blockade in $HLA\text{-}I^-$ tumours like Hodgkin's lymphoma[214], and detectable PD-L1 expression on NK cells[215]. Indeed, activated peripheral NK cells expressing CD69 are associated with improved response to melanoma ICB[216,217]. Globally, NK and T cell interactions and competition for IL-2 may influence the outcome of ICB activity[218].

#### *1.2.3.6 DCs*

There are three prototypic subsets of DC; conventional DC(cDC)1, cDC2 and plasmacytoid DC (pDC). cDC1 have enhanced cross-presentation capacity and are predominantly responsible

for $CD8^+$ T cell priming, whilst cDC2 have strong antigen presentation for $CD4^+$ T cells. Instead, pDCs are specialised for type I IFN production upon TLR7/9 stimulation.

Broadly, the contribution of cDCs to ICB response depends on the balance of priming and inhibitory functions they can enact. Murine studies have identified tumour antigens primarily drain to tdLNs in which mouse cDC1s prime tumour-reactive T cells[219–222]. In melanoma, this cascade appears to be triggered by skin Trm cells which promote maturation and migration of cDC1 to tdLNs and leads to tumour epitope spreading[223]. In accordance, following PD-1/PD-L1 blockade, increases in proliferating $Ki67^+$ $CD8^+$ T cells were observed in tdLNs only but not in non-tumour draining equivalents[224]. cDC2s instead uptake and present antigen primarily within the tumour[222]. This represents a possible divergence between tumour $CD8^+$ and $CD4^+$ T cell priming and activation locations. cDCs have also been implicated in the CXCR3-driven recruitment of T cells to tumours through production of CXCL9/10/11[225], particularly cDC1. Within tumours, cDC1 are often found in close proximity to $CD8^+$ T cells and their respective densities co-correlate[176]. Further, IFN-ɣ from intratumoural T cells stimulates IL-12 production from neighbouring tumour cDC1 which in turn reinforces T cell IFN-ɣ and cytotoxic function[226]. In turn however, cDCs can express high levels of PD-L1 following antigen uptake and T cell priming. Following antigen priming, IFN-ɣ produced by activated T cells stimulates PD-L1 upregulation, particularly on cDC1s[222]. PD-L1 is also a hallmark of other immunoregulatory molecules on DCs that collectively restrain T cell immunity[227]. However, several studies have associated PD-L1 expression on DCs with clinical responses to ICB. PD-L1 deletion specifically on DCs but not macrophages leads to increased anti-tumour activity and PD-L1 DCs appear to be required for α-PD-L1 responses[222,228]. Specifically, PD-L1 on DCs forms a *cis* interaction with CD80 that limits CD28 co-stimulation[229]. Following α-PD-L1 treatment, cDCs can be re-licensed for CD28 stimulation and accordingly, increased presence of intratumoural cDCs associates with enhanced T cell stimulation and therapy response[229,230].

The contribution of pDCs to ICB responses is less well defined than their conventional counterparts. pDCs in melanoma have conventionally been associated with poor prognosis and recruitment and maturation of Tregs[231–233]. pDCs are capable of upregulating PD-L1 upon stimulation, with $PD\text{-}L1^+$ pDCs having increased type I IFN production[234]. However, little is known about what happens to $PD\text{-}L1^+$ pDCs following α-PD-1/L1. Persistent intratumoural type I IFN signalling has been demonstrated to inhibit ICB treatment, with higher expression of *IFIT1* and *MX1* being associated with α-PD-1 treatment progression in melanoma[235]. However, pDCs have also been ascribed cross-priming potential[236]. pDCs also appear to recruit and activate NK cells via CCR5 chemotaxis and OX40L stimulation respectively,

leading to subsequent stimulation of cDCs and T cell activation[237]. As such, their role in immune responses to ICB remains underexplored.

## 1.3 Genetic sensitivity and resistance to ICB

In addition to cellular biomarkers of immune responses and stimulation during ICB, understanding how underlying germline genetics affects responses to treatment has gained recent traction. Given checkpoint blockers result in profound transcriptomic and cellular variation between patients, whether this can be attributed to a genetic cause and indeed how much this is responsible for this heterogeneity is of keen interest. Variation in the human genome occurs most commonly as single nucleotide polymorphisms (SNPs), most of which result in subtle and undetectable changes in phenotype. Rare examples of SNPs with an overwhelming immune effect include IL2RG and ADA mutations that lead to X-linked and autosomal severe immunodeficiency.

For the most part however, SNPs result in much more subtle changes in gene expression which can be detected using expression quantitative trait loci (eQTL) analysis. eQTL pairs describe a significant association between genotype at a given SNP (eSNP) and expression of a gene (eGene), with increasing or decreasing expression based on the number of alternate alleles carried (0=homozygous major, 1=heterozygous, 2=homozygous minor) (Figure 1.5). An example of an eQTL association is at rs10784774, where individuals homozygous for the major allele (AA) have significantly higher *LYZ* expression in monocytes compared to individuals with the heterozygous AG allele, with a further drop in GG allele carriers[238]. rs10784774 is located within 2.5 Mb of the LYZ promoter and is assumed to have a local or *cis*-acting effect. There are several ways in which cis-acting genetic variation can alter transcription; coding eSNPs can modify post-transcriptional processing and stability whilst non-coding eSNPs can affect mRNA splicing, transcription initiation and elongation, chromosomal secondary and tertiary structure and epigenetic regulation (reviewed in Pai et al.[239]). rs10784774 also shows significant association with genes located outside of this window (CREB1, DUSP19 and RAB27A)[238], also referred to as *trans*-eQTLs where a more complex relationship between the eSNP and eGene is assumed that may involve post-transcriptional interactions such as transcription factors and cellular receptors.

eQTL effects are often cell-type specific given the distinct transcriptional machinery and environment each cell subset operates in. For example, the rs10784774-LYZ eQTL from above is detected in monocytes, but shows no effect in B cells[238]. This separation of eQTLs across

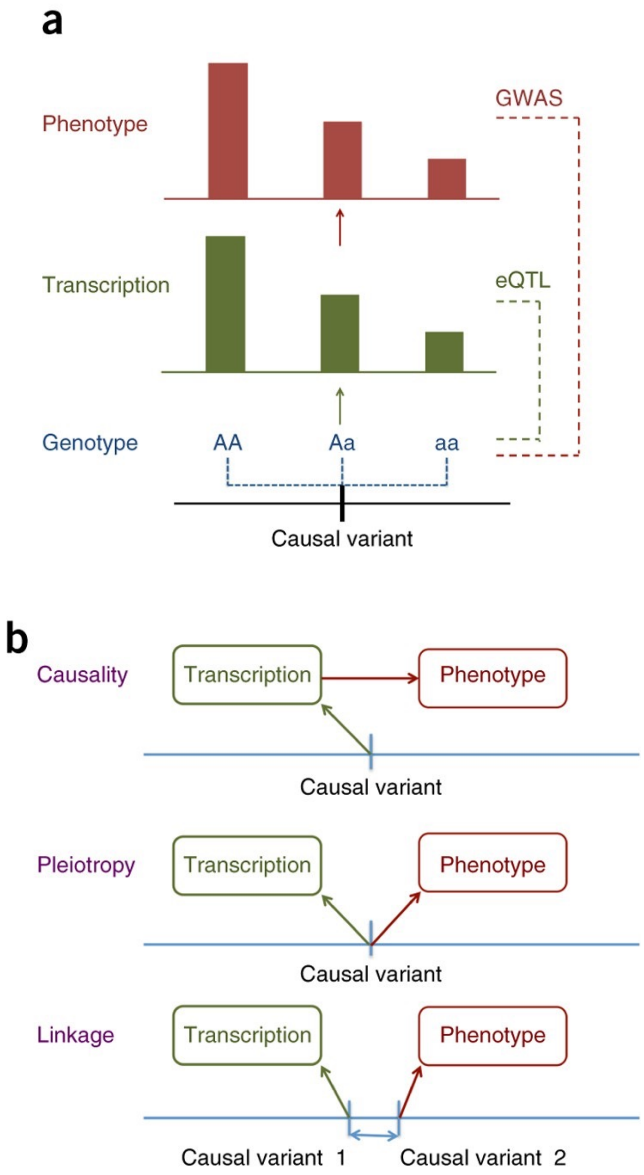



**Figure 1.5 Quantitative analysis of genetic variation. (a)** Genotypic variation at a causal variant leads to varying transcript levels and potentially divergent phenotypes, detected through expression quantitative trait locus (eQTL) and genome-wide association study (GWAS) analyses respectively. **(b)** How the genetic variation influences transcriptomic and phenotypic effects can be through directly causal or distinct (pleiotropic) mechanisms, or through co-inheritance with a separate genetic mutation (linkage disequilibrium) which is responsible for the observed effect. Adapted from[240].

cell types is representative of considerable overall specificity, whilst overlapping eQTLs are more common when comparing similar cell types such as $CD4^+$ and $CD8^+$ T cells[241]. In addition to their cell-type specificity, eQTLs are often context-specific, given how quickly transcriptional processes are induced and regulated upon stimulation. One of the early studies to examine how eQTLs change between resting and stimulated states was performed

in monocytes exposed *in vitro* to lipopolysaccharide or IFN-γ[242]. Of the eleven thousand microarray probes with at least one eQTL association, 43.4% were only observed after stimulation whilst more than half of the eQTLs found in resting monocytes were specific to this condition. Similar stimulation-specific eQTLs have been identified across T cells and DCs amongst other PBMC subsets[243–245].

By linking eSNPs to those identified in disease GWAS, key gene players that contribute to a given pathology can be uncovered. An example is the co-localisation of the type 1 diabetes (T1D) risk locus rs34843303 with *CTSH* expression in monocytes suggesting a monocytic contribution to T1D aetiology[246]. Context-specific eQTL are particularly important for uncovering genetic associations in a biological context and are enriched for overlap with GWAS risk loci above resting eQTLs[242]. A LPS-specific eQTL is observed in monocytes between *IRF8* and rs17445836, which forms a lead GWAS SNP for multiple sclerosis (MS)[247]. This SNP is associated with greater upregulation of interferon response genes in MS patient PBMCs[247], thus positioning monocytes as the key driver of this effect. Several studies have further explored genetic associations in proper disease or intervention contexts using isolated *ex vivo* cells following vaccination[248], dietary supplementation[249], as well as immunosuppressive treatment for lupus[250]. Although far fewer QTL associations were found in these analyses, each uncovered QTL may prove to be more informative in their disease relevance.

The majority of GWAS in melanoma has focused on treatment-naive cases to understand melanoma susceptibility, where *MC1R* and *CDK2NA* have been identified as important loci. Additional genes related to DNA damage (*ERCC2/5*[251], *PARP1*[252], *XRCC1*[253]), immunity (*HLA-DQ1*[254], *IFNW1*[255], *IL-10*[256]) and other processes (*EGFR*, *FLT1*, *PIK3CA*[256]) have also been posited as melanoma risk alleles but cannot be replicated upon genome-wide testing. However, limited work has been performed on underlying genetic causes of varying response to ICB in melanoma despite its strong immunological basis. Of these, several studies have focused on polymorphisms within CTLA-4 and PD-1/L1 as obvious initial targets. Breunis et al.[257] retrospectively assessed seven common *CTLA-4* polymorphisms for associations with ipilimumab outcome in 152 patients, identifying three SNPs (rs4553808, rs11571327, rs231775) significantly related to response within 4 weeks of treatment initiation. These associations could not be validated in a separate study by Quierolo et al., which identified two other CTLA-4 SNPs (rs11571316, rs3087243) associated with overall ipilimumab survival in an initial cohort of 14 individuals[258], followed by additional investigation in a cohort of ipilimumab-treated 173 patients[259]. Similarly, a SNP in PD-1 (rs11568821) was associated with longer median PFS in a cohort of 115 patients with MM treated with nivolumab[260],

with additional SNPs being identified as correlates of PD-1/L1 blockade across other cancer types (PD-L1 rs2282055 and rs4143815 in NSCLC[261], PD-L1 rs17718883 in gastric cancer[262], PD-L1 rs7041009 in NSCLC[263]). In particular, PD-L1 rs17718883 encodes a non-synonymous nonsense P146R mutation that weakens the PD-1/PD-L1 interaction, permitting higher native IFN-γ expression by T cells and weakening the extent α-PD-1 can restore immune function[262].

Although these SNPs were all identified in association with ICB outcome, studies have also begun to turn their attention to irAE occurrence, with rs10204525 in PD-1 recently associated with irAE occurrence following nivolumab in metastatic RCC[264]. It is important to note that many of these studies could not replicate SNP-outcome associations found in previous tests, either indicating cancer-specific behaviour of immune SNP variation or that greater powering is required to get a properly unbiased and complete insight into checkpoint molecule polymorphisms.

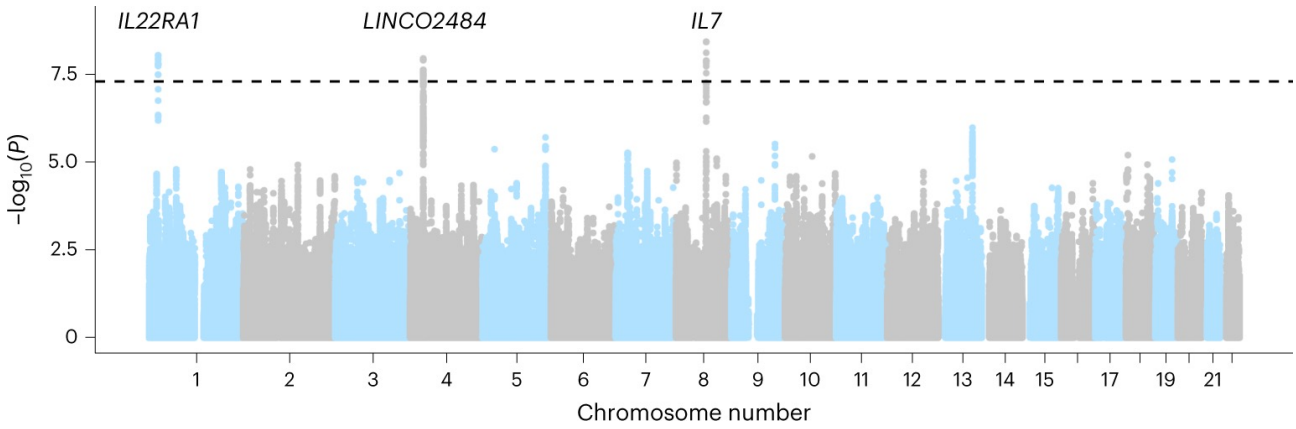



**Figure 1.6 GWAS analysis of irAE development in ICB.** Groha et al[265] performed a genome-wide association study of pan-cancer patients treated with ICB to detect genetic variants associated with immune-related adverse events (irAE), finding three loci below genome-wide significance.

Recently, datasets with sample sizes matching the scale required for GWAS studies of ICB responses have begun to emerge. A genome-wide study found three loci significantly associated with irAE occurrence in a cohort of 1751 advanced cancer patients; IL7 rs16906115, IL22RA1 rs75824728 and 4p15 rs113861051[265] (Figure 1.6). IL7 rs16906115 in particular replicated in two validation cohorts, thus identifying a novel genetic regulator of ICB outcomes. With the further increase in the number of ICB-treated patients globally, particularly as a first-line treatment for melanoma, additional GWAS loci for survival, irAE and other clinical manifestations will continue to be uncovered and provide novel insights into underlying genetic influences of ICB responses.

## 1.4 Key aims

Altogether, it is evident that identifying conserved features of the immune response to ICB that lead to clinical benefit is extremely important, but challenging given intra-patient and cellular variation. To tackle this, I will explore the following aspects:

- What are the characteristics of $CD8^+$ T cell response to ICB? Can we identify modules of gene expression that tend to be co-associated?
- How does the T cell response vary between $CD8^+$ T cell subsets? Can we embed clonal changes and dynamics to better understand this?
- Can we use descriptions of $CD8^+$ T cell responses to identify biological and clinical features associated with clinical benefit from ICB?
- How is the $CD8^+$ T cell response interlinked with that of other immune subsets? Can we identify parallel features of these cell types that regulate T cell immunity?
- How do we identify the specific subpopulations of these immune subsets that influence beneficial and detrimental T cell responses to ICB?
- How do genetic variants associated with divergent clinical responses to ICB enact their effects?

To answer these questions, I have collected peripheral blood samples from MM patients enrolled for treatment with ICB, across both single-agent and combination treatment, as part of a group-wide study. I will then isolate PBMCs and specific immune subsets ($CD8^+$ T cells, $CD14^+$ monocytes and $CD19^+$ B cells in particular) and assess their transcriptomic, proteomic and genetic profiles using bulk and single-cell RNAseq, flow cytometry and DNA array genotyping, both prior to ICB and following the completion of the first cycle of immunotherapy.

Using this data, I can therefore monitor the pre-treatment and on-treatment immune state of these MM patients, and assess the changes induced by ICB. By linking this with clinical information collected retrospectively, I have identified features that associate with clinical outcomes including progression, survival and toxicity development. These novel features can be used as potential tools for future patient stratification and novel treatment strategies in the fight against cancer.

# Chapter 2

# Methods

## 2.1 Patient and clinical cohort

Patients with metastatic melanoma were recruited via the Oxford Radcliffe Biobank (Oxford Centre for Histopathology Research ethical approval reference 19/SC/0173, projects 16/A019, 18/A064, and 19/A114). Healthy donors living in Oxford were recruited via the Oxford Biobank (Research ethical approval number 06/Q1605/55). All recruited individuals provided written consent for donation of blood samples and the collection of relevant biological and clinical information. MM patients were either treated with sICB (480 mg nivolumab monthly or 2 mg/kg pembrolizumab 3 weekly), or cICB (3 mg/kg ipilimumab plus 1 mg/kg nivolumab every 3 weeks for 4 treatment cycles followed by maintenance nivolumab). MM outcome data was collected based on clinical or radiological assessment at approximately 6 months following ICB treatment, and evaluated based on immune-related Response Evaluation Criteria in Solid Tumors v1.1 (irRECIST.1.1)[266]. Additional information regarding patient PFS, OS, and development of irAEs within 3 months as per National Cancer Institute Common Terminology Criteria for Adverse Events (CTCAE) was also collected[267].

## 2.2 Sample collection and preparation

Immediately prior to the initiation of immunotherapy and prior to subsequent cycles of treatment, peripheral blood samples (approximately 30-50 mL) were collected in 10 mL EDTA Vacutainers (BD Biosciences) (Figure 2.1) and diluted 1:2 in HBSS (Lonza) at room temperature (RT). 10-25 mL of the diluted samples were then layered onto 12.5 mL of Ficoll-Paque in a

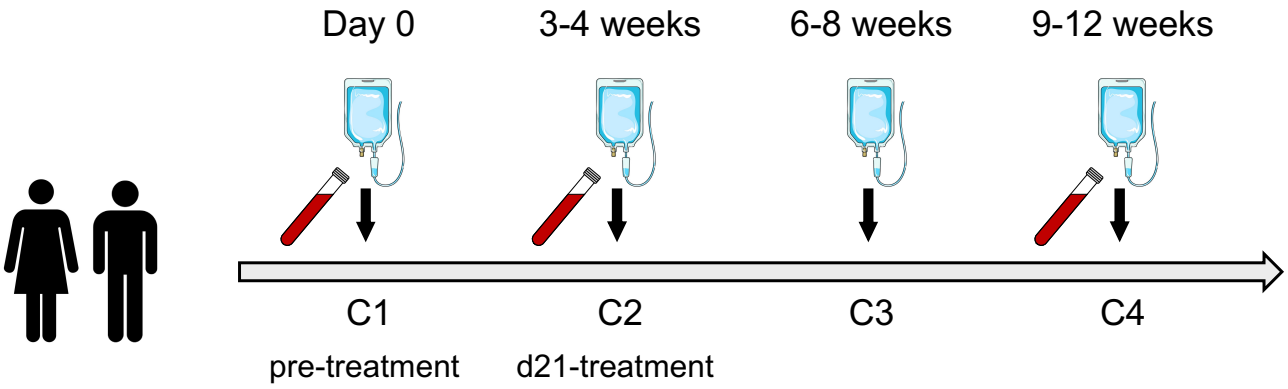



**Figure 2.1 Patient blood sample collection.** Schematic of sample collection for patients receiving ICB. Blood was collected immediately prior to ICB initiation and immediately prior to subsequent cycles of ICB across the duration of the patient's treatment regimen.

50 mL Falcon for density centrifugation at 400 g for 30 minutes with slow acceleration and no deceleration at RT. Plasma was slowly aspirated from the top of the resultant fractions, centrifuged at 16,000 g for 20 minutes at 4 °C and the resulting plasma supernatant snap frozen at 80 °C for ELISAs, cytometric bead arrays and CMV testing. PBMCs were collected from the buffy coat layer and washed twice in cold HBSS by centrifugation at 300 g for 10 minutes at 4 °C. PBMCs were counted by haemocytometer using Trypan Blue (ThermoFisher) to determine viability. 1.25x$10^6$ PBMCs were centrifuged and the pellet resuspended in 350 uL of RLT Plus Buffer (Qiagen) supplemented with 40 mM dithiothreitol (Merck), snap frozen at 80 °C for downstream RNA/DNA extraction. PBMCs were also cryopreserved in 90% FCS (Gibco) supplemented with 10% DMSO (Merck). The remaining PBMCs were used for magnetic-activated cell sorting using commercial kits from Miltenyi Biotec; CD8 MicroBeads, CD14 MicroBeads, CD19 MicroBeads, Memory CD4 T Cell Isolation Kit, NK Cell Isolation Kit according to the manufacturer's instruction using MACS Buffer (HBBS with 0.5% (v/v) FCS and 10 uM EDTA), MS columns and an OctoMACS separator (Miltenyi). Isolated cells were counted using the Countess II FL Automated Cell Counter (ThermoFisher), centrifuged and resuspended in 350 uL of RLT with dithiothreitol as described before. The sample processing approach and downstream assays are summarised in Figure 2.2.

## 2.3 Genotyping

Genomic DNA (gDNA) was isolated and array genotyped as previously described[268]. In particular, gDNA from healthy donors (HD) was isolated from whole blood using the

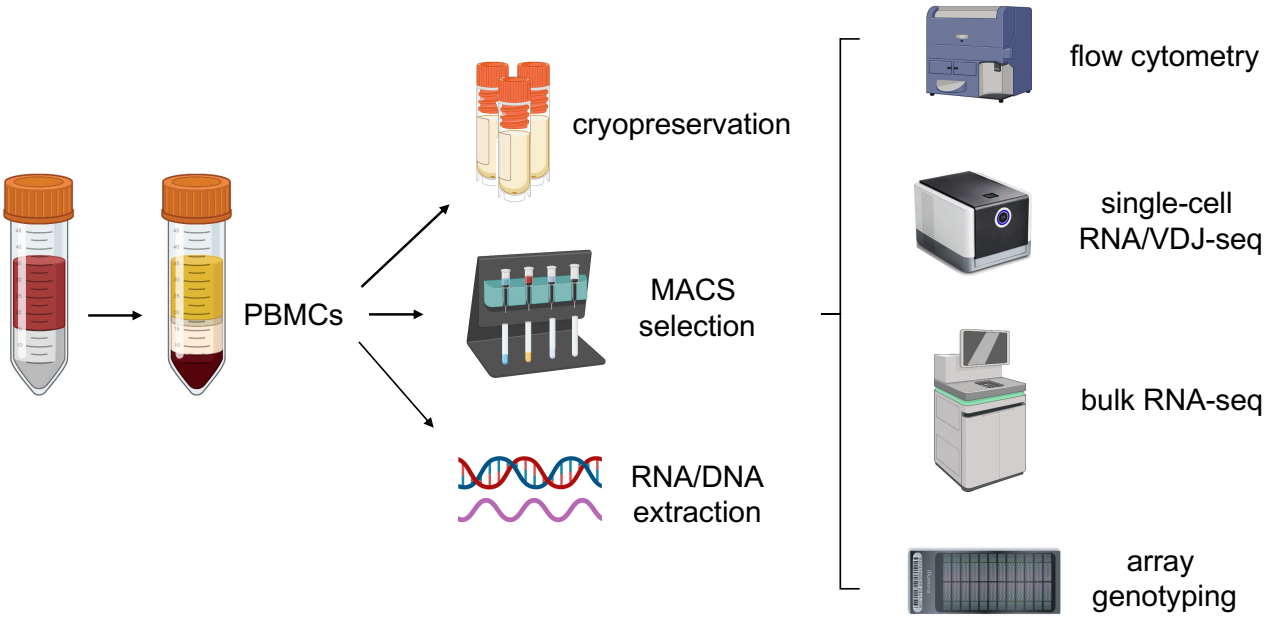



**Figure 2.2 Downstream assays for processed patient PBMCs.** Schematic of patient sample processing for PBMCs and subsequent aliquotting for cryopreservation, further magnetic isolation of subsets, and lysis for downstream RNA/DNA extraction. The assays performed on each processed sample type are depicted to the right.

Gentra Puregene Blood Kit (Qiagen) whilst gDNA from melanoma patients (MM) and some further HDs was isolated from PBMCs using the AllPrep DNA/RNA/miRNA Kit (Qiagen) after homogenisation using QIAshredder columns (Qiagen). HD gRNA was quantified by PicoGreen (Invitrogen) and then genotyped on the HumanOmniExpress-12v1.0 BeadChip (Illumina) spanning 733,202 loci. MM gRNA was quantified by Qubit DNA HS Assay Kit (ThermoFisher) and genotyped on the Infinium Global Screening Array 24v3 (Illumina) spanning 654,027 loci. SNP calls were initially filtered for minor allele frequency (MAF) >4%, Hardy-Weinberg equilibrium (HWE) p>1x10-10 and SNP missingness <2%. Samples with call rates <97% were excluded from downstream analysis. QC metrics were calculated in GenomeStudio v2.0 and PLINK v1.9[269]. HD and MM genotypes were then pre-phased and imputed using Eagle2[270] and Minimac4[271], with the Haplotype Reference Consortium v181 as a reference on the Michigan Imputation Server v1.2.483. Following imputation, SNPs with MAF>0.04, imputation R2>0.7 and HWE p>1x10-10 were retained as further QC. 52 overlapping genotypes across the HD and MM genotype sets were compared and loci with discordant calls removed, leading to a total of 5,477,998 remaining SNPs across 282 HDs and 215 MM patients.

## 2.4 Bulk RNAseq

RNA was isolated using the AllPrep DNA/RNA/miRNA Kit from PBMCs and isolated cell subsets. 100-800 ng of extracted RNA was used for mRNA library construction using the NEBNext Poly(A) mRNA Magnetic Isolation Module kit (New England Biolabs) and NEBNext Ultra II Directional RNA Library Prep Kit for Illumina (New England Biolabs) with SPRIselect beads (Beckman Coulter) used for DNA cleanup. In particular, a fragmentation of 8 minutes to achieve libraries of 400-550 bp size was selected. Prepared libraries were quantified by Qubit DNA HS Assay Kit and QCed using the TapeStation D1000 HS Kit on the TapeStation 2200 or 4000 (Agilent). Libraries were sequenced by the Oxford Genomics Centre on Illumina HiSeq 4000 (75bp paired-end) or NovaSeq 6000 (150bp paired-end) sequencers.

For general analysis, HISAT2[272] was used to align paired fastq files to the GRCh38/hg38 genome. samtools, picard and bamtools were used to sort the mapped bam file, mark duplicate reads and filter for paired reads. stringtie[273] was used for transcriptome reconstruction and HTSeq[274] used for gene count quantification. to generate final read count tables. mbv[275] from QTLtools and verifybamID[276] were used to identify sample contamination with a maximum cutoff of 2.5% mixing accepted.

For eQTL analysis, STAR[277] was used to align fastq files to the GRCh37/hg19 genome in an allele-blinded manner using the WASP algorithm[278] based on the corresponding genotyped vcf. samtools was used to sort the mapped bam and the bam was remapped using WASP, with reads failing to map back to the same location subsequently removed. HTSeq was used for gene count quantification as before.

Differential expression (DE) analysis and data normalisation was performed in DESeq2[279] using the expression matrices outputted by HTSeq. Gene counts were normalised and transformed based on size factor and dispersion estimates with genes with count <10 subsequently removed. Principal component analysis (PCA), correlation analysis and calculation of geometric mean composite scores were performed using normalised expression data. For DE analysis, a negative binomial generalised linear model was used, with confounding variables including age, sex and quantity of RNA library input regressed, or ID for paired analysis. Multiple testing correction was performed using Benjamini-Hochberg (BH) procedure, with adjusted p values <0.05 considered significant. Ensembl IDs were converted to gene symbol names using the mygene package. Pathway analysis was performed using the XGR package[280] using the Gene Ontology Biological Processes (GOBP) database with the hypergeometric test and BH procedure used for multiple testing corrections.

Significantly enriched pathways were identified with adjusted p value <0.05.

The MiXCR package[281] was used to recover TCR and BCR sequences from paired fastq files from bulk RNA-sequencing as previously described[147]. In particular, three mapping passes were made to maximise the number of assembled reads. T cell clones were defined on unique β chain CDR3 sequence, and TCR Shannon diversity assessed using the vegan package. Due to varying numbers of recovered reads per sample, data was subsampled 1,000 times using the mosaic package and the median value taken across subsamples. Expanding and involuting clones were defined as those with an increased repertoire proportion following treatment with significance determined by Fisher's exact test. Stable clones were identified as those present across multiple timepoints.

## 2.5 Single-cell RNAseq

Single-cell RNAseq was performed using the 10X Chromium 5' platform (10X Genomics) across three instances. Freshly isolated CD8 cells were subjected to 10X v1 sequencing in 2018, whilst cryopreserved PBMCs were used for 10X v2 sequencing and cryopreserved B and T cells were isolated and used for 10X v1.1 sequencing in 2021. Unless otherwise stated, all cells and reagents were kept on ice or at 4 °C during cell preparation. For v1 preparation, CD8 cells were isolated from separate fresh PBMC samples using CD8 MicroBeads (Miltenyi) as described above, and resuspended in HBSS supplemented with 5% FCS. Cells were loaded onto a Chip A for subsequent GEM generation, with each well representing cells from a single sample.

For v1.1 and v2 preparation, cryopreserved PBMCs were thawed at 37 °C and washed once in cold HBSS. For preparation of PBMCs, cells were counted on the Countess and identical numbers of live cells from different individuals were pooled together. The cell pool was passed through the Dead Cell Removal Kit (Miltenyi) according to the manufacturer's instructions using 100 uL of Dead Cell MicroBeads per sample. For preparation of T cells or B cells, cells from each sample were separately isolated using Dead Cell MicroBeads in combination with T or B Cell Isolation Kits (Miltenyi). Cells were incubated with 10 uL of biotin-conjugated selection antibodies and 40 uL of Dead Cell MicroBeads for 5 minutes at RT. 20 uL of anti-biotin MicroBeads and 30 uL of Dead Cell MicroBeads were subsequently added and incubated for 10 minutes at RT. Across both selection methods, the cell mixture was supplemented with Dead Cell Binding Buffer to a volume of 500 uL and passed through an MS column followed by 3 washes of 250 uL of Binding Buffer. Cells were spun down at 500 g for 5 minutes and resuspended in HBSS supplemented with 5% FCS. Isolated B or

T cells for v1.1 were then pooled together with an identical number of live cells from each individual added. Cells for v2 preparation were loaded onto a Chip K whilst cells for v1.1 were loaded onto a Chip G for GEM generation.

Libraries for gene expression and VDJ were constructed for each version according to manufacturer's instructions, using SPRIselect beads for DNA cleanups. In particular, TCR libraries were prepared for CD8 cells, PBMCs and T cells whilst BCR libraries were prepared for PBMCs and B cells. Libraries were quantified by Qubit DNA HS Assay Kit and QCed using the Bioanalyzer 2100 or the TapeStation D1000 and D5000 HS Kits (Agilent). Libraries were sequenced on an Illumina HiSeq 4000 for v1 at a targeted depth of 50,000 reads per cell for gene expression and 5,000 reads per cell for VDJ, or an Illumina NovaSeq 6000 for v1.1 and v2 at a targeted depth of 20,000 reads per cell for gene expression and 5,000 reads per cell for VDJ libraries.

An initial pre-processing pipeline was developed for fastqs from sequenced v1 libraries consisting of read mapping and counting using cellranger v3.0.2, followed by cell QC using scater[282] and scran[283] as previously described[147]. Doublets were estimated using the doubletCells function in scran. $CD8^+$ T cells were selected based on non-zero expression of *CD3D* and non-zero expression of *CD8A* or *CD8B*. Cells with <500 UMIs, <300 detected genes and mitochondrial gene percentage > 20% were excluded as low-quality cells whilst genes expressed in <5 cells were removed. The Seurat v3[284] package was then used for downstream normalisation, scaling, regression of UMI counts, mitochondrial gene percentage and cell cycle scores, and the identification of top variable features for dimensionality reduction. PCA was performed using the scaled data and the top 16 PCs selected for Louvain and UMAP clustering using a Scree plot. Cluster resolution was defined using hierarchical clustering in the clustree[285] package and a final resolution of 1.5 was selected. Cells were projected into the UMAP space in a total of 25 clusters, which were then annotated using the SingleR[286] package. Normalised TPM counts were constructed for all cells and reference datasets from 5 previous cancer T cell studies[112,135,287–289] and the reference labels projected onto each cell. The most abundant label for each Seurat cluster was used to identify its corresponding subset identity in conjunction with manual curation. Cellranger vdj was used for mapping of TCRs, with TCRs called as productive, full-length and TRA or TRB chains retained. Singlet TCRs were identified as carrying a single $\alpha$, single $\beta$, paired $\alpha\beta$ or dual $\alpha$ and a single $\beta$ chain.

A separate pre-processing pipeline was developed for the v2 PBMCs and v1.1 B and T cells. Read mapping and counting was performed using cellranger v6.0.1 followed by cell barcode recovery using the EmptyDrops[290] function from the DropletUtils package. Probable doublets and doublet scores were computed using the scrublet package[291]. Genetic demultiplexing of

pooled cells was performed using the cellsnp-lite package for genetic pileups and vireo[292] for demultiplexing and matching to genotypes from array genotyping. The SoupX package[293] was then used to correct for ambient RNA contamination. Similar QC filters were used to identify low-quality cells, namely those with <300 features and >20% mitochondrial gene percentage. Genotypic doublets identified by vireo were also removed prior to clustering. The Seurat v4 package[294] was also used for data normalisation, scaling and regression of UMI count, mitochondrial gene percentage and cell cycle scores, and identification of top variable features. Features matching those in a defined list of HLA, TCR and BCR genes were excluded as variable features to minimise artifacts during downstream dimensionality reduction. PCAs were then calculated and the Harmony package applied for batch correction, specifying each pool as the batch source. Louvain and UMAP clustering was then applied and cells projected into the UMAP space. Initial cluster resolutions of 5 and 2.5 were used for PBMCs and B or T cells respectively for population identification. Cell populations were identified using two parallel methods; semi-supervised reference transfer using SingleR and supervised marker expression across clusters. Specifically, expression of the following markers was associated with subset definition; CD3D and detected TCR (T cell), LYZ (monocyte), MS4A1, CD79A and detected BCR (B cell), FCER1A (cDC), GNLY (NK), CLEC4C (pDC), PPBP (platelet), HBB (red blood cell), with subsets positive for each marker being determined by local minima values. Doublet clusters were identified as having marker expression from multiple subsets, outlier scrublet score or predicted similarity to genotypic doublet clusters. TCR and BCR sequences were mapped using cellranger vdj and filtered for productive and full-length chains. Singlet TCRs were identified as before whilst singlet BCRs were identified as those carrying single light, single heavy, paired light and heavy chains or those with two light chains and one heavy chain where the ratio of light chain UMIs >8 as previously described[295]. Doublet T cells and B cells were also excluded as having doublet TCR or BCRs respectively. Doublet and contaminating clusters and cells were removed prior to reclustering as described in Figure X. In particular, PBMCs were originally clustered with a fine resolution of 5.0 as this retrieved a separate cluster of putative plasma cells with uniquely high percentage expression of immunoglobulin genes, resulting in 90 Seurat clusters. Contaminating B-T doublets, monocyte-B and monocyte-T doublets were removed prior to reclustering. In the second round of reclustering, a resolution of 5 was again selected to generate 85 Seurat clusters with 4 clusters having *HBB* expression close to 100% and removed as RBC contamination. Cells were then divided into five groupings; NK and T cells, B cells, monocytes, DC/HSCs, and all other remaining cells. For each group, cells were reclustered as above and doublet or contaminating cells were identified based on gene expression, outlier scrublet score, genotypic doublet expression similarity, platelet gene carriage and VDJ information. For

example, cells carrying a detected TCR in the B cell group were removed. In particular, a large group of *GNLY*$^+$ cells in the monocyte group were identified as contaminating NKs, based on genotypic doublet similarity despite the reported presence of GNLY$^+$ monocytes[296]. For the combined NK and T cells, removal of contaminating platelets, BCR-carrying cells and myeloid cells was first performed prior to reclustering. NK cell clusters were then identified based on geometric mean expression of a previously published NK cell gene signature[297], implemented using AddModuleScore in Seurat with thresholds determined by local minima. The NK cells were separated and reclustered. The remaining T cells were reclustered and roughly annotated into conventional CD4$^+$ and CD8$^+$ T cells, with these annotations refined upon separate reclustering of CD4$^+$ and CD8$^+$ T cells. Across all cell subsets, subgroups of 'dying' cells were identified as those with higher mitochondrial gene percentage accompanied by lower ribosomal gene percentage and were excluded for all analyses.

T cell clonality information was calculated for both sets of single-cell RNA-seq based on concatenated CDR3 amino acid sequence across the $\alpha$ and $\beta$ chains in the initial single-cell data, whilst the variable and joining chain type was incorporated in the second set of single-cell data. B cell clonality information was calculated using the immcantation pipeline[298]. Clone sizes were calculated based on the time of sampling (i.e. at baseline or on-treatment). Expanding, stable and involuting clones were defined as per the bulk MiXCR data. For recovery of expression information for certain genes, the MAGIC package was used[299]. The CellPhoneDB v2.1.0 package[300] was used for ligand-receptor interactions across subsets. Differential gene expression analysis was performed by either subsampling to identical numbers of cells across comparator groups across 100 iterations and performing a linear expression model with individual used as a random variable, or using the full dataset wherever indicated. Pathway analysis was performed using XGR as described before. Median expression scores were calculated using the AddModuleScore function in Seurat.

## 2.6 Flow cytometry

Flow cytometry was performed on 1x10$^6$ cryopreserved PBMCs as previously described[139,147,268]. In brief, cryopreserved PBMCs were thawed at 37 °C and washed in cold HBSS once. Cells were then stained with fixable amine dye (Live/Dead Near IR, ThermoFisher; Fixable Viability Stain 440UV, BD Biosciences) in 100 uL of a 1:1000 dilution with cold HBSS in a 96 well V bottom plate. Cells were incubated for 30 minutes at 4 °C and washed once in HBSS prior. 50 uL of surface antibody cocktail was then prepared in cell staining buffer (HBSS with 5% FCS) supplemented with Brilliant Stain Buffer. Following

incubation for 30 minutes at 4 °C, cells were washed once in cell staining buffer and if needed, cells were stained with 50 uL of secondary antibody as per the primary stain. For intracellular staining, cells were fixed and permeabilised with the Foxp3/Transcription Factor Staining Buffer Set (eBioscience) according to manufacturer's instructions, with 150 uL of permeabilisation reagent added to each plate well and incubated for 30 minutes at 4 °C. Cells were washed with 1x permeabilisation buffer and then 50 uL of intracellular antibody cocktail added. Cells were stained for 30 minutes at 4 °C and then washed with permeabilisation buffer. Fixation was then performed using 100 uL of 2% paraformaldehyde (Merck) and washed with cell staining buffer prior to acquisition on a BD LSR II, Fortessa X20 or X50 (BD Biosciences). Data was analysed using FlowJo v10.7.1 (BD Biosciences) and exported for statistical analysis in R.

## 2.7 General statistical analysis

Statistical analysis and plotting was performed in R v4.1 using baseR, rstatix or ggpubr for comparisons of two groups and correlation analysis, and lme4 lmerTest for linear effect models. Fisher's exact tests in baseR were used for enrichment analysis. Treg eQTL associations were performed using Pearson's correlations. Survival analysis was performed using the survival and survminer packages. ggplot2, UpSetR[301], networkD3, circlize[302], corrr and ComplexHeatmap[303] were used for visualization. For all data, *p<0.05, **p<0.01, ***p<0.001, and ****p<0.0001. Images were created using BioRender and Microsoft Powerpoint.

# Chapter 3

# $CD8^+$ T cell transcriptomic responses to ICB

## 3.1 Summary and Aims

$CD8^+$ T cells are key mediators of anti-tumour responses and have generally been pinpointed as the cell type reinvigorated by ICB given their high expression of PD-1. The pre-treatment presence of intra-tumoural $CD8^+$ T cells has previously been identified as a marker of successful ICB response, and many therapies designed to augment the effect of ICB primarily target markers expressed by exhausted or naive $CD8^+$ T cells. However, despite ICB proving successful in the clinic for MM and other cancer indications, its precise function and effect on T cells is largely still not understood. Few studies have examined $CD8^+$ T cells both before and after ICB, whilst those that have typically only focus on TILs and/or inadequately integrate transcriptomic and clonal information.

In this chapter, I will investigate how ICB modulates $CD8^+$ T cells transcriptomically and phenotypically through bulk and single-cell RNAseq and flow cytometry across paired pre-treatment and on-treatment samples collected at day 21 of treatment (d21). I have focused on the peripheral $CD8^+$ T cell response to ICB given its importance in supplying new T cells to tumour sites, and its relative ease of sampling which allows us to study larger patient cohorts. The specific aims I will cover are the following:

- What are the genes and pathways modulated by ICB in $CD8^+$ T cells?
- Are there correlations and overlap between these genes and pathways?
- What biological processes does ICB binding induce in $CD8^+$ T cells?

- What is the phenotype and distribution of peripheral $CD8^+$ T cell subsets in MM patients?
- Which subsets are the most clonally expanded and persist over ICB?
- How does ICB reinvigorate T cells on a clonal or transcriptomic basis?
- Which $CD8^+$ T cell subsets are the most sensitive to ICB?

## 3.2 Bulk RNAseq-based characterisation of the $CD8^+$ T cell response

To examine the $CD8^+$ T cell response to ICB, PBMCs from MM patients receiving sICB or cICB were isolated and the $CD8^+$ fraction was collected using magnetic cell sorting and subjected to bulk RNAseq. Paired pre-treatment and d21 on-treatment samples were collected from n=150 patients immediately prior to their first and second cycle of treatment respectively (C1 and C2). Differential expression (DE) analysis was performed using DESeq2, treating individual as a regressed pairwise variable. When comparing the differentially expressed genes (DEGs) modulated by sICB and cICB, I found that the majority of those altered during sICB also had differential expression following cICB (Figure 3.1a). Similarly, comparing the GOBP pathways enriched in each DEG geneset showed substantial overlap. The direction of effect across both treatment types was largely comparable, including for the most upregulated genes in both sICB and cICB (Figure 3.1b). This indicates both treatment types have similar transcriptomic effects in $CD8^+$ T cell, but to differing magnitudes.

I then examined the shared patterns of DE modulated by treatment. Firstly, I calculated gene expression deltas between C1 and C2 for each individual and performed heatmap clustering to examine DE similiarity between genes (Figure 3.1c). Upon visualisation of the gene-wise correlations, I found four clusters of genes with groups 1 & 2 (orange and yellow) being generally anti-correlated with groups 3 & 4 (blue and green). To understand the relevant biological processes that drive each module, I used GOBP enrichment analysis, demonstrating that groups 1 & 2 were comprised of genes related to cell division, amino acid metabolism, antigen presentation and glucose transport, whilst groups 3 & 4 involved pathways such as DNA-based transcription and protein targeting to membrane pathways (Figure 3.1d). When examining the fold changes of genes involved in groups 3 & 4, I found the majority were down-regulated by treatment, suggesting these pathways are suppressed at C2, whilst groups 1 & 2 are induced. Interestingly, when I looked at pro-inflammatory pathways canonically associated with immune stimulation, these were enriched in group 1 which seemingly

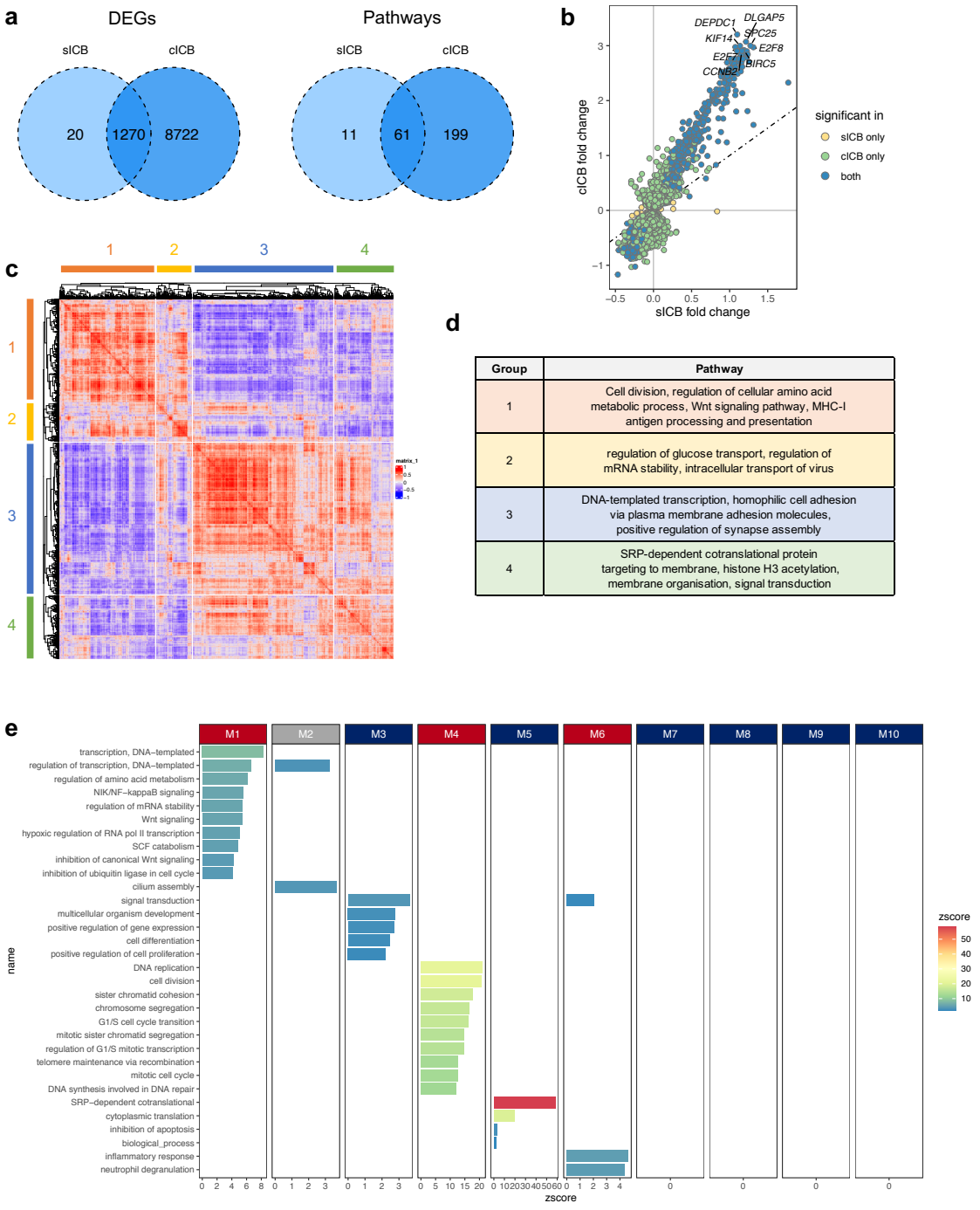



**Figure 3.1 Bulk RNAseq analysis of DEGs and pathways modulated by ICB. (a)** Venn diagrams comparing the DEGs (adjusted p value <0.05) and enriched GOBP pathways that sICB and cICB modulate in peripheral $CD8^+$ T cells. DEGs and pathway enrichment was called significant if adjusted p-value <0.05. **(b)** Dotplot comparing DEG fold changes following sICB vs cICB. **(c)** Delta values for significant DEGs were calculated across n=150 individuals based on normalised gene expression at C1 and C2. These values were used for a gene-gene co-correlation heatmap resulting in four distinct clusters of DEGs. **(d)** GOBP pathway enrichment was performed on each of the DEG clusters in (c), with the top most enriched pathways for each group shown. **(e)** Weighted gene correlation network analysis was performed using C1 and C2 DEG expression. The top five pathways enriched in each module are depicted. The colour of each facet represents whether the module score was significantly increased (red), decreased (blue) or unchanged (grey) from C1 to C2.

suggested T cell mitosis and immune responses are interlinked. To further dissect these broad modules and test whether mitosis and immune responses could be disentangled, I performed weighted gene co-expression network analysis (WGCNA) which uses a more comprehensive network and hub approach to define independently correlated groups of genes. Ten modules of genes were identified with M7-M10 consisting of very few numbers of genes (Figure 3.1e). I looked at module scoring to determine directionality of each module, finding three modules with significantly increased score following ICB; M1 contained genes associated with NF-$\varkappa$B signalling and Wnt signalling, with these pathways also being found in the upregulated pathways of Group 1 in the previous co-correlation heatmap. DNA-templated transcription was also enriched in M1 in the WGCNA analysis whilst being downregulated in Group 3 from the heatmap, suggesting a more granular understanding for this pathway is required. Module M4 was an additional module significantly induced by treatment and had a strong enrichment for cell division-related genes. Finally, inflammatory response was enriched in a separate module, M6, suggesting these are all possibly distinct facets of the immune awakening that ICB imparts.

Given many of the top DEGs and the most enriched pathways in ICB are related to mitotic responses, I wanted to further characterise this observation, and what other pathways mitosis correlates with. Using gene expression of the nuclear antigen *MKI67* as a proxy, I examined whether the increase in mitosis correlated with changes in eight selected signature genes representing T cell activation and cytotoxicity (*CTSW*, textitIFNG, *CXCL10*), as well as response to inflammatory cytokines (*JAK1*, *JAK2*, *STAT1*, *HLA-DRA*) and the type I interferon response (*MX1*). *MKI67* was significantly correlated with induction of *STAT1*, *IFNG* and *JAK2*, likely emblematic of autocrine signalling in association with T cell proliferation (Figure 3.2a). Intriguingly, *MX1* expression was not associated with increased mitotic activity, suggesting type I interferon production and signalling may be independently regulated or occur in disparate cell types or locations. Similarly, *CTSW*, encoding cathepsin W, was poorly correlated with *MKI67* and *IFNG*. To next examine global overlaps across these nine genes, I co-correlated the changes in each gene's expression after ICB and visualised the correlations using a heatmap (Figure 3.2b). This produced three groups of gene groups; one with *MKI67*, *IFNG* and STAT1, a moderately related group composed of *HLA-DR*, *JAK2* and *CXCL10*, and more distant group with *HLA-A*, *JAK1* and *CTSW*. These correlations were just between single genes, so to increase the robustness of these associations, I identified all genes associated with induction of the signature gene using a linear model. The results for *MKI67* are shown in Figure 3.2c as an example. As expected, the top-most correlated gene with *MKI67* was itself, followed by other canonical cell division-related genes such as *TOP2A*. Pathway enrichment

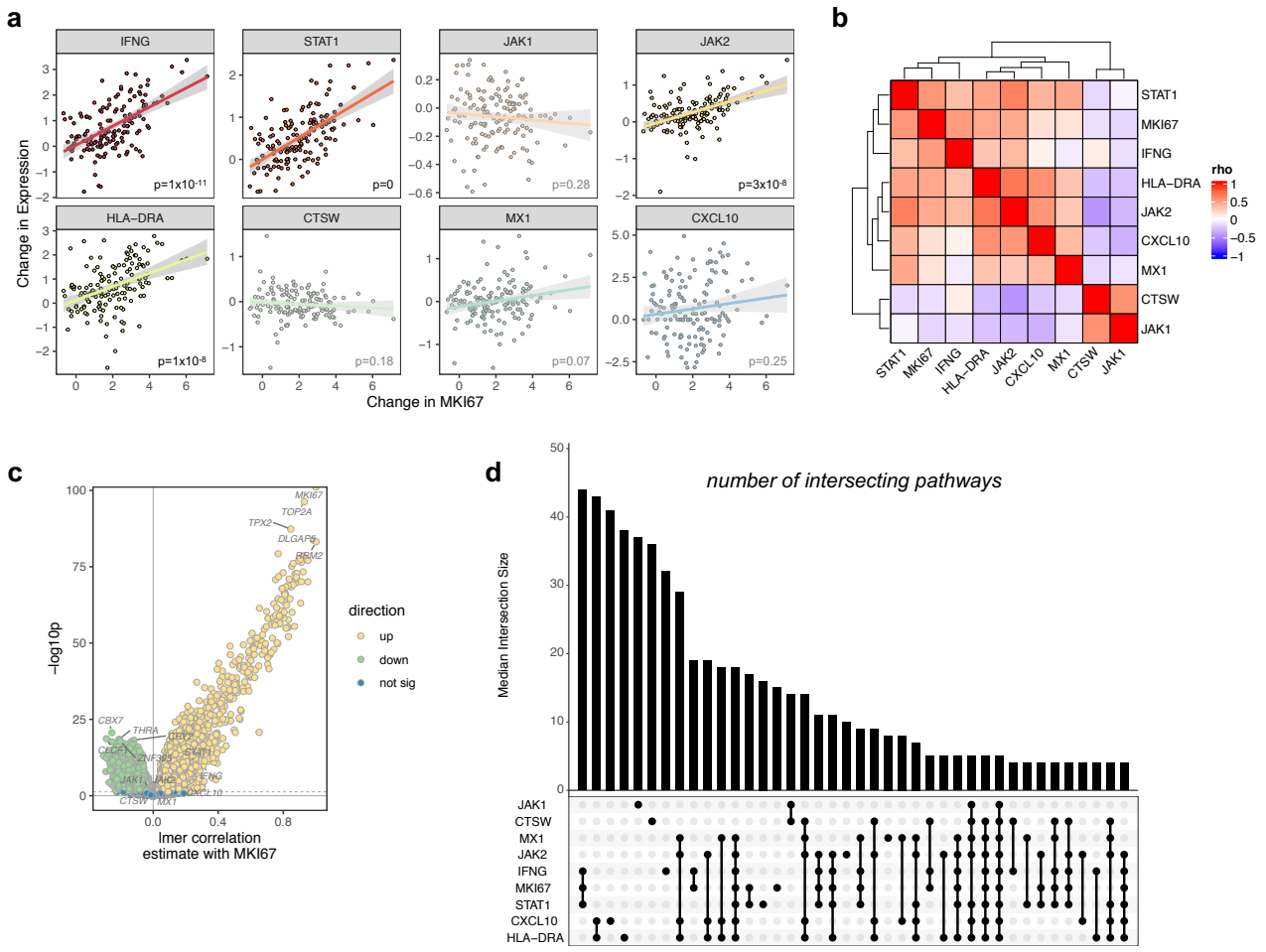



**Figure 3.2 Correlations between responses induced by ICB in CD8⁺ T cells. (a)** Correlations of expression deltas for *MKI67* and eight other selected signature genes between C1 and C2 (n=150, Spearman's rank test). **(b)** Correlation heatmap plotting Spearman's rho values using the deltas for the genes. **(c)** Volcano plot showing correlations with gene delta values and change in *MKI67*. Correlation estimates were generated using a linear model regressing age, sex and sequencing batch and significant genes having p value <0.05. **(d)** For each signature gene, GOBP pathway enrichment was performed on genes significantly correlated with its change in expression. The overlap in GOBP pathways was visualised using an Upset plot with the biggest intersecting sets positioned to the left of the plot.

across each analysis was then performed and I examined the overlapping pathways associated with each signature gene. Overlaps were visualised using an Upset plot[301], finding large similarity between *MKI67*, *IFNG* and *STAT1*-associated pathways, and *CXCL10* and *HLA-DRA* (Figure 3.2d). These results recapitulated the correlation heatmap between the single genes, demonstrating the validity of these previous associations. Overall, there seem to be several layers of T cell responses downstream of the mitosis induced by ICB, with two distinct groups of cytotoxicity represented by *IFNG* and *CTSW* respectively, which may potentially align with early and mature cytotoxic T cells.

To test whether these patterns of gene expression in patients were occurring directly downstream of ICB antibody binding on T cells, I stained PBMCs from n=106 patients, using an α-IgG4 antibody to detect pembrolizumab and nivolumab-bound cells. By flow cytometry, I found IgG4 was mostly restricted to T cells and was only observed at C2 as expected (Figure 3.3a). IgG4 staining masked PD-1 antibodies used for flow cytometry, explaining previous results in the lab showing PD-1 staining levels at C2 close to zero. The levels of IgG4 positivity was roughly in line with pre-treatment PD-1 staining (p=0.02, data not shown). Looking across the cohort, I saw significantly increased levels of IgG4 following both sICB and cICB, with higher IgG4 levels in cICB vs sICB-treated patients (Figure 3.3b), despite the higher dose of α-PD-1 used in monotherapy treatment compared to combination[32,34]. My flow cytometry panel also included intracellular Ki67 staining and I decided to see if its expression patterns matched that of IgG4. I saw a significant increase in $Ki67^+$ $CD8^+$ T cells following cICB to a similar order of magnitude to IgG4. To see broadly what DEGs are modified in association with IgG4, I performed correlation analysis between IgG4 measured by flow cytometry, and gene expression deltas from bulk RNAseq data in matching individuals. Two examples I pulled out were *MKI67* and *IFNG* which both showed a significant correlation even when factoring in treatment type as a covariate (Figure 3.3c). Globally, increased IgG4 was associated with an enrichment of genes associated with DNA replication, mitochondrial metabolism and cell cycle amongst many other pathways (Figure 3.3d). As a further characterisation, I performed dendrogram clustering on pathways that correlate with the signature genes I previously explored as well as those modulated by increased IgG4 flow binding. I found that pathways downstream of IgG4 correlated very strongly with those associated with *IFNG*, *MKI67* and *STAT1*, again suggesting these may be directly downstream of α-PD-1 signalling (Figure 3.3e). The other distinct groups were *CXCL10*, *HLA-DRA*, *MX1* and *JAK2*, and *CTSW* and *JAK2*, in accordance with the overlap analysis that was previously shown (Figure 3.2d). Given *MKI67* appeared to be directly downstream of IgG4 and both markers were present on the same flow panel, I was

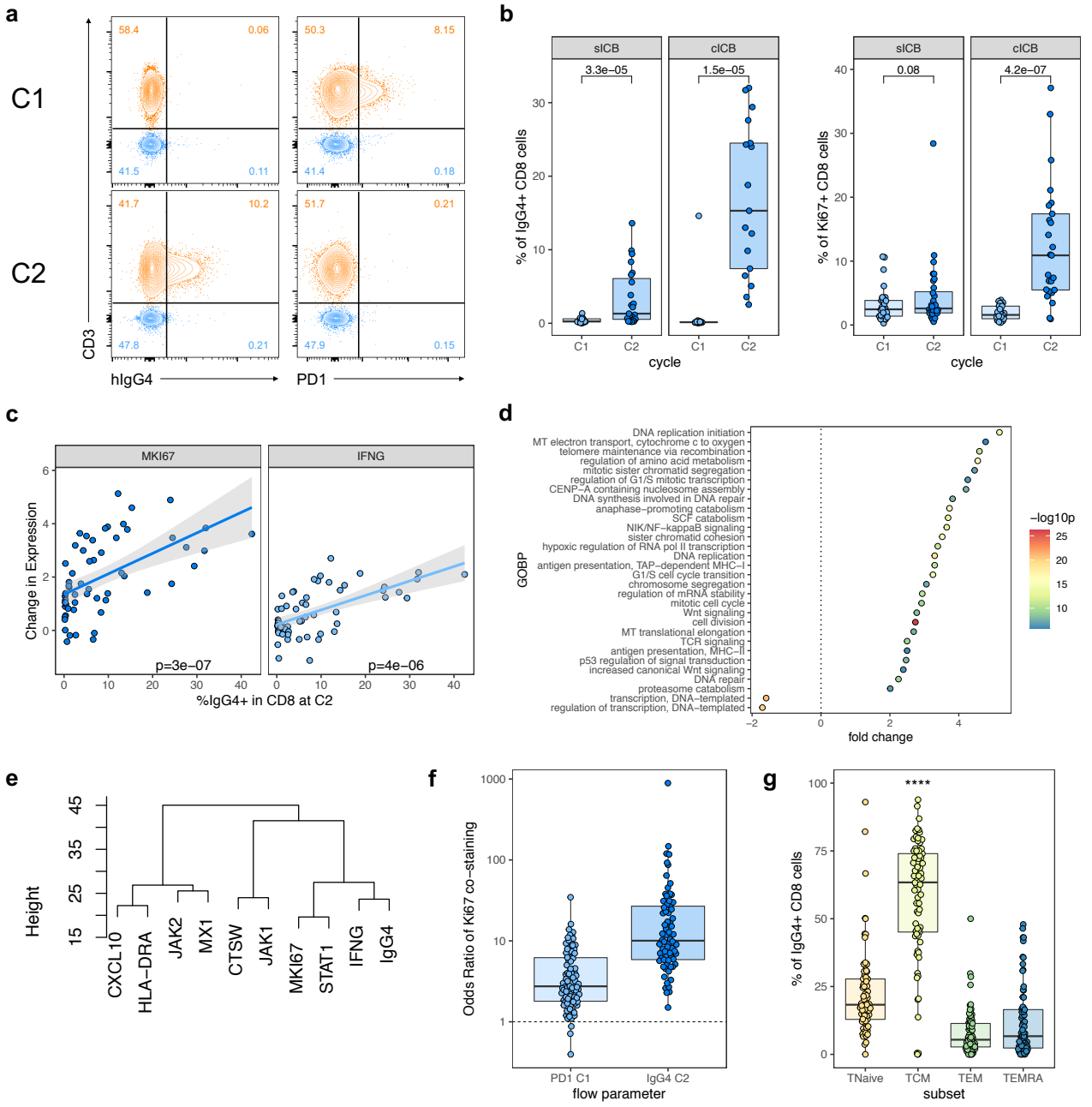



**Figure 3.3 Associations between IgG4 staining and CD8⁺ T cell responses to ICB. (a)** Representative flow cytometry plots of PD-1 and IgG4 staining in PBMCs at C1 and C2. **(b)** IgG4⁺ and Ki67⁺ cells are significantly increased following sICB and cICB (n=17-32, two-sided Wilcoxon signed-rank test). **(c)** Correlation between IgG4 staining by flow cytometry at C2 and changes in the expression of *MKI67* and *IFNG* by bulk RNAseq (n=57, Spearman's rank test). **(d)** GOBP pathway enrichment based on gene deltas that significantly correlate with levels of IgG4 staining at C2. Correlation estimates were generated using a linear model regressing age, sex and sequencing batch and significant genes having p value <0.05. **(e)** Dendrogram clustering using GOBP pathways associated with changes in eight signature genes and IgG4 staining at C2 to determine similarity in downstream signalling between these genesets. **(f)** Fisher's odds ratios of co-staining between PD-1 and Ki67 at C1, and IgG4 and Ki67 at C2 (n=93 and 73). **(g)** Subset proportions of IgG4⁺ CD8⁺ T cells (n=73, two-sided Wilcoxon signed-rank test with Bonferroni correction for multiple testing).

able to discern whether IgG4-bound CD8$^+$ T cells were also co-expressing Ki67 directly. I performed Fisher's exact tests to look at statistical overlap on a per-individual basis. Plotting the enrichment odds ratios across all individuals in this analysis, I saw that on average, IgG4$^+$ cells were 10.1 times more likely to also be Ki67$^+$ (Figure 3.3f). There was marked co-expression of Ki67 and PD-1 on the same cell at baseline albeit to a lesser degree, which potentially suggests that mitotic state encapsulates cells that have been chronically activated to a point near exhaustion. Lastly, I examined which CD8$^+$ T cell subsets carried the highest levels of IgG4 and Ki67 staining following ICB. Surprisingly, the central memory (CM) subset had the highest levels of peripheral IgG4 positivity, significantly higher than the more differentiated effector (Eff) and effector memory (EM) subsets (Figure 3.3g). A similar result was observed for Ki67 staining (data not shown). As such, rather than the canonical theory of more cytotoxic Eff CD8$^+$ T cells receiving direct 'reinvigoration' from ICB, it appears that $\alpha$-PD-1 predominantly binds and induces proliferation in CM cells, which may then interact with other cell subsets in a downstream manner. Characterising the proliferative response to ICB and disentangling it from cytotoxicity, given the low levels of cytotoxic and activation markers on CM cells by flow cytometry, was one of the rationales behind extending my analysis to the single-cell RNAseq level.

## 3.3 Single-cell RNAseq characterisation of the CD8$^+$ T cell response

### 3.3.1 Describing single-cell peripheral CD8$^+$ T cell subsets

I investigated the response of CD8$^+$ T cells to ICB using the 10X Chromium platform to perform single-cell RNAseq. 5' mRNA capture and targeted amplification of the TCR was employed to embed transcriptomic data with T cell clonality. PBMCs were isolated at C1 and C2 for 8 MM patients and the CD8$^+$ fraction sorted before droplet encapsulation and sample processing and sequencing. Following pre-processing of the returned data, 22445 live, singlet CD8$^+$ T cells were obtained, which clustered into 7 distinct subsets; Naive, CM, EM, Eff, Mitotic, gamma delta ($\gamma\delta$) and mucosal-associated invariant T cells (MAITs) based on an overclustering approach utilising SingleR[286] for label transfer (Figure 3.4a). The top most distinguishing markers for each subset were in line with expected genes, such as *CCR7* and *TCF7* for Naive cells, *LTB* and *IL7R* for CM, *GZMK* for EM, *GZMB/H* for Eff and *MKI67*, *TRDV2* and *KLRB1* for Mitotic cells, $\gamma\delta$s and MAITs respectively (Figure 3.4b). I further characterised each subset based on the expression of the previous signature genes used in the

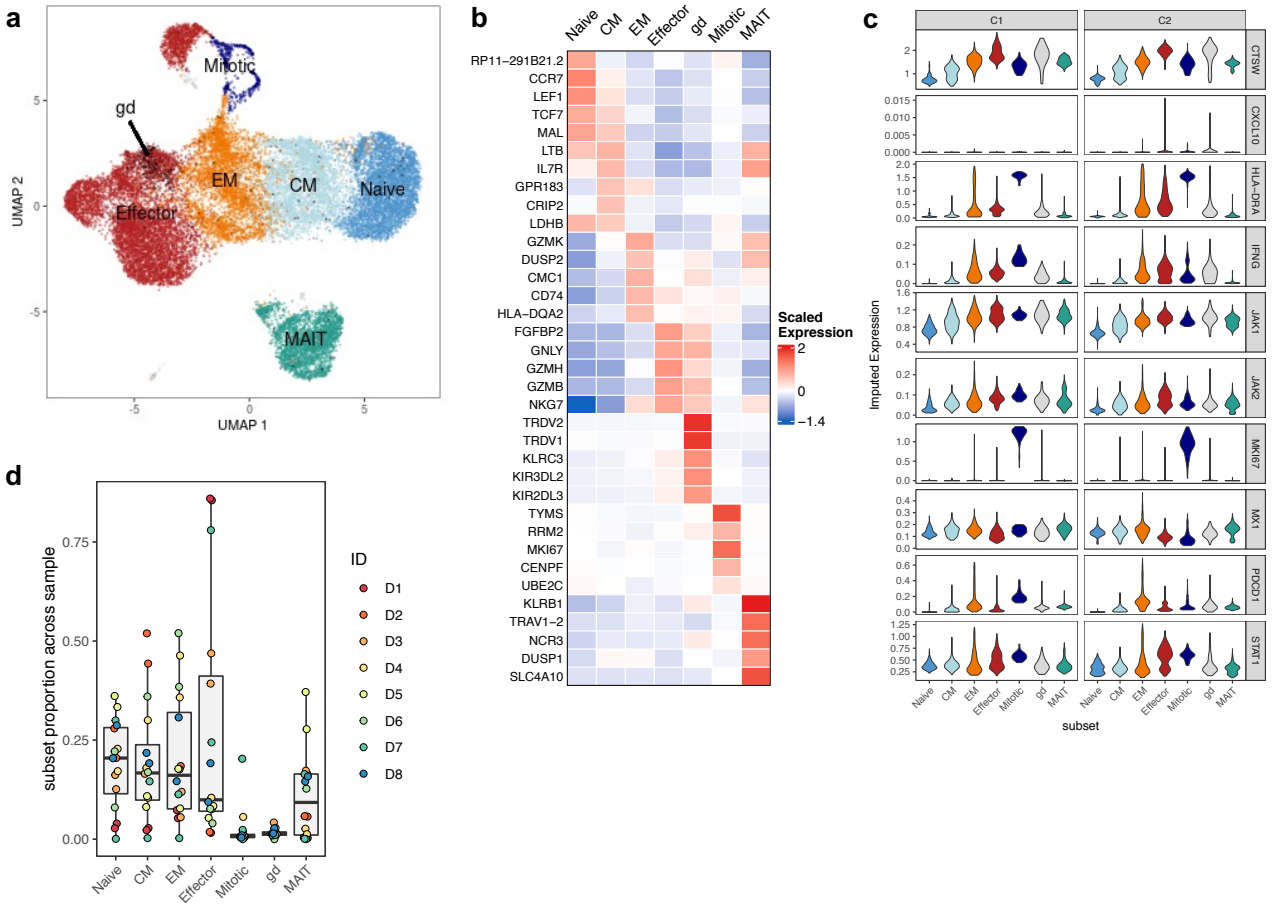



**Figure 3.4 Single-cell RNAseq of CD8⁺ T cells.** **(a)** UMAP clustering of n=22445 single CD8⁺ T cells from eight MM patients at C1 and C2. **(b)** Heatmap of top five most distinguishing genes per single-cell subset. **(c)** Expression of selected genes of interest across each single-cell subset at C1 and C2. **(d)** Subset proportion for each single-cell sample.

bulk analysis and *PD-1*. Mitotic cells were the primary subset expressing *MKI67* at both C1 and C2 and therefore represent the cycling cells that form the mitotic response. They had marked expression of *STAT1*, *HLA-DRA* and to a lesser extent, *IFNG* (Figure 3.4c), potentially explaining the strong correlations observed in the bulk data across these markers with mitosis (Figure 3.2a,d). Additionally, Mitotic cells had the highest median expression of *PDCD1* at C1 in accordance with the enrichment of PD-1 and Ki67 co-expression observed previously, but fell by C2 ostensibly due to α-PD-1 treatment. Looking at the expression of *CTSW* and also *IFNG* at C2, it seems that Eff cells are the main 'canonical' cytotoxic subset, followed by γδ cells. Across individuals, there were variable proportions of each subset but what I noticed was that individuals with predominance of one subset tended to have consistently high proportions of the same subset even after treatment (Figure 3.4d).

Given the slightly inconsistent patterns between *IFNG* and *CTSW* expression, I generated a cytotoxicity score for each individual cell based on the expression of 50 genes most-correlated with *IFNG*, including *NKG7* and *PRF1*. I found Eff had the highest median score value, suggesting that these are the key cytotoxic cells that potentiate immune responses, although mitotic cells had an intermediate score comparable to EMs (Figure 3.5a). To further characterise these subsets, I compared the GOBP pathways inferred from the significant DEGs across each subset. Processes associated with transcription and RNA processing were enriched in Naive cells and to a lesser extent, CMs, whilst EMs and Effs were enriched for pro-inflammatory and immune pathways (Figure 3.5b). Aside from cell division, Mitotic cells also had higher expression of genes relating to mitochondrial metabolism such as respiratory chain and electron transport.

Finally, to examine peripheral exhaustion, I looked at the expression of canonical exhaustion markers such as *TOX*, *ENTPD1* and *HAVCR2*. I found higher mean expression of exhaustion-related genes on EM cells at both timepoints whilst Mitotic, Eff and γδ subsets had intermediate to low expression, and negligible expression was observed on Naive and CM cells (Figure 3.5c-d). Focusing in on *PDCD1* expression, I found that EM and Mitotic subsets were significantly enriched for cells with >0 expression (Figure 3.5e). This link between *PDCD1* and Mitotic cells may relate to chronic antigen stimulation required to drive such a strong proliferative response but the rationale behind why EM cells are the most exhausted subset peripherally remains less well understood. EM cells have higher expression of *CD74* and *KLRD1* which have previously been defined as markers of 'circulating TILs'[138] and may therefore represent exhausted T cells from the tumour microenvironment that have subsequently egressed into the circulation, given they also tend to have more CD103 expression transcriptomically and by flow cytometry (data not shown).

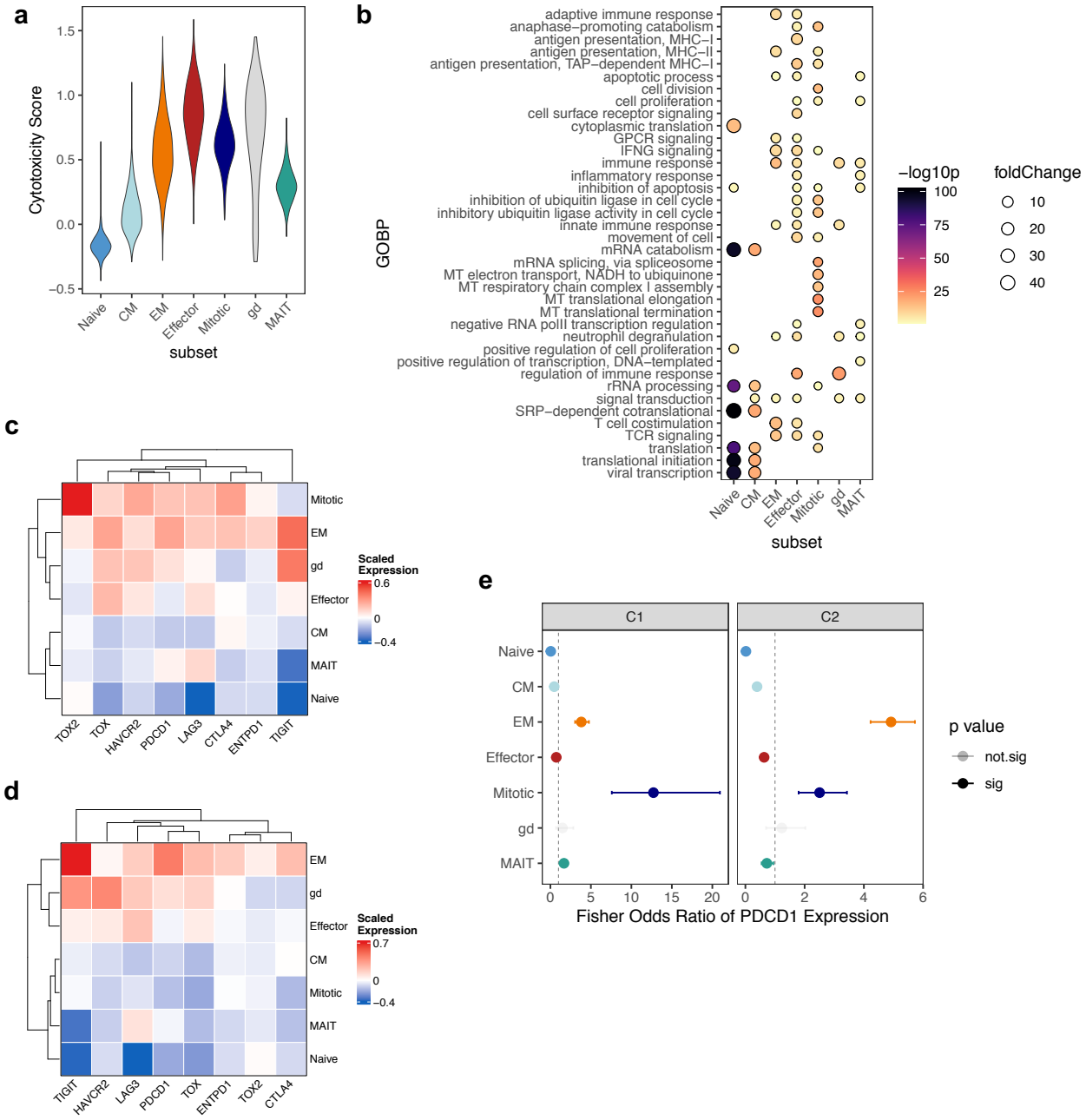



**Figure 3.5 Expression and pathway characterisation of CD8⁺ T cell subsets.** **(a)** Cytotoxicity scores generated from the expression of the top 50 genes correlating with *IFNG* across each single-cell subset. **(b)** GOBP pathways enriched for expression in each subset. The genes that are significantly distinct across each subset, identified using *FindAllMarkers* in Seurat were subjected to GOBP pathway enrichment analysis and significantly enriched pathways plotted. **(c-d)** Expression of selected exhaustion markers across subsets at C1 (c) and C2 (d). **(e)** Subset enrichment for *PDCD1*⁺ cells based on Fisher's exact tests at C1 and C2.

### 3.3.2 Describing the clonal dynamics of CD8⁺ T cell subsets following ICB at single-cell resolution

I next explored the interplay of T cell clonality data obtained from VDJ sequencing and the cell subsets described previously. Clonal expansion of $CD8^+$ T cells is canonically associated with antigen stimulation and in the context of ICB, has been linked to improved outcomes and parallel intratumoural T cell infiltration and expansion[135,147]. To identify expanded T cell clones in this data, I downsampled cells from each sample to 300 cells and defined clones based on identical variable and joining chains and CDR3 sequence, with those comprised of >1 member being defined as expanded. When I compared the mean clone size per individual across each subset, I found that there was a stepwise increase from the least differentiated Naive subset, which were uniformly singleton clones, through to CM and EM, and then Effs which represent the most clonally expanded subset (Figure 3.6a). Interestingly, despite their robust expression of division and proliferation markers, Mitotic cells tended to have low clonal expansion, with the majority of clones appearing to be singletons across both timepoints, indicating they may derive from naive cells. I also assessed the proportion of cells in each subset that belonged to an expanded clonotype, demonstrating similar findings of clonally expanded Effs and non-expanded Mitotic cells (Figure 3.6b). Relating this to the group's previous descriptions of the clinical importance of 'large' clones, namely those that occupy >0.5% of the TCR repertoire, I observed that the majority of large clones had an Eff phenotype at C1 and either an Eff/EM phenotype at C2 (Figure 3.6c). This suggested that following ICB, there is an emergence of clonally expanded cells with an EM phenotype.

I then wanted to trace clones between C1 and C2 across each individual. When I plotted the proportion of the repertoire occupied by each clone at C1 and C2, coloured by the predominant subset phenotype of the clone members at C1, there was relative stability in size of many large clones although a notable amount of inter-individual heterogeneity was observed that could not be directly linked back to treatment type, age, sex or other covariates (Figure 3.6d). To examine whether any subsets were more likely to comprise persistent clones, namely those found at both C1 and C2, I performed Fisher's exact tests for the number of cells at C2 in each subset with a matching C1 clonotype. I found that invariant T cells (MAITs and γδs) had the highest clonal persistance, likely due to the reduced repertoire combinations for these cells (Figure 3.6e). Of the remaining cell types, persistent cells were significantly over-represented in EM and Eff cells whilst Naive and surprisingly, Mitotic cells were significantly under-represented. This indicated that Mitotic cells at C1 tend not to persistent through treatment and their C2 counterparts represent *de novo* clones not derived

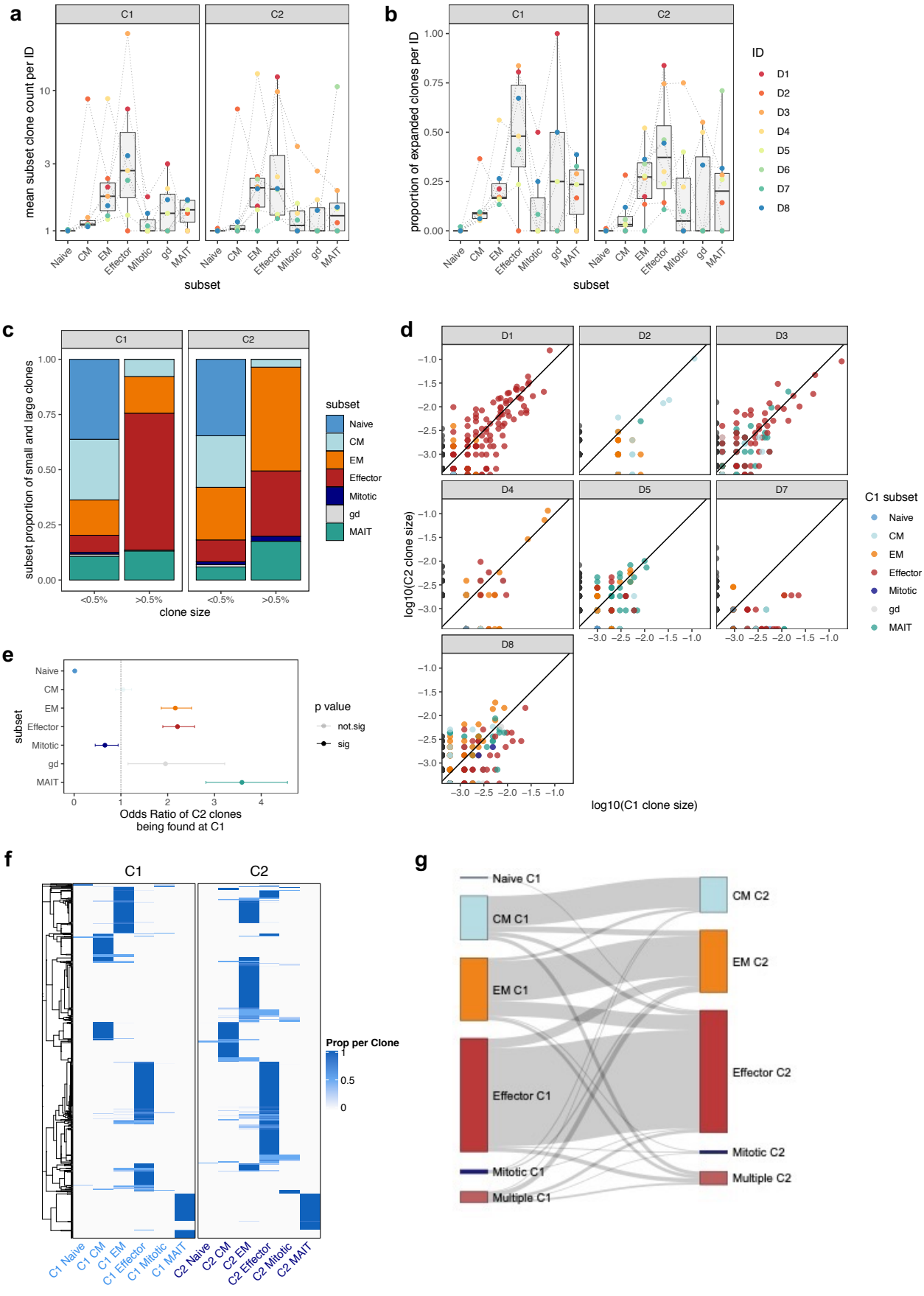

a
C1
C2
mean subset clone count per ID
subset
Naive
CM
EM
Effector
Mitotic
gd
MAIT
b
proportion of expanded clones per ID
ID
D1
D2
D3
D4
D5
D6
D7
D8
c
subset proportion of small and large clones
clone size
<0.5%
>0.5%
d
log10(C2 clone size)
log10(C1 clone size)
C1 subset
e
Odds Ratio of C2 clones being found at C1
p value
not.sig
sig
f
Prop per Clone
C1 Naive
C1 CM
C1 EM
C1 Effector
C1 Mitotic
C1 MAIT
C2 Naive
C2 CM
C2 EM
C2 Effector
C2 Mitotic
C2 MAIT
g
Naive C1
CM C1
EM C1
Effector C1
Mitotic C1
Multiple C1
CM C2
EM C2
Effector C2
Mitotic C2
Multiple C2

**Figure 3.6 Clonal characteristics and dynamics of CD8⁺ T cell subsets during ICB. (a-b)** Subsamples of 300 cells per individual at C1 and C2 were generated and the size of each T cell clone was calculated. The mean clone size of cells (a) and proportion of cells belonging to a clone with >1 member (b) in each subset was plotted per sample. **(c)** Subset proportion of small and large clones (those occupying less or more than 0.5% of the TCR repertoire) at C1 and C2. **(d)** C1 and C2 size of each clone per individual coloured by their C1 subset phenotype. **(e)** Fisher's exact tests were performed per subset to assess the number of persistent clones defined as clonotypes present at both C1 and C2. **(f)** Heatmap of subset proportion at C1 and C2 for all clones in the single-cell dataset. **(g)** Sankey plot tracing the predominant subset phenotype at C1 and C2 for clones present at both timepoints.

from pre-treatment T cells. More globally, examining the subset distribution of all clonotypes across C1 and C2 showed that a large proportion of EM, Eff and MAIT cells were not only found at both timepoints, but also maintained the same phenotype across ICB (Figure 3.6f). A considerable proportion of CM clones found at C1 were undetectable at C2, possibly having been not re-sampled due to their small clonal size. In line with previous observations, there was marked emergence of EM cells at C2 with a similar but less prominent effect for Effs and CMs. To confirm and visualise this surprising observation of largely maintained subset phenotypes despite treatment with ICB and the passage of 28 days between sampling, I selected the clones found at both C1 and C2. I examined the subset flux of clones across ICB, again based on the predominant subset composition for that clone at each timepoint (Figure 3.6g). I recapitulated these prior results, identifying that the majority of Eff clones at C1 remain the same subset at C2 with comparable but slightly subdued degrees of stability for CM and EM clones across treatment.

Although this description of 'stable' Eff cells is relatively novel in cancer and immunotherapy, I was able to find observations of an analogous 'long-lived effector cell' (LLEC) population that emerge in later stages of chronic viral infections, made by Sara Hamilton's group[304] during lymphocytic choriomeningitis virus infection. These cells peaked at 90 days after initial challenge and were defined by high expression of KLRG1, low expression of CD27, and increased expression of CX3CR1, T-bet and EOMES. They also appeared to undergo homeostatic proliferation rather than rapid antigen-induced expansion. To explore whether this precise phenotype matched the stable Eff phenotype detected in our patients, I imputed the expression of KLRG1 and CD27 in the single-cell data using MAGIC[299] to recover technical drop-outs. I used a cutoff of 1.15 for the ratio of *KLRG1*:*CD27* expression to call cells LLECs vs non-LLECs, determined to be the local minimum value of the bimodally distributed ratio values (Figure 3.7a). I then examined the expression of the additional markers (*CX3CR1*, *TBX21* encoding T-bet and *EOMES*) used to describe LLECs, finding that these were enriched on the LLEC population compared to the non-LLECs (Figure 3.7b). In keeping with an

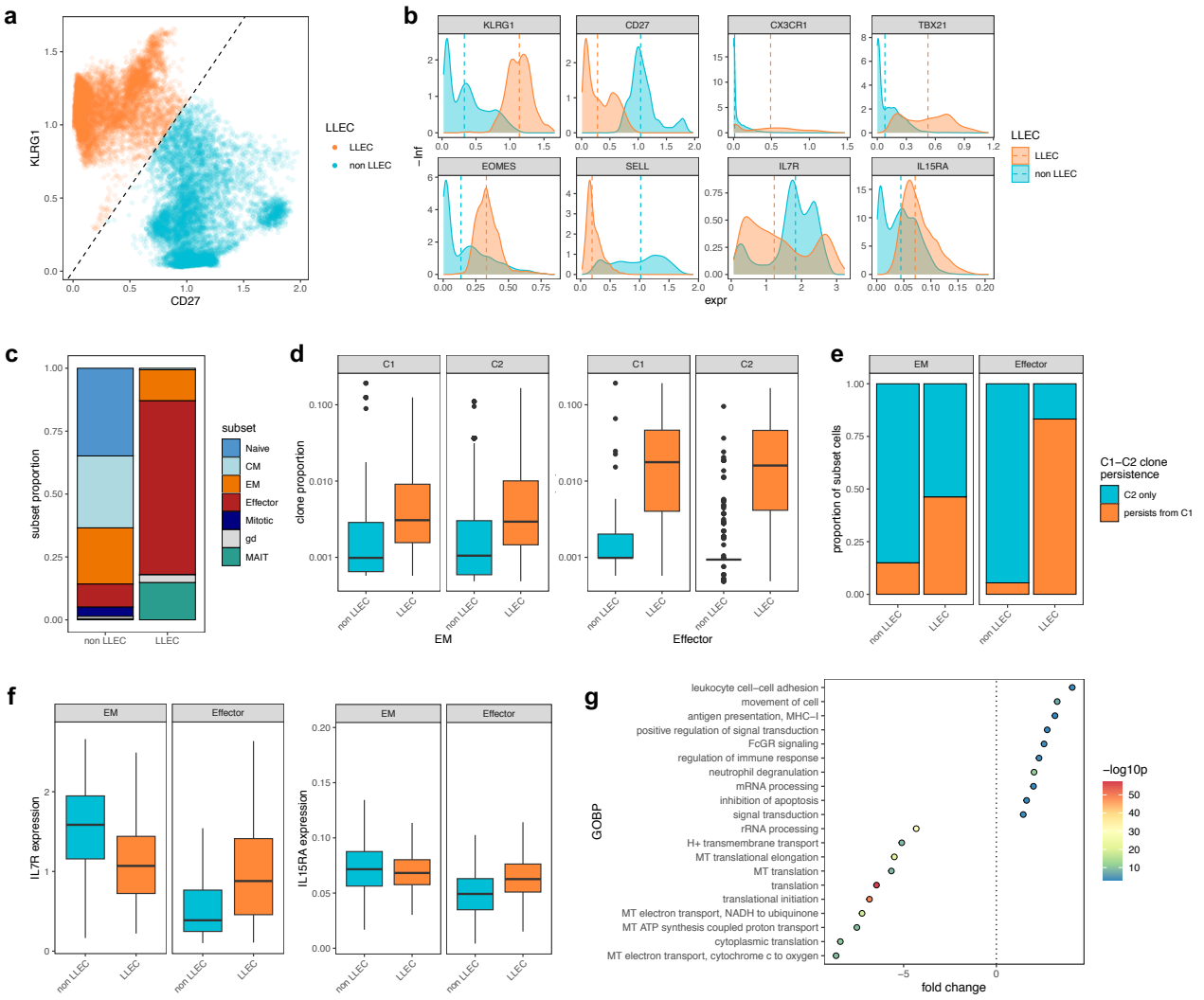



**Figure 3.7 Characterisation of long-lived effector cells. (a)** Gating strategy for defining long-lived effector cells (LLECs) and non-LLEC populations based on KLRG1 and CD27 expression. **(b)** Expression of additional supporting markers on LLECs and non-LLECs. **(c)** Subset proportion of LLEC and non-LLEC. **(d)** Clone size as a proportion of the TCR repertoire for LLEC and non-LLECs within EM (left) and Eff (right). **(e)** Proportion of persistent clones in LLEC and non-LLEC in EM and Eff. **(f)** Expression of *IL7R* and *IL15RA* in EM and Eff LLEC and non-LLEC. **(g)** GOBP pathways enriched in Eff LLECs relative to Eff non-LLECs based on differential gene expression using *FindAllMarkers*.

increased homeostatic proliferation potential, I observed LLECs had intermediate expression of *IL7R* and increased expression of *IL15RA*, which are receptors for the homeostatic cytokines IL-7 and IL-15 respectively. Altogether, it appears that the LLEC phenotype can also be observed within cancer patients and is preserved across immunotherapy, with relatively stable LLEC proportions also found across C1 and C2 (data not shown). In terms of subset phenotype, LLECs were mainly effectors as expected (Figure 3.7c), with minor contribution from EM and MAIT cells, and were also more clonally expanded than their non-LLEC counterparts even when comparing within the same subset (Figure 3.7d). The majority of LLEC clones did not significantly change in size between C1 and C2 (data not shown) and had significantly greater likelihood of persisting across treatment than their non-LLEC counterparts (Figure 3.7e). Interestingly, when I examined expression of *IL7R* and *IL15RA*, LLEC Effs had significantly higher expression of both markers compared to non-LLEC Effs, whilst this pattern was not observed in EMs (Figure 3.7f). This suggests that LLEC Effs may be particularly adept at maintaining their clonally expanded size through homeostatic proliferation, and provides a hypothesis as to why these cells are expanded, persistent and phenotypically stable, even despite low expression of *MKI67* and other genes involved in cell division. To further characterise the pathways that demarcate LLEC and non-LLEC Effs, I performed differential gene expression analysis and pathway enrichment across these two populations. LLEC Effs had an enrichment of pathways associated with class I MHC antigen presentation and inhibited apoptosis, whilst the non-LLEC counterparts had markedly greater mitochondrial-related metabolism (Figure 3.7g). Although metabolic pathways in T cell subsets and activation are incompletely understood, mitochondria-associated oxidative phosphorylation and the citric acid cycle are traditional pathways through which naive and memory T cells maintain their cellular energy stores, and dysregulation of this process can lead to cellular exhaustion[100]. Effector cells however are often attributed alternative bio-energetic sources such as cholesterol metabolism and glycolysis[305] and the maintenance of the cellular machinery for sustained effector function likely requires metabolic reshuffling away from mitochondrial activity.

As a point of comparison to this stable Eff phenotype, I also analysed the clonal features of mitotic cells. I previously demonstrated that the majority of Mitotic cells were unexpanded and recapitulated this by correlating clone size and *MKI67* expression across all cells at C2 (Figure 3.8a). This produced a negative association between the two, again underscoring that higher proliferation does not necessarily generate large expanded T cells. Looking at the clone size distribution of Mitotic cells, I found the majority were singleton whilst a small number belonged to clonotypes with 4+ members (Figure 3.8b). Conversely however,

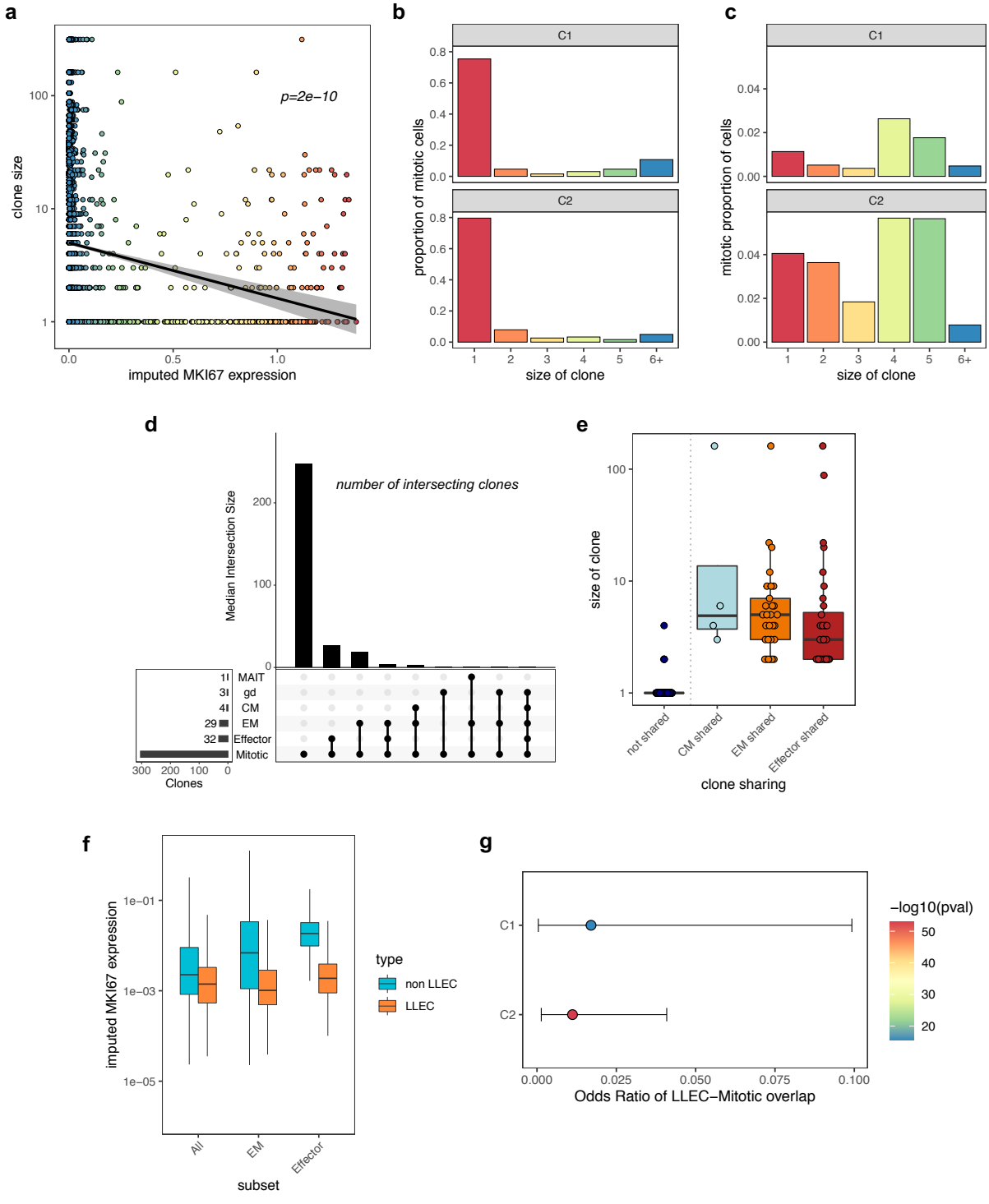



**Figure 3.8 Characterisation of the mitotic response at a clonal level.** **(a)** Correlation of clone size and *MKI67* expression imputed using MAGIC at C2 (n=7873 cells, Spearman's rank test). **(b)** Clonal size distribution of mitotic cells at C1 and C2. **(c)** Proportion of cells in the Mitotic subset for clones of varying size. **(d)** Upset plot showing clonal overlap between Mitotic cells and other cell subsets at C2. **(e)** Clonal size for cells in the Mitotic subset grouped by clonal sharing with other subsets. **(f)** Expression of *MKI67* across LLEC and non LLEC populations in all cells, or just EM or Eff subsets. **(g)** Odds ratios from Fisher's exact tests examining the overlap between LLECs and Mitotic cells.

expanded clones did have a similar proportion of Mitotic members to non-expanded clones suggesting active proliferation does contribute to select clonal expansion events (Figure 3.8c). When I looked at clonotype sharing between Mitotic cells and other subsets at C2, the majority of clones were unique to the Mitotic subset, no surprise given their singleton status, but there was some sharing with Eff and EM (Figure 3.8d). Examining the size of clones based on their sharing status, I found there was limited clonal expansion of just Mitotic cells, whilst those shared with CM and EM cells in particular accounted for the expanded Mitotic clones identified earlier (Figure 3.8e). This is in concordance with my flow cytometry data showing the highest Ki67 staining in CM $CD8^+$ T cells, and suggests mitosis does contribute to expansion of some CM and EM cells. To understand whether this also extends to LLECs, I compared the *MKI67* expression of LLEC and non-LLECs both across all cells and just EMs and Effs (Figure 3.8f). LLECs had consistently lower expression of *MKI67* despite being characteristically more clonally expanded. Examining the overlap between LLECs and Mitotic cells once more, I found there was extremely low overlap between these two groups (Figure 3.8g). Overall, it appears that the Mitotic response during ICB may not contribute to $CD8^+$ T cell effector stability, nor the clonal expansion posited to be clinically beneficial and related to anti-tumour reactivity.

### 3.3.3 Assessing $CD8^+$ T cell subset changes during ICB

Finally, I wanted to describe the global effects ICB has on the $CD8^+$ T cell compartment - both in terms of changes in subset composition and gene expression within each subset. Initially, when examining subset proportions between C1 and C2 for the single-cell patients, I found a significant decrease in CM proportion following ICB (Figure 3.9a) although the data was most likely underpowered to detect most effects, such as the expected increase in Mitotic cell proportion reflecting my previous bulk and flow results. To circumvent this, I applied my single-cell subset descriptions to the bulk RNAseq cohort where there was much better statistical power, by generating subset scores per bulk sample. To do this, I identified the twenty most discriminating genes for each subset in the single cell data, with independent identification of genes across C1 and C2 to avoid biasing from post-ICB gene expression. Using the intersection of the genes from the two lists, I calculated the geometric mean of these subset 'signature' genesets to define a score. When looking to see what changed between C1 and C2, I identified drops in Naive and CM score accompanied by increases in EM and Mitotic score (Figure 3.9b), all of which mirror the trends found in the single-cell analysis. This increase in EM score is particularly interesting given how it mirrors the observed expansion of a small group of *de novo* EM clones. Effector score remained mostly

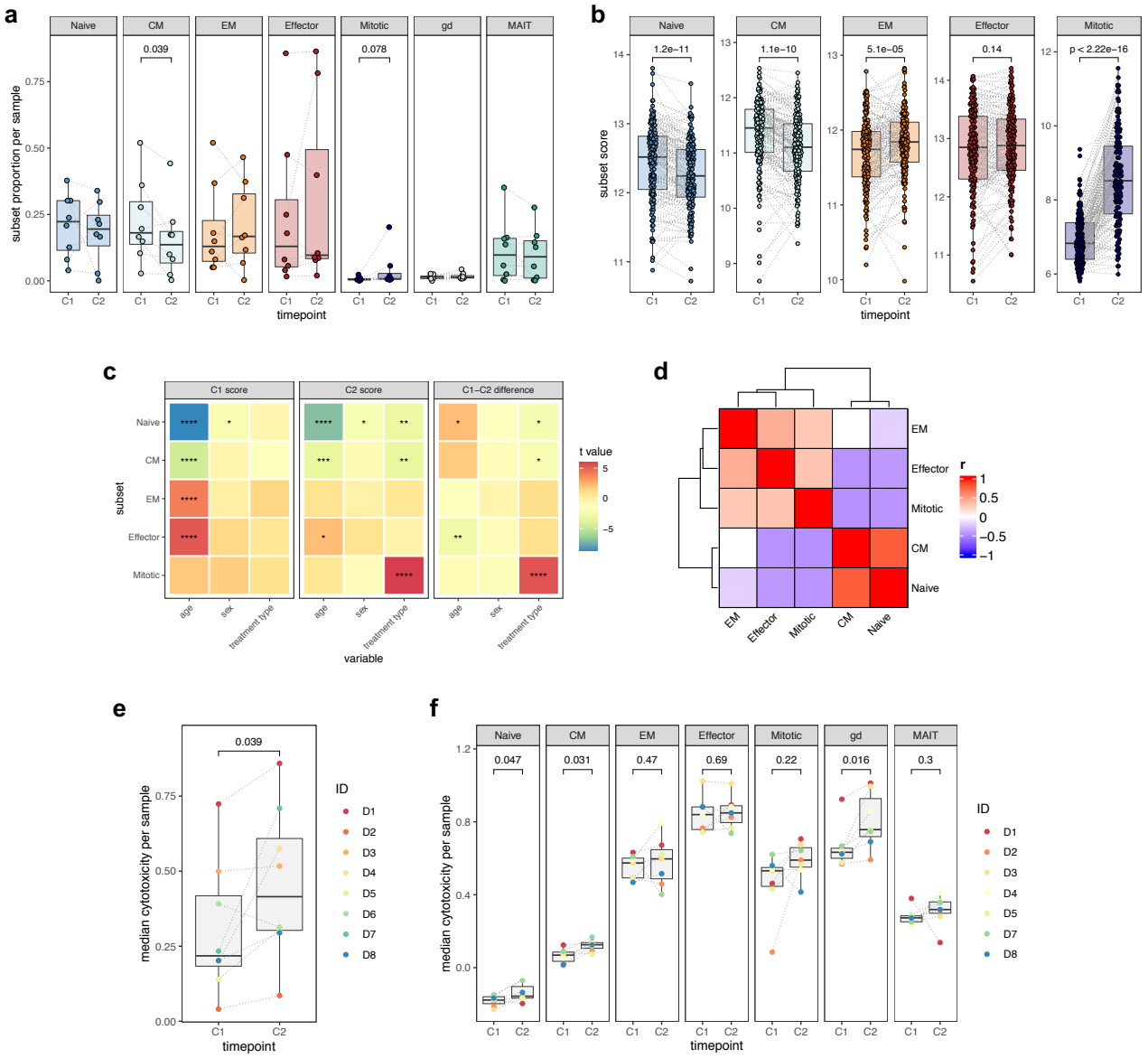



**Figure 3.9 Changes in CD8⁺ T cell subset proportion during ICB. (a)** Change in single-cell subset proportions per individual between C1 and C2 (n=8, two-sided Wilcoxon rank-test). **(b)** Change in subset scores calculated in CD8 bulk RNAseq samples between C1 and C2, based on geometric mean expression of top discriminating genes per subset identified by single-cell (n=150, two-sided Wilcoxon rank-test). **(c)** Linear model estimates for correlations between subset scores at C1, C2 and delta values, with clinical covariates (n=150). **(d)** Correlation heatmap of bulk RNAseq subset score, using the deltas between C1 and C2 scores (n=150, Pearson's correlation test). **(e)** Change in median cytotoxicity score per sample in single-cell data (n=8, two-sided Wilcoxon signed-rank test). **(f)** Change in median cytotoxicity score in each subset per sample in single-cell data (n=8, two-sided Wilcoxon signed-rank test).

constant between C1 and C2, again reflecting the relative stability of the Eff compartment. I next examined how these scores corresponded with various clinical variables through linear models, finding that patient age had a marked influence on C1 subset scores and to a lesser extent, C2 scores (Figure 3.9c). Both these associations occurred in the same direction where older individuals had low Naive and CM scores and higher Effector score, in line with the inflationary and repertoire narrowing effects of age and CMV. Looking at the change in subset scores during treatment, I found that older individuals were more likely to have increases in Naive scoring and decreases in Eff score, possibly showing a reduced propensity to respond immunologically to ICB. Treatment with cICB (Figure 3.9c, treatment type) was associated with a greater magnitude of change, namely greater increase in Mitotic score, and larger decreases in Naive and CM score. When co-correlating changes in subset score, I found that Naive and CM score tended to decrease in a paired fashion but had no strong correlations with EM, Effector or Mitotic score change (Figure 3.9d). As such, it was difficult to weigh whether the observed loss of Naive and CM cells is due to their transition into EM cells, which was observed to a small degree, or instead results from movement into other tissues, cell death, or disproportionate expansion of other subsets types such as EM. Collectively, these changes in subset composition are in line with the proposed stimulatory effect of ICB and overall stronger immune responses following treatment.

To follow this up, I examined whether the median cell cytotoxicity per sample was increased in the single-cell data after ICB. I found a significant increase in cytotoxicity across the single-cell patients, with 7 out of 8 individuals having increased cytotoxicity at C2 (Figure 3.9e). To explain this, I checked whether cytotoxicity was consistently increased across all cell types, or instead whether expansion of more cytotoxic subsets accounted for this increase. I found that median per-subset cytotoxicity was not generally changed across C1 to C2 with the exception of Naive, CM and γδ cells (Figure 3.9f), with Naive and CM cells having low starting cytotoxicity and falling in subset proportion following treatment . I inferred that cytotoxicity increases were principally driven by expansion and contraction of highly and weakly cytotoxic subsets respectively. Overall, this reflects that changes in $CD8^+$ T cell transcriptomes are likely driven by both within-subset and across subset changes.

To therefore examine within-subset changes from ICB more comprehensively, I performed DE analysis comparing C1 to C2 cells for the main four single-cell subsets, excluding Mitotic, γδ and MAIT cells due to their smaller subset size being prohibitive of sufficient power to detect DEGs. Since the number of cells affects the number of detected DEGs, I subsampled each subset 100 times before differential gene expression, performing subsampling analysis across increasing numbers of cells. Effs had consistently higher numbers of DEGs than EM, CM and

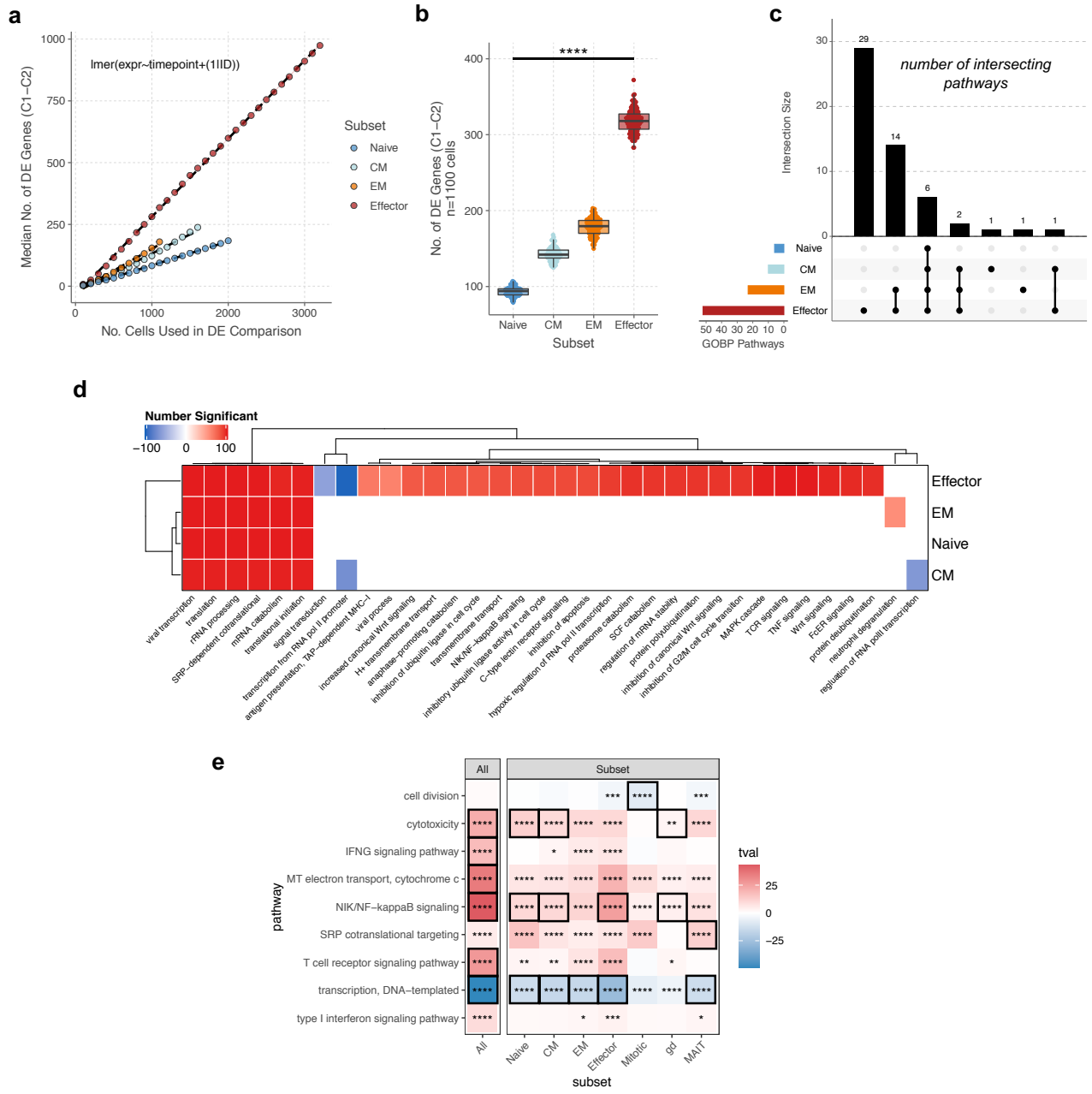



**Figure 3.10 Gene expression changes within CD8⁺ T cell subsets during ICB. (a)** Number of DEGs in each subset following ICB. Subsets were downsampled to the indicated numbers of cells at C1 and C2 and differential expression tested across 100 bootstraps using the indicated linear model. **(b)** Numbers of DEGs across each subset when using n=1100 cells for subsampling ($p<0.0001$, two-sided Wilcoxon signed-rank test). **(c)** Upset overlap plot for the number of significant pathways modulated by ICB in each subset using the differentially expressed genes obtained in (b). Only pathways modulated in >50 subsamples were included. **(d)** Heatmap of pathways modulated by ICB for each subset with shading representing how many subsamples the pathway was found to be significantly induced or suppressed in out of the total 100 subsamples. **(e)** T values for score changes of selected pathways between C1 and C2 in the single-cell data. Genes from each GOBP pathway were used to calculate per-pathway scores in each cell using *AddModuleScore* in Seurat. Linear models with individual as a fixed variable were constructed to see if the pathway score was significantly increased or not in that population. Boxes with bold outline were detected as significant using a more conservative two-sided Wilcoxon signed-rank test for score medians per sample.

Naive (Figure 3.10a), especially when comparing results from the maximum common number of cells used for subsampling across all subsets (Figure 3.10b). For subsequent analyses, I selected this subsample size of n=1100 cells. Assessing the pathways associated with these DEGs, I found that Eff cells demonstrated the largest number of DE pathways, many of which were uniquely induced relative to EM, CM and Naive cells, which instead seemed to upregulate common pathways (Figure 3.10c). This suggested that ICB has both a global effect on all cells, as well as a unique stimulatory activity on Effs. The pathways that were uniquely upregulated by ICB in Effs were consistently immune response-related, such as TCR signalling, MAPK cascade and TNF signalling (Figure 3.10d), suggesting these cells receive large functional benefit from treatment with ICB, and to a much greater extent than other $CD8^+$ T cell subsets.

I finally tried to account for expression changes in pathways that ICB modulates that were also identified in bulk RNAseq, using the single-cell data. I scored some of the most strongly modulated pathways by ICB across each single $CD8^+$ T cell, and then determined whether their within-subset expression increased following treatment (Figure 3.10e). For cell division, I found a significant decrease in pathway score in the Mitotic subset, indicating that the increased mitotic response detected transcriptomically stems purely from an expansion of the Mitotic subset rather than a per-cell increase in mitotic activity. The increase in IFN-$\gamma$ signalling and NF-$\kappa$B signalling responses from ICB is likely due to both upregulated signalling across certain cell types such as EM/Eff and also expansion of EM cells. For mitochondrial electron transport, higher bulk expression could be attributed to an expansion of Mitotic cells, which are enriched for mitochondrial-associated genes, as well as globally increased mitochondrial expression across all subsets. The SRP co-translational targeting to membrane pathway was increased in expression across all subsets which may compensate for the fall in Naive and CM cells that occurs with ICB, given these two subsets have maximal enrichment for this pathway. TCR and type I IFN signalling responses were also uniformly increased across all subsets. As such, there appears to be a dual effect of both within subset-expression increases as well as skewing towards the subsets with relative enrichment for these pathways. Overall, ICB has a varied pattern of effect on $CD8^+$ T cells at the subset level - being seen to induce more immune stimulation in each individual cell, in particular Eff cells, as well as shift the composition of T cells towards a more activated and differentiated state.

## 3.4 Conclusions and Discussion

I dissected the responses of peripheral CD8$^+$ T cells to ICB using bulk RNAseq to capture the breadth of responses across a large patient cohort and flow cytometry to measure these changes phenotypically, and integrated these results with the granularity of single-cell RNAseq. To summarise some of the results of this chapter:

- Mitotic responses are induced by ICB and correlate with increased antigen presentation and immune activation
- Mitotic responses specifically correlate with *IFNG* and *STAT1* responses, whilst *HLA-DR*, *CXCL10*, *JAK2*, *MX1*, and *CTSW*, *JAK1* form distinct expression groups that are induced distinctly as a possible paracrine secondary response
- ICB binding occurs principally on T cells and associates strongly with mitosis
- Single-cell RNAseq resolves seven subsets of CD8$^+$ T cells with Eff cells being the most cytotoxic, whilst Mitotic and EM cells are the most peripherally exhausted
- Eff CD8$^+$ T cells are the most clonally expanded at both C1 and C2 with remarkable subset stability, possibly in part due to a 'long-lived effector cell' phenotype whilst Mitotic responses tend to be transient and less clonally expanded
- ICB leads to a shift towards more EM responses and away from Naive and CM signatures with an overall increase in peripheral cytotoxicity
- Eff ICB has a uniquely stimulatory effect on CD8$^+$ T cells, but both changes in subset expression and composition contribute to its transcriptomic effects

By comparing C1 and C2 transcriptomes, I identified an increase in EM signatures following ICB, in line with emergence of a group of clonally expanded EM cells. This is consistent with other studies of the peripheral and intratumoural CD8$^+$ compartment upon checkpoint immunotherapy[105,143,306]which have also described memory and EM expansion. However, how this relates to the mitotic response identified at C2 is not entirely clear, given that the majority of Ki67$^+$ cells at C2 were of a CM phenotype by flow cytometry, and not clonally expanded. It may be that EM expansion occurs early on during ICB, such as in the initial seven days where mitosis purportedly peaks[307], whilst cells continuing to proliferate by C2 represent dysfunctional cells or off-target proliferation resulting from cytokine stimulation or reduced TCR signalling strength needed for activation. Future exploration of the TCR specificity of three main groups of cells; (a) Mitotic cells at d21, (b) expanded EM cells and (c) stable Eff cells, would be particularly interesting. This could be done through *in silico* TCR specificity predictions using algorithms such as TCRMatch[308] or GLIPH2[309], or through *in vitro* antigen specificity experimental pipelines[310–312]. Whether mitotic cells at C2 all target

similar or different antigens would help to gauge their relevance to immune response of ICB. Indeed, given that mitotic cells and EMs expressed some markers of T cell exhaustion and several papers suggest that exhausted cells are epigenetically locked out of activation and proliferation[108–111], their contribution to beneficial T cell states required for clinical responses is unclear. It could also be the case that low levels of mitosis, such as those stemming from homeostatic proliferation, do not push cells past an activation barrier that leads to exhaustion whilst the highly cycling fraction represented by Mitotic cells surpass this threshold. These different signal and proliferation strengths may relate to the binding strength of TCRs with their antigens and is another impetus behind performing detailed specificity characterisation.

Overall, I posit that EM expansion contributes to maintenance of large clone counts, which act as a biomarker for tumour reactivity, whilst Eff cells are a functional cell type that contribute to anti-tumour cytotoxicity, given their non-exhausted state, stable phenotype, metabolic features and unique induction of immune signalling pathways during ICB. Following up on the biological mechanisms through which this non-exhausted Eff phenotype is maintained across treatment would be particularly insightful and may provide a rationale for adjuvant design to complement ICB. Tracking these LLEC clones across longer periods of time, such as throughout a patient's two year regimen of ICB, would also be informative.

An interesting observation made was that there are higher rates of α-PD-1 binding in individuals treated with cICB vs sICB, despite there being at least three times more α-PD-1 given to sICB patients. Since α-PD-1 binding also reflects the levels of circulating PD-1 on T cells, it potentially suggests that there is a higher amount of T cell activation which may be potentiated by the presence of α-CTLA-4. It would be interesting to sort $CD8^+$ T cells based on whether they have IgG4 staining for downstream single-cell RNAseq, or to use IgG4 in a CITE-seq panel to discern the functional, subset and VDJ characteristics of this cell population. The higher levels of IgG4 staining with cICB also reflects the increased mitotic and overall transcriptomic activity seen in these patients, and provides a suggested mechanism behind this phenomenon; IgG4 binding leads to mitotic activity and *IFNG* and *STAT1* expression in T cells, which in turn stimulates a second group of immune events such as MHC expression, *JAK2* and chemokine expression, eventually culminating in upregulation of canonical cytotoxic molecules such as *CTSW* and *JAK1*. Due to increased activity at the top of this cascade, cICB may therefore lead to greater downstream signalling and transcriptomic change. Understanding the specific importance of α-PD-1 binding as well as the contribution of α-CTLA-4 in this process is important due to the emergence of additional checkpoint blocker drugs, and understanding how these blockade combinations function will inform future clinical strategies.

# Chapter 4

# Examining CD8$^+$ T cell heuristics associated with clinical response

## 4.1 Summary and Aims

Understanding the mechanisms behind ICB's therapeutic success in some patients, whilst not delivering clinical benefit for others, is a key question in the immunotherapy field. Many papers have tried to identify predictive markers of clinical response within the tumour, identifying factors such as CD8$^+$ T cell infiltration, PD-L1 positivity, tumour mutation burden. From a translational perspective, a simple blood-based biomarker would be much more desirable given easier sampling and routine blood tests already being embedded within hospital care. Recent work is also demonstrating the interconnectedness of peripheral and tumour immunity[135] meaning that blood biomarkers likely describe a direct contribution to intratumoural immune responses.

Here, I will describe and investigate peripheral markers of clinical response to ICB within CD8$^+$ T cells, starting with the group's observations around clonal expansion. For each marker, I will trace its transcriptomic and immunological associations to describe more central tenets of patient ICB response. These analyses will utilise results from bulk RNAseq, flow cytometry and clinical follow-up of MM patients during the course of their ICB treatment. The specific aims I will cover are:

- What are cohort-wide transcriptomic associations with CD8$^+$ T cell clonal expansion?
- Which subsets associate with clonal expansion across the cohort and can this be used as a clinical biomarker?

- Is it possible to translate these biological associations into a hospital-based heuristic of ICB response?
- What are the cellular and transcriptomic associations of this hospital biomarker?
- How does this marker associate with other clinical predictors of outcome such as autoimmune side-effects?
- Can our findings be used to identify a pre-treatment predictor of poor clinical response to ICB?

## 4.2 Clonal expansion of CD8$^+$ T cells

In the case of diseases requiring cell-mediated immunity such as cancer, clonal expansion of CD8$^+$ T cells is usually attributed to antigen recognition and increased potential for tumour killing and patient responses. We were one of the first groups to formally demonstrate this in peripheral blood in 2020, where we identified that patients with an increased number of 'large' clones occupying >0.5% of the TCR repertoire after ICB had longer survival and improved clinical responses[147]. However, the underlying expression and biological pathways that drive this process of peripheral clonal expansion are still incompletely understood. Given the now expanded size of our cohort, I first validated whether improved clinical responses were still associated with higher numbers of on-treatment expanded clones. I used MiXCR to recover TCR chains from our bulk RNAseq data and downsampled to 1000 TCR-$\alpha$ or TCR-$\beta$ chains per sample, as the minimum number of chains seen across our samples. I measured whether patients that had clinical responses by 6 months of treatment i.e. radiological shrinking and regression of their tumours, had more large clones at C2, measured by CDR3 sequence. Responding individuals had significantly higher large clone counts across both TRA and TRB chains, indicating this unlikely to be a chance observation restricted to one of the chains (Figure 4.1a). From here, I used TCR-$\beta$ chain sequences to define clones, given its wider prevalence in clonality studies compared to the $\alpha$ chain. To assess long-term outcomes, patients were also grouped by whether they had an above median number of large clones or not, and their length of survival without evidence of cancer progression i.e. progression-free survival (PFS), was tracked. Indeed, patients with high numbers of large clones had significantly better PFS than those with below median count (Figure 4.1b).

I next identified genes and pathways that correlate with increased numbers of large clones either at C1 or at C2. I performed differential gene expression analysis in DESeq2, with the number of large clones as the modelling variable whilst regressing for age, sex, quantity of input RNA used for sequencing, and sequencing batch. Amongst the top genes associated

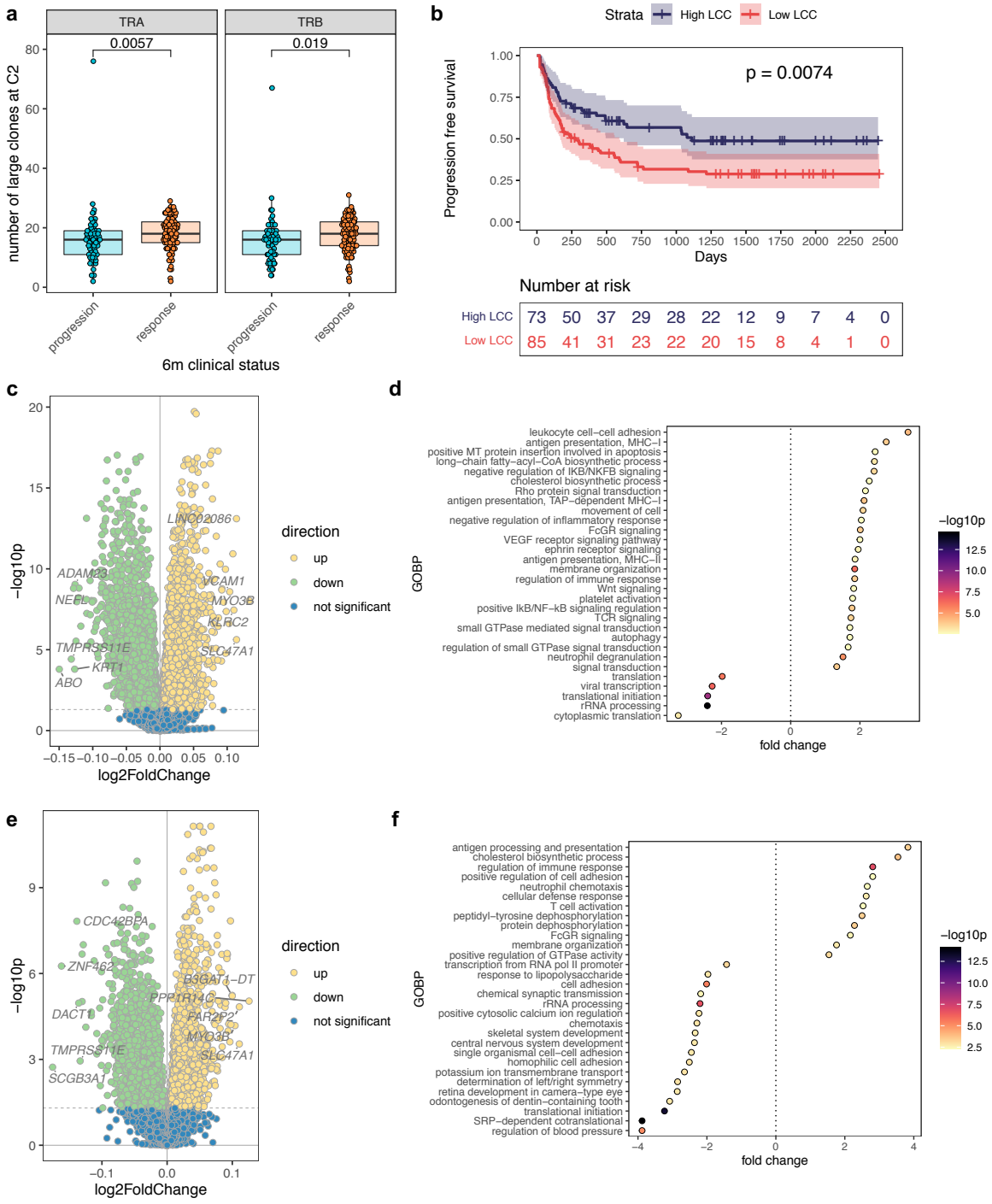



**Figure 4.1 Clinical and transcriptomic associations of CD8⁺ T cell clonal expansion.** **(a)** Comparison between numbers of large clones comprising >0.5% of the TCR repertoire, measured by TCR-a or TCR-b chain, in individuals with clinical response or progression based on 6 month radiological scan (n=158, two-sided Wilcoxon signed-rank test). **(b)** Kaplan Meier survival curve comparing progression free survival (PFS) of individuals with above and below median large clone count at C2 (n=158, two-sided log-rank test). **(c,e)** Volcano plot showing correlations with gene expression and large clone count at C1 (c) and C2 (e). Correlation estimates were generated using DESeq2 regressing age, sex and sequencing batch and significant genes having adjusted p value <0.05. **(d,f)** GOBP pathways enriched in expanded clones based on differentially expressed genes at C1 (d) and C2 (f), with significant pathways having adjusted p value <0.05.

with clonal expansion were *VCAM1* which may contribute to non-cytotoxic anti-viral responses[313], *MYO3B* which may contribute to immunological synapse maturation and TCR force generation required for T cell activation[314,315], and *SLC47A1*, a hitherto underexplored drug and solute transporter[316] (Figure 4.1c,e). Examining the corresponding pathways at C1 and C2, I found that class I MHC presentation and cholesterol biosynthesis were strongly associated with clonal expansion as well as T cell activation and GTPase activity which both support stimulatory post ligation TCR signalling[317] (Figure 4.1d,f). Increased enrichment of cholesterol metabolism also parallels previous observations around LLEC function, and further understanding how metabolic states relate to clonal expansion and sustained effector responses especially in the absence of exhaustion is particularly interesting. Pathways that were under-represented during clonal expansion include those relating to general transcriptional and translation processes which were associated with Naive and CM cells in the previous single-cell analysis. Altogether, this suggests that clonal expansion is associated with specific transcriptomic pathways supporting T cell activation and that these pathways remain consistent throughout ICB.

## 4.3 Subset-associated signatures

After reinforcing the importance of assessing peripheral clonal expansion, I wanted to assess which $CD8^+$ T cell subsets were major contributors to this. I previously demonstrated by single-cell analysis that the majority of large clones were of an Eff phenotype at C1 and Eff/EM at C2. To validate this across the bulk cohort, I correlated the number of large clones with the subset scores previously generated in the bulk RNAseq data, using a linear model to regress other covariates such as treatment type, age and sex. I performed this analysis at either C1, C2 or using the difference between metrics across treatment. Eff score was the only score significantly correlated with large clone count at C1 whilst EM and Eff score were both correlated with clonality at C2 (Figure 4.2a), perfectly mirroring my single-cell observations. Change in EM was uniquely correlated with changes in the number of large clones which again recapitulates single-cell observations of EM expansion. Altogether, having a sizeable Eff compartment is closely linked to clonal expansion, whilst there appears to be added contribution from a group of expanded EMs at C2.

Given effector cells were strongly associated with expanded clones, I next assessed whether higher on-treatment effector score associated with long-term response to ICB. I similarly stratified individuals on whether they had above or below median Eff score at C2 and compared their PFS and overall survival (OS). Above median (high) Eff score was strongly

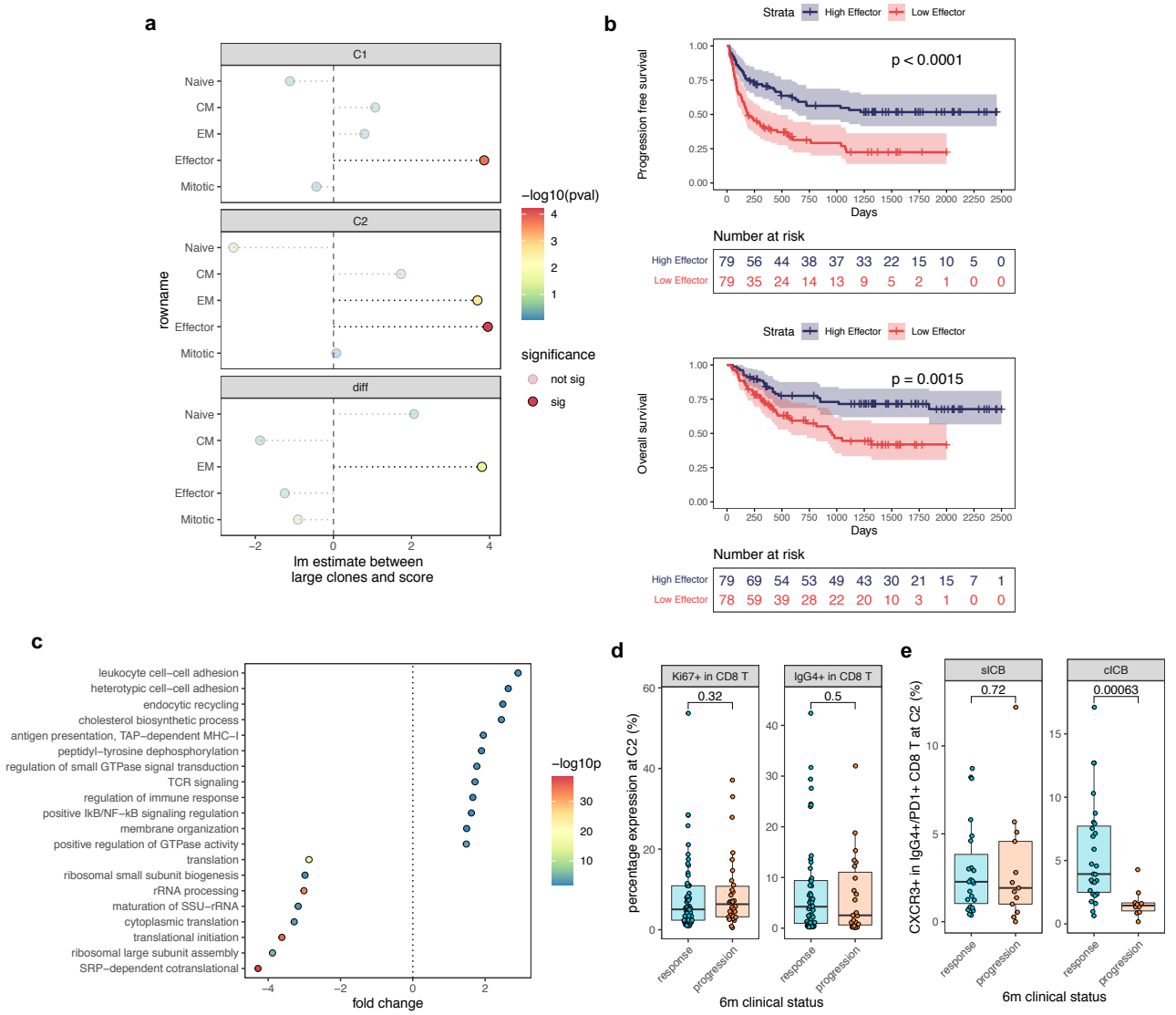



**Figure 4.2 Subset score associations with clonality, clinical outcome and transcriptomics. (a)** Correlation estimates between large clone count and subset score at C1, C2 or based on difference across timepoint. Correlations were performed using a linear model regressing age, sex and treatment type. **(b)** Kaplan Meier survival curve comparing progression free survival (PFS, top) and overall survival (OS, bottom) of individuals with above and below median Effector score at C2 (n=158, two-sided log-rank test). **(c)** C1 GOBP pathways enriched in individuals with above median Eff score at C2 based on differential gene expression using DESeq2. **(d)** Comparison of C2 mitotic and IgG4 responses in individuals split by clinical response status at 6 months (n=89 and 73, two-sided Wilcoxon signed-rank test). **(e)** Comparison of C2 CXCR3$^+$ proportion in IgG4$^+$ or PD-1$^+$ CD8$^+$ T cells across sICB and cICB for individuals split by clinical response status at 6 months (n=36 and 37, two-sided Wilcoxon signed-rank test).

associated with improved survival across both measures (Figure 4.2b). These results suggest that $CD8^+$ T cell antigen recognition (clonal expansion) and functionality (Eff score) are both required for successful anti-tumour responses driven by ICB. Interestingly, no associations were observed between outcome and higher EM score at C2 or its relative change between C1 and C2, which hints at a slight separation between processes that drive clonal expansion and cytotoxic capacity. I also examined pre-treatment pathways that influence Effector score at C2, finding that increased baseline cholesterol metabolism, MHC-I antigen presentation and GTPase signalling were all predictive of a higher on-treatment Effector composition, reinforcing the importance of these biological pathways in promoting immune response to ICB (Figure 4.2c).

Previous literature has identified that peripheral mitotic responses during ICB may be predictive of clinical benefit[104]. However, I observed that dividing cells are usually CM in phenotype by flow cytometry and often belong to small, unexpanded clones which are less likely to have reacted to cancer antigens. I tested to see if responding individuals to ICB at 6 months had differing proportions of $Ki67^+$ or $IgG4^+$ cells in their $CD8^+$ T cell population measured by flow cytometry, and found no significant difference (Figure 4.2d). In their study, Huang et al[104] associated a mitotic response coupled with active reductions in tumour burden with beneficial patient outcome, potentially suggesting that mitotic cells need to accompany an effective anti-tumour response in order to be clinically relevant. To explore this, I examined the expression of the chemokine receptor CXCR3 at C2 on $CD8^+$ T cells and on a smaller subset of $IgG4^+$ or $PD\text{-}1^+$ T cells. These cells represent those likely to be undergoing a degree of activation or acute TCR stimulation. CXCR3 in particular has been previously implicated as an essential chemokine receptor for TIL recruitment[106,107] and so I reasoned its expression marked a population of possible tissue/tumour-homing T cells. Although no association between CXCR3 expression on all $CD8^+$ T cells and 6 month clinical status was seen, there was significantly higher CXCR3 positivity within the $IgG4^+$ or $PD\text{-}1^+$ fraction of $CD8^+$ T cells in responding individuals for cICB, but not sICB (Figure 4.2e). Understanding the precise function and biological origin of this population would be particularly interesting; are $CXCR3^+$ $IgG4^+$ cells a small population of tumour-reactive TILs that have recirculated and become 'reinvigorated'? Instead, do they represent peripheral T cells capable to tumour reactivity that are now heading to tumour sites to carry out some cytotoxic function? Alternatively, could these be bystander cells that simply reflect successful immune stimulation on other cells and general 'reinvigoration'? Linking these cellular phenotypes with peripheral and intratumoural clonality may help to unpick their purpose.

## 4.4 Clinical lymphocyte stability

To translate clonal expansion and increased Effector score into a clinically tractable predictor of outcome, I next examined whether hospital lymphocyte count could be used as an easily measured and minimally invasive biomarker. Our group had previously assessed if there was a relationship between C1 and C2 lymphocyte count and patient survival but found no significant association in a multivariate Cox model[44]. Since temporal stability was a shared feature of large clones and Effector cells - both of which being the key heuristics identified so far, I wondered whether steady lymphocyte counts across C1 and C2 would instead predict outcome. I calculated the ratio of C1:C2 lymphocyte counts based on routine blood tests as part of patient hospital monitoring, with this ratio termed lymphocyte stability (LS) (Figure 4.3a). A LS value >1 represents an increase in lymphocyte count across treatment following treatment whilst LS <1 corresponds to a fall in count. In our cohort of n=126 patients, the minimum LS value was 0.27, depicting a 5-fold decrease in lymphocytes across treatment, whilst the maximum was 2.31. Across this, the majority of individuals had an LS <1 with the median fall in LS being 0.8. I used this as a threshold cut-off, grouping patients with LS >0.8 as stable whilst those with LS <0.8 were classified as having falling LS. Comparing PFS and OS across these two groups, there was a strongly significant difference in ICB outcome, with stable LS individuals having superior survival (Figure 4.3b). Upon testing whether LS was associated with other clinical variables such as progression, death status, irAE development, sex, CMV status and HLA features, I found it was associated only with 6 month clinical status, overall progression and death status, and predominantly in individuals treated with sICB (Figure 4.3c).

I next tried to identify the biological drivers of lymphocyte stability by correlating LS with various cellular and clonal measures. Firstly, I examined the proportions of major immune subsets within PBMCs measured by flow cytometry, finding an expected correlation between T cell proportion and LS (Figure 4.4a). Of interest, NK cell proportions were also correlated with LS, whilst monocyte proportions were anti-correlated. Overall B cell proportion was not associated with LS. LS was specifically associated with increased $CD8^+$ T cell proportion of all PBMCs (Figure 4.4b), and as expected, anti-correlated with increased T cell naivety (Figure 4.4c). Upon examining the relationship between LS and clonality, increased clonal expansion at C1 and C2 associated with the degree of lymphocyte stability, when measured by numbers of large clones, mean clone size and smaller numbers of clones (Figure 4.4d-e). To understand how the functional state of T cells was associated with LS, I measured the levels of CD38 and HLA-DR as activation markers, and granzyme-B (GZMB) and perforin

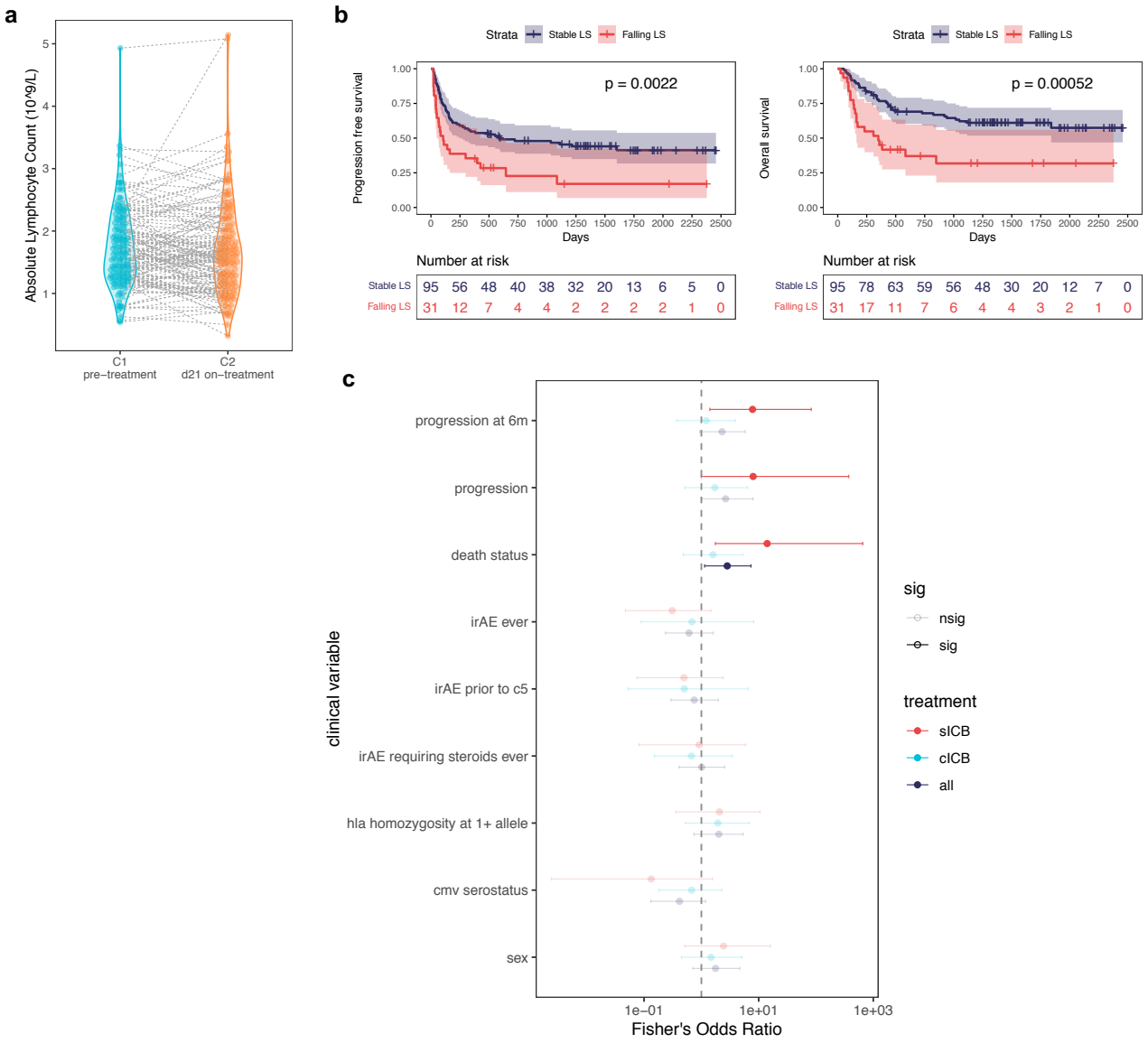



**Figure 4.3 Stability of hospital lymphocyte counts associates with long-term ICB survival. (a)** Patient lymphocyte count measured during routine hospital blood tests at C1 and C2 (n=126). **(b)** Kaplan Meier survival curve comparing progression free survival (PFS, left) and overall survival (OS, right) of individuals with stable lymphocyte stability (LS) (ratio of C2 and C1 count >0.8) and falling LS (LS <0.8) (n=126, two-sided log-rank test). **(c)** Odds ratios from Fisher's exact tests comparing overlap between LS groups (stable vs falling) with other binary clinical variables.

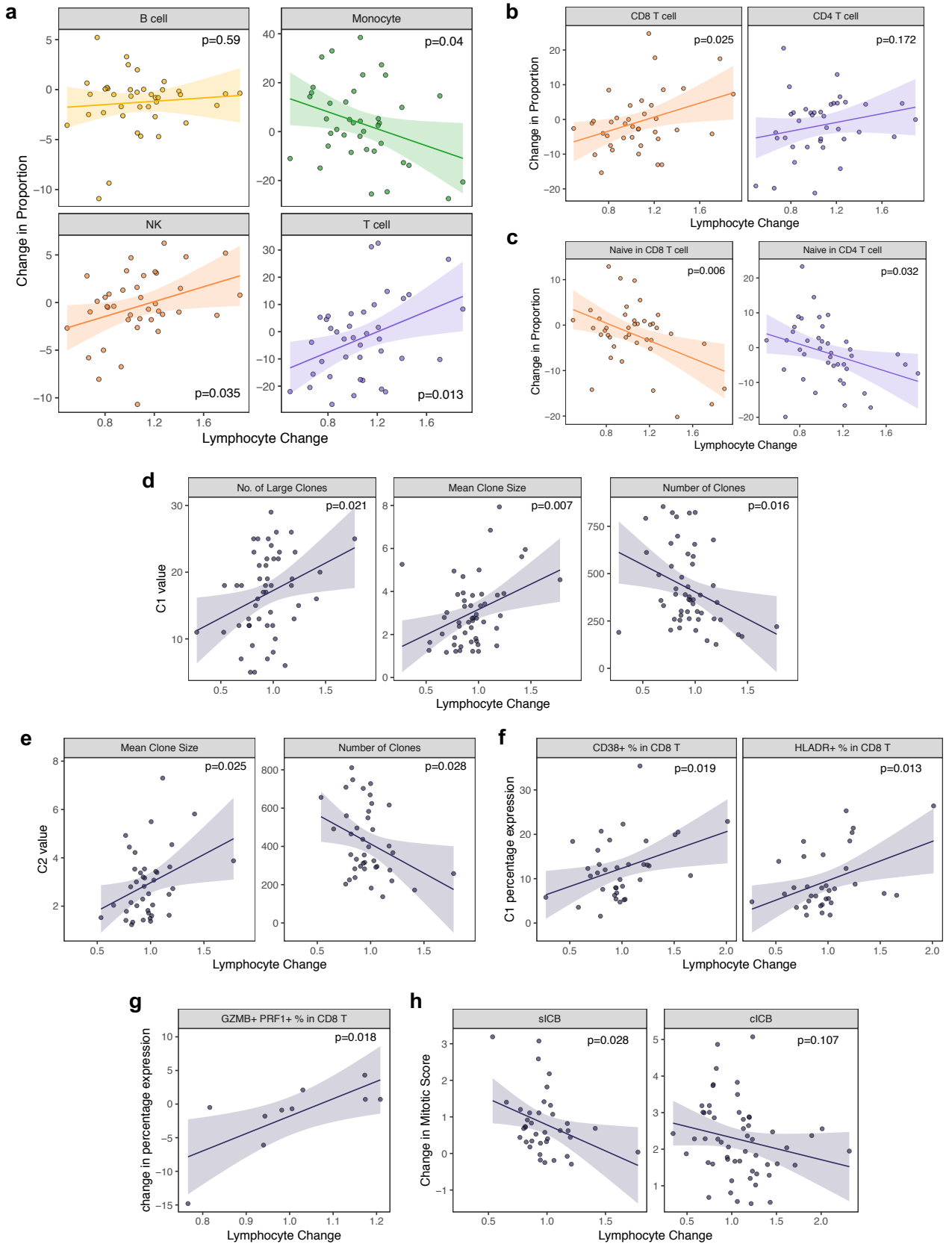

a
B cell
p=0.59
Monocyte
p=0.04
NK
p=0.035
T cell
p=0.013
Change in Proportion
Lymphocyte Change
b
CD8 T cell
p=0.025
CD4 T cell
p=0.172
Change in Proportion
Lymphocyte Change
c
Naive in CD8 T cell
p=0.006
Naive in CD4 T cell
p=0.032
Change in Proportion
Lymphocyte Change
d
No. of Large Clones
p=0.021
Mean Clone Size
p=0.007
Number of Clones
p=0.016
C1 value
Lymphocyte Change
e
Mean Clone Size
p=0.025
Number of Clones
p=0.028
C2 value
Lymphocyte Change
f
CD38+ % in CD8 T
p=0.019
HLADR+ % in CD8 T
p=0.013
C1 percentage expression
Lymphocyte Change
g
GZMB+ PRF1+ % in CD8 T
p=0.018
change in percentage expression
Lymphocyte Change
h
sICB
p=0.028
cICB
p=0.107
Change in Mitotic Score
Lymphocyte Change

**Figure 4.4 Phenotypic, clonal and subset associations with lymphocyte stability. (a-c)** Correlation between lymphocyte stability (LS) values (i.e. ratio change in lymphocyte count between C1 and C2) and change in flow cytometry proportions between C1 and C2 of (a) PBMC subsets, (b) $CD8^+$ and $CD4^+$ T cell proportions and (c) naive T cell proportion within $CD8^+$ and $CD4^+$ T cells (n=38, Spearman's rank test). **(d-e)** Correlations between LS values and $CD8^+$ T cell clonality metrics measured by MiXCR in bulk RNAseq data at either C1 (d) or C2 (e) (n=52, Spearman's rank test). **(f-g)** LS values correlated with flow cytometry proportions of $CD38^+$ and $HLADR^+$ cells within the $CD8^+$ T cell compartment at C1 (f) or the change in granzyme B $(GZMB)^+$ perforin-1 $(PRF1)^+$ cells within $CD8^+$ T cells between C1 and C2 (g) (n=10-36, Spearman's rank test). **(h)** Correlation between LS values and change in mitotic score measured in the bulk RNAseq data (n=51 and 71, Spearman's rank test).

(PRF)-1 positivity as cytotoxic markers within $CD8^+$ T cells. LS was associated with increased CD38 and HLA-DR expression at C1 (Figure 4.4f), and an increase across treatment in double positive $GZMB^+$ $PRF1^+$ cells (Figure 4.4g). LS was also significantly correlated with Eff score at C2, both when using bulk RNAseq score and flow cytometry (data not shown). Altogether, this suggests that a stable lymphocyte response may require 3 aspects: (1) clonal expansion, (2) T cell activation as evidenced by CD38 and HLA-DR expression, which unpublished data from Victoria Woodcock suggests is a hallmark of ICB-driven immune awakening, and (3) functional cytotoxicity based on GZMB/PRF1 expression and Effector composition. In line with previous data showing LLECs having less mitotic activity, LS was negatively correlated with changes in Mitotic score across treatment, with a significant anti-correlation seen in sICB and the same trend for cICB patients (Figure 4.4h).

To further these observations, I examined transcriptomic correlates of LS using bulk RNAseq data. To do this, I segregated patients by LS (stable vs falling) and looked separately at the DE genes modulated by ICB for each group using DESeq2. Comparable numbers of differential genes were found in each analysis, with a similar ratio of induced and suppressed genes (Figure 4.5a). Comparing the magnitude of DE for each gene, I found a large number of genes were significantly modulated in both groups although the degree of DE was generally higher in the falling LS group (Figure 4.5b). In particular, *MYO3B*, which was previously associated with clonal expansion, was significantly induced only in stable LS patients. To understand the distinct biological pathways modulated by ICB in each group, I performed GOBP pathway analysis on each set of DEGs and compared pathway enrichment values. Similar to the DEG analysis, many pathways were modulated in both groups to a similar degree based on fold changes (Figure 4.5c). However, focusing on the pathways that were significantly enriched only in one group, pathways relating to metabolism and T cell homeostatis were exclusively induced in stable LS $CD8^+$ T cells. In contrast, $CD8^+$ T cells from falling LS patients had disproportionately increased signalling related to mitosis, in accordance with previous observations, and type I IFN signalling. How these two biological modules contribute to T

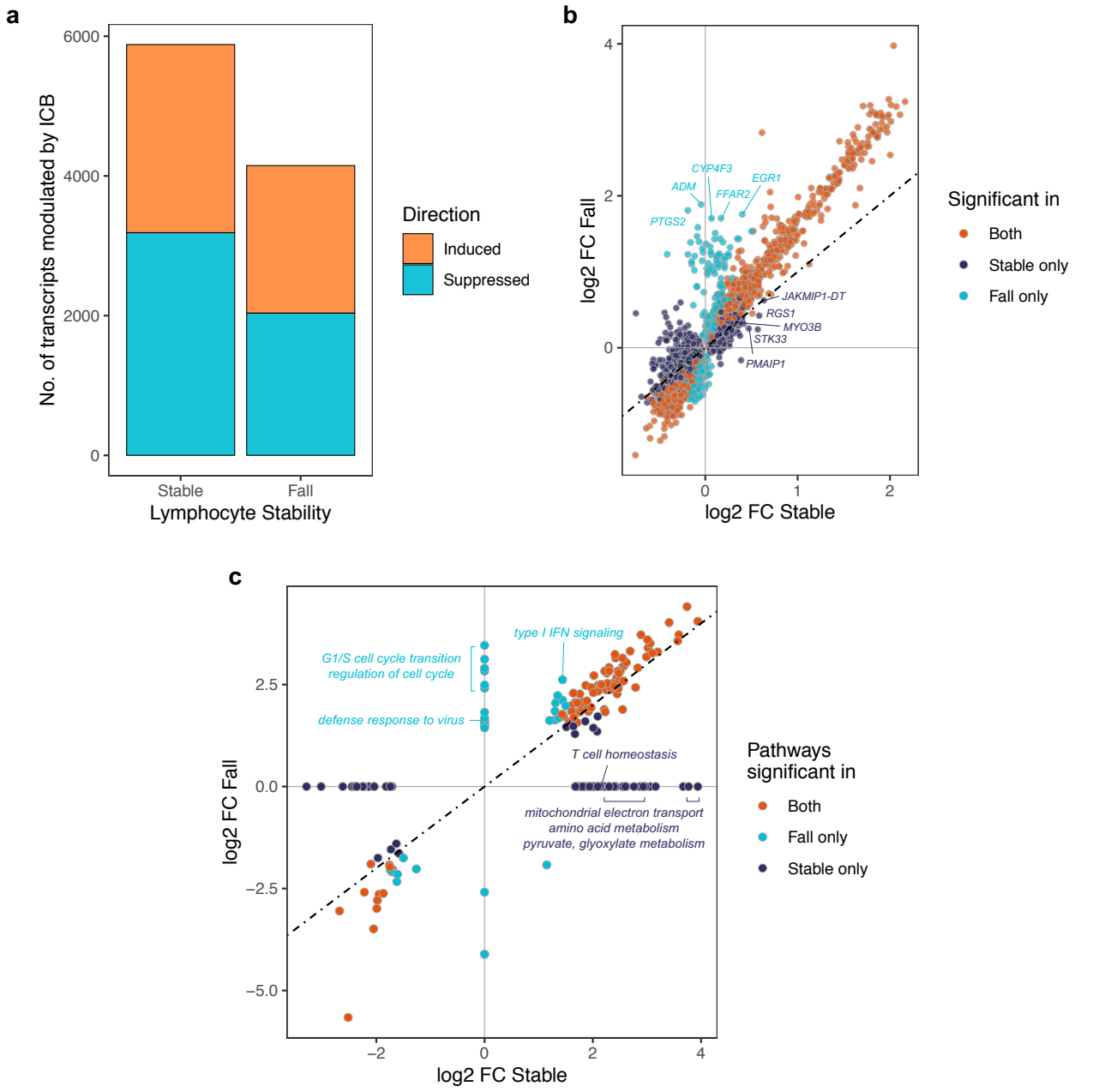



**Figure 4.5 Transcriptomic differentiators between stable and falling lymphocyte stability. (a)** Patients with paired C1 and C2 CD8⁺ T cell bulk RNAseq data were separated into stable and falling LS groups and differential gene expression analysis between C1 and C2 performed for each group separately. The number of induced and suppressed genes in the stable and falling LS groups are represented. **(b)** Dotplot comparing DEG fold changes across the stable vs falling LS groups. Points were coloured based on whether the gene was significantly modulated in both or only one of the groups. **(c)** GOBP pathway enrichment was performed on each geneset and the pathway fold changes were then plotted, with colouring according to whether the pathway was significantly enriched in both genesets, or only in one group.

cell instability remains interesting to explore further but is in keeping with absent Effector and clonal expansion responses.

I lastly investigated the interplay between LS and irAEs further, given this is another well-established clinical biomarker of ICB response. In my previous co-variate analysis, no overlap between the two metrics was seen, and in keeping with this, when individuals with irAEs prior to C5 were excluded, stable LS was still associated with significantly higher PFS and OS (Figure 4.6a). I validated that irAE development was still associated with clinical responses to sICB or cICB in our cohort, with the observation that it is a much stronger predictor of response for cICB patients (Figure 4.6b). To understand this lack of interaction between LS and irAEs, I examined whether large clone count was significantly different between patients who developed autoimmunity by C5 or not, finding minimal difference (Figure 4.6c). This suggests that clonality, Eff score and LS require almost completely separate T cell drivers compared to irAEs, and potentially have distinct prognostic benefits for sICB and cICB. Indeed, when I examined the relationship between irAEs and CXCR3 expression in the IgG4$^+$/PD-1$^+$ population, which I previously demonstrated to be associated with 6 month clinical status in cICB but not sICB, CXCR3 proportion was consistently increased in irAE-developing individuals across both treatment types (Figure 4.6d). This indicates that T cell trafficking may be an important determinant for irAE development, which synergises with cICB outcome, but beneficial CD8$^+$ T cell states in sICB instead focus on stability.

## 4.5 Pre-existing CD8$^+$ T cell IFN responses

As part of the analysis of lymphocyte stability, increased type I IFN signalling was one of the pathways associated with falling LS. To test whether this represented an indicator of poorer CD8 and ICB response, I scored bulk RNAseq samples for genes involved in this pathway to generate a proxy type I IFN signature. I looked to see whether high type I IFN signalling at baseline associated with worse survival upon treatment, finding it was indeed indicative of significantly worse PFS and OS (Figure 4.7a), thus identifying a relevant biomarker of response that is tractable at C1. When I explored the transcriptomic pathways that correlated with high type I IFN signatures, they spanned pathways of generalised inflammation such as interferon responses, JAK-STAT cascade, TLR signalling and immune response whilst also correlating with increased cell proliferation and division (Figure 4.7b). One particular pathway that caught my interest was complement activation, which suggests a degree of monocyte involvement and possible interaction between monocytes and CD8$^+$ T cells. Given the anti-correlation between monocyte and T cell proportions observed by flow cytometry, I

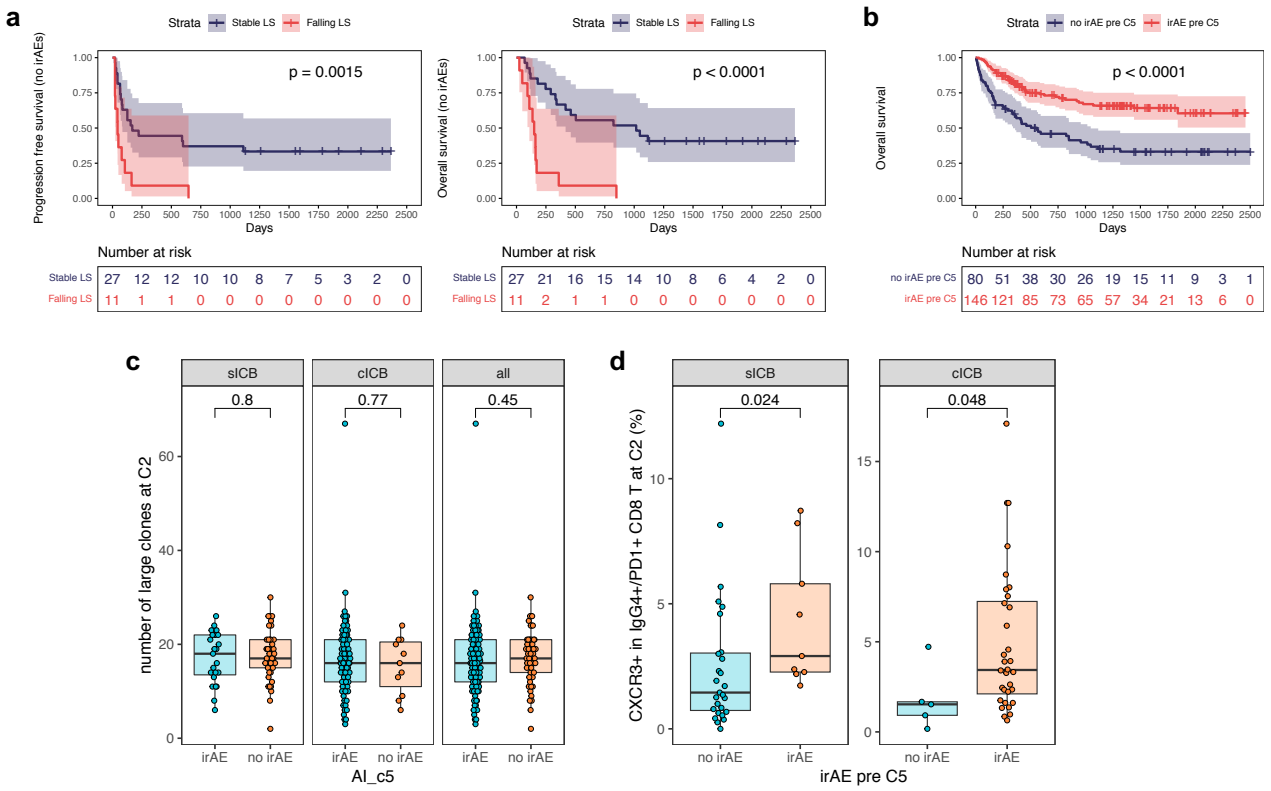



**Figure 4.6 Distinct patient responses underlying lymphocyte stability and immune-related adverse events.** **(a)** Kaplan Meier survival curves for patients with stable vs falling lymphocyte stability (LS) who did not develop immune-related adverse events (irAEs) prior to C5, examining their progression-free survival (left) or overall survival (OS, right) (36, two-sided log-rank test). **(b)** Kaplan Meier survival curve for patient OS based on development of irAEs prior to C5 (n=226, two-sided log-rank test). **(c)** Comparison of numbers of large $CD8^+$ T cell clones at C2 in individuals who develop irAEs prior to C5 or do not (n=159, two-sided Wilcoxon signed-rank test). **(d)** CXCR3 positivity in the $IgG4^+$ or $PD\text{-}1^+$ compartment of $CD8^+$ T cells based on development of irAEs prior to C5 (n=36 and 37, two-sided Wilcoxon signed-rank test).

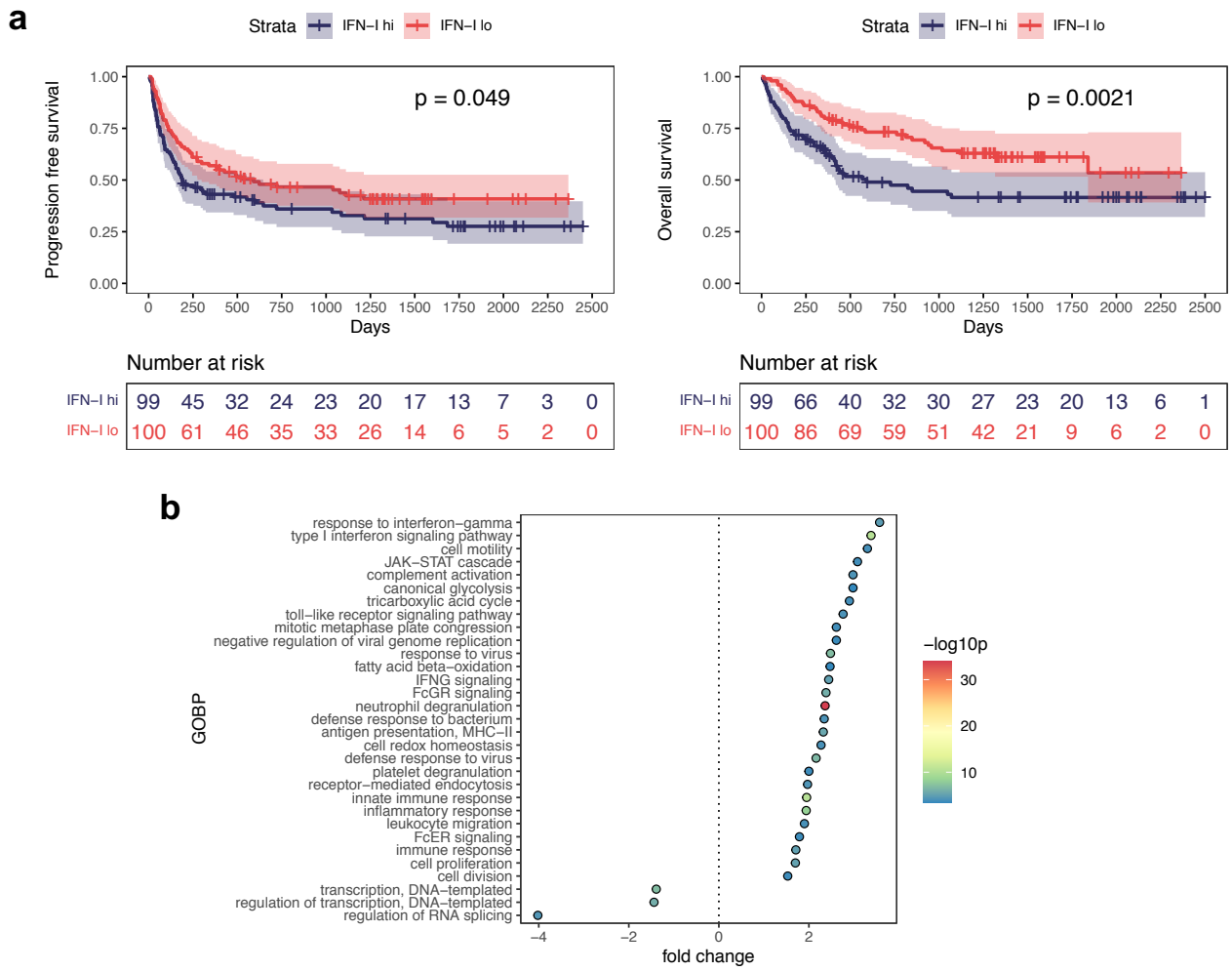



**Figure 4.7 Pre-treatment type I IFN responses associate with clinical outcome. (a)** Kaplan Meier survival curves for patients based on their type I interferon (IFN-I) expression score in bulk $CD8^+$ T cell samples. Genes associated with the 'type I interferon signaling' GOBP pathway were identified and the geometric mean of expression per $CD8^+$ T cell sample was calculated. Individuals were separated based on whether they had above or below median score and their relative progression free survival (left) and overall survival (right) was determined (n=199, two-sided log-rank test). **(b)** Differential gene expression analysis was performed using the IFN-I high and low groups as per (a) to identify genes correlated with type I IFN signatures at C1. GOBP pathway enrichment was subsequently performed on the significant genes (adjusted p-value <0.05) and pathway fold changes plotted for significant pathways (adjusted p-value <0.05).

decided to explore interactions between CD8$^+$ T cells and other peripheral immune subsets further, forming the basis of the next chapter's findings.

## 4.6 Conclusions and Discussion

Building off our group's previous observations and the results from the previous chapter, I was able to identify multiple characteristics of pre-existing and on-treatment CD8$^+$ T cell responses that predict response to ICB. Most significantly, these could be converted into a clinically tractable marker, lymphocyte stability, which can be calculated from measurements already taken as part of standard hospital care, thus making it particularly easy to translate into an actionable biomarker. To summarise some of the results of this chapter:

- CD8$^+$ T cell clonal expansion is associated with antigen presentation and cholesterol metabolism, and demarcates individuals with longer PFS
- Effector score at C2 is a strong predictor of PFS and OS whilst mitotic score does not associate with improved survival
- Stable hospital lymphocyte counts in patients between C1 and C2 of ICB is associated with long term outcome
- Lymphocyte stability is driven by CD8$^+$ T cells and correlates with clonal expansion, activation and increased cytotoxicity following ICB, and anti-correlates with mitotic and type I interferon signatures
- Lymphocyte stability and autoimmune toxicity are largely distinct clinical markers
- Pre-treatment type I interferon score is significantly associated with poorer survival with ICB

In these analyses, I identified two biomarkers of CD8$^+$ T cell responses that correspond with improved outcome with ICB; clonal expansion and effector function. Although there is a large degree of overlap between these markers, such as in the pathways that contribute to these processes (Figure 4.1f,4.2c), they putatively represent slightly distinct biological facets of CD8$^+$ T cells. Peripheral clonal expansion is assumed to reflect tumour reactivity with Wu et al[135] in particular demonstrating that expanded clones in circulation are not only found infiltrating tumours but are also often clonally expanded within tumours as well. Separately, non-exhausted cytotoxic phenotypes are needed for CD8$^+$ T cells to enact their functional killing role, acting as a quasi second-signal for anti-tumour response. Notably, the cytotoxicity of peripheral CD8$^+$ T cells correlates with TIL cytotoxicity[137,138], suggesting that individuals with a large number of peripheral expanded Eff clones at C2 have sufficient anti-tumour responses to enable cancer regression. To what extent these circulating cells are directly

involved in the anti-tumour ICB response is unclear; Yost et al[112] demonstrated that ICB is potentiated by influx of novel peripheral clones into the tumour whilst there is also evidence of increased levels of the chemoattractant CXCL10 following treatment in the plasma of MM patients by ELISA (unpublished data from Chelsea Taylor).

Having identified hospital lymphocyte stability as a highly attractive biomarker for ICB - based on its ease of measurement and the earliness of its readout, a central question was what LS represents. Based on my analyses, LS may be a robust biomarker because it encapsulates both clonal expansion and effector function. The anti-correlation between LS and mitotic responses also re-emphasises that mitosis is not clinically beneficial, and perhaps represents either off-target proliferation, particularly in cICB where peripheral tolerance via CTLA-4 is hampered, or instead reflects tumour persistence as other papers have suggested[116]. It would be interesting to explore whether long-term lymphocyte stability i.e. between C2 and C4 or later timepoints, also associates with clinical benefit or whether ICB outcome is determined by this initial burst of immune activity within the first cycle of treatment. This would have implications for treatment resistance and duration should ICB have such immediate dichotomisation in outcomes within the first month of treatment, including whether to offer earlier tumour scans to patients. Finally, it is worth noting that LS is associated with increased OS, both in a separate American cohort of pan-cancer ICB patients[265], most of whom were treated with sICB, as well as in follow-up analyses across multiple tumour types in a wider cohort of Oxford ICB patients dating back to 2014 (unpublished data from the Fairfax group). As such, understanding further biological mechanisms that underpin lymphocyte stability, such as epigenetic variability, is an area of substantial research interest and may lead to the development of novel combination therapies with ICB.

Another interesting biomarker associated with clinical benefit from ICB was lower levels of pre-treatment type I IFN signalling. Conventionally, type I IFN responses have been thought to lead to improved T cell function, $CD4^+$ T cell help and the upregulation of inflammatory cytokines and chemokines, such as CXCL9-11[318]. Our observations run counter to this traditional viewpoint, but has a strong immunological basis in chronic infections such as LCMV models[319] and HIV-I in humans[320], where sustained IFN-I contributes to pathogenesis. More recently, sustained IFN-I signalling has been described as negatively prognostic in the context of PD-1 blockade by two papers. Jacquelot et al[321] described that chronic IFN-I leads to an intratumoural accumulation of suppressive Tregs and myeloid cells, and in turn, increased PD-L1 and NOS2 expression in tumour cells and DCs. In a similar vein, Boukhaled et al[322] described that type I IFN 'responsiveness' upon stimulation predicted poor effector T cell responses associated with decreased chromatin accessibility and an increase in markers

of dysfunction such as *TOX*. In accordance with these, our data seems to suggest that IFN-Is associate with (a) generalised inflammatory and mitotic pathways in the absence of TCR signalling (Figure 4.7b) and (b) decreased lymphocyte stability (Figure 4.5c) which associates with increased monocyte count and a skewing towards naive T cell proportions. How precisely IFN-Is drive these effects is difficult to disentangle but it would be interesting to stimulate PBMCs from patients in our cohort with a variety of IFN-Is and subject the treated cells to single-cell RNAseq to dissect its functions, especially on mitosis and clonality, and to perform follow-on cytotoxicity assays. This data also points towards a detrimental effect of peripheral monocytes for ICB responses, which has previously been described[323] but remains incompletely understood and informs our interest in exploring $CD8^+$ T cell interactions with other immune subsets across the next chapters.

# Chapter 5

# Assessing related changes across PBMC subsets during ICB

## 5.1 Summary and Aims

Although $CD8^+$ T cells have been the primary focus of studies exploring the the effect of ICB, there has been growing recognition that ICB modifies immunity in other cell subsets and that clinical response is influenced by the phenotypes of these populations. A large number of studies have looked at peripheral PBMC subsets for response biomarkers such as Krieg et al[323] but have not conducted larger scale transcriptomic analysis to support their proteomic findings from flow cytometry or CyTOF, nor tried to link the underlying mechanisms behind phenotype changes across subsets. Given the group has matching bulk RNAseq data across multiple cell subsets from the same patients, both prior to treatment and on therapy, this data is well placed to begin addressing these two questions.

In this chapter, I will investigate how transcriptomic changes from ICB are shared between major cell subsets; $CD8^+$ T cells, $CD14^+$ monocytes and $CD19^+$ B cells. Although a variety of other cell subsets were isolated in blood, such as memory and naive $CD4^+$ T cells, there was sufficient sample size only across these cell types to uncover relevant changes. The specific aims I will cover are the following:

- How do pathways associated with IgG4 binding correlate across different cell subsets?
- What are global patterns of gene expression modulation by ICB across cell subsets?
- How do pathways correlated with CD8 mitosis, interferon gamma and type I IFN signalling vary across cell subsets?

- What pathways in other cell subsets associate with T cell clonality and effector presence?
- How does variation in the context of lymphocyte stability correlate across cell subsets?
- What impact does BCR chain usage have on CD8$^+$ T cell profiles?
- How can we understand the relationship between all these different factors across the three cell subsets?

## 5.2 Changes associated with differential ICB binding across cell subsets

I previously assessed the transcriptomic associations of ICB binding measured through IgG4 staining by flow cytometry on the CD8$^+$ T cell compartment, finding a strong associated upregulation of mitosis, *IFNG* expression and inflammation. Interestingly, not all of these pathways were clinically beneficial and α-PD-1 binding levels alone did not predicte improved survival. To dissect what effects ICB binding has on CD14$^+$ monocytes and CD19$^+$ B cells, I interrogated bulk RNAseq data from these two subsets. Specifically, I calculated the delta values between C1 and C2 across genes for each subset, and tested which genes were modulated by ICB in correlation with IgG4 positivity. Linear model correlations were used to regress variation from age, sex and sequencing input and batch. For CD14$^+$ monocytes, the genes induced by treatment that correlated most with ICB binding were *CXCL13* and *PDCD1*, whilst *SEMA6B* and *ATP2A3* were amongst the most anti-correlated with IgG4 levels (Figure 5.1a). *CXCL13* and *PDCD1* are upregulated upon type I IFN and IFN-ɣ signalling respectively, and so these results appear consistent with activation of these pathways in CD8$^+$ T cells during ICB. Expression of both of these genes in monocytes has prominent downstream implications. Much like in CD8$^+$ T cells, PD-1 can be seen as an exhaustion marker on monocytes, but its expression is often seen in dysfunctional immune contexts such as sepsis where it exacerbates non-specific inflammation[324]. CXCL13 is a ligand that recruits CXCR5$^+$ cells, mainly B cells, to tissues and stimulates B cell germinal centre reactions to produce increased amounts of antibodies and undergo class switching. Comparatively less is known about *SEMA6B* and *ATP2A5*, although it has been reported that *SEMA6B* associates with immunosuppression[325] whilst *ATP2A5* influences mitochondrial metabolism. Collectively, based on differential gene expression analysis, it seems that ICB binding on CD8$^+$ T cells directly associates with accelerated monocyte-driven inflammation, with additional modulation of monocyte metabolism and potential B cell recruitment and homeostasis. To verify these broad patterns, I used GOBP enrichment to analyse the positively and negatively correlated genes, finding that pathways associated with inflammatory genes were indeed

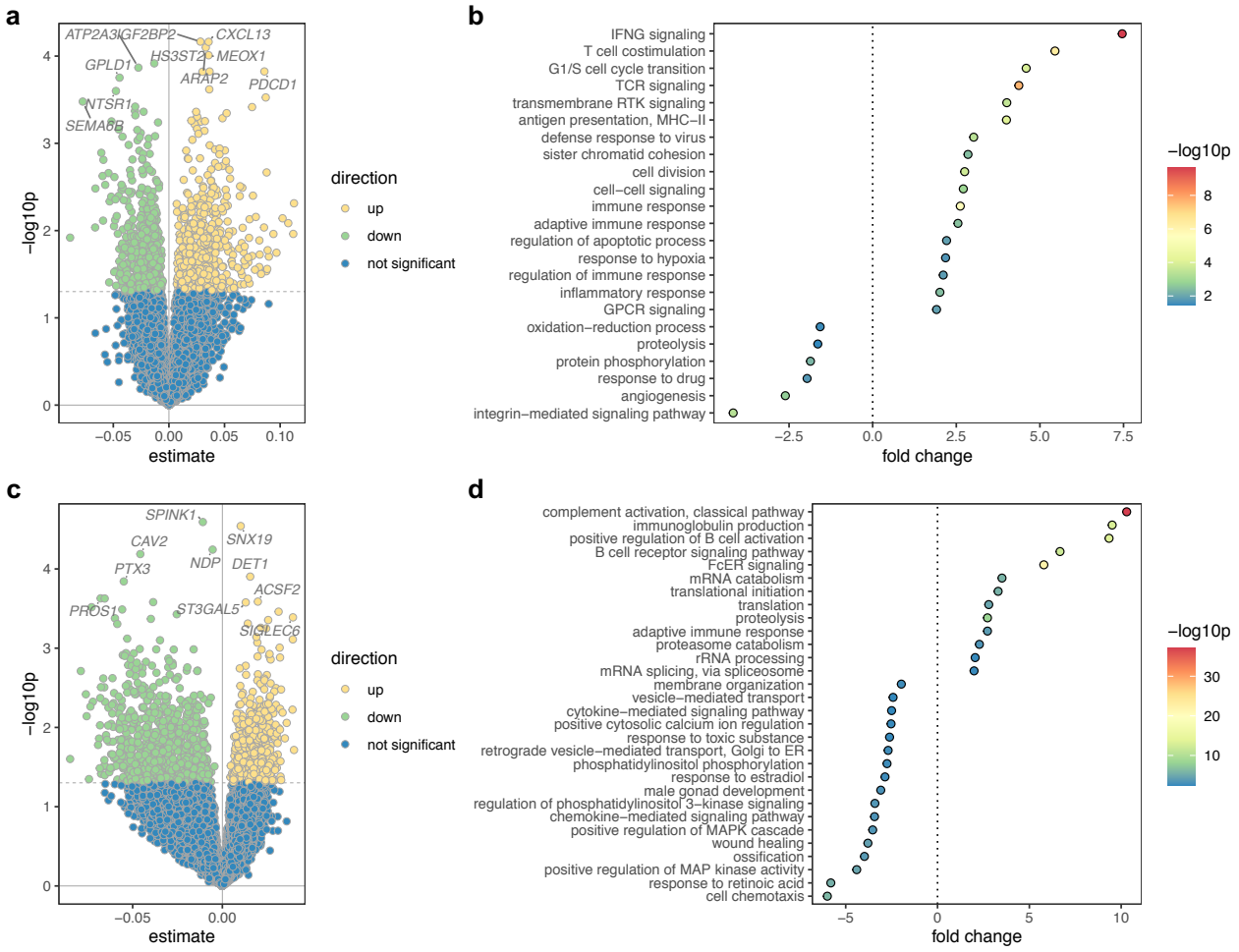



**Figure 5.1 Transcriptomic associations of monocytes and B cells with IgG4 binding. (a, c)** Volcano plot of genes in CD14$^+$ monocytes (a) or CD19$^+$ B cells (b) with expression difference between C1 and C2 that significantly correlate with the amount of IgG4 binding. Gene expression delta values were correlated with the levels of IgG4 at C2 on the corresponding CD8$^+$ T cells when measured by flow cytometry, using linear models to regress age, sex and sequencing input RNA and batch covariates. **(b, d)** Significantly enriched GOBP pathways for the corresponding monocyte genes in (a) and (c) respectively.

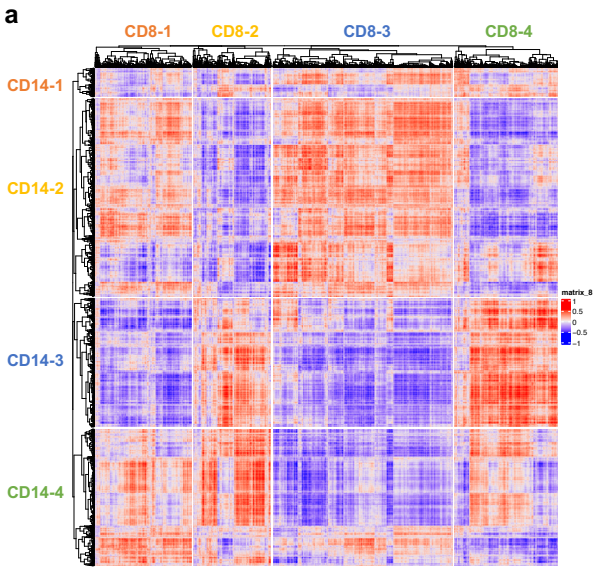
enriched in association with increased IgG4 binding, but did not form the most significant pathways (Figure 5.1b). Instead IFN-ɣ signalling was the top most induced pathway, likely reflecting the marked increase in *IFNG* expression detected in $CD8^+$ T cells previously. Other monocyte pathways that emerged in this analysis included mitotic and type I IFN signalling, suggesting global features of the ICB response are conserved across cell types, as well as T cell costimulation and class I/II MHC upregulation. These latter two processes are likely supportive of T cell growth but whether they influence clonal expansion or instead seemingly less desirable mitotic responses is unclear. It is also worth noting TCR signalling was a pathway that was associated with IgG4 staining, which seems to reflect a degree of T cell contamination in this bulk RNAseq data. This could be a secondary reflection of monocyte inflammation and/or physical monocyte-T cell interactions, supported by MHC-I expression. However, it potentially complicates interpretation of the expression of certain genes and pathways, such as *PDCD1* which is natively expressed by $CD8^+$ T cells to a higher degree.

I looked at similar analysis for the $CD19^+$ B cells, where the genes most induced in accordance with ICB binding included the endoplasmic reticulum associated *SNX19*[326], *ACSF2* which is involved in mitochondrial metabolism, and *SIGLEC6* which is purported to encourage cell-cell interactions[327] (Figure 5.1c). The genes most downregulated in B cells in association with IgG4 binding (*PTX3*, *CAV2*) were less well biologically described but decreased *PTX3* expression has been associated with lupus development[328]. Globally in B cells, I found that complement and immunoglobulin pathways were most strongly associated with ICB binding, with additional B cell activation and adaptive immune responses also being upregulated (Figure 5.1d). This likely represents a shift towards an increased antibody-secreting cell (ASC) phenotype following ICB, as described in unpublished data by Chelsea Taylor. One other increased pathway of note was complement activation, and again, whether this represents monocyte contamination or shared signalling molecules between complement and antibody secretion is unclear. Conversely, MAPK pathways and interestingly, chemotaxis and retinoic acid signalling were strongly anticorrelated with increased IgG4 binding. In B cells, decreased MAPK often associates with increased cell proliferation, and retinoic acid has been demonstrated to facilitate IgA class switching and T-cell independent humoral responses[329]. This therefore suggests a sensitisation of B cells to inflammation and proliferation in association with increased IgG4 binding on $CD8^+$ T cells. Overall, monocyte and B cell pathways downstream of $CD8^+$ ICB responses often revolve around parallel inflammation and mitotic processes, whilst also promoting monocyte co-stimulation and B cell antibody secretion.

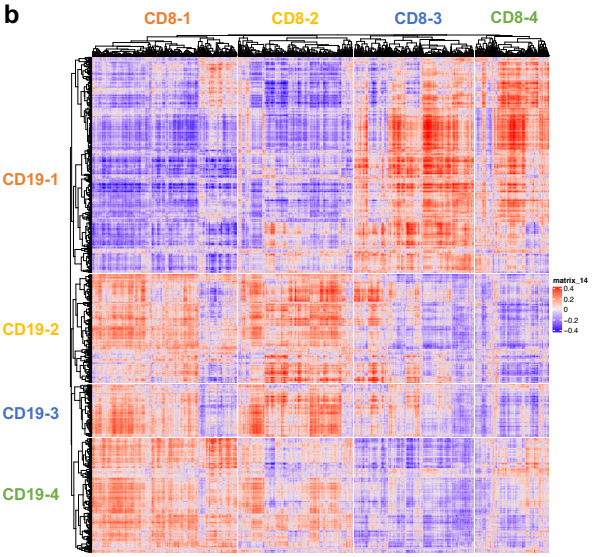
## 5.3 Global transcriptomic correlates across peripheral immune subsets

To further analyse pathway correlations between different cell types, I co-correlated subset-specific gene expression changes occurring during ICB. This processed involved using per-gene C1-C2 expression delta values across each subset, taking only genes found to be differentially expressed across treatment. Pearson's correlations were performed between pairs of genes, one gene from each cell type being compared. I then plotted the correlation coefficients of the gene pairs as a heatmap, where columns represent genes from subset one and rows represent genes from subset two (Figure 5.2). Hierarchical cluster analysis revealed the responding genes formed four major clusters per cell type. I identified the biological processes represented in each cluster using GOBP pathway enrichment analysis - which is summarised in the righthand tables. When looking at CD8 and CD14 correlation, CD8 Group 1, which was demarcated by naive-associated pathways, had a negative correlation with CD14 Group 3, representing type I IFN and inflammatory pathways (Figure 5.2a). This suggests that CD14 upregulation of IFN-I and inflammation is linked with decreased CD8 naive responses, as would be expected biologically. CD8 Group 4, comprised of genes related to cell division, was negatively associated with CD14 Group 2 (Rho and GTPase pathways) and instead associated with the aforementioned IFN-I and inflammatory CD14 Group 3. Interestingly monocyte Rho and GTPase pathways were associated with naive and transcription-based CD8 pathways, which suggests some elements of immunosuppression.

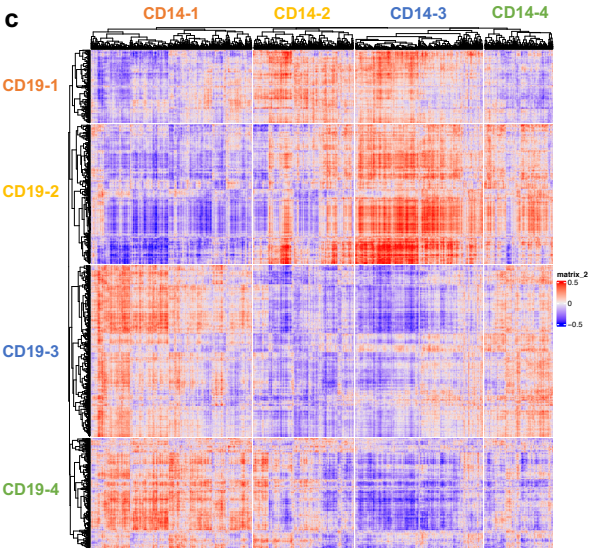
When looking at similar analysis across $CD8^+$ T cells and B cells, induction of naive and transcription-related CD8 pathways (CD8 Group 1 and 2) was positively associated with upregulated B cell transcription, and complement and migration pathways in CD19 Group 4, which also contained some inflammatory-associated genes (Figure 5.2b). These $CD8^+$ T cell processes were anti-correlated with B cell upregulation of MHC, IFN-I and cell division (CD19 Group 1), which was instead associated with T cell mitosis and inflammatory responses (CD8 Group 3 and 4). Finally, between monocytes and B cells, I observed less obvious correlation patterns but CD14 Group 3 (IFN-I and MHC) was positively correlated with CD19 Group 2 (B cell mitosis and IFN-I) and Group 1 (endoplasmic reticulum activity) representative of antibody production (Figure 5.2c). Collectively, these results can be used to begin to understand how gene expression changes between subsets are interlinked, with evidence of shared IFN-I and to a lesser extent, mitotic responses following ICB.




| Group | CD8 Pathway | CD14 Pathway |
|---|---|---|
| 1 | Naïve-associated pathways | |
| 2 | Mitochondrial, NFkB and TNF pathways | Rho and GTPase pathways |
| 3 | Transcription-related pathways | Type I IFNs and inflammatory pathways |
| 4 | Cell division and mitosis-related pathways | Class I MHC and mitosis-related pathways |




| Group | CD8 Pathway | CD19 Pathway |
|---|---|---|
| 1 | Naïve-associated pathways | MHC, type I IFN and cell division pathways |
| 2 | Transcription-related pathways | DNA-templated transcription |
| 3 | Cell division and mitosis-related pathways | DNA-templated transcription |
| 4 | Mitochondrial, NFkB and TNF pathways | Complement and leukocyte migration pathways |




| Group | CD14 Pathway | CD19 Pathway |
|---|---|---|
| 1 | Rho and GTPase pathways | Golgi to ER transport and protein folding |
| 2 | IFkB and phosphorylation pathways | Cell division and type I IFN pathways |
| 3 | Type I IFN and antigen presentation pathways | BCR and GPCR signalling |
| 4 | Mitochondrial and T cell costimulatory pathways | DNA-templated transcription |

**Figure 5.2 Gene correlation heatmaps across subset pairs.** DEGs significantly modulated by ICB across each subset were identified and the change in expression across ICB was calculated. The gene expression delta values per individual for each subset were then cross-correlated by Pearson's correlation for each pair of subsets, using only individuals with sequencing data across both subsets. Correlation heatmaps were then plotted with clustering into 4 modules for each subset based on correlation coefficients and GOBP pathway enrichment analysis performed for each module. Heatmaps and summarised pathways for each module are provided for comparisons between **(a)** $CD8^+$ T cells and $CD14^+$ monocytes, **(b)** $CD8^+$ T cells and $CD19^+$ B cells and **(c)** $CD14^+$ monocytes and $CD19^+$ B cells.

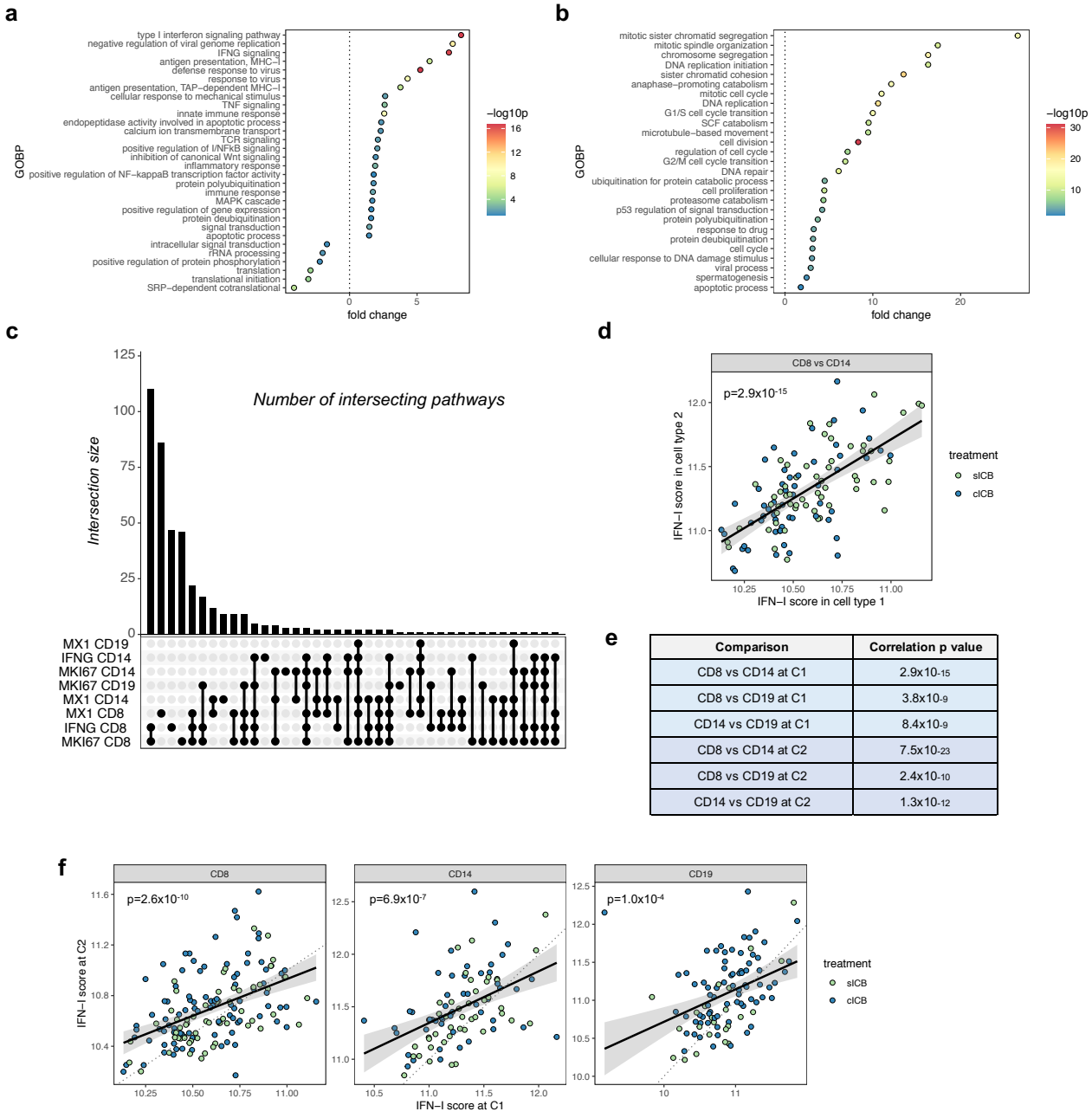
## 5.4 Changes in monocytes and B cells according to T cell factors

To elaborate on some of these cross-subset observations, I next focused on pathways modulated in $CD14^+$ monocytes and $CD19^+$ B cells in accordance with certain biological and clinical $CD8^+$ T cell measures. By connecting these pathways with those engaged by $CD8^+$ T cells within these contexts, a more granular understanding of cross-subset associations, and monocyte and B cell processes that associate with clinical ICB responses, could be developed.

### 5.4.1 T cell mitotic and interferon signatures

I first explored what pathways in monocytes and B cells associated with the mitotic T cell response, given how strongly it links to IgG4 binding and is likely to be immediately downstream of ICB. I used normalised expression of *MKI67* in $CD8^+$ T cells as a proxy for mitosis, calculating its difference between C1 and C2 and fitting linear models to identify genes that change in expression accordingly. After fitting monocyte genes to this *MKI67* change and performing GOBP pathway analysis, I found that the top pathway was type I IFN signalling rather than mitosis, with analogous 'negative regulation of viral genome replication' and 'defense response to virus' pathways also being highly enriched (Figure 5.3a). ICB is unlikely to bind directly to monocytes, evidenced by the lack of flow IgG4 staining on monocytes, and so it appears that the IFN-I monocyte response may be triggered downstream of $CD8^+$ T cells. Additional pathways that were strongly linked to the CD8 mitotic response were monocyte IFN-ɣ signalling and MHC-I upregulation, which both likely result from IFN-ɣ production by mitotic $CD8^+$ T cells. When performing similar analysis for B cells, I found that CD8 mitosis paralleled the induction of mitosis in B cells, with few other pathways related to discernable biological processes being significantly enriched (Figure 5.3b).

To build on these results, I similarly identified the monocyte and B cell pathways correlating




| Comparison | Correlation p value |
|---|---|
| CD8 vs CD14 at C1 | 2.9x10-15 |
| CD8 vs CD19 at C1 | 3.8x10-9 |
| CD14 vs CD19 at C1 | 8.4x10-9 |
| CD8 vs CD14 at C2 | 7.5x10-23 |
| CD8 vs CD19 at C2 | 2.4x10-10 |
| CD14 vs CD19 at C2 | 1.3x10-12 |

**Figure 5.3 Monocyte and B cell associations with CD8⁺ T cell mitosis, IFN-I and IFNg signatures. (a-b)** Gene expression changes between C1 and C2 in monocytes (a) and B cells (b) were correlated against *MKI67* in CD8⁺ T cells following ICB. Significant correlation was detected using a linear model regressing out age, sex, sequencing RNA input and batch covariates, and GOBP pathway enrichment was performed on the significant genes. **(c)** Similar pathway analysis was conducted across CD8⁺ T cells, monocytes and B cells using change in expression of *MKI67*, *MX1* and *IFNG* as variables. The overlap in significant pathways was plotted using an Upset plot. **(d-e)** IFN-I signatures were scored in each subset at C1 and C2 using the geometric mean expression of genes enriched in the 'type I interferon signaling pathway' from GOBP. CD8⁺ T cell and CD14⁺ monocyte scores at C1 (d) and across all other subset pairs at C1 and C2 (e) were plotted and the correlation p-values calculated (n=44-119, Pearson's correlation test). **(f)** IFN-I signatures at C1 and C2 were correlated within the same subset (n=150, 96 and 99, Pearson's correlation test).

with T cell type I IFN and IFN-ɣ signalling, using *MX1* and *IFNG* for proxy expression. I compared the pathways that were modified in accordance with CD8 mitosis, IFN-I and IFN-ɣ across the three cell types, visualising similarity using an Upset plot (Figure 5.3c). This demonstrated that $CD8^+$ T cell *IFNG* and *MKI67* expression shares the most downstream signalling similarity whilst across subsets, there was greatest overlap between T and B cell pathways downstream of CD8 mitosis and IFN-ɣ signalling. This was followed by overlap between IFN-I associated pathways in CD8 and CD14 genesets. Given all the shared pan-subset IFN-I signatures observed, I decided to formally investigate this by generating IFN-I scores across each subset's RNAseq samples, basing this off the geometric mean expression of genes in the GOBP pathway 'type I interferon signaling' - in an identical method to previous analysis of CD8 IFN-I scores and clinical outcome. I correlated scores across pairs of subsets at either C1 or C2, finding individuals with higher CD8 IFN-I signalling also tended to have increased CD14 and CD19 IFN-I signalling score as well (Figure 5.3d-e). The most significant correlation was between CD8 and CD14 cells, possibly reflecting the more concordant gene expression changes observed between these two subsets, as well as greater statistical power from more overlapping samples. These correlations were not sensitive to patient age, sex or treatment type, or sequencing-related covariates. Finally I tested whether individuals with higher C1 IFN-I signalling also had higher IFN-I score at C2, performing within subset correlations of socres at these two timepoints. Scores were strongly correlated across all cell types irrespective of these other variables (Figure 5.3f). Overall it appears that CD8 mitosis and the associated IFN-ɣ produced by this cell population correlates with parallel processes in $CD14^+$ monocytes, whilst mainly inducing mitosis in B cells instead, with a global wave of IFN-I signalling also emerging.

### 5.4.2 T cell clonality and effector score

I next tried to understand how T cell clonality relates to monocyte/B cell gene expression profiles. I used DESeq2 to identify the C1 and C2 genes that correlate with CD8 Gini index values at C1 or C2. The Gini index ranges from 0 to 1 and is a measure of clonal inequality i.e. many large clones will shift the index more towards 1 whilst an abundance of unexpanded clones will lower it towards 0. Gini values were used as a quasi-normalised metric to increase power to detect relevant correlations. To gauge the strength of the relationship between T cel clonality and the transcriptomic profiles of monocytes and B cells, I counted the number of enriched pathways for each set of significant genes (Figure 5.4a). I found limited evidence of interaction between monocytes and CD8 clonality except when looking at C1 Gini correlations with C2 monocyte gene expression. Whether this reflects limited interaction,

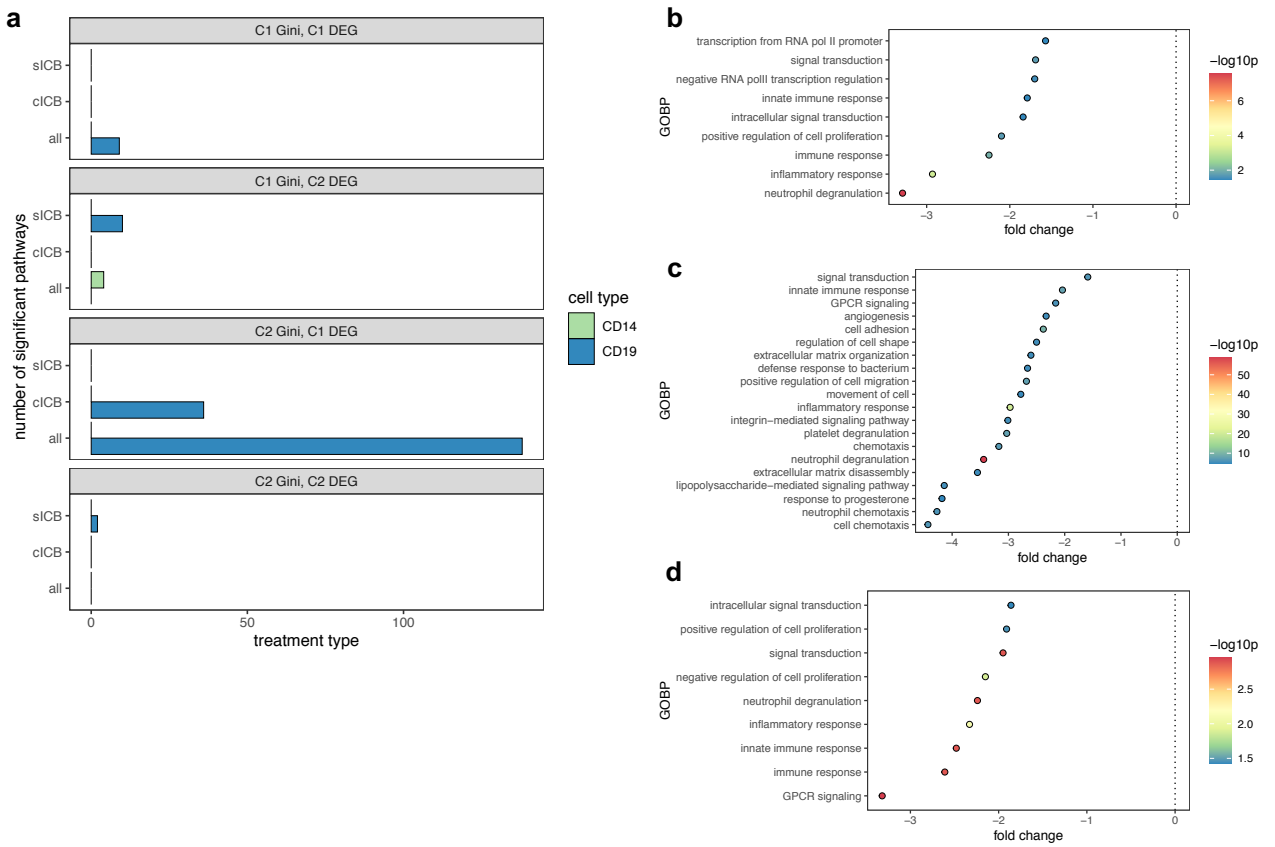



**Figure 5.4 Monocyte and B cell associations with CD8⁺ T cell clonality.** **(a)** Monocyte and B cell gene expression was correlated with CD8⁺ T cell Gini index values in DESeq2, regressing out age, sex, sequencing RNA input and batch covariates. Significantly correlated genes were subjected to GOBP pathway enrichment analysis and the number of significant pathways was plotted (adjusted p <0.05). Analysis was conducted at C1 or C2 for gene expression and Gini index values, and across different ICB treatment types. **(b-c)** Significant B cell pathways at C1 that correlate with C1 Gini index (b) and C2 Gini index (c) were plotted. **(d)** C1 B cell genes that significantly correlate with CD8⁺ T cell Effector score at C2 were identified using the same differential expression analysis as in (a) and significantly enriched pathways in that geneset were plotted.

or instead, limited statistical power is unclear. Looking at B cells, there was saw evidence of some CD8-B cell associations at C1, with the observed pathways shown in Figure 5.4b. Interestingly, these pathways, most of which were inflammatory, were universally associated with reduced Gini values, suggesting B cell inflammation is linked to T cell naivety, even in the absence of ICB. Although no pathways were identified when examining if baseline CD8 Gini values influence C2 B cell expression, a large number of C1 B cell genes and pathways were found to predict on-treatment CD8 clonal inequality (Figure 5.4c). Many of these pathways were similar to Figure 5.4b, and in the same direction, again showing that many aspects of immunity are remarkably preserved across ICB treatment, and reinforcing that B cell inflammation associates with greater numbers of small clones. The abundance of B cell pathways that correlated with lower clonality was intriguing, so I also tested what observations could be seen when examining B cell pathways that predict Effector score. Looking at C1 CD19 expression associated with Effector score at C2, B cell genes within inflammation, GPCR signalling and signal transduction pathways associated with decreased Effector presence (Figure 5.4d). This ultimately suggests that the early inflammatory B cell state leads C2 clonal equality and weaker Effector responses, and overall poorer T cell responses to ICB.

### 5.4.3 Lymphocyte stability

In association with T cell clonality and effector function, I previously identified the clinical relevance of monitoring lymphocyte stability across the first cycle of ICB. Assessing genes and pathways that were uniquely modulated in $CD8^+$ T cells depending on stable vs falling LS groups, mitosis and IFN-I were found to associate with falling LS whilst T cell homeostatis and metabolism were linked with stable responses. I performed analogous analysis using CD14 and CD19 RNAseq data to identify uniquely modulated pathways across LS in these cell types. Plotting the enrichment fold changes of pathways modulated in monocytes revealed that stable LS responses required monocyte class I MHC upregulation and T cell co-stimulation, whilst limiting the IFN-I response and innate inflammation (Figure 5.5, left). These collectively mimic the results found in the $CD8^+$ T cell analysis, and again reinforces this pattern of shared type I IFN responsivity being detrimental to overall outcome. In B cells, I saw falling LS was accompanied by large degrees of B cell transcriptional activity, typified by IFN-I and innate inflammatory pathways (Figure 5.5, right). Altogether, this suggests that individuals with falling LS have universal and non-specific innate-type immune responses to ICB, whilst those with stable LS have increased T cell expansion and activation, supported in part by monocyte co-stimulation. The observed increase in transcriptomically-active B cells

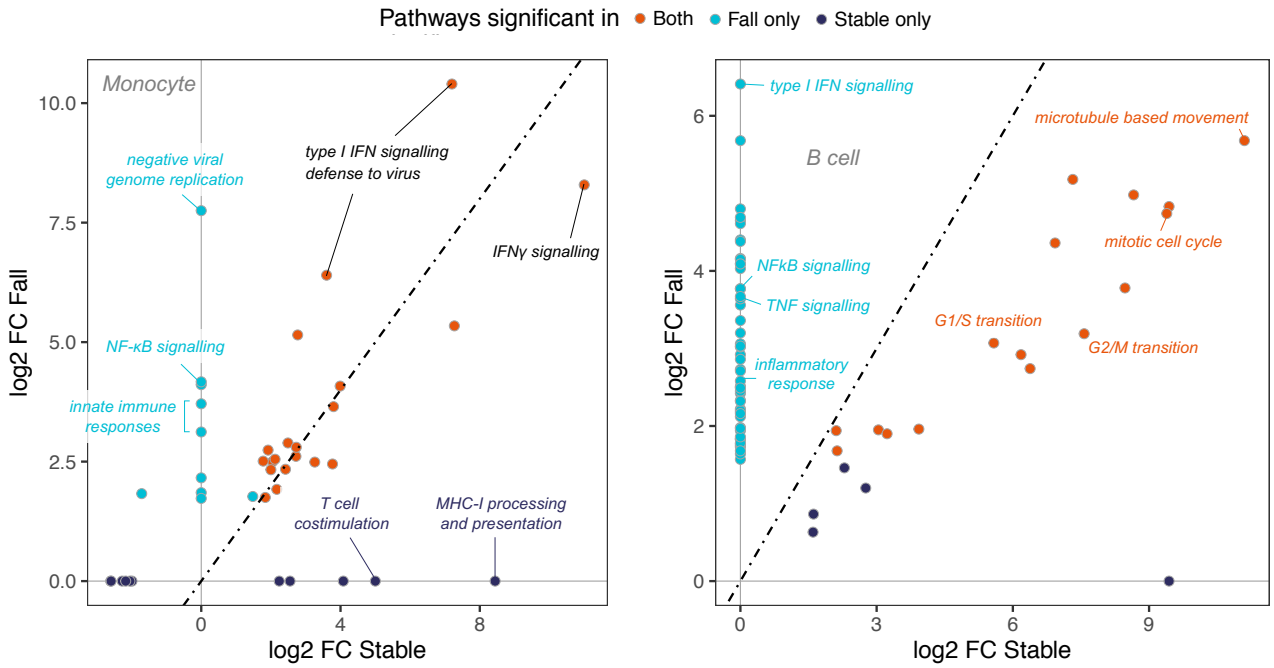



**Figure 5.5 Monocyte and B cell transcriptomic associations with lymphocyte stability.** Patients were separated into those with stable or falling LS and the monocyte and B cell genes significantly modulated by ICB in each LS group were identified. GOBP pathway enrichment analysis was performed on each geneset and pathways were plotted based on the pathway fold change values, and classified based on whether they were significant across both LS groups, or unique to either the stable or falling groups.

seemingly contributes to generalised inflammation and poorer $CD8^+$ T cell responses.

To further dissect subset-based contributions to lymphocyte stability, I leveraged the results of a GWAS performed by Groha et al[265] which demonstrated that lymphocyte stability was associated with the SNP rs16906115 in the *IL7* locus. In this paper, it was identified that individuals homozygous for the major allele had significantly reduced lymphocyte stability relative to individuals carrying at least one copy of the minor allele. I first checked whether these results could be replicated using array genotyping data from the patient cohort. When I examined lymphocyte count at C1 and C2 for the cohort separated by major allele carriage, I saw that there was indeed a significant reduction in lymphocyte count in the dominant allele carriers but not in those with the alternate allele (Figure 5.6a). To establish that this difference did not arise from differences in statistic power, I compared the magnitude of lymphocyte count changes between major and minor allele carriers, finding a significant difference in delta values (Figure 5.6b). Given I had previously demonstrated that LS correlated with increased on-treatment clonality, I checked to see if there was an effect of the rs16906115 SNP on $CD8^+$ T cell clonal measures at C2. Separating individuals based on treatment type, I found SNP carriers had significantly increased clonal inequality, in line with their LS values (Figure 5.6c). This effect was most prominent for sICB-treated individuals, who also had significantly higher clonality when measured through other readouts like total number of T cell clones, and large clone count (Figure 5.6d). Interestingly, SNP carriers also had significantly higher percentages of $CD8^+$ T cell clones found at both C1 and C2 (Figure 5.6d, right), in line with the increase in clonal persistence associated with LS and the homeostatic effects of IL7.

I then wanted to understand how this SNP had such major downstream effects, far above typical cis-acting SNPs with the most likely explanation being that the SNP modulates levels of IL7, leading to changes in T cell clonality. I therefore assessed the levels of *IL7* expression across different cell types that bulk RNAseq had been performed on. *IL7* expression was by far the highest in B cells across all major peripheral PBMC subsets and particularly enriched in melanoma patients (Figure 5.6e), although there was no difference in *IL7* expression following treatment (data not shown). I next checked whether the expression levels of IL7 in B cells were affected by rs16906115 genotype. Interestingly, individuals with the alternate alelle had significantly higher B cell *IL7*, particularly at C1, whilst the same genotypic effect was not observed in healthy donors despite the comparatively larger sample size (Figure 5.6f). This suggests that the phenotypic variation modulated by variation at this SNP may require the context of chronic stimulation to become evident, but whether this is a cancer-specific observation is unclear. To understand what aspects of B cell phenotype also are associated with rs16906115, I calculated the percentage of chain usage across B cell clones, given that

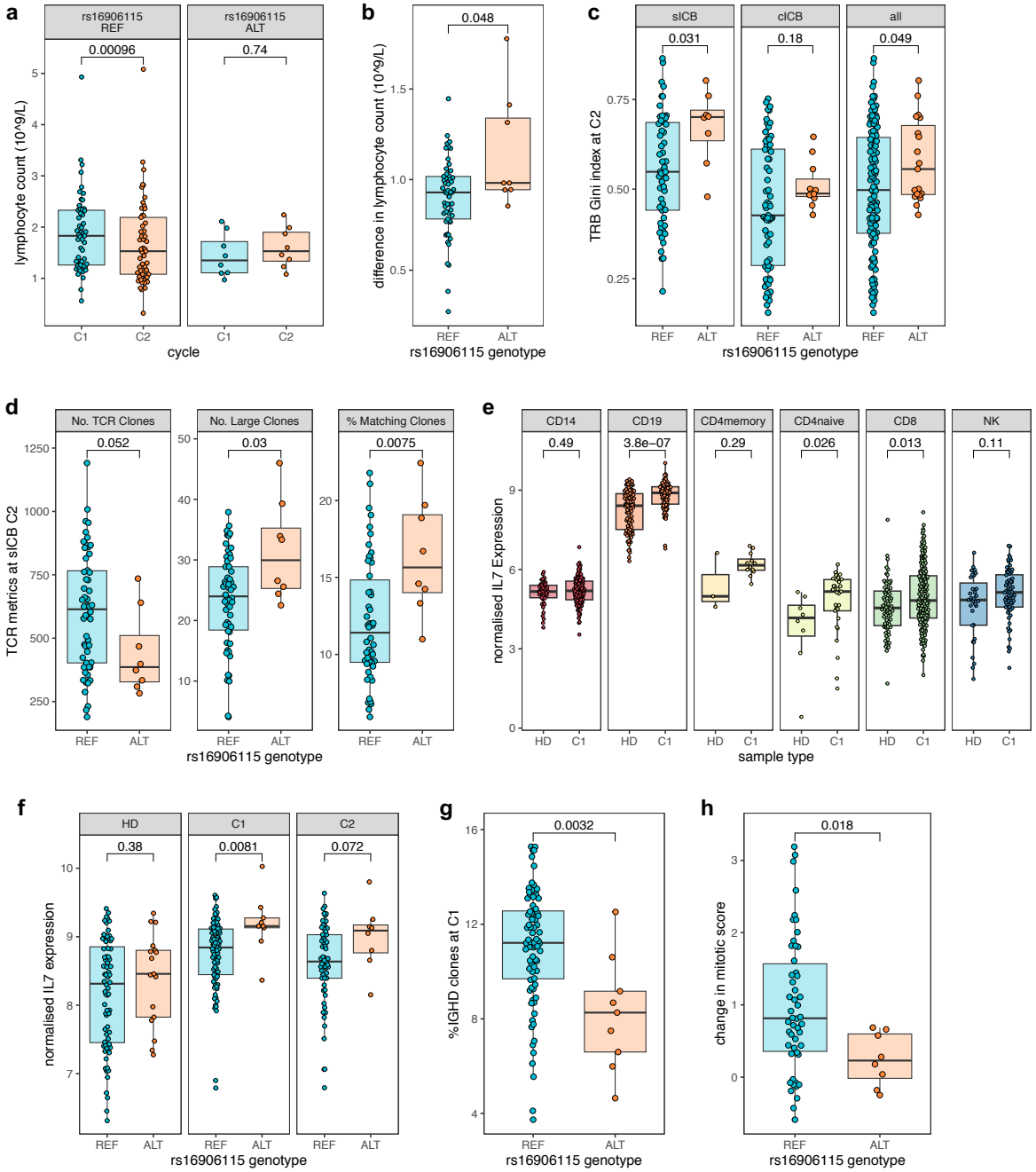



**Figure 5.6 Immunological associations with the *IL7* SNP rs16906115. (a)** Lymphocyte count across C1 and C2 for sICB-treated patients homozygous for the major allele at rs16906115 (REF), or carrying the alternate allele instead (ALT) (n=53 and 8). **(b)** Absolute change in lymphocyte count in REF vs ALT sICB treated patients (n=61). **(c)** Difference in C2 Gini index values for $CD8^+$ T cells for REF and ALT individuals across ICB treatment type (n=138). **(d)** Difference in total numbers of TCR clones, number of large clones and percentage of clones with matching TRB sequences between C1 and C2 across REF and ALT alleles (n=61). **(e)** Bulk RNAseq expression of *IL7* across different peripheral immune subsets. Expression was compared between healthy individuals (HD) and C1 melanoma patients (n=15-243). **(f)** Change in *IL7* expression in B cells according to rs16906115 genotype (n=93, 89 and 66). **(g)** IGHD clone usage at C1 by rs16906115 genotype, based on MiXCR BCR recovery in B cell bulk RNAseq data (n=89). **(h)** The change in $CD8^+$ T cell mitotic score between C1 and C2 was calculated and compared in individuals with major and alternate allele carriage for rs16906115 (n=61). All statistical comparisons were performed using two-sided Wilcoxon signed-rank tests.

increased IgD and IgM clones frequently associate with B cell naivety. Whilst no other differences in chain usage were observed, carriage of the alternative rs16906115 allele was associated with significantly lower IgD usage (Figure 5.6g). IgD is expressed to a lower extent in memory B cells and antibody secreting cells, possibly suggesting that SNP carriage is associated with altered subset frequency - as opposed to a direct trans-effect on *IGHD* expression. Lastly, to reaffirm some of the prior observations around lymphocyte stability, homeostatic proliferation and *MKI67* expression, I found that SNP carriage was associated with significantly lower mitotic induction, as measured by the change in mitotic score between C1 and C2, particularly for sICB patients (Figure 5.6h). Collectively, this suggests that variation in B cell *IL7* is linked to downstream impacts on T cells at C2, again affirming the influence of the baseline B cell state and cross-subset cytokine behaviour on $CD8^+$ T cell changes during ICB.

## 5.5 Changes in T cells based on B cell chain usage

Given C1 B cell chain usage (IgD) and $CD8^+$ T cell response to ICB were associated, I investigated whether other B cell chains had similar observable effects. Using the chain frequencies of IgA, IgD, IgE, IgG1-4 and IgM, I constructed linear model arguments to identify $CD8^+$ T cell genes that changed in expression across ICB in accordance with the proportions of each chain. To compare the transcriptomic impacts of differential chain usage, I performed pathway enrichment for each associated geneset and used a clustered heatmap for visualisation. C1 IgE proportion was strongly linked to many downregulated pathways in $CD8^+$ T cells following ICB (Figure 5.7a), spanning IFN-ɣ and TLR signalling, inflammatory response, TNF production and chemotaxis, and altogether suggesting there is an immunosuppressive interaction between IgE and $CD8^+$ T cells. Across other B cell chains, less of an effect was seen. A unique set of $CD8^+$ T cell pathways was upregulated in individuals with greater IgM, including SRP-dependent cotranslational and rRNA processing, DNA-templated transcription and mitotic signalling. Many of these pathways are enriched in the naive compartment of $CD8^+$ T cells, again suggesting that baseline naive B cell responses are linked to parallel CD8 naivety. Higher IgA was associated with increased CD8 immune responses and GTPase activity, which was pathway previously seen to be associated with $CD8^+$ T cell clonal expansion (Figure 4.1), and so may be relevant for T cell activation post ICB. Finally IgD, which was anti-correlated with clonal expansion in the context of variation at rs16906115, was associated with generalised inflammation pathways, but unlike IgA, anti-correlated with GTPase activity (Figure 5.7b). Overall, this suggests that B cell naivety

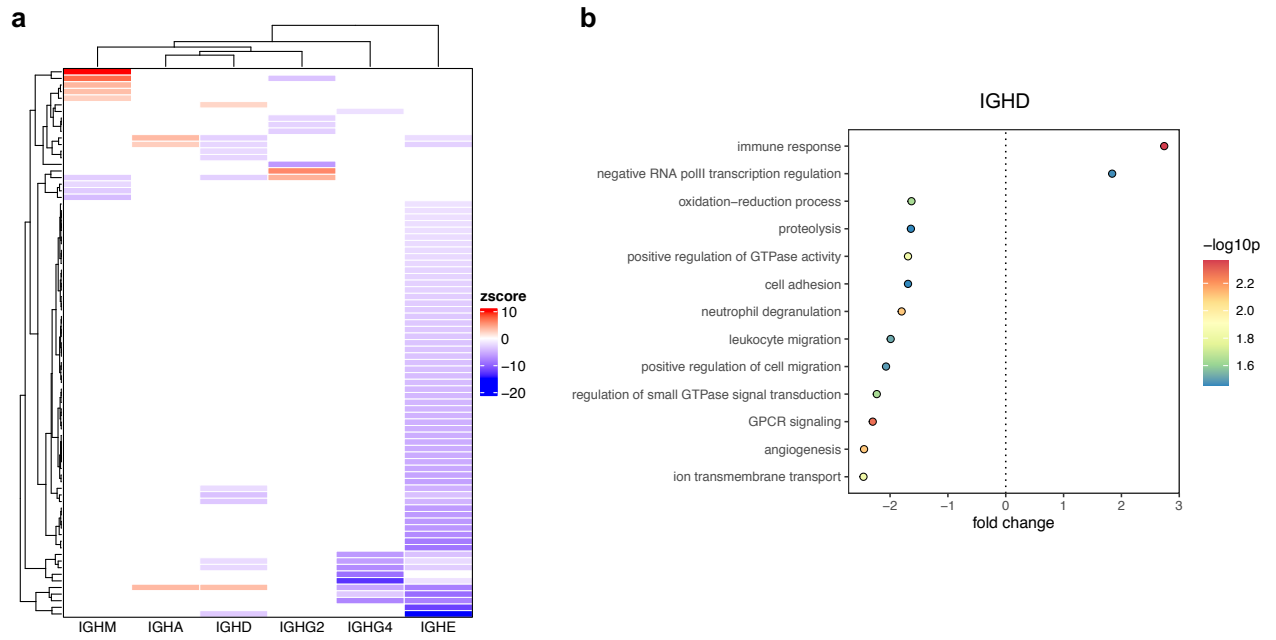



**Figure 5.7 CD8⁺ T cell transcriptomic associations with B cell chain usage. (a)** Change in CD8⁺ T cell gene expression between C1 and C2 was calculated and correlated with the proportion of chain usage for each B cell sample. B cell chains were recovered using MiXCR on C1 B cell bulk RNAseq and chain information extracted from heavy Ig chains. Correlations were performed using linear models regressing out age, sex, sequencing RNA input and sequencing batch. GOBP pathway enrichment was then performed on each geneset and the pathway zscores used to generate a clustered heatmap. **(b)** Significant CD8⁺ T cell GOBP pathways associated with higher C1 IGHD chain usage.

(represented by IgM) and aberrant IgE signalling act as immune dampeners on the $CD8^+$ T cell responses to ICB. IgD and IgA perform potentially opposing roles for T cell activation where they encourage decreased and increased GTPase signalling respectively. Baseline B cell chains appear to have limited effects on type I IFN signalling changes in $CD8^+$ T cells, suggesting perhaps these signals instead come mainly from monocytes.

## 5.6 Overall associations of cross-subset heuristics

Given a large number of subset factors were identified that seem to be correlated or anti-correlated with each other, I was interested in seeing whether a network plot that linked all of these together could be constructed. I curated scores for $CD8^+$ T cell subsets, large clone count, lymphocyte stability, T cell IgG4 binding, cell-type type I IFN scores and B cell IL7 expression, and generated a correlation matrix. I then used the corrr package to create a network, where the strength of shading represents the correlation between two factors (Figure 5.8). Two connected factors acted as central nodes; CD8 IgG4 binding and Mitotic score at C2 on $CD8^+$ T cells. This is interesting given I hypothesised that downstream signalling of IgG4 on CD8s drives the main signalling patterns observed on all cell subsets, and the two are tightly correlated. The degree of IgG4 binding was mostly aligned with $CD8^+$ T cell subset scores, grouped on the right side of the network, specifically being correlated with Naive and CM subset score whilst anti-correlating with Effector score. An additional T cell metric on the right side of the network was large clone count, which was positioned between Effector and EM score. Interestingly, EM score was distally positioned relative to all other metrics, suggesting that this subset may have a distinct interactions with other peripheral factors, and could also be influenced by non-peripheral features.

On the left side of the network, mitotic $CD8^+$ T cell score was linked with IFN-I scores, forming a pan-cell type IFN-I module. Interestingly, this was anti-correlated with B cell *IL7* expression, which reflects its opposing relationship with lymphocyte stability; IL7 promotes lymphocyte stability which is instead negatively associated with type I IFN responses. It is also interesting to observe the separation between subset-based scoring and biological processes such as mitosis and type I IFN response, suggesting that inter-individual variation at both of these levels may trump the strength of subset-pathway associations. Overall, there appears to be 3 distinct facets of the immune response to ICB shown in the network; a potential dysfunctional module characterised by unwanted or excessive type I IFNs and mitosis (bottom left), a secondary group reflecting cell naivety and quiescence (bottom right), and a final group representing desirable T cell immune function (top and upper right).

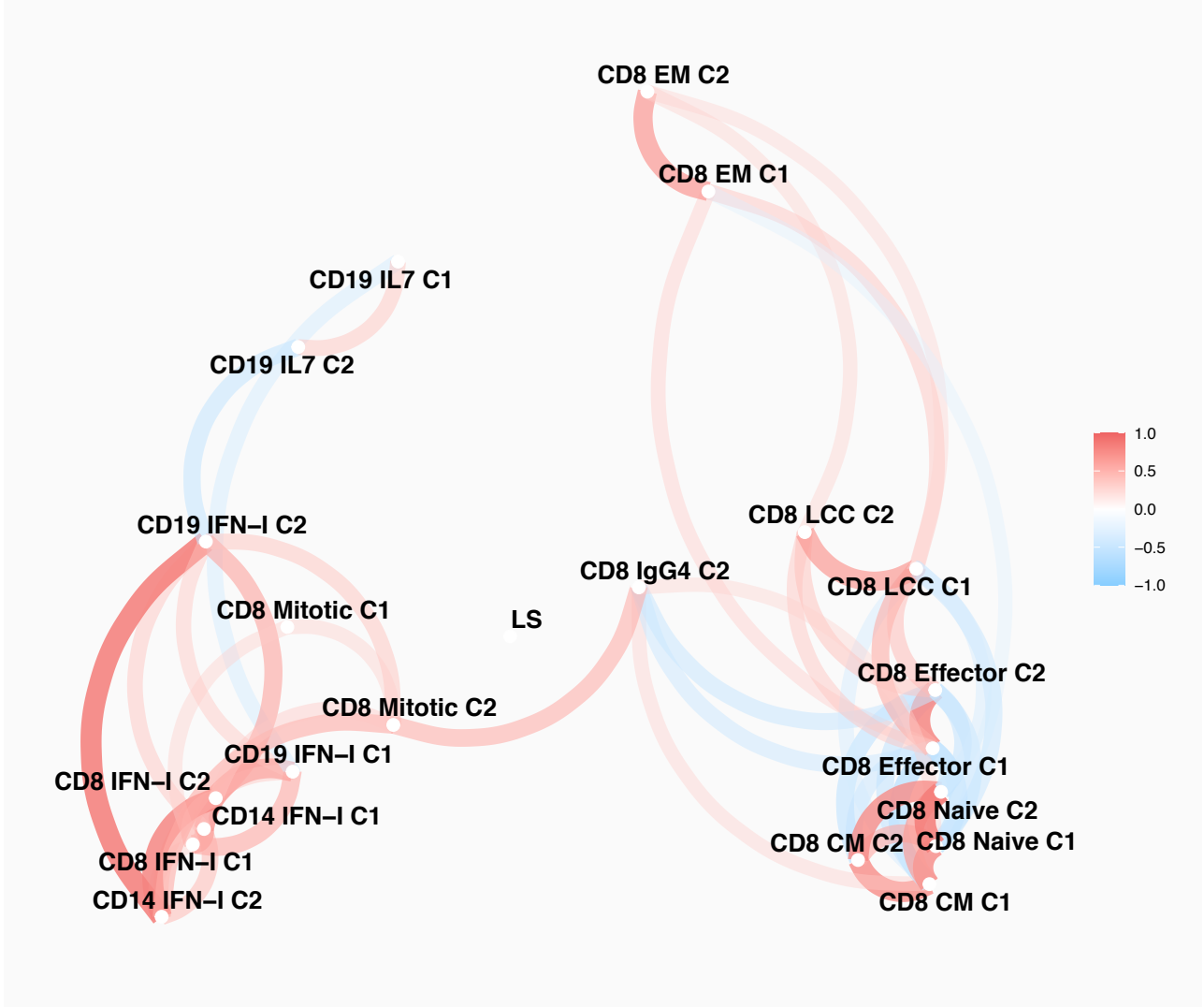



**Figure 5.8 Pan-subset heuristic correlation network.** Different measures identified across bulk RNAseq analyses such as CD8$^+$ T cell subset scores, proportion of IgG4 flow cytometry staining in CD8$^+$ T cells, subset IFN-I scores, B cell *IL7* expression and lymphocyte stability were correlated and the corrr package used to construct a correlation network. The strength and direction of correlations is represented by the shading and colour of the connector, with non-significant correlations as determined by Pearson's correlations not shaded.

## 5.7 Conclusions and Discussion

By comparing $CD8^+$ T cell responses with those from $CD14^+$ monocytes and $CD19^+$ B cells, I was able to understand global patterns of gene expression shared across PBMC subsets, and uncover potential interacting patterns between subset pairs. To summarise some of the results of this chapter:

- IgG4 binding in $CD8^+$ T cells leads to monocyte IFNG and mitotic signalling, and $CD19^+$ immunoglobulin production and activation
- There is strong sharing of transcriptomic modules between $CD8^+$ and $CD14^+$ cells with naive-associated pathways globally correlating across all cell subsets
- IFN-I signalling is conserved across all subsets whilst CD8 mitosis appears to particularly associate with CD14 IFN-I responses
- Baseline B cell activation is associated with limited clonal expansion and Effector presence at C2
- Monocyte and B cell IFN-I and generalised inflammation are both associated with poorer LS responses, whilst monocyte MHC-I presentation is upregulated in stable LS
- *IL7* expression is enriched in B cells and promotes T cell expansion as revealed by analysis of genetic variation at rs16906115
- Higher IgD chain usage in B cells associates with reduced receptor signalling and increased inflammation in $CD8^+$ T cells
- A network correlation model recapitulates observations around cross-subset interactions and the effects of ICB

Although a myriad of monocyte and B cell pathways that associate with CD8 activity following ICB were identified, I focused on a few particular characteristics such as shared IFN-I signalling and mitosis. CD8 mitosis was tightly linked to CD14 IFN-ɣ signalling, with a likely explanation being directly increased IFN-ɣ production from $IgG4^+$ $CD8^+$ T cells, also leading to CD14 activation, and class I MHC upregulation. Based on their increased amounts of type I IFN machinery[330,331], it is tempting to then speculate monocytes drive the IFN-I response which then has downstream paracrine signalling influences on the other immune subsets. In support of this, CD8 mitosis and IFN-I signalling were typically clustered in separate hierarchical groups in earlier analysis, and no direct enrichment of IFN-I signalling was observed in mitotic $CD8^+$ T cells by single-cell RNAseq. Interestingly, CD8 α-IgG4 staining and mitosis associated with a variety of distinct pathways that were upregulated in monocyte, namely both IFN-I signalling, which may contribute to hypofunctional $CD8^+$ T cells and poor ICB outcome, as well as class I MHC, which LS analysis seems to indicates

is beneficial to $CD8^+$ T cell responses. It could be that monocyte responses to ICB are dictated by a balance between MHC-I expression and IFN-I production, particularly if these are differentially expressed across monocyte subsets. Exploring this hypothesis through single-cell RNAseq would definitely be of interest. Krieg et al[323] identified that monocytes with higher expression of HLA-DR correlated with $\alpha$-PD-1 outcome in their study, reinforcing the potential importance of adequate T cell co-stimulation from monocytes for clinical ICB benefit. In further support of this, Zemek et al[331] identified that fast-off modulation of monocyte IFN-$\beta$ signaling was associated with clinical outcomes for ICB in dual-tumour murine models, whilst non-responders maintained high levels of monocyte IFN-I following tumour implantation and ICB treatment. Globally, general monocyte count, IFN-I and inflammation all associated with poor LS and presumed poor response to ICB, in accordance with many previous studies[140,142]. It is therefore tempting to speculate that generalised inflammation helps drive the non-productive mitotic signature seen in $CD8^+$ T cells, given that this seems to be distinct from antigen-driven clonal expansion. Collectively, these observations indicate that the monocyte compartment can contribute to beneficial immunity during ICB, but often associates with generalised inflammation that dampens productive T cell responses instead.

For B cells, one of the most striking observations made was around the impact of baseline B cell transcriptomic activity and activation, and the suboptimal T cell responses this is associated with. One such example was increased IgD proportions corresponding with reduced induction of GTPase signalling in $CD8^+$ T cells, thus limiting downstream TCR activation[317]. Interestingly, when investigating transcriptomic associations across all BCR chains, IgE was associated with reduced T cell function, potentially in line with its relationship with Th2 responses[332], as well as increase in generalised inflammation, in keeping with its role in allergy auto-immunity. Outside of chain usage, baseline B cell activation generally anti-correlated with CD8 clonal expansion and effector function at C2. Much like how aberrant monocyte inflammation is linked to auto-immune diseases[333], inflammatory B cells are implicated in lupus and multiple sclerosis development[334,335]. In a parallel manner to monocytes, it may be that the B cell balance of *IL7* expression and T cell co-stimulation, versus their inflammatory behaviour, dictates whether they are beneficial or not in the context of ICB. Furthermore, how antibody production fits into this dynamic model is unclear, particularly given that cancer-specific immunoglobulins are thought to license enhanced tumour killing[194]. More generally, understanding the directionality of the cross subset interactions would be valuable, as the driver cells and processes that lead to type I IFN responses, inflammation and expanded T cells could then be inferred. This could potentially be achieved by adapting

statistic tests used in network topology and/or genetics analysis such as the Steiger test[336]. Lastly, further exploration around relevant monocyte and B cell pathways, as well as how ICB impacts other peripheral immune cell types such as $CD4^+$ T cells, and adding these factors into the network analyses, will improve the resolution of how ICB is understood to work on a cellular and clinical basis.

# Chapter 6

# Identifying subset interactions in single-cell RNAseq analysis of PBMCs

## 6.1 Summary and Aims

Increasingly, single-cell sequencing methods are being employed to understand biological heterogeneity in new detail, and particularly in the diverse landscapes of cancer and immunity. Throughout my previous analysis, I have combined analyses across bulk RNAseq of $CD8^+$ T cells, $CD14^+$ monocytes and $CD19^+$ B cells, single-cell RNAseq of $CD8^+$ T cells and flow cytometry. To therefore unify and validate some of these observations across these disparate platforms, I performed single-cell RNAseq of PBMCs from n=22 melanoma patients and healthy donors.

In this chapter, I will describe single-cell PBMC populations in melanoma in detail and then investigate how their peripheral proportions and interactions are modulated by different clinical and biological contexts. The specific aims I will cover are the following:

- What subsets are PBMCs from melanoma patients comprised of at single-cell resolution?
- How does single-cell resolution improve our understanding of biological processes such as *IL7* expression in B cells?
- How do proportions of subsets across cell types correspond with each other?
- What additional information can cell-cell interaction analysis tell us of clinical contexts such as lymphocyte stability?
- What specific peripheral subsets have the greatest amounts of interaction?
- How do regulatory T cell correlations, expansion and expression correspond with

clinical responses to ICB?
- Do subset interactions capitulate our observations in bulk RNAseq?

## 6.2 Annotating subsets in single-cell RNAseq of melanoma and healthy PBMCs

I performed single-cell RNAseq on PBMC samples across melanoma and healthy donors with my experimental and analytical pipeline described in detail in the Methods (Figure 6.1). In short, I batched paired C1 and C2 samples from MM patients receiving cICB, along with healthy donors and subjected them to 5' gene expression and VDJ-sequencing, recovering n=236,661 cells after pre-processing and genetic demultiplexing to remove heterotypic doublets. I performed subset annotations across two stages, where I initially clustered all recovered cells and then removed identifiable clusters of homotypic doublets, based on their VDJ information, cluster gene expression, expression similarity to genotypic doublets, and reference mapping using SingleR. In particular for the cluster gene expression approach, I calculated the proportion of cells in each cluster that expressed key cell type genes such as *CD3E* (T cells), *LYZ* (monocytes), *CD79A* (B cells) etc, and looked at their distribution. For many of these markers, I found a bimodal expression pattern and so used the local minimum inflexion as a cutoff for marker positivity of each cluster. Using this method, Clusters that had positive expression of *CD3E* were identified as T cells, whilst those with expression of both *CD3E* and *LYZ* were characterised as T cell-monocyte doublets. After removing identifiable doublets, I then reclustered the remaining cells and re-annotated using the aforementioned approach, thereby identifying a cluster of B cells adjacent to small groups of plasmablasts (PB) and plasmacytoid DCs (pDC), which formed a bridge to a group of conventional DCs (DC) loosely connected to a cluster of monocytes (Myeloid). Separate to these clusters was a joined group of T cell and NK cells, with cells resembling megakaryocytes (Mega) present in the middle of the UMAP projection. To annotate subsets within each cell type, I separately reclustered each of the key cell types, using additional marker expression and SingleR inferences to label each specific subset. Altogether, I identified 10 subsets of B cells, 6 subsets of monocytes, 4 DC subsets, 8 NK subsets and 18 T cell subsets separated into 7 $CD4^+$ T cell subsets and 8 $CD8^+$ T cell subsets, and 4 unconventional and mitotic subsets. Subsets and key markers identifying each cell subset are presented in the Appendix. Of note, many cell types had a specific subset that was enriched for IFN-I signalling genes such as *MX1* and *ISG15*, suggesting that the IFN-I responses previously observed are actually limited to a specific population of cells, rather than across the whole cell type. As a further

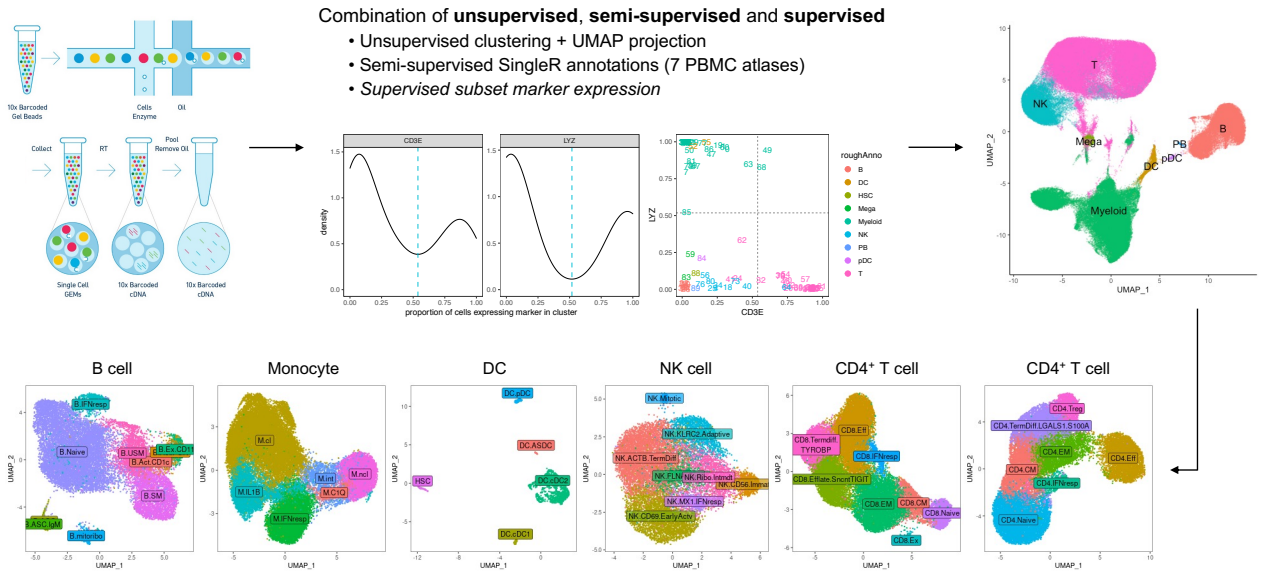



**Figure 6.1 Single-cell RNAseq workflow for sample batching, PBMC clustering and subset annotation.** Schematic demonstrating droplet encapsulation of single-cells using 10x Genomics, followed by bioinformatic processing of the single-cell sequencing data. A combination of three bioinformatic approaches were used to annotate PBMC clusters, including one where cell type signature genes were scored across each cluster and distributions plotted (Methods). For subset annotations, cells types were individually reclustered and annotated in finer resolution.

characterisation of all PBMC subsets, I identified the significantly distinguishing markers across subsets within a cell type using Seurat's *FindAllMarkers* function, and performed GOBP pathway analysis (Figure 6.2). Comparing pathways across PBMC subsets, I identified shared enrichment of certain subset pathways across cell types, such as (1) SRP-dependent cotranslational processing in naive B, monocyte, NK and T cell subsets, (2) inflammatory response in switched memory B cells, all DC subsets, all monocyte subsets except non-classical monocytes, immature NK cells and several T cell subsets, (3) IFN-ɣ signalling in activated and exhausted B cells, intermediate, non-classical, complement-enriched and IFN-I responsive monocytes, and differentiated CD8$^+$ T cells, and (4) MHC-I enrichment in antibody-secreting B cells, non-classical and IFN-I responsive monocytes, terminally differentiated NK cells, and Effector CD8$^+$ and gamma-delta T cells. Altogether, I identified a total of 48 specific subsets across 8 different cell populations.




**Figure 6.2 GOBP pathway characterisation of PBMC pathways.** Differentially expressed genes across subsets within a cell type were identified using Seurat's *FindAllMarkers*. The significantly distinguishing genes were then passed through pathway enrichment analysis and pathways amongst the top 10 most significantly enriched across subsets were plotted.

## 6.3 Using single-cell RNAseq to uncover B cell dynamics associated with IL7

To demonstrate the power of single-cell RNAseq data to extend my previous observations, I focused on understanding the expression patterns of *IL7* across B cell subsets, given its clinical and biological relevance to lymphocyte stability and T cell clonality. To increase statistical power, I combined B cells from this single-cell PBMC dataset with additional single-cell RNAseq data of isolated B and T cells from other patients in our cohort to form a B cell dataset composed of healthy donor and C1 MM B cells (n=16,028 cells and 29 individuals). For simplicity in this dataset, I grouped cells into the four main B cell subsets of Naive, unswitched memory (USM), switched memory (SM) and antibody-secreting cells (ASCs), with clustering and phenotyping data in the Appendix. Bulk RNAseq analysis had previously showed that *IL7* expression was highest in peripheral B cells, increased in melanoma patients relative to healthy controls and that carriage of the alternate allele of the *IL7* SNP rs16906115 was associated with increased B cell *IL7*. I was able to replicate all of my aforementioned bulk observations using this single-cell data, showing highest *IL7* expression in B cells (data not shown), significantly higher median B cell *IL7* in each melanoma patient compared to healthy donors (p=0.00011, data not shown) and that patients with the alternate rs16906115 allele had significantly higher median B cell *IL7* versus those with just the reference allele (Figure 6.3a).

I aimed to understand how this difference in B cell *IL7* expression resulting from rs16906115 was mediated across subsets. I first compared *IL7* expression across the four B cell subsets, finding that USM B cell had the highest *IL7* expression across these four subsets, followed by SM, Naive and then ASCs (Figure 6.3b). I then looked at *IL7* expression based on rs16906115 genotype within each subset, finding no significant difference (Figure 6.3c). I wondered whether variation at this SNP instead influences the proportions of B cell subsets, such as by increasing numbers of *IL7*-high USM and SM cells. I calculated the proportion of each subset out of all B cells per individual, and found alternate allele carriage was indeed associated with significantly higher USM proportion, with parallel trends of increases in SM and decreased Naive B cells (Figure 6.3d). These results are consistent with my observation that the rs16906115 alternate allele was associated with lower amounts of IgD, with USM, SM and ASCs having minimal *IGHD* expression compared to Naive B cells (Appendix). Finally, I wanted to understand whether increased B cell *IL7* was associated with B cell clonal expansion in a similar manner to T cells. I used the original PBMC single-cell RNAseq data, since both subset and gene expression information and processed BCR sequencing was

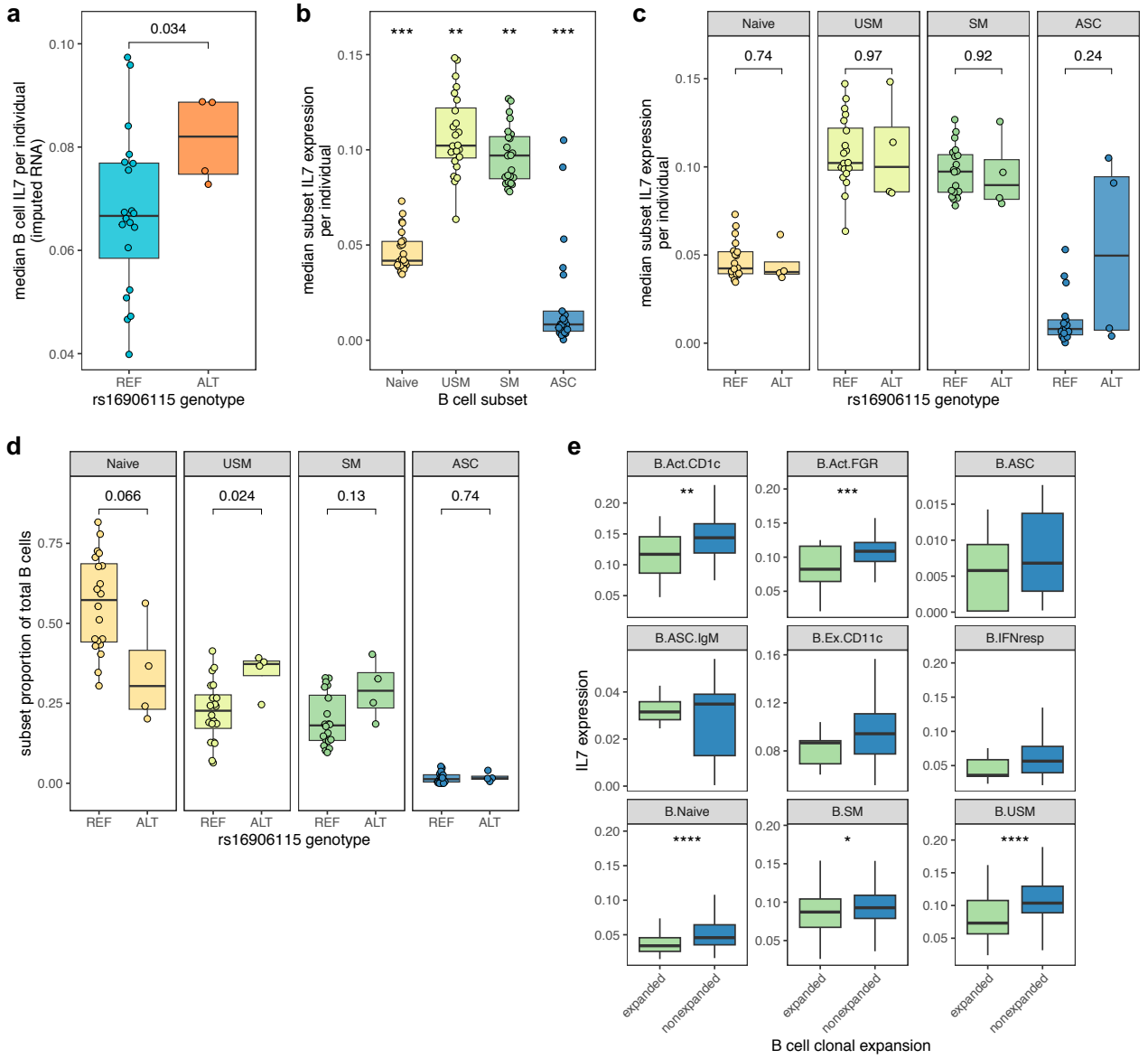


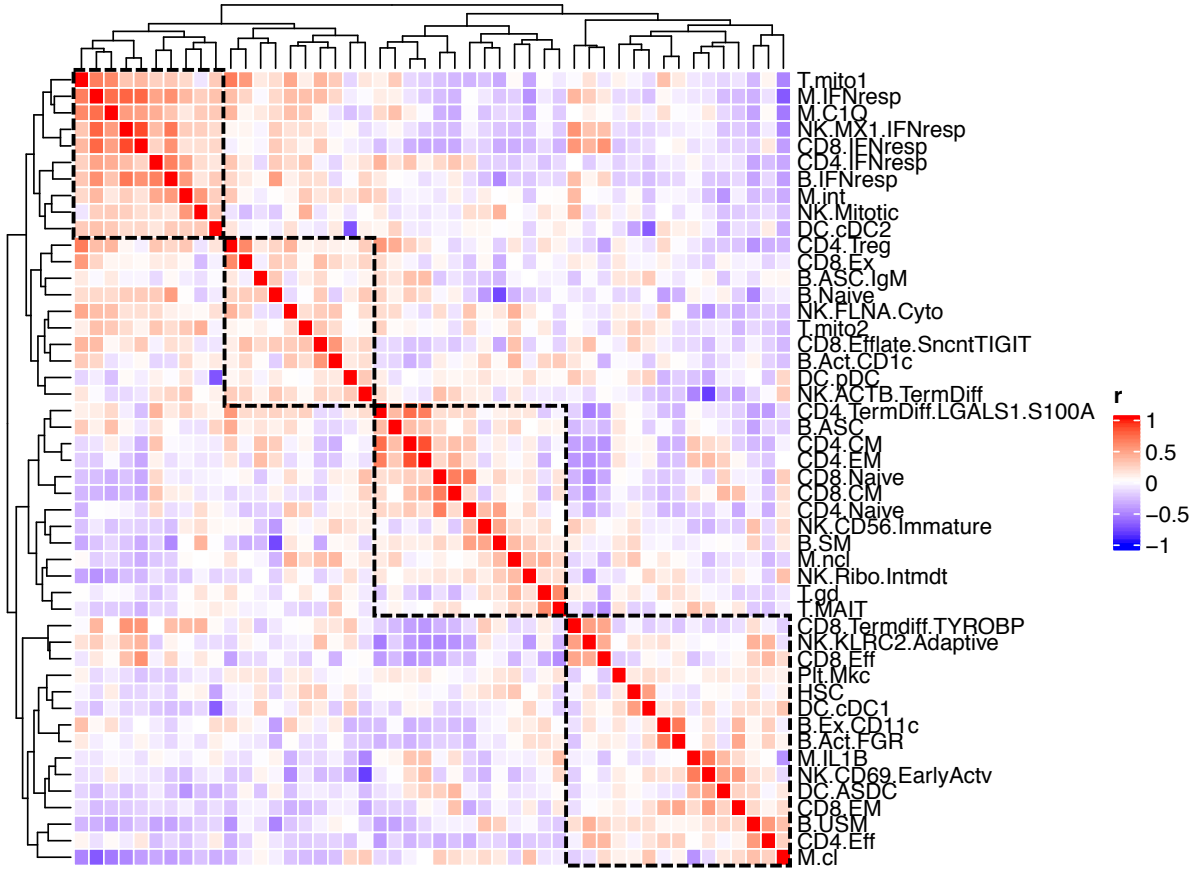

**Figure 6.3 Single-cell characterisation of B cell *IL7* expression. (a)** The median level of MAGIC imputed *IL7* expression within C1 B cells from MM patients was compared on the basis of genetic variation at rs16906115 (n=23). **(b)** Median expression of imputed *IL7* across B cell subsets per individual (n=23). **(c)** Comparison of median subset *IL7* expression across rs16906115 genotype (n=23). **(d)** B cell subset proportion across individuals separated by rs16906115 genotype (n=23). Significance for (a-d) was determined by two-sided Wilcoxon signed-rank tests. **(e)** Imputed *IL7* expression across clonally expanded and non-expanded B cells within each subset (those with >1 clonal member). Significance was tested using a linear model with individual as a fixed variable.

available in this dataset. Looking within each of the B cell subsets, I found *IL7* expression was actually increased in non-expanded B cells across most subsets, in particular USM B cells (Figure 6.3e). This suggests that B cell clonal expansion follows very different patterns to $CD8^+$ T cell expansion, in accordance with unpublished analyses performed by Chelsea Taylor, and that *IL7* may have stronger paracrine effects on $CD8^+$ T cells than autocrine B cell signalling. Altogether, these single-cell analyses pinpoint USM B cells as a particular subset of interest for influencing lymphocyte stability and T cell responses to ICB.

## 6.4 Correlating cell type proportions across single-cell RNAseq PBMCs

I next wanted to examine how subset proportions are correlated within PBMCs as a potential explanation for my observations around pan-subset IFN-I signalling, mitosis and IFN-I signature correlation, and anti-correlation between mitosis and Effector activity. I calculated the proportions of each subset within cell types for melanoma patient samples and correlated these across all subsets to generate a correlation heatmap (Figure 6.4a). Heatmap clustering revealed four main subset groups, with the constituent populations listed in the table in Figure 6.4b. Group 1 was comprised of all of the IFN-I responsive subsets across monocytes, NK cells, $CD8^+$ T cells, $CD4^+$ T cells and B cells. Other subsets present in Group 1 were mitotic T cells and NK cells, complement-enriched (C1Q) and intermediate monocytes and cDC2s. This again reaffirms the parallel mitotic and IFN-I signalling observed across many cell types, suggesting there is intrinsic interaction and feedback between these subsets that leads to their shared presence. Group 2 consisted of many subsets that shared a degree of dysfunctional activity, most notably $CD4^+$ regulatory T cells (Treg) and exhausted $CD8^+$ T cells which had well correlated subset proportions, and plasmacytoid DCs, which are amongst the highest producers of type I IFNs due to their high TLR7/9 expression. On the other hand, Groups 3 and 4 were characterised by an abundance of intermediately differentiated and memory phenotypes, and activated and effector subset types respectively. In particular, I found that USM B cells, Effector, terminally differentiated and EM $CD8^+$ T cells and Effector $CD4^+$ T cells were all present in Group 4, along with cross-presenting cDC1s, pointing to greater degrees of stimulatory T cell activity. Globally, Groups 1 and 2 clustered together and were on the opposite phylogenetic branch to Groups 3 and 4, reinforcing this division between mitosis, IFN-I and immunosuppresive responses, and T cell functionality.

**a**




**b**

| Group | Subsets | | | |
|---|---|---|---|---|
| 1 | T.Mito<br>M.IFNresp<br>M.C1Q<br>NK.IFNresp | CD8.IFNresp<br>CD4.IFNresp<br>B.IFNresp | M.Int<br>NK.Mito<br>cDC2 | Mitotic/ IFNs |
| 2 | CD4.Treg<br>CD8.Ex<br>B.ASC.IgM<br>B.Naïve | NK.Cyto<br>T.Mito<br>CD8.Eff.late | B.Act.CD1c<br>pDC<br>NK.TermDiff | Dysfunctional |
| 3 | CD4.TermDiff<br>B.ASC<br>CD4.CM<br>CD4.EM | CD8.Naive<br>CD8.CM<br>CD4.Naive<br>NK.Immature | B.SM<br>M.Ncl<br>NK.Intermediate<br>T.gd, MAIT | Intermediate/ Memory |
| 4 | CD8.TermDiff<br>NK.Adaptive<br>CD8.Eff<br>Plt.Mkc<br>HSC | cDC1<br>B.Ex.CD11c<br>B.Act.FGR<br>M.IL1B<br>NK.EarlyActv | ASDC<br>CD8.EM<br>B.USM<br>CD4.Eff<br>M.cl | Effector/ Activated |

**Figure 6.4 Correlations of subset proportion across cell types. (a)** The proportion of subsets within each cell type was calculated on a per-sample basis and then co-correlated across all subset pairs, with the resultant correlation values plotted as a clustered heatmap (Pearson's correlation test). **(b)** Summarised cluster membership for subsets based on the heatmap in (a).

## 6.5 Exploring cell-cell interactions in the context of lymphocyte stability

I next looked at gene-gene interactions across cell types using the ligand-receptor analysis package CellPhoneDB[300] to dissect specific interactions relevant to ICB responses. This analysis involves correlating the expression of a receptor gene on a primary subset and its cognate ligand on a secondary subset, thus identifying putative cell-cell interactions mediated by that ligand-receptor pair. Given I had explored transcriptomic and cellular associations with lymphocyte stability in detail, I focused on comparing ligand-receptor interactions in patients with stable vs falling LS. After identifying unique interactions across each LS group, I counted the number of interactions across each cell type pair, subtracting the number of interactions in falling LS individuals from those in stable individuals. This generated a global picture of which cell-cell interactions contribute positively or regulatory to lymphocyte stability. At C1, I found $CD4^+$ and $CD8^+$ T cell interactions generally promoted lymphocyte stability, possibly reminiscent of $CD4^+$ T cell help for $CD8^+$ T cells, whilst interactions between other cell types were associated with falling LS instead, particularly monocytes and T cells (Figure 6.5a). At C2, I found preservation of CD4-CD8 interactions as associated with stable LS whilst there were newly pro-LS interactions between T cells, cDCs and B cells that may reflect a degree of immune reinvigoration. Interestingly, pDC interactions were consistently associated with lymphocyte instability, possibly reflecting their IFN-I activity. I then specifically examined the unique ligand-receptor interactions between T cells and myeloid cells (monocytes and DCs) at C2 for each LS group, given that distinct T cell and monocyte pathways were particularly identifiable in stable vs falling LS. Many interactions between T cells and cDCs were generally enriched in stable LS individuals with a notable example being a predicted interaction between *CD244* expressed on $CD8^+$ T cells, and *CD48* expressed on cDCs and monocytes (Figure 6.5c). CD244 is an immunostimulatory receptor associated with TCR signalling and activation[337], and so this interaction may potentially contribute to monocyte-dependent T cell co-stimulation, in support of T cell homeostasis. On the other hand, interaction between $CD4^+$ T cell *CD40L* and its receptor *CD40* on monocytes was only observed in falling LS individuals, and may link to increased monocyte inflammation, given stimulation of CD40 has been demonstrated to increase TNF-$\alpha$, IL-6 and IL-8 production in monocytes[338]. As such, this interaction provides a possible causative link to increased monocyte inflammation and NF-$\varkappa$B signalling observed in falling LS contexts.

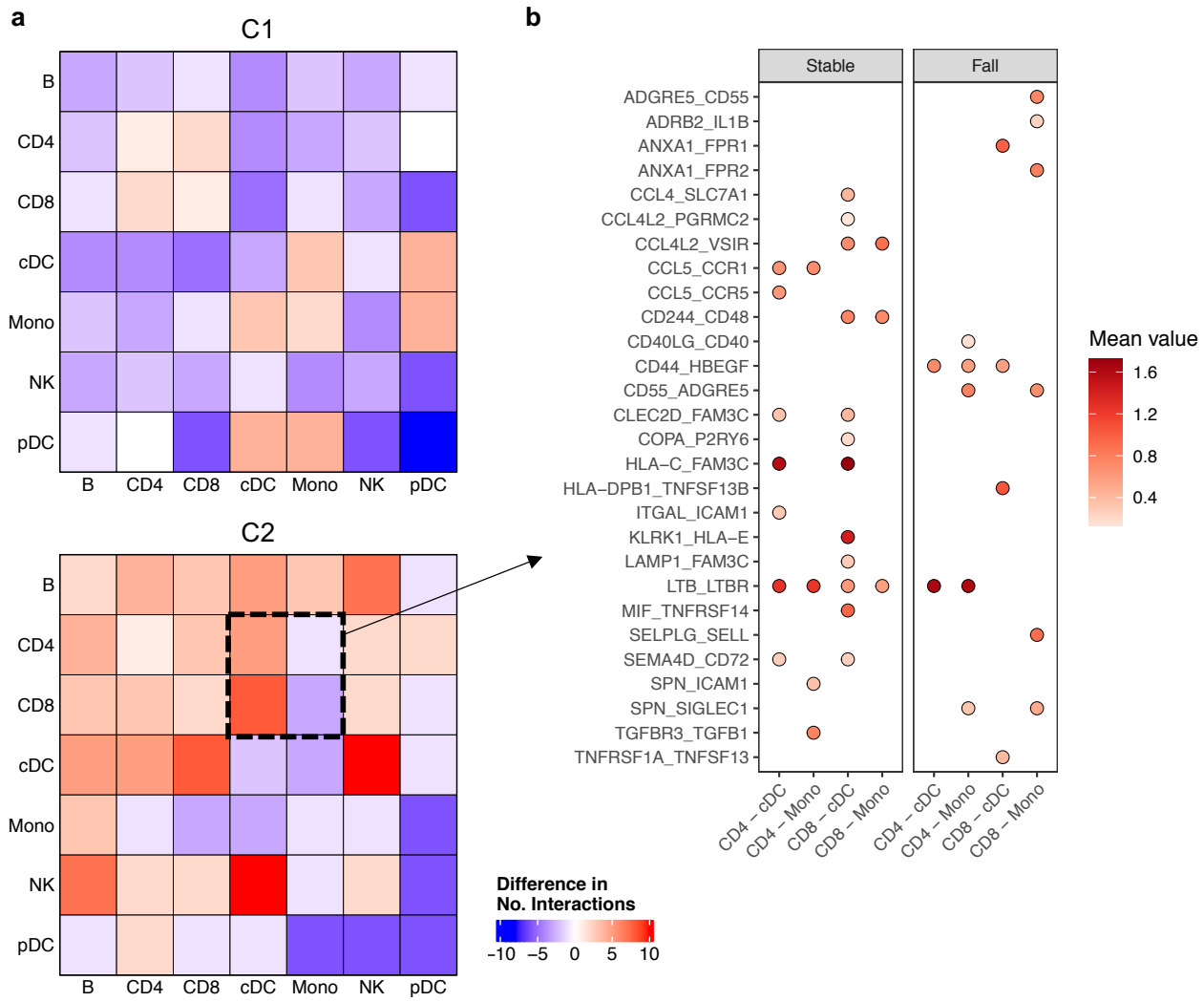



**Figure 6.5 Ligand-receptor interaction analysis across cell types in the context of LS. (a)** Using CellPhoneDB, the number of significant interactions between cell types was calculated for individuals with stable LS and falling LS separately, at C1 or C2. The number of interactions observed in falling LS was subtracted from those found in stable LS, and the resulting number plotted as heatmaps. **(b)** The unique interactions to stable and falling LS individuals across T cells and myeloid cells were plotted, with the ligand-receptor pair and cell-cell pair displayed on the y and x axis respectively.

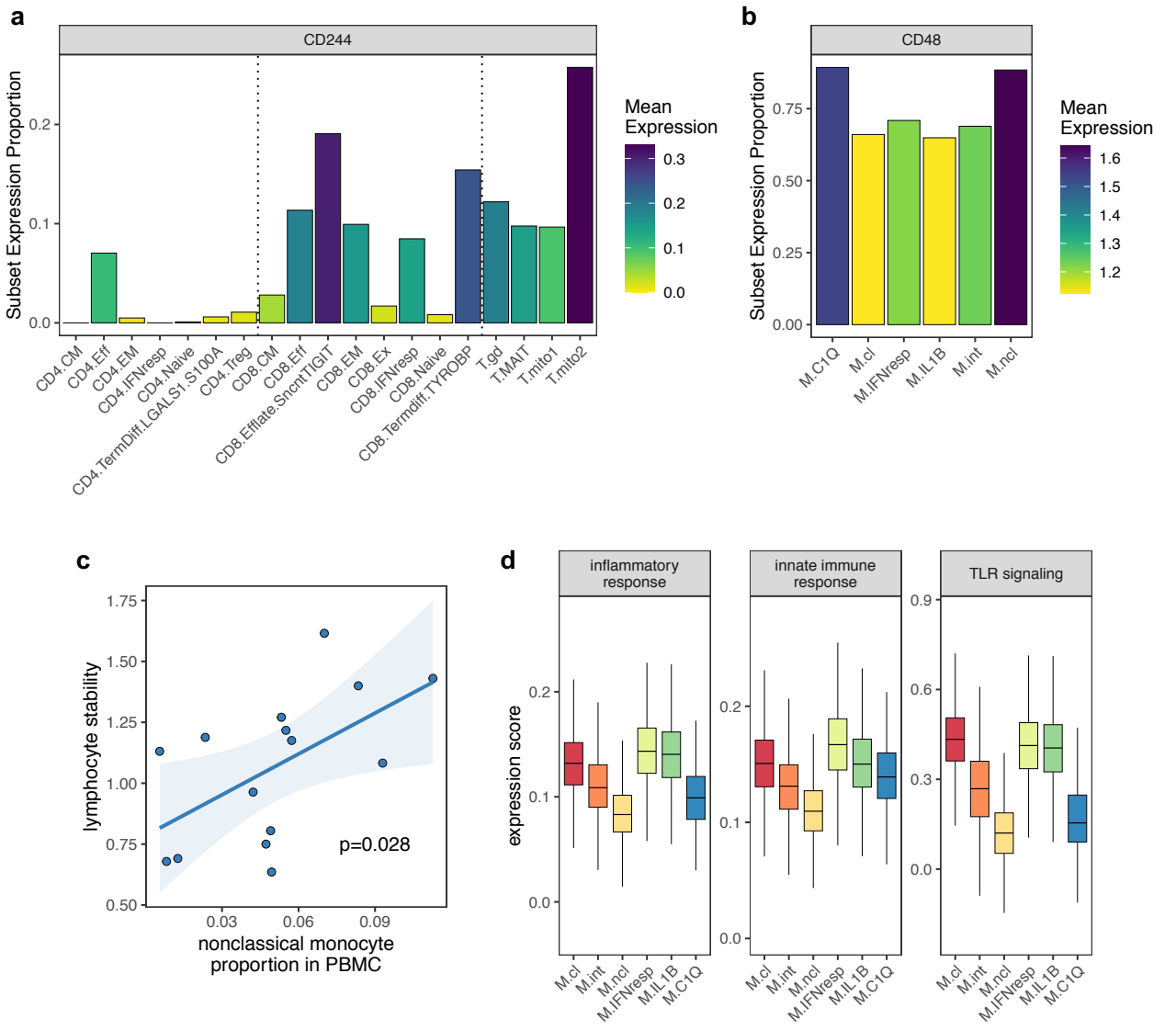



**Figure 6.6 Analysis of monocyte and T cell subsets enriched for CD244-CD48 interactions.** **(a)** Expression of *CD244* on T cells and **(b)** *CD48* on monocytes was compared across subsets. **(c)** The proportion of non-classical monocytes of all PBMCs was correlated with hospital lymphocyte stability values(n=15, two-sided Wilcoxon signed-rank test). **(d)** GOBP pathways related to inflammation were scored in single-cell monocytes. The constituent genes for each pathway were identified and used to generate a per-cell score via SeurattextitAddModuleScore function. Pathway expression per monocyte subset was then compared.

To begin pinpointing what specific $CD8^+$ T cell and monocyte subsets might be involved in promoting or preventing lymphocyte stability, I looked at the expression of *CD244* across T cell subsets, and *CD48* on monocytes. *CD244* was mostly enriched in $CD8^+$ T cells, and was particularly high in late Effector $CD8^+$ T cells, followed by terminally differentiated and effector subsets (Figure 6.6a). Notably, *CD244* was under-expressed in Naive and exhausted $CD8^+$ T cells, signifying its potential involvement in stimulating desirable effector $CD8^+$ function, as opposed to less relevant naive or exhausted phenotypes. When looking at CD48 expression on monocytes, I found that it was highest in non-classical monocytes, followed narrowly by complement-enriched monocytes (Figure 6.6b). Given their increased *CD48* expression and enrichment of MHC-I antigen presentation and processing (Figure 6.2), I wondered whether non-classical monocytes may enhance T cell responses, and thereby associate with positive lymphocyte stability despite overall monocyte count being negatively associated with LS. To validate this hypothesis, I correlated the proportion of non-classical monocytes of all PBMCs, as measured by the single-cell data, with clinical LS values. I found a significant positive correlation, suggesting that this subset is indeed relevant for maintaining stable T cell responses (Figure 6.6c). More globally, I also wondered whether there were distinct expression patterns of inflammation across monocyte subsets, particularly relevant given the negative association between generalised monocyte inflammation and LS values. I generated scores for multiple GOBP pathways related to inflammation using the *AddModuleScore* function from Seurat, and compared these across monocyte subsets. Consistently, non-classical monocytes had the lowest level of pro-inflammatory scoring (Figure 6.6d), in accordance with the prior pathway analysis across subsets showing they were the only monocyte subset without enrichment for the 'inflammatory response' pathway (Figure 6.2). This is also consistent with my correlational proportion analysis in Figure 6.3a, in which non-classical monocytes were the only monocyte subset that was clustered into Group 4, which contains the majority of effector-related subsets. Overall, this analysis suggests that non-classical monocytes are a key subset that contributes to T cell responses whilst other monocyte subsets may indeed negatively impact general immunity due to CD40-stimulation leading to inflammation.

## 6.6 Understanding specific $CD4^+$ and $CD8^+$ subset interactions with other cell types

My previous ligand-receptor interaction analysis yielded an interesting result where CD4 and CD8 T cell interactions were often stimulatory, with greater numbers of ligand-receptor

interactions seen in individuals with stable lymphocyte counts. I wanted to examine how these interactions varied across more granular $CD4^+$ and $CD8^+$ T cell subsets. Using CellPhoneDB, I identified significant interactions between specific T cell subsets, counting the number of subset-subset interactions and plotting these as heatmaps. I found that more differentiated $CD8^+$ T cell subsets (terminally differentiated, late effector) had higher numbers of interactions with $CD4^+$ T cells, with the greatest number of ligand-receptor interactions occurring across terminally differentiated subsets of both cell types (Figure 6.7a). This suggests that $CD4^+$ interactions which may constitute T cell help, come particularly from differentiated $CD4^+$ T cells, and likewise, may favourably impact more differentiated $CD8^+$ T cells, thus playing a positive role in T cell immune activity. Interestingly, the $CD4^+$ T cell subset seen to interact most with exhausted $CD8^+$ T cells was $CD4^+$ Tregs, in line with their immunosuppressive activity. Upon examining interactions between $CD8^+$ T cells and B cell subsets, I found a comparable pattern where B-CD8 interactions were concentrated in differentiated $CD8^+$ T cell subsets, with the greatest interactions occurring between late Effectors and activated B cells (Figure 6.7b). Looking specifically at USM B cells, I found there were also greater interactions with more differentiated $CD8^+$ T cells. Interestingly, I saw that exhausted, and to a lesser extent, terminally differentiated $CD8^+$ T cells had the highest levels of interaction with exhausted B cells, despite B-T cell interactions typically being as immunostimulatory. I lastly examined interactions between B cells and $CD4^+$ T cells, finding that Tregs interacted with exhausted B cells to a much greater degree than any other subsets (Figure 6.7c). This was followed by interactions between IFN-I responsive $CD4^+$ T cells and exhausted and activated B cell subsets. Overall, these results appear to reinforce the importance of global CD8-CD4 interactions, and potentially those between $CD8^+$ T cells and B cells, whilst CD4-B cell interactions are less obviously beneficial to immune responses during ICB, which is possibly a reflection of the detrimental effects of inflammatory B cells that become licensed by $CD4^+$ T cell help.

## 6.7 Interactions between regulatory T cells and conventional $CD8^+$ and $CD4^+$ T cells

Since the previous subset proportion and ligand-receptor analysis identified that Tregs associated with T and B cell exhaustion, and there is a body of pre-existing literature suggesting Treg immunosuppression contributes to poorer responses to ICB, I developed a flow cytometry panel to detect Tregs based on intracellular staining of the transcription factor Foxp3 and surface expression of CD25 (Figure 6.8a). Tregs had lower expression of

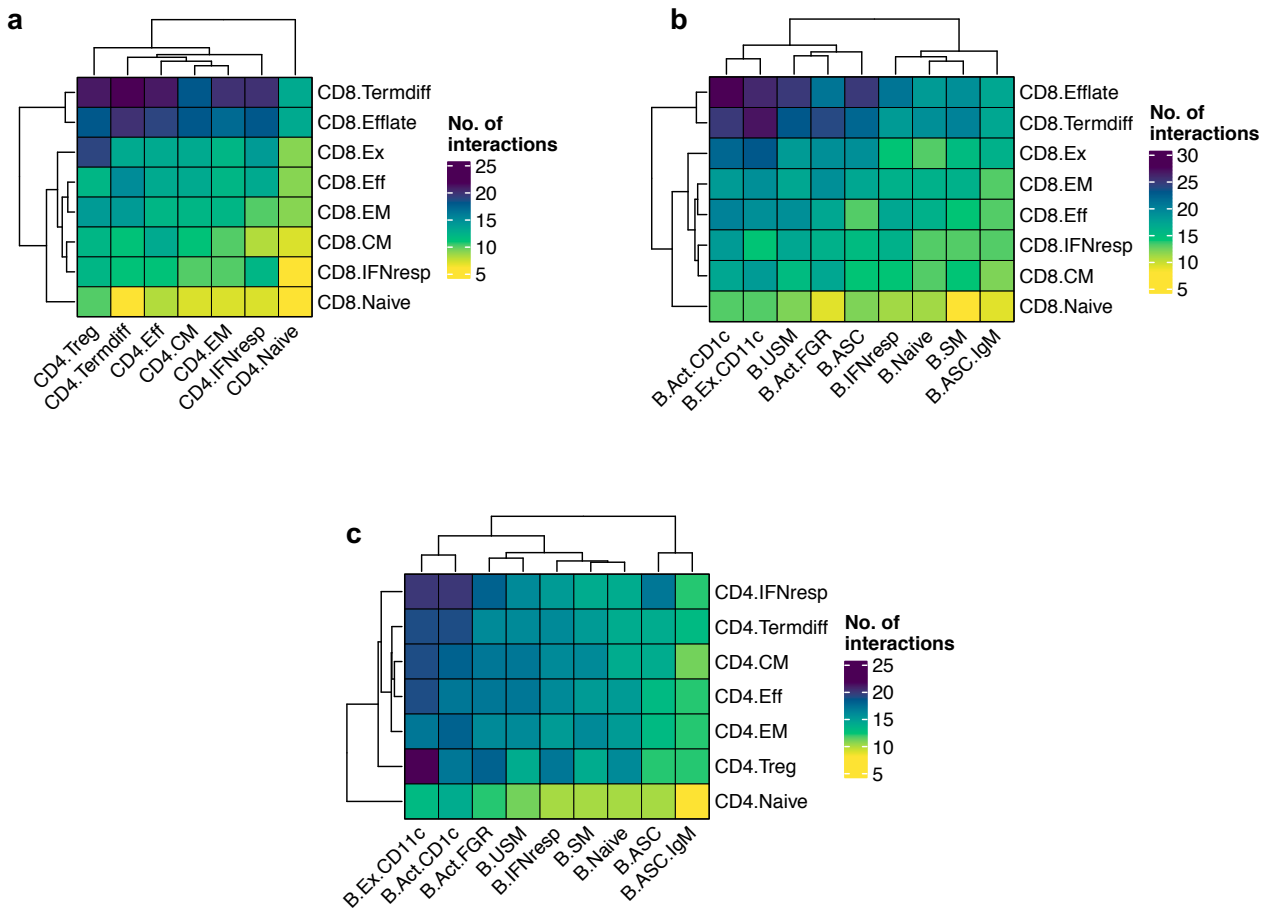



**Figure 6.7 Analysis of CD8⁺, CD4⁺ and B cell subset interactions.** Using CellPhoneDB, ligand-receptor interactions between subsets were identified and counted across **(a)** CD4⁺ and CD8⁺ T cells, **(b)** CD8⁺ T cells and B cells, and **(c)** CD4⁺ T cells and B cells.

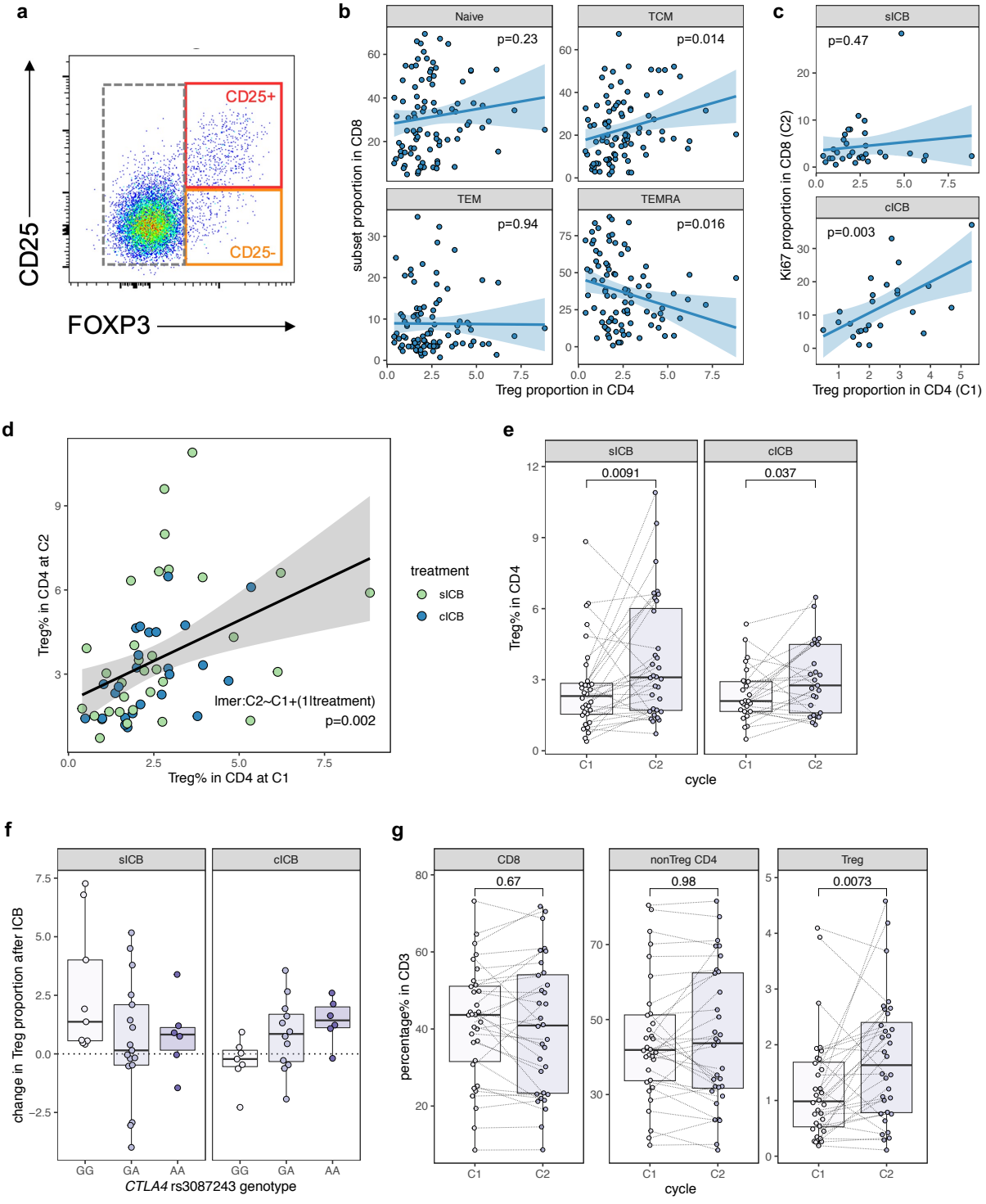



**Figure 6.8 Regulatory CD4⁺ T cell dynamics. (a)** Flow cytometry detection of Tregs as CD4⁺ T cells that stain positively for FOXP3 and CD25 (red square). **(b)** Correlations between Treg proportion and CD8⁺ T cell subset proportions (n=91, Pearson's correlation test). **(c)** Correlation between Treg proportion at C1 and Ki67⁺ CD8⁺ T cells following sICB or cICB (n=57, Pearson's correlation test). **(d)** Correlation between Treg proportion at C1 and C2 using a linear model, including treatment type as a fixed variable (n=57). **e** Change in Treg proportion between C1 and C2 for sICB and cICB (n=57, two-sided Wilcoxon signed-rank test). **(f)** QTL association between genotype at rs3087243 and change in Treg proportion (n=57, Pearson's correlation test). **(g)** Change in proportions of T cell populations following sICB (n=32, two-sided Wilcoxon signed-rank test).

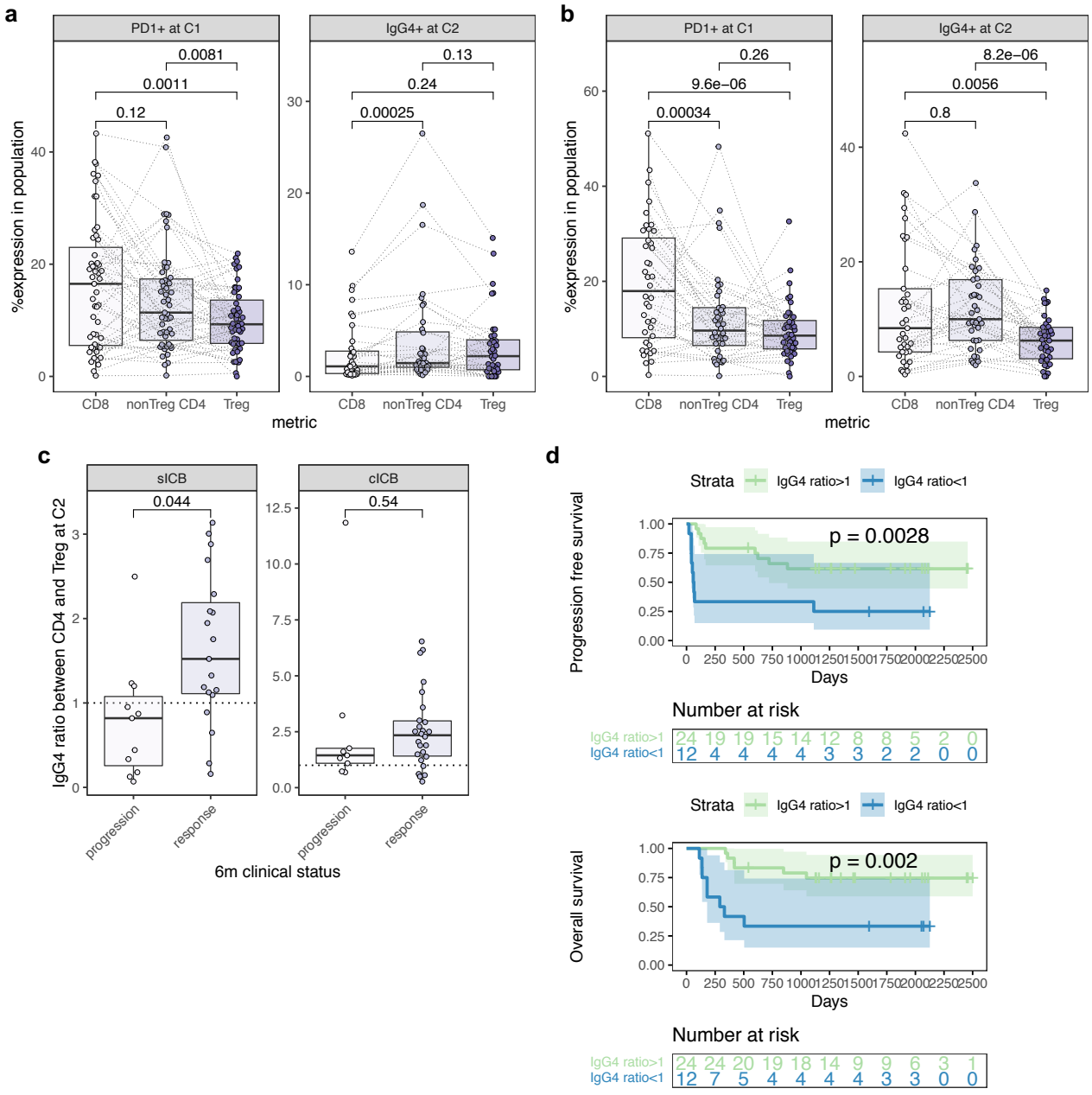



**Figure 6.9 Regulatory CD4⁺ T cell phenotype. (a-b)** Flow cytometry staining of PD-1 at C1 and IgG4 at C2 across conventional CD8⁺ T cells, CD4⁺ T cells and Tregs in patients treated with sICB (a) or cICB (b) (n=51 and 36 for sICB, 40 and 37 for cICB, two-sided Wilcoxon signed-rank test). **(c)** Ratio of IgG4 staining positivity on CD4⁺ T cells versus Tregs for sICB and cICB patients separated by 6 month clinical response (n=36 and 37, two-sided Wilcoxon signed-rank test). **(d)** Kaplan Meier survival curves for sICB treated patients based on CD4:Treg IgG4 ratio values above or below, across progression-free (top) and overall survival (bottom) (n=36, two-sided log-rank test).

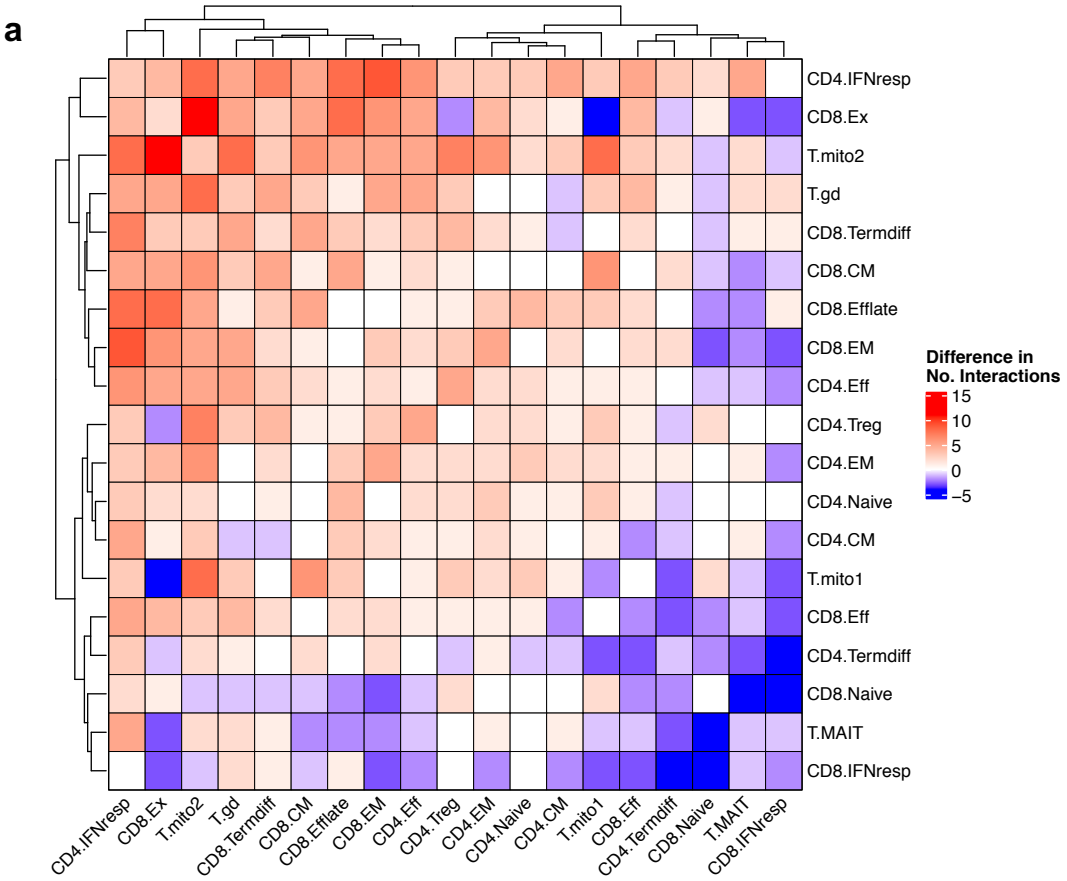
CD127 and were enriched for expression of both surface and intracellular CTLA-4 (data not shown). I first tried to understand how Tregs correlated with $CD8^+$ T cell subset proportions by flow cytometry, finding Treg proportion amongst $CD4^+$ T cells and $CD8^+$ TEMRA proportion was anti-correlated, whilst Tregs correlated positively with TCMs (Figure 6.8b). This suggests that higher peripheral Treg counts skew T cell responses away from an effector phenotype at pre-treatment, and since effector counts across ICB are relatively stable, such early Treg responses may dampen immunity throughout treatment. Interestingly, when I correlated pre-treatment Treg proportion with the number of $Ki67^+$ mitotic cells post-ICB, I found a significant positive correlation particularly in cICB (Figure 6.8c). At first, this seems counter-intuitive given typical 'immunosuppressive' Treg function but this observation is perhaps in keeping with my exploration of mitosis as a possibly hypofunctional and mostly non-expanded T cell response. High Treg proportion at C1 was significantly predictive of a sustained higher proportion of Tregs at C2 irrespective of treatment type (Figure 6.8d), again demonstrating the importance of pre-treatment immunity in determining ICB responses. Comparing the proportions of Tregs at C1 and C2, Tregs were significantly expanded following treatment with sICB or cICB, but with increased significance in sICB (Figure 6.8e). I wondered whether the addition of $\alpha$-CTLA-4 as part of cICB would influence how Treg proportion changes over ICB, given previous literature suggests ipilimumab binds to Tregs and encourages ADCC based on its IgG1 backbone. To explore this, I leveraged genetic variation at a common autoimmune associated *CTLA4* SNP, rs3087243, exploring whether there was any association between allele carriage and Treg expansion. To my interest, I found a QTL association between minor allele carriage and change in Treg proportion between C1 and C2, with a significant effect only observed in cICB (Figure 6.8f). This result indicates that changes in Treg proportion are quite distinct between sICB and cICB, with genetic variation possibly influencing ICB immunity through variations in Treg activity.

To gain a global picture of the changes in Treg proportion relative to all T cells, I compared how the proportion of $CD8^+$, conventional $CD4^+$ (non Foxp3+ CD25+) and Tregs of the total $CD8^+$ T cell population changed across treatment. I found that Tregs were the only subset that showed significant expansion following treatment, and only in sICB (Figure 6.8g). To further understand the therapeutic implications of Tregs in ICB, I compared the relative levels of exhaustion and reinvigoration across conventional and regulatory T cell populations, measured by PD-1 staining at C1 and IgG4 staining at C2. I performed this analysis separately across sICB and cICB, given the possible distinct behaviour of Tregs within these two treatment types. At C1, I observed the highest levels of PD-1 on $CD8^+$ T cells, followed by conventional $CD4^+$ T cells and then Tregs (Figure 6.9a-b). At C2, I

saw slightly different patterns of IgG4 staining between sICB and cICB but consistently higher IgG4 levels on conventional $CD4^+$ T cells. Since α-PD-1 binding on Tregs purportedly restores the immunosuppressive functions of Tregs[163], I wondered whether the ratio of α-PD-1 binding on conventional T cell subsets versus Tregs could be predictive of ICB outcome. When looking at sICB, individuals with treatment responses by 6 months had significantly higher amounts of IgG4 staining on conventional CD4 T cells versus on Tregs, whilst most progressing individuals had more IgG4 staining on their Tregs instead (Figure 6.9c). I segregated sICB-treated individuals into those with higher IgG4 staining on $CD4^+$ T cells vs Tregs (IgG4 ratio >1) and lower staining (IgG4 ratio <1), and found there was significant difference in PFS and OS (Figure 6.9d), but did not observe parallel results for cICB. Collectively these results indicate that Tregs dampen pre-existing T cell responses, promote T and B cell exhaustion, are expanded following ICB, and accordingly, reinvigoration of Tregs by ICB has a negative effect for clinical outcome, particularly for sICB.

## 6.8 Describing T cell interaction networks associated with clinical response to ICB

To relate these broader interaction analyses to clinical outcome, I lastly assessed which T cell subset interactions were enriched in 6 month responding individuals versus those progressing on treatment. I found that many T cell interactions were enriched in responding individuals, as expected given my previous LS analyses, but there was a sizeable group of cells that had interactions enriched in progressors (Figure 6.10a). These cells were clustered in the lower right of the interaction heatmap, spanning Tregs, naive T cells and IFN-I responsive subsets. I plotted these interactions with greater enrichment in treatment progressors as a force-directed network, finding two key nodal groups of IFN-I responsive and naive $CD8^+$ T cells (Figure 6.10b). These subsets had strong network links to mitotic T cells, as well as exhausted $CD8^+$ T cells, but also demonstrated some interactions with a variety of CD4 subsets, such as naive, terminally differentiated and EM populations. These results are concordant with many of my observations using bulk RNAseq, thus supporting my findings made in a larger cohort but with less granularity. Overall, this highlights these two peripheral $CD8^+$ T cell populations as key targets for additional therapeutic interventions that may sensitise individuals to ICB, and exploring the interactions of these cells with other subsets may pinpoint additional cell types that influence the treatment course of immunotherapy.


a
CD4.IFNresp
CD8.Ex
T.mito2
T.gd
CD8.Termdiff
CD8.CM
CD8.Efflate
CD8.EM
CD4.Eff
CD4.Treg
CD4.EM
CD4.Naive
CD4.CM
T.mito1
CD8.Eff
CD4.Termdiff
CD8.Naive
T.MAIT
CD8.IFNresp
Difference in
No. Interactions
15
10
5
0
−5

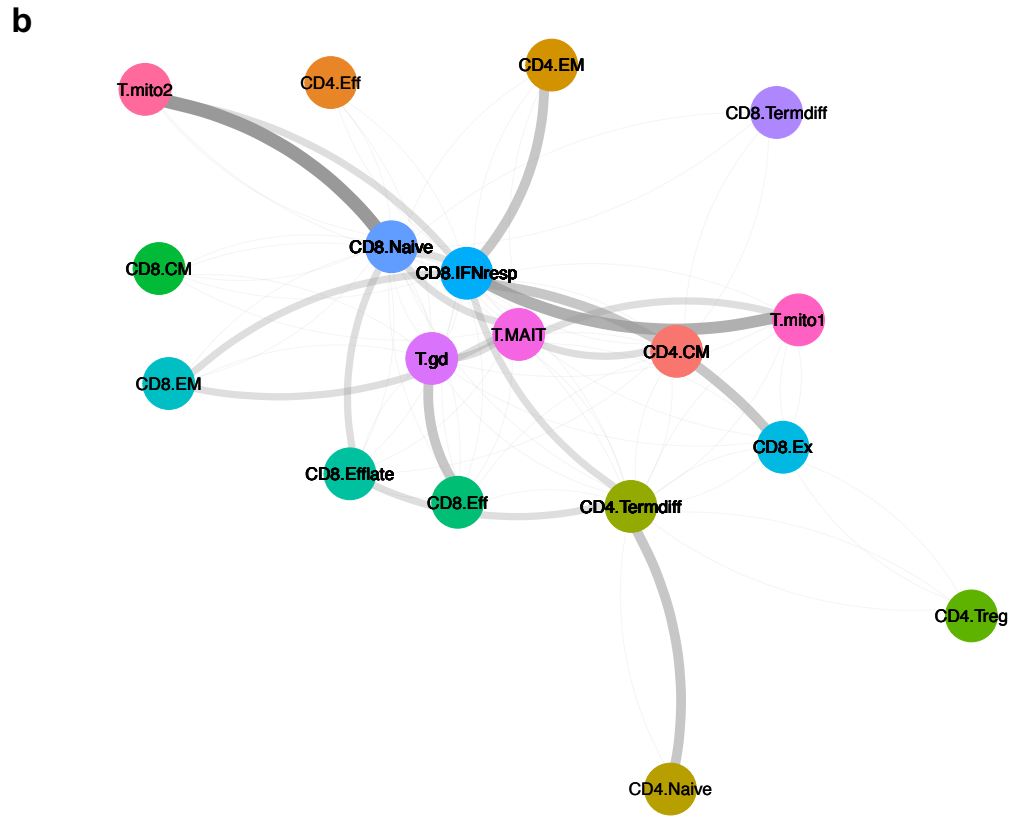

b
T.mito2
CD4.Eff
CD4.EM
CD8.Termdiff
CD8.Naive
CD8.CM
CD8.IFNresp
T.mito1
T.MAIT
CD4.CM
T.gd
CD8.EM
CD8.Ex
CD8.Efflate
CD8.Eff
CD4.Termdiff
CD4.Treg
CD4.Naive

**Figure 6.10 T cell interaction network enriched in progressing individuals. (a)** CellPhoneDB was used to identify interactions between T cell subsets in clinical responders and progressors by 6 months. The number of interactions found across each subset pair in progressors was substracted from responders and counted for plotting on a clustered heatmap. **(b)** The interaction values that were increased in progressor individuals were input into a force-directed graph model to generate a network of subset interactions that are active in ICB progression.

## 6.9 Conclusions and Discussion

By leveraging the power of single-cell RNAseq, I was able to identify specific cell populations that contribute to biological and clinical processes that previously described, such as B cell *IL7* expression, lymphocyte stability and T cell interactions. To summarise some of the results of this chapter:

- PBMCs were comprised of 8 main cell types, which spanned 48 unique subsets including specific IFN-I responsive cells within most subsets
- B cell *IL7* is mainly expressed in unswitched memory B cells, and genetic variation at rs16906115 modulates subset proportions to increase overall *IL7* expression
- Proportional analysis identified cross-subset clusters of IFN-I responsive and mitotic cells, dysfunctional cells, intermediate and memory cells, and effector populations
- Interactions between CD244-CD48 and CD40L-CD40 on T cells and monocytes respectively potentially contribute to lymphocyte stability, with non-classical monocytes being the sole monocyte population that supports LS
- Differentiated $CD8^+$ T cells and $CD4^+$ T cells had the greatest number of cross-T cell interactions, whilst also being enriched across a network of exhausted $CD8^+$ T cells, B cells and regulatory T cells
- Tregs anti-correlate with effector T cell proportions and are expanded after treatment, whilst the ratio of IgG4 staining on conventional $CD4^+$ T cells versus Tregs is significantly associated with outcome
- Assessing subset-subset interactions within T cells based on 6 month clinical response shows similar network associations to previous bulk analysis

I developed a moderately high throughput single-cell RNAseq pipeline where six to eight samples from different individuals were batched onto the same single-cell chip. This allowed me to generate data from a greater number of individuals with increased statistical power to understand subset proportions. However it also resulted in a more challenging pre-processing pipeline where doublet removal was more intensive, and there was a considerable number of monocytes that could not be reliably assigned genetic identities. It was interesting to

note how this single-cell PBMC dataset also contained additional $CD8^+$ T cell subsets that were not identified in the single-cell $CD8^+$ T cell data used in Chapter 3. Whether this was due to a technical improvement in the single-cell technology (v2 10x chemistry vs v1), an increased number of cells allowing more confident clustering and assignment of rarer subsets, or an expanded repertoire of reference data, is unclear, but allowed me to identify that there are unique subsets of cells enriched for many of the IFN-I ISGs that correspond with the type I IFN signalling pathway. Of the pathways enriched in IFN-I responsive $CD8^+$ T cells, GTPase activity was not present, suggesting that these cells have minimal TCR signalling capacity, and perhaps exist in a setting of more generalised inflammation, rather than targeted T cell killing. IFN-I monocytes were one of the few IFN-I subsets enriched for IFN-ɣ signalling, further suggesting IFN-ɣ from sources like $CD8^+$ T cells leads to downstream IFN-I signalling on paracrine cells. It would be interesting to examine the expression of cytokine receptors and transcription factor networks, using a package such as SCENIC[339] to identify if IFN-I monocytes are indeed more predisposed to IFN-ɣ signalling. The other key subset observations I made were (a) identifying a population of regulatory $CD4^+$ Tregs which expressed many similar pathways to other $CD4^+$ T cell subsets, and (b) that USM B cells, and to a lesser extent their switched memory counterparts, are predominant expressors of *IL7*. The exact biological mechanisms that drive this, as well as why melanoma patients have increased levels of B cell *IL7*, and the interaction between this, the rs16906115 SNP and subset proportions is an area of ongoing interest in the group.

From ligand-receptor analysis, I identified that non-classical monocytes may be advantageous for lymphocyte stability during ICB as they had higher levels of the costimulatory molecules *CD48*. Non-classical monocytes are typically regarded as less pro-inflammatory compared to classical monocytes, as confirmed by the pathway scoring data I generated across monocytes. Since monocyte inflammation seems to be associated with poorer ICB responses, and $CD14^+$ monocytes also encompass myeloid-derived suppressor cells, it is perhaps less surprising that a preponderance of non-classical monocytes appears to be associated with stronger ICB immunity. Indeed, analysis of ipilimumab-treated individuals has shown that an increased number of $CD16^+$ monocytes corresponds with improved response to α-CTLA-4, with a purported mechanism being increased ADCC of α-CTLA-4 bound Tregs, mediated through CD16 as an Fc receptor[340]. Whether there is a more direct mechanism behind this effect is unclear, with my ligand-receptor analysis not showing a particularly strong interaction between non-classical monocytes and T cells relative to other monocyte subsets. It would have been interesting to extend my network analysis of responder vs progressor subset interactions to additional subsets, and creating a holistic map across all PBMC subsets, but

this would probably require a more detailed examination of whether each interactions can be considered stimulatory or suppressive. Approaches using mathematical modelling and machine learning could also be employed, such as in Kirouac et al[341], where toggle-switch signalling and subset-transcriptomic prediction algorithms were used to identify responding factors for CAR-T cell therapy.

Lastly, I identified a potential role for Tregs in association with $CD8^+$ T cell and B cell exhaustion and so explored the dynamics of Tregs in more detail. I found several intriguing parallels between Tregs and mitotic $CD8^+$ T cells - such as baseline Treg proportion associating with induction of T cell mitosis during cICB, selective expansion of Tregs following treatment in contrast to total conventional T cells, and comparable levels of IgG4 staining at C2 between Tregs and $CD8^+$ T cells. Whether Treg expansion is mediated by clonal expansion of effector Tregs, also referred to as natural Tregs, or conversion of $CD4^+$ T cells into induced Tregs, was not explored, but would be possible to answer using the single-cell data by looking at Treg clonal expansion and relatedness to pre-existing $CD4^+$ T cells. Furthermore, how ICB binding affects $CD8^+$ T cells, $CD4^+$ T cells and Tregs would be interesting to understand at single-cell resolution. Few studies have examined facets of the peripheral $CD4^+$ T cell response to ICB, with a paper by Lozano et al[158] identifying that $CD4^+$ T cell expansion associates with the development of autoimmune toxicities, but not investigating the transcriptomic changes that occur across treatment. Whether IgG4 binding is also tangentially associated with clonal expansion in $CD4^+$ T cells would be interesting to understand, given that the lack of change in $CD4^+$ T cell proportions of all T cells during treatment seems to point away from this. Why Tregs are the only cell type to undergo significant increases in subset count also remains unclear and understanding the precise PD-1 associated machinery in these cells relative to other T cells is important. Multiple papers have confirmed that intratumoural $\alpha$-PD-1 ligation lifts an exhausted phenotype on Tregs[163,342] and in accordance with the paper by Kumagai et al[163], the ratio of 'reinvigoration' on T cells versus Tregs is predictive of outcome. Understanding the transcriptomic profile of Tregs from responding individuals versus progressors would also be valuable in deciphering the exact contributions of these cells to the ICB response, and for being able to characterise a patient as 'immuno-receptive' or immuno-resistant to therapy.

# Chapter 7

# Summary and future work

## 7.1 Overall summary

In this thesis, I have characterised the peripheral immune response to immune checkpoint blockade, with an initial focus on $CD8^+$ T cells but subsequently expanding analysis to look at interactions between cell types and subsets. I used bulk and single-cell RNA/VDJseq as well as flow cytometry as the predominant techniques to perform this analysis. Overall, across my results, I identified four themes that I considered particularly interesting:

- $CD8^+$ T cell clonal expansion, effector cells and long-lived effector cell phenotypes
- IgG4-binding of T cells, downstream signalling and distinct effects across cell types
- Clinical significance of lymphocyte stability and its relation with B cell *IL7* expression
- Associations between ICB immunity and genetic variation at rs16906115 and rs3087243

## 7.2 Clonal expansion, effector cells and long-lived effector phenotypes

Conventional models of T cell responses to acute exposure to a pathogen, describe a rapid expansion of naive T cells recognising the antigen stimulus, to generate large amounts of clonally expanded effector T cells which clear the pathogen. Following clearance, T cells responses wane with most effector T cells undergoing apoptosis, whilst some develop into memory T cells to respond upon repeat stimulation. In this process, antigen-driven T cell stimulation leads to clonal expansion within approximately 7-14 days, such as for

SARS-CoV2[343]. However, for chronic diseases such as cancer, this process of clonal expansion is less well defined. Clonal expansion is perhaps one of the best markers of an individual's capability to recognise tumours but effective T cell responses are constrained by functional processes such as exhaustion and anergy. T cell exhaustion, originally a process to rein in aberrant immunity, is well evidenced in tumour-specific resident memory T cells due to persistent stimulation and has been associated with both beneficial and detrimental response rates to ICB[101,125].

My results suggest that both clonal expansion and T cell functionality, evidenced by higher amounts of effector cells that don't display exhaustion markers, are both required for effective anti-tumour responses to ICB. I demonstrated that individuals with above median clonal expansion and effector score separately have longer progression free and overall survival. Since these two metrics are generally well-correlated, it is difficult to understand which factor is either more important, or perhaps drives the other. Indeed, there may be a feedback mechanism between these factors, in that effector T cells are capable of responding to tumour antigens and thus undergoing clonal expansion, whilst clonal expansion also drives this effector phenotype. What this indicates overall is that clonal expansion, and tumour exhaustion is a likely surrogate for tumour recognition potential, whilst effector skewing of T cell phenotypes represents cytolytic activity. The intersection point of these two aspects may be long-lived effector cells, which we've found to be clonally expanded, persistent clones that maintain a relatively stable clone size and effector phenotype. It is interesting to note that these cells also appear to have altered metabolism and this opens up further avenues of exploration to identify metabolic adjuvants for immunotherapy that may allow more persistent and functional T cell responses.

It's worth noting that these observations have relied upon peripheral blood samples, without matching to any tumour or normal adjacent tissue. As such, I am unable to describe how our results relate to intratumoural activity although there is a body of evidence to suggest that (a) peripheral T cells contribute to intratumoural cytotoxic responses during ICB[112], (b) peripheral T cell expansion mirrors intratumoural T cell expansion[135], and (c) peripheral T cell cytotoxicity mirrors intratumoural T cell cytotoxicity[138]. In particular, many papers have suggested that non-exhausted replenishment of tumour-reactive T cells, such as from tumour-draining lymph nodes[132,133] and peripheral blood[112,146], is key for tumour regression given pre-existing Trms tend to be exhausted and functionally inert[109]. One particular study of ICB-treated MM patients in complete remission i.e. cancer-free for up to 3 years showed that the resident memory T cell clones found prior to treatment were present in normal adjacent skin and blood at 3 year follow-up, adopting a phenotype with enrichment of *NKG7*, *GZMH*,

*CX3CR1* and *KLRG1*, markers similar to the LLEC phenotype I described. This appears to indicate that these cells are present at baseline prior to ICB and persist throughout treatment, up to and including during remission. It would be extremely interesting to perform similar analysis with longitudinal samples in our cohort but across both progressors (i.e. treatment cycles immediately prior to progression or treatment cessation), and long-term responders. Further pairing of these analyses with samples from archival tumour would be extremely valuable to understand the relationship between this peripheral expansion and functional T cell signature and the TME, particularly relative to tumour mutational burden and the immunosuppressive fibroblast and tumour environment as some previous studies have begun doing[175,344,345]. Lastly, exploring additional aspects of T cell tumour recognition, such as measures like TCR convergence[346,347], TCR specificity groups[112,348] and immunogenicity predictions, may be valuable particularly when embedded with transcriptomic profiling through single-cell RNA/VDJseq.

## 7.3 ICB binding, downstream signalling and effects on various T cell types

One of the most unexpected observations I made was that α-PD-1 after the first cycle of ICB appears to be mainly bound on central memory T cells, which are less differentiated and clonally expanded than other subsets. IgG4 staining was significantly enriched on mitotic $CD8^+$ T cells, hence my interest in understanding the mitotic response to ICB in more depth. To my surprise, I found that mitotic cells were largely non-clonally expanded, but instead formed the likely start of a signalling cascade that involved CD8 *IFNG* expression, IFN-γ signalling across cell-type but particularly in monocytes, and global IFN-I and inflammatory signatures. By single-cell RNAseq, mitotic cell populations were mostly distinct from those enriched for IFN-I stimulated genes across multiple cell types, further supporting that these processes are related but occur in distinct cell populations or with different tempos. Although I started to dissect all of these aforementioned signalling modules, further analysis using *ex vivo*, *in vitro* and *in silico* approaches could boost this effort. By collecting patient samples at earlier timepoints throughout treatment, it would be interesting to trace the tempo of each pathway to understand at what point each module peaks in expression and whether there are different dynamics across each cell type. Additionally, exposing patient PBMCs to ICB in culture in combination with various pathway inhibitors could create an image of pathway dependency and co-modulation. To extend these *in vitro* results, performing a single-cell CRISPR screen using guides targeted to specific transcription factors or signalling molecules

that support each biological process would allow for additional specificity, especially if cell-specific targeting can be achieved such as by an antibody-conjugated approach[349].

Multiple components of this mitotic, IFN-I and inflammatory cascade are negatively associated with clinical response to ICB, both in this cohort as well as in other studies[321,322,331,350]. Interestingly, Zemek et al[331] found that sustained IFN-I signalling from monocytes leads to aberrant inflammatory responses, again suggesting that inflammation is downstream of IFN-I signalling. Generalised peripheral inflammation from cell types such as monocytes is generally associated with poor ICB response, with papers showing detrimental effects of high IL-6[351] and IL-8[352] whilst IL-1β is associated with aberrant IL-7-mediated T cell homeostasis[353]. Many of these observations of biological processes being negatively deterministic of treatment outcome were made using baseline samples, suggesting that there may be an element of epigenetic regulation that influences ICB responses. Performing ATAC-seq and DNA methylation analyses, and integrating this with single-cell RNA/VDJseq information, would be useful to understand the epigenetic profile of inflammatory or IFN-ɣ responsive monocytes, so as to limit this signalling cascade from derailing ideal immune responses to ICB.

Although I didn't observe ICB binding on other cell types, IgG4 staining was seen on both conventional $CD8^+$ and $CD4^+$ T cells, and even regulatory T cells. Indeed, the amount of IgG4 staining was generally highest on conventional $CD4^+$ T cells out of these three cell populations. Whether IgG4 binding in $CD4^+$ T cells and Tregs also leads to similar mitosis and IFN-ɣ production is unclear, and how this interacts with the transcriptomic modulation witnessed on other cell types is also not well understood. Given $CD4^+$ T cells provide much needed stimulation for $CD8^+$ T cells, increased CD4 reinvigoration with α-PD-1 is likely beneficial to immune function and possibly explains why higher ratios of IgG4 staining on conventional CD4s versus Tregs is a positive predictor of clinical ICB response. Identifying which specific $CD4^+$ T cell subsets have greatest ICB binding, and how this response is different from that of CD8s, will further enable selective tuning of $CD8^+$ T cell potency.

## 7.4 Lymphocyte stability as a clinical marker and relation with B cell *IL7*

Across the results presented in this thesis, I found that measuring patient's lymphocyte counts before and after the first cycle of treatment, as per standard hospital care, was one of the most valuable predictors of long-term survival on ICB. Lymphocyte stability incorporated

multiple facets of dynamic T cell responses including clonal expansion, effector phenotype, activation and increased cytotoxicity, potentially explaining why it serves as such a strong biomarker of response. Interestingly, T cell clonal persistence beyond C2, such as out to C4, seems to be generally anti-correlated with beneficial responses based on unpublished data from this cohort and may instead reflect tumour persistence given many transcriptomic effects elevated at C2 tend to subside by C4. It would be interesting to understand whether LS also reflects a more immunogenic tumour and/or a permissive TME, thus allowing for T cell clones to react to tumour and persist through antigen stimulation and re-populating the peripheral repertoire. Since LS is predictive in sICB but less so in cICB, it would also be potentially useful to treat it as an early biomarker for whether sICB-treated individuals should have their immunotherapy escalated to cICB or not, depending on whether they have detectable LS changes or not. A detailed analysis of the utility and relevance of LS across multiple tumour types would also be important, given that it seems to be clinically relevant for metastatic melanoma and renal cell carcinoma (unpublished data, Robert Watson).

Lymphocyte stability appeared to be both linked with *IL7* from B cells, identified via a genetic effect, and non-classical monocyte subset proportion, based on single-cell interaction analysis. To what extent these interactions between T cells and B cells or monocytes are mediated by cell-cell interactions or instead paracrine cell signalling is unclear. When I assessed the number of BCR chains that were co-purified in bulk $CD8^+$ T cell RNAseq samples, I found significantly more BCRs were recovered from individuals with higher B cell *IL7* (unpublished data). This points to direct CD8-B cell interactions being potentially important for sustaining T cell responses. In line with this, published data suggests that B-T cell proximity within the tumour predicts responses to TIL therapy[354] whilst broadly, murine models have identified that B cells support $CD8^+$ T cell anti-tumour responses[355]. Given both monocytes and B cells tend to have high levels of MHC expression, this may make physical interactions with T cells more likely. This hypothesis of cell-cell interactions being required for T cell responses could be tested using a method such as PIC-seq[356], and would be interesting to understand in relation to B cell *IL7* for two reasons. Firstly, IL-7 has a short half-life with studies modifying its stability showing increased T cell persistence in a chimeric antigen receptor setting[357], and whether cell-associated IL-7 can similarly achieve such an effect would be interesting for both biological and therapy reasons. Secondly, it would give greater impetus to uncovering how B cell *IL7* gets induced in melanoma patients compared to healthy donors, in order to develop a therapeutic B-cell based agonist, as opposed to just delivering supra-biological infusions of recombinant IL-7 to patients. All in all, these findings appear to revitalise interest in the therapeutic use of IL-7 as an adjuvant to ICB[358] and may allow for pre-conditioning of

immune responses before immunotherapy treatment.

## 7.5 Developing an understanding of genetic determinants of ICB immunity

Finally, I made some interesting observations around genetic variation at two SNPs that affect ICB responses. The first was at the rs16906115 SNP within the *IL7* locus which appears to influence lymphocyte stability and T cell clonality, specifically in sICB, as well as subset proportions of USM B cells, and therefore total levels of B cell expression of *IL7*. How cell-count QTLs enact their effects is still very underexplored, although for a homeostatic cytokine such as IL-7, it would be tempting to explore whether levels of its cognate receptor *IL7R* are differentially expressed across different B cell subsets, and if this could help rationalise the genetic effects observed. Whether there is a transcriptomic mediator behind rs16906115's effects on *IL7* is unclear given the lack of difference in expression resulting from SNP variation within each subset, although cis or trans-acting QTLs very typically involve some degree of transcriptional perturbation. Traditional techniques commonly used for understanding how SNPs mediate transcriptomic variation include enzymatic probing and circular dichroism to examine mRNA folding[359,360], haplotype analysis for Kozak sequence alterations[361], and luciferase and RNA decay assays for identifying new open reading frames[362]. It would be interesting to understand (a) is there a difference in protein levels of IL-7 produced by B cells, (b) whether there is a difference in the levels of receptors and signalling proteins downstream of IL-7R and (c) whether these two factors therefore contribute to this shift in B cell subset proportions. Although rs16906115 also has pleiotropic effects in modulating T cell clonality, and lymphocyte stability as a clinical phenotype, it would be surprising if these effects were not mediated through these changes in *IL7* levels in peripheral blood.

The second SNP-phenotype observation I made was a QTL effect between Treg expansion and the rs3087243 SNP in the *CTLA4* locus. Single-cell eQTL studies have previously identified that minor allele carriage is associated with decreased levels of *CTLA4* particularly in conventional $CD4^+$ and $CD8^+$ T cells although a significant effect is still seen in Tregs[363,364]. As such, this potentially suggests that Tregs from minor allele carriers have decreased ipilimumab binding and undergo less ADCC. Given α-PD-1 appears to induce Treg proliferation and immunosuppression intratumourally[165], it seems that cICB does indeed lead to competing forces on Treg expansion, and hence genotypic effects may be more visible.

It is interesting to note that I didn't see any genotypic effects of rs3087243 when looking at changes in conventional T cell proportions, suggesting that the higher levels of CTLA-4 on Tregs are required to detect this SNP effect. To further dissect the effects of the rs3087243 SNP on Treg responses, it would be useful to perform Treg immunosuppression assays[365] using PBMCs from genotypically varied individuals both before and after treatment. Although no statistical differences in surface or intracellular expression levels of CTLA-4 in Tregs were observed by flow cytometry, it would be valuable to re-evaluate this after expanding the size of the patient cohort used for flow analysis.

More broadly, it would be extremely interesting to perform transcriptome-wide eQTL analysis using this bulk RNAseq and genotyping data. This could identify both melanoma-specific immune SNPs, as well as ICB context-specific QTLs. Some preliminary unpublished data suggests that eQTLs for $CD8^+$ T cell expression changes during ICB exist and have sufficient effect size to be detected in our cohort of n=151 individuals. Intriguingly, one eSNP identified in this analysis formed a cis-eQTL for *IFITM2*, which could potentially allow us to trace the directionality of downstream signalling related to type I IFN responses in $CD8^+$ T cells. Furthermore, it would be possible to begin investigating the genetic variation that contributes to changes in T cell clonality, and subset-subset interactions on a genome-wide scale, with the potential for validation using single-cell eQTL analysis.

# Chapter 8

# Appendix

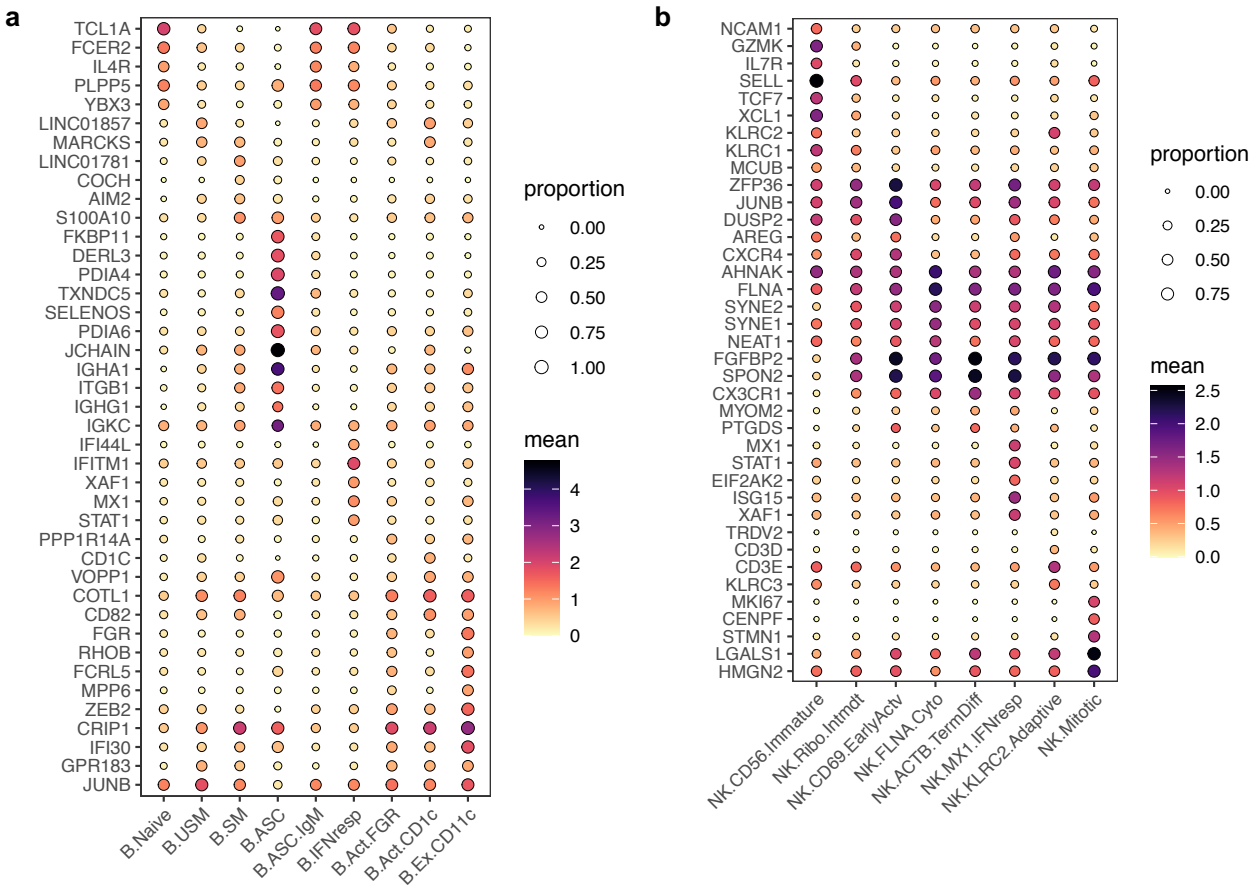



**Figure 8.1 Subset gene expression in B cells and NK cells.** The top 5 most distinguishing genes per subset were identified within each cell using Seurat's *AddModuleScore* function within B cells (a) and NK cells (b).

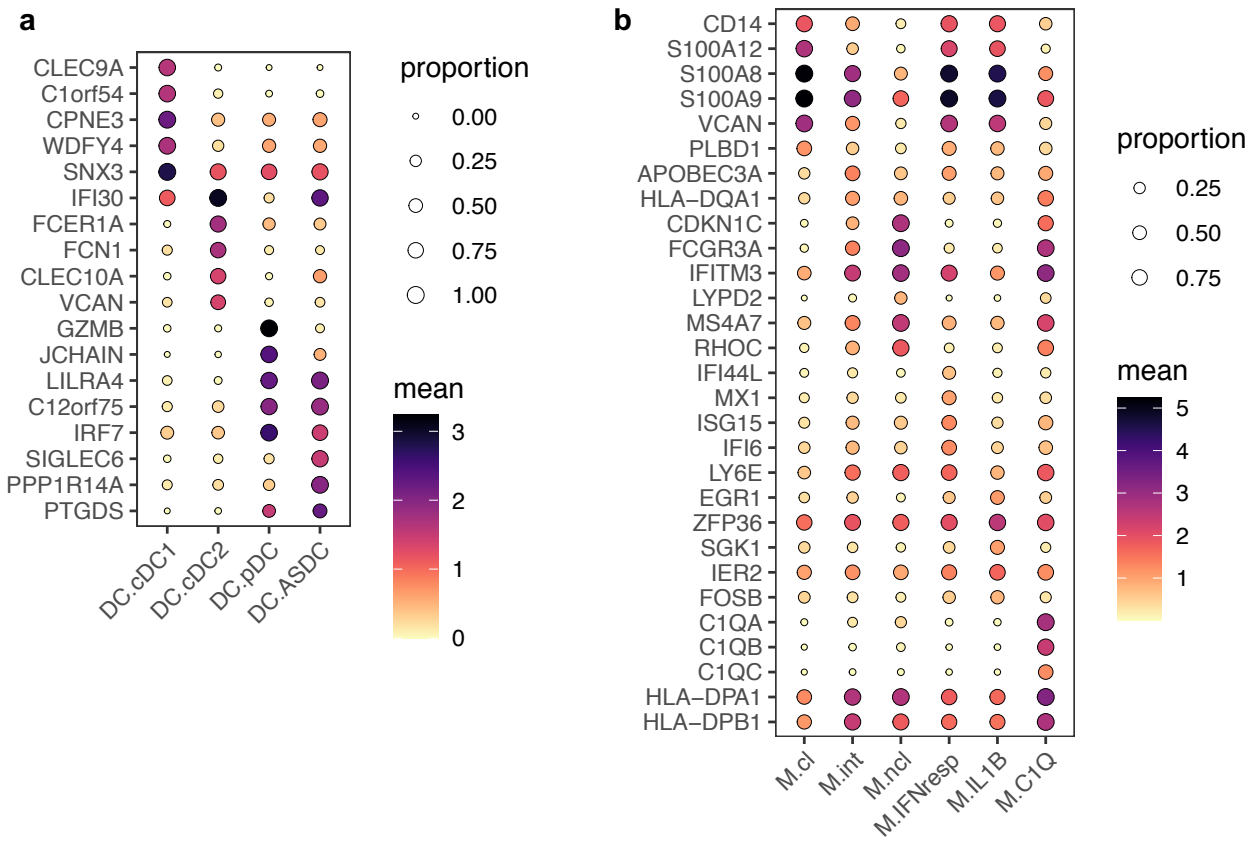



**Figure 8.2 Subset gene expression in DCs and monocytes.** The top 5 most distinguishing genes per subset were identified within each cell using Seurat's *AddModuleScore* function within DCs (a) and monocytes (b).

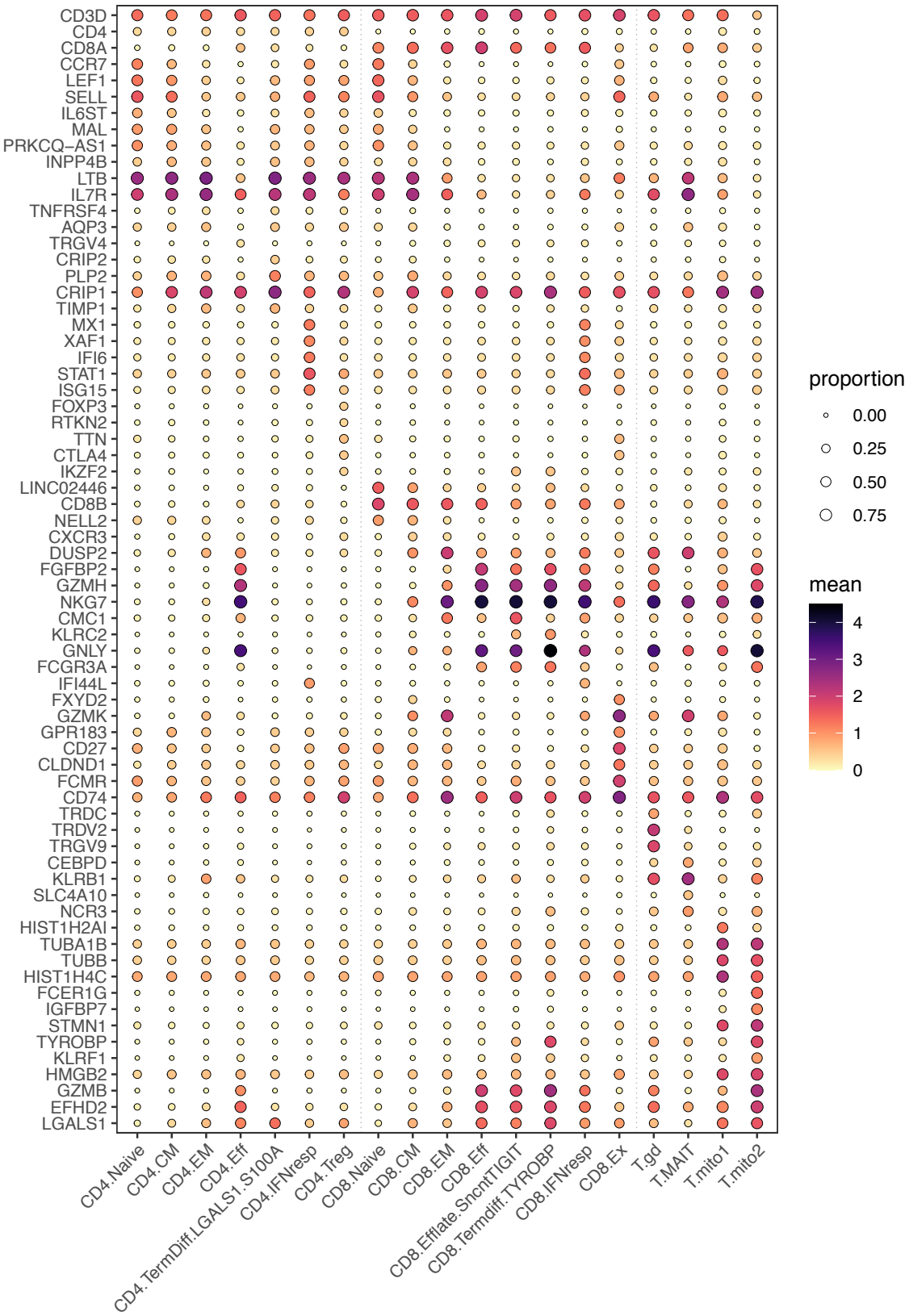



**Figure 8.3 Subset gene expression in DCs and monocytes.** The top 5 most distinguishing genes per subset were identified within each cell using Seurat's *AddModuleScore* function within T cell subsets.

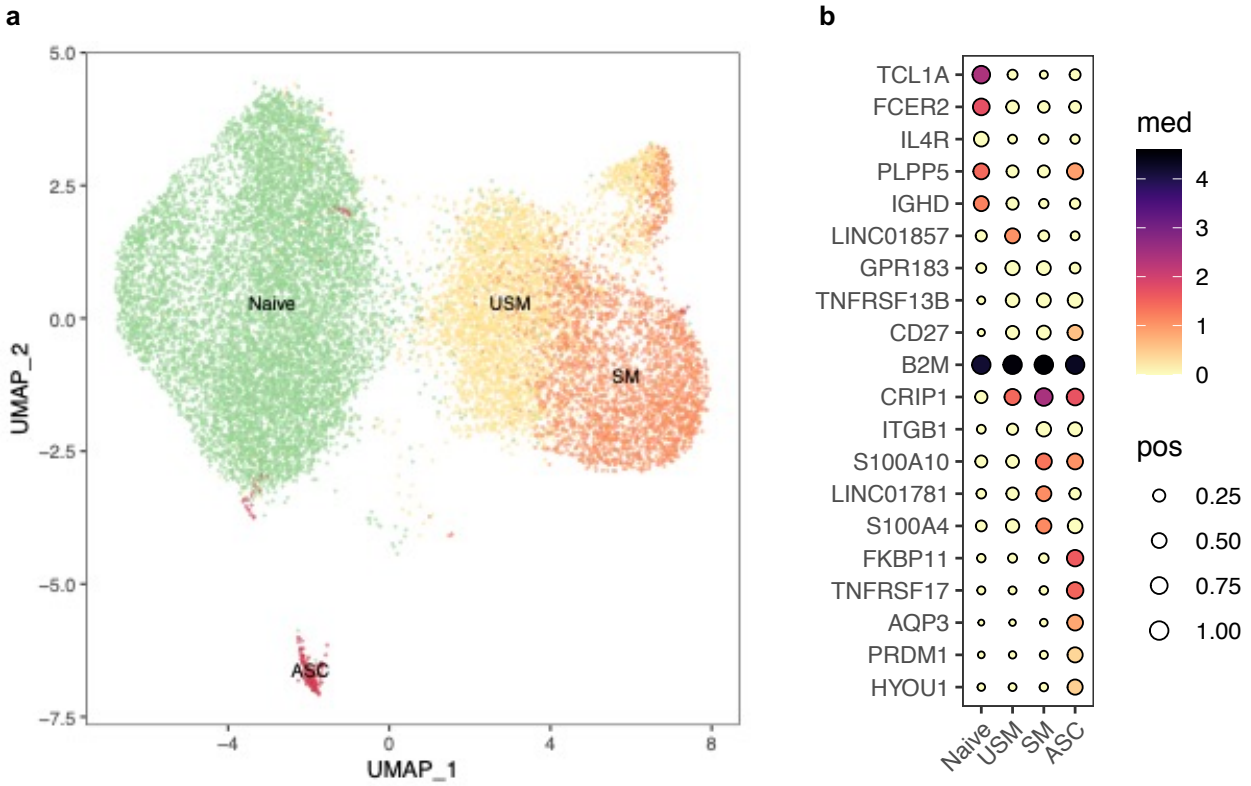



**Figure 8.4 UMAP and B cell subsets for combined single-cell RNAseq dataset. (a)** B cells from single-cell PBMC data and from a separate dataset from the same cohort were merged, clustered and re-annotated. (b) Subset gene expression across the B cell subsets. The top 5 most distinguishing genes per subset were identified within each cell using Seurat's *AddModuleScore* function within B cell subsets.

# Bibliography


1. CRUK. *Melanoma Skin Cancer* https://www.cancerresearchuk.org/health-professional/cancer-statistics/statistics-by-cancer-type/melanoma-skin-cancer.
2. NICE. *Melanoma: assessment and management* https://www.nice.org.uk/guidance/ng14.
3. Ward, W. Cutaneous Melanoma: Etiology and Therapy ([2017]).
4. Hayward, N. Whole-genome landscapes of major melanoma subtypes. Nature *545*, 175–180 (2017).
5. Bishop, D. Genome-wide association study identifies three loci associated with melanoma risk. Nature Genetics *41*, 920–5 (2009).
6. Helgadottir, H. Germline CDKN2A Mutation Status and Survival in Familial Melanoma Cases. Journal of the National Cancer Institute *108*, 11 (2016).
7. Lawrence, M. Mutational heterogeneity in cancer and the search for new cancer-associated genes. Nature *499*, 214–218 (2013).
8. Alexandrov, L. Signatures of mutational processes in human cancer. Nature *500*, 415–421 (2013).
9. Charoentong, P. Pan-cancer Immunogenomic Analyses Reveal Genotype-Immunophenotype Relationships and Predictors of Response to Checkpoint Blockade. Cell Reports *18*, 248–262 (2017).
10. Lennerz, V. The response of autologous T cells to a human melanoma is dominated by mutated neoantigens. PNAS *102*, 16013–16018 (2005).
11. Schumacher, T. Neoantigens in cancer immunotherapy. Science *348*, 69–74 (2015).
12. Kalialis, L. Spontaneous regression of metastases from melanoma: review of the literature. Melanoma Research *19*, 275–82 (2009).

13. Quaglino, P. Vitiligo is an independent favourable prognostic factor in stage III and IV metastatic melanoma patients: results from a single-institution hospital-based observational cohort study. Annals of Oncology *21*, 409–414 (2010).

14. Fishman, P. Vitiligo autoantibodies are effective against melanoma. Cancer *72*, 2365–9 (1993).

15. Clemente, C. Prognostic value of tumor infiltrating lymphocytes in the vertical growth phase of primary cutaneous melanoma. Cancer *77*, 1303–10 (1996).

16. Azimi, F. Tumor-infiltrating lymphocyte grade is an independent predictor of sentinel lymph node status and survival in patients with cutaneous melanoma. Journal of Clinical Oncology *30*, 2678–83 (2012).

17. Thomas, N. Tumor-infiltrating lymphocyte grade in primary melanomas is independently associated with melanoma-specific survival in the population-based genes, environment and melanoma study. Journal of Clinical Oncology *31*, 4252–9 (2013).

18. Bourke, J. Management of adverse events related to new cancer immunotherapy (immune checkpoint inhibitors). Medical Journal of Australia *205*, 418–424 (2016).

19. Essner, R. Contemporary surgical treatment of advanced-stage melanoma. Archives of Surgery *139*, 961–6 (2004).

20. Hanahan, D. Hallmarks of Cancer: New Dimensions. Cancer Discovery *12*, 31–46 (2022).

21. Leach, D. Enhancement of antitumor immunity by CTLA-4 blockade. Science *271*, 1734–6 (1996).

22. Hodi, F. Improved survival with ipilimumab in patients with metastatic melanoma. New England Journal of Medicine *363*, 711–23 (2010).

23. Robert, C. Ipilimumab plus dacarbazine for previously untreated metastatic melanoma. New England Journal of Medicine *364*, 2517–26 (2011).

24. Ishida, Y. Induced expression of PD-1, a novel member of the immunoglobulin gene superfamily, upon programmed cell death. The EMBO Journal *11*, 3887–95 (1992).

25. Nishimura, H. Development of lupus-like autoimmune diseases by disruption of the PD-1 gene encoding an ITIM motif-carrying immunoreceptor. Immunity *11*, 141–51 (1999).

26. Iwai, Y. Involvement of PD-L1 on tumor cells in the escape from host immune system and tumor immunotherapy by PD-L1 blockade. PNAS *99*, 12293–7 (2002).

27. Brahmer, J. Phase I study of single-agent anti-programmed death-1 (MDX-1106) in refractory solid tumors: safety, clinical activity, pharmacodynamics, and immunologic correlates. Journal of Clinical Oncology *28*, 3167–75 (2010).

28. Robert, C. Nivolumab in previously untreated melanoma without BRAF mutation. New England Journal of Medicine *372*, 320–30 (2015).

29. Robert, C. Pembrolizumab versus Ipilimumab in Advanced Melanoma. New England Journal of Medicine *372*, 2521–32 (2015).

30. NICE. *Ipilimumab for previously treated advanced (unresectable or metastatic) melanoma* `https://www.nice.org.uk/guidance/ta268`.

31. NICE. *Pembrolizumab for advanced melanoma not previously treated with ipilimumab* `https://www.nice.org.uk/guidance/ta366`.

32. NICE. *Nivolumab for treating advanced (unresectable or metastatic) melanoma* `https://www.nice.org.uk/guidance/ta384`.

33. Larkin, J. Combined Nivolumab and Ipilimumab or Monotherapy in Untreated Melanoma. New England Journal of Medicine *373*, 23–34 (2015).

34. NICE. *Nivolumab in combination with ipilimumab for treating advanced melanoma* `https://www.nice.org.uk/guidance/ta400`.

35. NICE. *Nivolumab for adjuvant treatment of completely resected melanoma with lymph node involvement or metastatic disease* `https://www.nice.org.uk/guidance/ta684`.

36. Weber, J. Adjuvant Nivolumab versus Ipilimumab in Resected Stage III or IV Melanoma. New England Journal of Medicine *377*, 1824–1835 (2017).

37. Tawbi, H. Relatlimab and Nivolumab versus Nivolumab in Untreated Advanced Melanoma. New England Journal of Medicine *386*, 24–34 (2022).

38. Sandru, A. Survival rates of patients with metastatic malignant melanoma. Journal of Medicine and Life *7*, 572–6 (2014).

39. Robert, C. Five-Year Outcomes With Nivolumab in Patients With Wild-Type BRAF Advanced Melanoma. Journal of Clinical Oncology *38*, 3937–3946 (2020).

40. Hamid, O. Five-year survival outcomes for patients with advanced melanoma treated with pembrolizumab in KEYNOTE-001. Annals of Oncology *30*, 582–588 (2019).

41. Larkin, J. Five-Year Survival with Combined Nivolumab and Ipilimumab in Advanced Melanoma. New England Journal of Medicine *381*, 1535–1546 (2019).

42. Wang, Q. What Happens to the Immune Microenvironment After PD-1 Inhibitor Therapy? Frontiers in Immunology *12*, 773168 (2021).

43. Emens, L. Cancer immunotherapy: Opportunities and challenges in the rapidly evolving clinical landscape. European Journal of Cancer *81*, 116–129 (2017).

44. Ye, W. Checkpoint-blocker-induced autoimmunity is associated with favourable outcome in metastatic melanoma and distinct T-cell expression profiles. British Journal of Cancer *124*, 1661–1669 (2021).

45. Del Castillo, M. The Spectrum of Serious Infections Among Patients Receiving Immune Checkpoint Blockade for the Treatment of Melanoma. Clinical Infectious Diseases *63*, 1490–1493 (2016).

46. Petrelli, F. Association of Steroids use with Survival in Patients Treated with Immune Checkpoint Inhibitors: A Systematic Review and Meta-Analysis. Cancers *12*, 546 (2020).

47. Maslov, D. Timing of steroid initiation and response rates to immune checkpoint inhibitors in metastatic cancer. Journal of Immunotherapy for Cancer *9*, e002261 (2021).

48. Zhang, H. Impact of corticosteroid use on outcomes of non-small-cell lung cancer patients treated with immune checkpoint inhibitors: A systematic review and meta-analysis. Journal of Clinical Pharmacy and Therapeutics *46*, 927–935 (2021).

49. Sallusto, F. Central memory and effector memory T cell subsets: function, generation, and maintenance. Annual Reviews in Immunology *22*, 745–63 (2004).

50. Fritsch, R. Stepwise differentiation of CD4 memory T cells defined by expression of CCR7 and CD27. Journal of Immunology *175*, 6489–97 (2005).

51. Gattinoni, L. A human memory T cell subset with stem cell-like properties. Nature Medicine *17*, 1290–7 (2011).

52. Gebhardt, T. Different patterns of peripheral migration by memory CD4+ and CD8+ T cells. Nature *477*, 216–9 (2011).

53. Watanabe, K. Human skin is protected by four functionally and phenotypically discrete populations of resident and recirculating memory T cells. Science Translational Medicine *7*, 279ra39 (2015).

54. Martin, M. Phenotypic and Functional Alterations in Circulating Memory CD8 T Cells with Time after Primary Infection. PLos Pathogens *11*, e1005219 (2015).

55. Detjen, K. Interferon gamma inhibits growth of human pancreatic carcinoma cells via caspase-1 dependent induction of apoptosis. Gut *49*, 251–62 (2001).

56. Wang, L. TNF-alpha induces two distinct caspase-8 activation pathways. Cell *133*, 693–703 (2008).

57. Martini, M. IFN-gamma-mediated upmodulation of MHC class I expression activates tumor-specific immune response in a mouse model of prostate cancer. Vaccine *28*, 3548–57 (2010).

58. Bhat, P. Interferon-ɣ derived from cytotoxic lymphocytes directly enhances their motility and cytotoxicity. Cell Death and Discovery *8*, e2836 (2017).

59. Kearney, C. Tumor immune evasion arises through loss of TNF sensitivity. Science Immunology *3*, eaar3451 (2018).

60. Cachot, A. Tumor-specific cytolytic CD4 T cells mediate immunity against human cancer. Science Advances *7*, eabe3348 (2021).

61. Oh, D. Intratumoral CD4 + T Cells Mediate Anti-tumor Cytotoxicity in Human Bladder Cancer. Cell *181*, 1612–1625.e13 (2020).

62. Oliviera, G. Landscape of helper and regulatory antitumour CD4 + T cells in melanoma. Nature *605*, 532–538 (2022).

63. Dhatchinamoorthy, K. Cancer Immune Evasion Through Loss of MHC Class I Antigen Presentation. Frontiers in Immunology *12*, 636568 (2021).

64. Kuiper, H. Activated T cells can induce high levels of CTLA-4 expression on B cells. Journal of Immunology *155*, 1776–83 (1995).

65. Wang, X. Expression of CTLA-4 by human monocytes. Scandinavian Journal of Immunology *55*, 53–60 (2002).

66. Wang, X. CTLA4 is expressed on mature dendritic cells derived from human monocytes and influences their maturation and antigen presentation. BMC Immunology *12*, 21 (2011).

67. Brunner, M. CTLA-4-Mediated inhibition of early events of T cell proliferation. Journal of Immunology *162*, 5813–20 (1999).

68. Egen, J. Cytotoxic T lymphocyte antigen-4 accumulation in the immunological synapse is regulated by TCR signal strength. Immunity *16*, 23–35 (2002).

69. Linsley, P. CTLA-4 is a second receptor for the B cell activation antigen B7. Journal of Experimental Medicine *174*, 561–9 (1991).

70. Collins, A. The interaction properties of costimulatory molecules revisited. Immunity *17*, 201–10 (2002).

71. Van de Merwe, P. CD80 (B7-1) binds both CD28 and CTLA-4 with a low affinity and very fast kinetics. Journal of Experimental Medicine *185*, 393–403 (1997).

72. Lee, K. Molecular basis of T cell inactivation by CTLA-4. Science *282*, 2263–6 (1998).

73. Fraser, J. CTLA4 ligation attenuates AP-1, NFAT and NF-kappaB activity in activated T cells. European Journal of Immunology *29*, 838–44 (1999).

74. Qureshi, O. Trans-endocytosis of CD80 and CD86: a molecular basis for the cell-extrinsic function of CTLA-4. Science *332*, 600–3 (2011).

75. Tivol, E. Loss of CTLA-4 leads to massive lymphoproliferation and fatal multiorgan tissue destruction, revealing a critical negative regulatory role of CTLA-4. Immunity *3*, 541–7 (1995).

76. Waterhouse, P. Lymphoproliferative disorders with early lethality in mice deficient in Ctla-4. Science *270*, 985–8 (1995).

77. Wing, K. CTLA-4 control over Foxp3+ regulatory T cell function. Science *322*, 271–5 (2008).

78. Schumann, K. Functional CRISPR dissection of gene networks controlling human regulatory T cell identity. Nature Immunology *21*, 1456–1466 (2020).

79. Ramagopal, U. Structural basis for cancer immunotherapy by the first-in-class checkpoint inhibitor ipilimumab. PNAS *114*, e4223–e4232 (2017).

80. Chen, H. Anti-CTLA-4 therapy results in higher CD4+ICOShi T cell frequency and IFN-gamma levels in both nonmalignant and malignant prostate tissues. PNAS *106*, 2729–34 (2009).

81. Tang, D. Increased frequency of ICOS+ CD4 T cells as a pharmacodynamic biomarker for anti-CTLA-4 therapy. Cancer Immunology Research *1*, 229–34 (2013).

82. Fan, X. Engagement of the ICOS pathway markedly enhances efficacy of CTLA-4 blockade in cancer immunotherapy. Journal of Experimental Medicine *211*, 715–25 (2014).

83. Wei, S. Distinct Cellular Mechanisms Underlie Anti-CTLA-4 and Anti-PD-1 Checkpoint Blockade. Cell *170*, 1120–1133.e17 (2017).

84. Robert, L. CTLA4 blockade broadens the peripheral T-cell receptor repertoire. Clinical Cancer Research *20*, 2424–32 (2014).

85. Kvistborg, P. Anti-CTLA-4 therapy broadens the melanoma-reactive CD8+ T cell response. Science Translational Medicine *6*, 254ra128 (2014).

86. Wei, S. Fundamental Mechanisms of Immune Checkpoint Blockade Therapy. Cancer Discovery *8*, 1069–1086 (2018).

87. Ribas, A. Cancer immunotherapy using checkpoint blockade. Science *359*, 1350–1355 (2018).

88. Vargas, F. Fc Effector Function Contributes to the Activity of Human Anti-CTLA-4 Antibodies. Cancer Cell *33*, 649–663 (2019).

89. Simpson, T. Fc-dependent depletion of tumor-infiltrating regulatory T cells co-defines the efficacy of anti-CTLA-4 therapy against melanoma. Journal of Experimental Medicine *210*, 1695–710 (2013).

90. Sharma, A. Anti-CTLA-4 Immunotherapy Does Not Deplete FOXP3 + Regulatory T Cells (Tregs) in Human Cancers. Clinical Cancer Research *25*, 1233–1238 (2019).

91. Freeman, G. Engagement of the PD-1 immunoinhibitory receptor by a novel B7 family member leads to negative regulation of lymphocyte activation. Journal of Experimental Medicine *192*, 1027–34 (2000).

92. Agata, Y. Expression of the PD-1 antigen on the surface of stimulated mouse T and B lymphocytes. International Immunology *8*, 765–72 (1996).

93. Mimura, K. PD-L1 expression is mainly regulated by interferon gamma associated with JAK-STAT pathway in gastric cancer. International Immunology *109*, 43–53 (2018).

94. Shephard, K. PD-1 inhibits T-cell receptor induced phosphorylation of the ZAP70/CD3zeta signalosome and downstream signaling to PKCtheta. FEBS Letters *574*, 37–41 (2004).

95. Hui, E. T cell costimulatory receptor CD28 is a primary target for PD-1-mediated inhibition. Science *355*, 1428–1433 (2017).

96. Karwacz, K. PD-L1 co-stimulation contributes to ligand-induced T cell receptor down-modulation on CD8+ T cells. EMBO Molecular Medicine *3*, 581–92 (2011).

97. Patsoukis, N. Selective effects of PD-1 on Akt and Ras pathways regulate molecular components of the cell cycle and inhibit T cell proliferation. Science Signaling *5*, ra46 (2012).

98. Patsoukis, N. PD-1 alters T-cell metabolic reprogramming by inhibiting glycolysis and promoting lipolysis and fatty acid oxidation. Nature Communications *6*, 6692 (2015).

99. Buck, M. Mitochondrial Dynamics Controls T Cell Fate through Metabolic Programming. Cell *166*, 63–76 (2016).

100. Bengsch, B. Bioenergetic Insufficiencies Due to Metabolic Alterations Regulated by the Inhibitory Receptor PD-1 Are an Early Driver of CD8(+) T Cell Exhaustion. Immunity *45*, 358–73 (2016).

101. Thommem, D. A transcriptionally and functionally distinct PD-1 + CD8 + T cell pool with predictive potential in non-small-cell lung cancer treated with PD-1 blockade. Nature Medicine *24*, 994–1004 (2018).

102. Fessas, P. A molecular and preclinical comparison of the PD-1–targeted T-cell checkpoint inhibitors nivolumab and pembrolizumab. Seminars in Oncology *44*, 136–140 (2017).

103. Riaz, N. Tumor and Microenvironment Evolution during Immunotherapy with Nivolumab. Cell *171*, 934–949.e16 (2017).

104. Huang, A. T-cell invigoration to tumour burden ratio associated with anti-PD-1 response. Nature *545*, 60–65 (2017).

105. Ribas, A. PD-1 Blockade Expands Intratumoral Memory T Cells. Cancer Immunology Research *4*, 194–203 (2016).

106. Chow, M. Intratumoral activity of the CXCR3 chemokine system is required for the efficacy of anti- PD-1 therapy. Immunity *50*, 1498–1512.e5 (2019).

107. House, I. Macrophage-Derived CXCL9 and CXCL10 Are Required for Antitumor Immune Responses Following Immune Checkpoint Blockade. Clinical Cancer Research *26*, 487–504 (2020).

108. Pauken, K. Epigenetic stability of exhausted T cells limits durability of reinvigoration by PD-1 blockade. Science *354*, 1160–1165 (2016).

109. Sen, D. The epigenetic landscape of T cell exhaustion. Science *354*, 1165–1169 (2016).

110. Ghoneim, H. De Novo Epigenetic Programs Inhibit PD-1 Blockade-Mediated T Cell Rejuvenation. Cell *170*, 142–157.e19 (2017).

111. Philip, M. Chromatin states define tumour-specific T cell dysfunction and reprogramming. Nature *545*, 452–456 (2017).

112. Yost, K. Clonal replacement of tumor-specific T cells following PD-1 blockade. Nature Medicine *25*, 1251–1259 (2019).

113. Nagasaki, J. PD-1 blockade therapy promotes infiltration of tumor-attacking exhausted T cell clonotypes. Cell Reports *38*, 110331 (2022).

114. Amaria, R. Neoadjuvant immune checkpoint blockade in high-risk resectable melanoma. Nature Medicine *24*, 1649–1654 (2018).

115. Tumeh, P. PD-1 blockade induces responses by inhibiting adaptive immune resistance. Nature *515*, 568–71 (2014).

116. Oliviera, G. Phenotype, specificity and avidity of antitumour CD8 + T cells in melanoma. Nature *596*, 119–125 (2022).

117. Woolaver, R. Differences in TCR repertoire and T cell activation underlie the divergent outcomes of antitumor immune responses in tumor-eradicating versus tumor-progressing hosts. Journal of Immunotherapy for Cancer *9*, e001615 (2021).

118. Simoni, Y. Bystander CD8 + T cells are abundant and phenotypically distinct in human tumour infiltrates. Nature *557*, 575–579 (2018).

119. Banchereau, R. Intratumoral CD103+ CD8+ T cells predict response to PD-L1 blockade. Journal of Immunotherapy for Cancer *9*, e002231 (2021).

120. Koh, J. MDSC subtypes and CD39 expression on CD8 + T cells predict the efficacy of anti-PD-1 immunotherapy in patients with advanced NSCLC. European Journal of Immunology *50*, 1810–1819 (2020).

121. Attrill, G. Higher proportions of CD39+ tumor-resident cytotoxic T cells predict recurrence-free survival in patients with stage III melanoma treated with adjuvant immunotherapy. Journal of Immunotherapy for Cancer *10*, e004771 (2022).

122. Luoma, A. Tissue-resident memory and circulating T cells are early responders to pre-surgical cancer immunotherapy. Cell *185*, 2918–2935.e29 (2022).

123. Jaiswal, A. An activation to memory differentiation trajectory of tumor-infiltrating lymphocytes informs metastatic melanoma outcomes. Cancer Cell *40*, 524–544.e5 (2022).

124. Principe, N. Tumor Infiltrating Effector Memory Antigen-Specific CD8 + T Cells Predict Response to Immune Checkpoint Therapy. Frontiers in Immunology *11*, 584423 (2020).

125. Sade-Feldman, M. Defining T Cell States Associated with Response to Checkpoint Immunotherapy in Melanoma. Cell *175*, 998–1013.e20 (2018).

126. Gattinoni, L. Wnt signaling arrests effector T cell differentiation and generates CD8+ memory stem cells. Nature Medicine *15*, 808–13 (2009).

127. Siddiqui, I. Intratumoral Tcf1 + PD-1 + CD8 + T Cells with Stem-like Properties Promote Tumor Control in Response to Vaccination and Checkpoint Blockade Immunotherapy. Immunity *50*, 195–211.e10 (2019).

128. Liu, B. Temporal single-cell tracing reveals clonal revival and expansion of precursor exhausted T cells during anti-PD-1 therapy in lung cancer. Nature Cancer *3*, 108–121 (2022).

129. Burger, M. Antigen dominance hierarchies shape TCF1 + progenitor CD8 T cell phenotypes in tumors. Cell *184*, 4996–5014.e26 (2021).

130. Dammeijer, F. The PD-1/PD-L1-Checkpoint Restrains T cell Immunity in Tumor-Draining Lymph Nodes. Cancer Cell *38*, 685–700.e8 (2020).

131. Li, C. A high OXPHOS CD8 T cell subset is predictive of immunotherapy resistance in melanoma patients. Journal of Experimental Medicine *219*, e20202084 (2022).

132. Connolly, K. A reservoir of stem-like CD8 + T cells in the tumor-draining lymph node preserves the ongoing antitumor immune response. Science Immunology *6*, eabg7836 (2021).

133. Schenkel, J. Conventional type I dendritic cells maintain a reservoir of proliferative tumor-antigen specific TCF-1 + CD8 + T cells in tumor-draining lymph nodes. Immunity *54*, 2338–2353.e6 (2021).

134. Voabil, P. An ex vivo tumor fragment platform to dissect response to PD-1 blockade in cancer. Nature Medicine *27*, 1250–1261 (2021).

135. Wu, T. Peripheral T cell expansion predicts tumour infiltration and clinical response. Nature *579*, 274–278 (2020).

136. Aoki, H. Greater extent of blood-tumor TCR repertoire overlap is associated with favorable clinical responses to PD-1 blockade. Cancer Science *112*, 2993–3004 (2021).

137. Pauken, K. Single-cell analyses identify circulating anti-tumor CD8 T cells and markers for their enrichment. Journal of Experimental Medicine *218*, e20200920 (2021).

138. Lucca, L. Circulating clonally expanded T cells reflect functions of tumor-infiltrating T cells. Journal of Experimental Medicine *218*, e20200921 (2021).

139. Watson, R. Immune checkpoint blockade sensitivity and progression-free survival associates with baseline CD8 + T cell clone size and cytotoxicity. Science Immunology *6*, eabj8825 (2021).

140. Hong, J. Hepatocellular carcinoma patients with high circulating cytotoxic T cells and intra-tumoral immune signature benefit from pembrolizumab: results from a single-arm phase 2 trial. Genome Medicine *14*, 1 (2022).

141. Yamauchi, T. T-cell CX3CR1 expression as a dynamic blood-based biomarker of response to immune checkpoint inhibitors. Nature Communications *12*, 1402 (2021).

142. De Lima, V. Immune Cell Profiling of Peripheral Blood as Signature for Response During Checkpoint Inhibition Across Cancer Types. Frontiers in Oncology *11*, 558248 (2021).

143. Valpione, S. Immune-awakening revealed by peripheral T cell dynamics after one cycle of immunotherapy. Nature Cancer *1*, 210–221 (2020).

144. Shen, R. LAG-3 expression on peripheral blood cells identifies patients with poorer outcomes after immune checkpoint blockade. Science Translational Medicine *13*, eabf5107 (2021).

145. Kato, T. Peripheral T cell receptor repertoire features predict durable responses to anti-PD-1 inhibitor monotherapy in advanced renal cell carcinoma. Clinical and Translational Oncology *23*, 1646–1656 (2021).

146. Han, J. Resident and circulating memory T cells persist for years in melanoma patients with durable responses to immunotherapy. Nature Cancer *2*, 300–311 (2021).

147. Fairfax, B. Peripheral CD8+ T cell characteristics. Nature Medicine *26*, 193–199 (2020).

148. Au, L. Determinants of anti-PD-1 response and resistance in clear cell renal cell carcinoma. Cancer Cell *39*, 1497–1518.e11 (2021).

149. Holm, J. Neoantigen-specific CD8 T cell responses in the peripheral blood following PD-L1 blockade might predict therapy outcome in metastatic urothelial carcinoma. Nature Communications *13*, 1935 (2022).

150. Snell, L. Dynamic CD4 + T cell heterogeneity defines subset-specific suppression and PD-L1-blockade-driven functional restoration in chronic infection. Nature Immunology *22*, 1524–1537 (2021).

151. Veatch, J. Neoantigen-specific CD4+ T cells in human melanoma have diverse differentiation states and correlate with CD8+ T cell, macrophage, and B cell function. Cancer Cell *40*, 393–409.e9 (2022).

152. Cui, C. Neoantigen-driven B cell and CD4 T follicular helper cell collaboration promotes anti-tumor CD8 T cell responses. Frontiers in Immunology *184*, 6101–6118.e13 (2021).

153. Yi, R. MHC-II Signature Correlates With Anti-Tumor Immunity and Predicts anti-PD-L1 Response of Bladder Cancer. Frontiers in Cellular and Development Biology *10*, 757137 (2022).

154. Alspach, E. MHC-II neoantigens shape tumour immunity and response to immunotherapy. Nature *574*, 696–701 (2019).

155. Spitzer, M. Systemic Immunity Is Required for Effective Cancer Immunotherapy. Cell *168*, 487–502.e15 (2017).

156. Zuazo, M. Functional systemic CD4 immunity is required for clinical responses to PD-L1/PD-1 blockade therapy. EMBO Molecular Medicine *11*, e10293 (2019).

157. Kagamu, H. CD4 + T-cell Immunity in the Peripheral Blood Correlates with Response to Anti-PD-1 Therapy. Cancer Immunology Research *8*, 334–344 (2020).

158. Lozano, A. T cell characteristics associated with toxicity to immune checkpoint blockade in patients with melanoma. Nature Medicine *28*, 353–362 (2022).

159. Jordan, M. Thymic selection of CD4+CD25+ regulatory T cells induced by an agonist self-peptide. Nature Immunology *2*, 301–6 (2001).

160. Ottonello, S. Association Between Response to Nivolumab Treatment and Peripheral Blood Lymphocyte Subsets in Patients With Non-small Cell Lung Cancer. Frontiers in Immunology *11*, 125 (2020).

161. Schoonderwoerd, M. Targeting Endoglin-Expressing Regulatory T Cells in the Tumor Microenvironment Enhances the Effect of PD1 Checkpoint Inhibitor Immunotherapy. Clinical Cancer Research *26*, 3831–3842 (2020).

162. Feng, M. Pharmacological inhibition of β-catenin/BCL9 interaction overcomes resistance to immune checkpoint blockades by modulating T reg cells. Science Advances *5*, eaau5240 (2019).

163. Kumagai, S. The PD-1 expression balance between effector and regulatory T cells predicts the clinical efficacy of PD-1 blockade therapies. Nature Immunology *21*, 1346–1358 (2020).

164. Perry, J. PD-L1-PD-1 interactions limit effector regulatory T cell populations at homeostasis and during infection. Nature Immunology *23*, 743–756 (2022).

165. Kamada, T. PD-1 + regulatory T cells amplified by PD-1 blockade promote hyperprogression of cancer. PNAS *116*, 9999–10008 (2019).

166. Masuda, K. Multiplexed single-cell analysis reveals prognostic and nonprognostic T cell types in human colorectal cancer. Journal of Clinical Investigations Insight *7*, e154646 (2022).

167. Chen, Y. Tumor-associated macrophages: an accomplice in solid tumor progression. Journal of Biomedical Science *26*, 78 (2019).

168. Qu, Y. Baseline Frequency of Inflammatory Cxcl9-Expressing Tumor-Associated Macrophages Predicts Response to Avelumab Treatment. Cell Reports *32*, 107873 (2020).

169. Li, S. Metabolism drives macrophage heterogeneity in the tumor microenvironment. Cell Reports *39*, 110609 (2022).

170. Kersten, K. Spatiotemporal co-dependency between macrophages and exhausted CD8 + T cells in cancer. Cancer Cell *40*, 624–638.e9 (2022).

171. Braun, D. Progressive immune dysfunction with advancing disease stage in renal cell carcinoma. Cancer Cell *39*, 632–648.e8 (2021).

172. Bassez, A. A single-cell map of intratumoral changes during anti-PD1 treatment of patients with breast cancer. Nature Medicine *27*, 820–832 (2021).

173. Sumitomo, R. PD-L1 expression on tumor-infiltrating immune cells is highly associated with M2 TAM and aggressive malignant potential in patients with resected non-small cell lung cancer. Lung Cancer *136*, 136–144 (2019).

174. Gordon, S. PD-1 expression by tumour-associated macrophages inhibits phagocytosis and tumour immunity. Nature *545*, 495–499 (2017).

175. Bagaev, A. Conserved pan-cancer microenvironment subtypes predict response to immunotherapy. Cancer Cell *39*, 845–865.e7 (2021).

176. Hammerl, D. Spatial immunophenotypes predict response to anti-PD1 treatment and capture distinct paths of T cell evasion in triple negative breast cancer. Nature Communications *12*, 5668 (2021).

177. Zhang, S. The Role of Myeloid-Derived Suppressor Cells in Patients with Solid Tumors: A Meta-Analysis. PLoS One *11*, e0164514 (2016).

178. Meyer, C. Frequencies of circulating MDSC correlate with clinical outcome of melanoma patients treated with ipilimumab. Cancer Immunology and Immunotherapy *63*, 247–57 (2014).

179. Strauss, L. RORC1 Regulates Tumor-Promoting "Emergency" Granulo-Monocytopoiesis. Cancer Cell *28*, 253–69 (2015).

180. Bronte, V. Recommendations for myeloid-derived suppressor cell nomenclature and characterization standards. Nature Communications *7*, 12150 (2016).

181. Li, L. Irf8 regulates macrophage versus neutrophil fate during zebrafish primitive myelopoiesis. Blood *117*, 1359–69 (2011).

182. Langlais, D. The macrophage IRF8/IRF1 regulome is required for protection against infections and is associated with chronic inflammation. Journal of Experimental Medicine *213*, 585–603 (2016).

183. Singh, S. IL-1α Mediates Innate and Acquired Resistance to Immunotherapy in Melanoma. Journal of Immunology *206*, 1966–1975 (2021).

184. Millrud, C. On the origin of myeloid-derived suppressor cells. Oncotarget *8*, 3649–3665 (2017).

185. Flores-Toro, J. CCR2 inhibition reduces tumor myeloid cells and unmasks a checkpoint inhibitor effect to slow progression of resistant murine gliomas. PNAS *117*, 1129–1138 (2020).

186. Chasseuil, E. Blood Predictive Biomarkers for Nivolumab in Advanced Melanoma. Acta Dermato-Venereologica *98*, 406–410 (2018).

187. Rad Pour, S. Predicting anti-PD-1 responders in malignant melanoma from the frequency of S100A9+ monocytes in the blood. Journal of Immunotherapy for Cancer *9*, e002171 (2021).

188. Gentles, A. The prognostic landscape of genes and infiltrating immune cells across human cancers. Nature Medicine *21*, 938–945 (2015).

189. Anagnostou, V. Integrative Tumor and Immune Cell Multi-omic Analyses Predict Response to Immune Checkpoint Blockade in Melanoma. Cell Reports Medicine *1*, 100139 (2020).

190. Helmink, B. B cells and tertiary lymphoid structures promote immunotherapy response. Nature *577*, 549–555 (2020).

191. Cabrita, R. Tertiary lymphoid structures improve immunotherapy and survival in melanoma. Nature *577*, 561–565 (2020).

192. Griss, J. B cells sustain inflammation and predict response to immune checkpoint blockade in human melanoma. Nature Communications *10*, 4186 (2019).

193. Patil, N. Intratumoral plasma cells predict outcomes to PD-L1 blockade in non-small cell lung cancer. Cancer Cell *40*, 289–300.e4 (2022).

194. Meylan, M. Tertiary lymphoid structures generate and propagate anti-tumor antibody-producing plasma cells in renal cell cancer. Immunity *55*, 527–541.e5 (2022).

195. Fässler, M. Antibodies as biomarker candidates for response and survival to checkpoint inhibitors in melanoma patients. Journal of Immunotherapy for Cancer *7*, 50 (2019).

196. Diem, S. Immunoglobulin G and Subclasses as Potential Biomarkers in Metastatic Melanoma Patients Starting Checkpoint Inhibitor Treatment. Journal of Immunotherapy *42*, 89–93 (2019).

197. Lynch, K. Heterogeneity in tertiary lymphoid structure B-cells correlates with patient survival in metastatic melanoma. Journal of Immunotherapy for Cancer *9*, e002273 (2021).

198. Vanhersecke, L. Mature tertiary lymphoid structures predict immune checkpoint inhibitor efficacy in solid tumors independently of PD-L1 expression. Nature Cancer *2*, 794–802 (2021).

199. Zhang, Y. Single-cell analyses reveal key immune cell subsets associated with response to PD-L1 blockade in triple-negative breast cancer. Cancer Cell *39*, 1578–1593.e8 (2021).

200. Rodriguez, A. Immune mechanisms orchestrate tertiary lymphoid structures in tumors via cancer-associated fibroblasts. Cell Reports *36*, 109422 (2021).

201. Litchfield, K. Meta-analysis of tumor- and T cell-intrinsic mechanisms of sensitization to checkpoint inhibition. Cell *184*, 596–614.e14 (2021).

202. Xia, L. Predictable Roles of Peripheral IgM Memory B Cells for the Responses to Anti-PD-1 Monotherapy Against Advanced Non-Small Cell Lung Cancer. Frontiers in Immunology *10*, 757137 (2021).

203. Carril-Ajuria, L. Baseline circulating unswitched memory B cells and B-cell related soluble factors are associated with overall survival in patients with clear cell renal cell carcinoma treated with nivolumab within the NIVOREN GETUG-AFU 26 study. Journal of Immunotherapy for Cancer *10*, e004885 (2022).

204. Das, R. Early B cell changes predict autoimmunity following combination immune checkpoint blockade. Journal of Clinical Investigation *128*, 715–720 (2018).

205. DeFalco, J. Non-progressing cancer patients have persistent B cell responses expressing shared antibody paratopes that target public tumor antigens. Clinical Immunology *187*, 37–45 (2018).

206. Niu, C. PD-1-positive Natural Killer Cells have a weaker antitumor function than that of PD-1-negative Natural Killer Cells in Lung Cancer. International Journal of Medical Sciences *17*, 1964–1973 (2020).

207. Norris, S. PD-1 expression on natural killer cells and CD8(+) T cells during chronic HIV-1 infection. Viral Immunology *25*, 329–32 (2012).

208. Park, I. Tumor-derived IL-18 induces PD-1 expression on immunosuppressive NK cells in triple-negative breast cancer. Oncotarget *8*, 32722–32730 (2017).

209. Hsu, J. Contribution of NK cells to immunotherapy mediated by PD-1/PD-L1 blockade. Journal of Clinical Investigation *128*, 4654–4668 (2018).

210. Quatrini, L. The Immune Checkpoint PD-1 in Natural Killer Cells: Expression, Function and Targeting in Tumour Immunotherapy. Cancers *12*, 3285 (2020).

211. Judge, S. Minimal PD-1 expression in mouse and human NK cells under diverse conditions. Journal of Clinical Investigation *130*, 3051–3068 (2020).

212. Erdag, G. Immunotype and immunohistologic characteristics of tumor-infiltrating immune cells are associated with clinical outcome in metastatic melanoma. Cancer Research *72*, 1070–80 (2012).

213. Sconocchia, G. Melanoma cells inhibit NK cell functions. Cancer Research *72*, 5428–9 (2012).

214. Ansell, S. PD-1 blockade with nivolumab in relapsed or refractory Hodgkin's lymphoma. New England Journal of Medicine *372*, 311–9 (2015).

215. Dong, W. The Mechanism of Anti-PD-L1 Antibody Efficacy against PD-L1-Negative Tumors Identifies NK Cells Expressing PD-L1 as a Cytolytic Effector. Cancer Discovery *9*, 1422–1437 (2019).

216. Subrahmanyam, P. Distinct predictive biomarker candidates for response to anti-CTLA-4 and anti-PD-1 immunotherapy in melanoma patients. Journal of Immunotherapy for Cancer *6*, 18 (2018).

217. De Coaña, Y. PD-1 checkpoint blockade in advanced melanoma patients: NK cells, monocytic subsets and host PD-L1 expression as predictive biomarker candidates. Oncoimmunology *9*, 1786888 (2020).

218. Alvarez, M. Indirect Impact of PD-1/PD-L1 Blockade on a Murine Model of NK Cell Exhaustion. Frontiers in Immunology *11*, 7 (2020).

219. Marzo, A. Tumor antigens are constitutively presented in the draining lymph nodes. Journal of Immunology *162*, 5838–45 (1999).

220. Hargadon, K. Incomplete differentiation of antigen-specific CD8 T cells in tumor-draining lymph nodes. Journal of Immunology *177*, 6081–90 (2006).

221. Salmon, H. Expansion and Activation of CD103(+) Dendritic Cell Progenitors at the Tumor Site Enhances Tumor Responses to Therapeutic PD-L1 and BRAF Inhibition. Immunity *44*, 924–38 (2016).

222. Peng, Q. PD-L1 on dendritic cells attenuates T cell activation and regulates response to immune checkpoint blockade. Nature Communications *11*, 4835 (2020).

223. Menares, E. Tissue-resident memory CD8 + T cells amplify anti-tumor immunity by triggering antigen spreading through dendritic cells. Nature Communications *10*, 4401 (2019).

224. Fransen, M. Tumor-draining lymph nodes are pivotal in PD-1/PD-L1 checkpoint therapy. JCI Insight *3*, e124507 (2018).

225. Chow, M. Intratumoral Activity of the CXCR3 Chemokine System Is Required for the Efficacy of Anti-PD-1 Therapy. Immunity *50*, 1498–1512.e5 (2019).

226. Garris, C. Successful Anti-PD-1 Cancer Immunotherapy Requires T Cell-Dendritic Cell Crosstalk Involving the Cytokines IFN-ɣ and IL-12. Immunity *49*, 1148–1161.e7 (2018).

227. Maier, B. A conserved dendritic-cell regulatory program limits antitumour immunity. Nature *580*, 257–262 (2020).

228. Oh, S. PD-L1 expression by dendritic cells is a key regulator of T-cell immunity in cancer. Nature Cancer *1*, 681–691 (2020).

229. Mayoux, M. Dendritic cells dictate responses to PD-L1 blockade cancer immunotherapy. Science Translational Medicine *12*, eaav7431 (2020).

230. Duraiswamy, J. Myeloid antigen-presenting cell niches sustain antitumor T cells and license PD-1 blockade via CD28 costimulation. Cancer Cell *39*, 1623–1642.e20 (2021).

231. Sharma, M. Plasmacytoid dendritic cells from mouse tumor-draining lymph nodes directly activate mature Tregs via indoleamine 2,3-dioxygenase. Journal of Clinical Investigation *117*, 2570–82 (2007).

232. Aspord, C. Plasmacytoid dendritic cells support melanoma progression by promoting Th2 and regulatory immunity through OX40L and ICOSL. Cancer Immunology Research *1*, 402–15 (2013).

233. Aspord, C. Melanoma hijacks plasmacytoid dendritic cells to promote its own progression. Oncoimmunology *3*, e27402 (2014).

234. Alculumbre, S. Diversification of human plasmacytoid predendritic cells in response to a single stimulus. Nature Immunology *19*, 63–75 (2018).

235. Benci, J. Tumor Interferon Signaling Regulates a Multigenic Resistance Program to Immune Checkpoint Blockade. Cell *167*, 1540–1554.e12 (2016).

236. Nierkens, S. Immune adjuvant efficacy of CpG oligonucleotide in cancer treatment is founded specifically upon TLR9 function in plasmacytoid dendritic cells. Cancer Research *71*, 6428–37 (2011).

237. Liu, C. Plasmacytoid dendritic cells induce NK cell-dependent, tumor antigen-specific T cell cross-priming and tumor regression in mice. Journal of Clinical Investigation *118*, 1165–75 (2008).

238. Fairfax, B. Germline variants associated with immunotherapy-related adverse events. bioRxiv (2022).

239. Pai, A. The genetic and mechanistic basis for variation in gene regulation. PLoS Genetics *11*, e1004857 (2015).

240. Zhu, Z. Integration of summary data from GWAS and eQTL studies predicts complex trait gene targets. Nature Genetics *46*, 481–487 (2016).

241. Kasela, S. Pathogenic implications for autoimmune mechanisms derived by comparative eQTL analysis of CD4+ versus CD8+ T cells. PLoS Genetics *13*, e1006643 (2017).

242. Fairfax, B. Innate immune activity conditions the effect of regulatory variants upon monocyte gene expression. Science *343*, 1246949 (2014).

243. Ye, C. Intersection of population variation and autoimmunity genetics in human T cell activation. Science *345*, 1254665 (2014).

244. Lee, M. Common genetic variants modulate pathogen-sensing responses in human dendritic cells. Science *343*, 1246980 (2014).

245. Quach, H. Genetic Adaptation and Neandertal Admixture Shaped the Immune System of Human Populations. Cell *167*, 643–656.e17 (2016).

246. Guo, H. Integration of disease association and eQTL data using a Bayesian colocalisation approach highlights six candidate causal genes in immune-mediated diseases. Human Molecular Genetics *24*, 3305–13 (2015).

247. De Jeger, P. Meta-analysis of genome scans and replication identify CD6, IRF8 and TNFRSF1A as new multiple sclerosis susceptibility loci. Nature Genetics *41*, 776–82 (2009).

248. Franco, L. Integrative genomic analysis of the human immune response to influenza vaccination. eLife *2*, e00299 (2013).

249. Berlanga-Taylor, L. Genomic Response to Vitamin D Supplementation in the Setting of a Randomized, Placebo-Controlled Trial. eBioMedicine *31*, 133–142 (2018).

250. Davenport, E. Discovering in vivo cytokine-eQTL interactions from a lupus clinical trial. Genome Biology *19*, 168 (2018).

251. Schrama, D. ERCC5 p.Asp1104His and ERCC2 p.Lys751Gln polymorphisms are independent prognostic factors for the clinical course of melanoma. Journal of Investigative Dermatology *131*, 1280–90 (2011).

252. Davies, J. Inherited variation in the PARP1 gene and survival from melanoma. International Journal of Cancer *135*, 1625–33 (2014).

253. Figl, A. Single nucleotide polymorphisms in DNA repair genes XRCC1 and APEX1 in progression and survival of primary cutaneous melanoma patients. Mutation Research *661*, 78–84 (2009).

254. Lee, J. Malignant melanoma: relationship of the human leukocyte antigen class II gene DQB1*0301 to disease recurrence in American Joint Committee on Cancer Stage I or II. Cancer *78*, 758–63 (1996).

255. Lenci, R. Influence of genetic variants in type I interferon genes on melanoma survival and therapy. PLoS One *7*, e50692 (2012).

256. Park, J. Gene variants in angiogenesis and lymphangiogenesis and cutaneous melanoma progression. Cancer Epidemiology, Biomarkers Prevention *22*, 827–34 (2013).

257. Breunis, W. Influence of cytotoxic T lymphocyte-associated antigen 4 (CTLA4) common polymorphisms on outcome in treatment of melanoma patients with CTLA-4 blockade. Journal of Immunotherapy *31*, 586–90 (2008).

258. Quierolo, P. Association of CTLA-4 polymorphisms with improved overall survival in melanoma patients treated with CTLA-4 blockade: a pilot study. Cancer Investigation *31*, 336–45 (2013).

259. Quierolo, P. Association of CTLA-4 Gene Variants with Response to Therapy and Long-term Survival in Metastatic Melanoma Patients Treated with Ipilimumab: An Italian Melanoma Intergroup Study. Frontiers in Immunology *8*, 386 (2017).

260. Parakh, S. PDCD1 Polymorphisms May Predict Response to Anti-PD-1 Blockade in Patients With Metastatic Melanoma. Frontiers in Immunology *12*, 672521 (2021).

261. Nozimo, T. Clinical Impact of Single Nucleotide Polymorphism in PD-L1 on Response to Nivolumab for Advanced Non-Small-Cell Lung Cancer Patients. Scientific Reports *7*, 45124 (2017).

262. Li, Q. PD-L1 P146R is prognostic and a negative predictor of response to immunotherapy in gastric cancer. Molecular Therapy *30*, 621–631 (2022).

263. Machado-Rugolo, J. Relevance of PD-L1 Non-Coding Polymorphisms on the Prognosis of a Genetically Admixed NSCLC Cohort. Pharmacogenomics and Personalised Medicine *14*, 239–252 (2021).

264. Kobayashi, M. Severe Immune-Related Adverse Events in Patients Treated with Nivolumab for Metastatic Renal Cell Carcinoma Are Associated with PDCD1 Polymorphism. Genes *13*, 1204 (2022).

265. Groha, S. Germline variants associated with toxicity to immune checkpoint blockade. Nature Meidince, 2584–2591 (2022).

266. Henze, J. RECIST 1.1, irRECIST 1.1, and mRECIST: How to Do. Current Radiology Reports *4* (2016).

267. NIH. *Common Terminology Criteria for Adverse Events (CTCAE) — Protocol Development* `https://ctep.cancer.gov/protocoldevelopment/electronic%%205C_applications/ctc.htm#ctc%5C%5C_40`..

268. Gilchrist, J. Natural Killer cells demonstrate distinct eQTL and transcriptome-wide disease associations, highlighting their role in autoimmunity. Nature Communications *13*, 4073 (2022).

269. Chang, C. Second-generation PLINK: rising to the challenge of larger and richer datasets. Gigascience *4*, 7 (2015).

270. Loh, P. Reference-based phasing using the Haplotype Reference Consortium panel. Nature Genetics *48*, 1443–1448 (2016).

271. Das, S. Next-generation genotype imputation service and methods. Nature Genetics *48*, 1284–1287 (2016).

272. Kim, D. Graph-based genome alignment and genotyping with HISAT2 and HISAT-genotype. Nature Biotechnology *37*, 907–915 (2019).

273. Pertea, M. StringTie enables improved reconstruction of a transcriptome from RNA-seq reads. Nature Biotechnology *33*, 290–5 (2015).

274. Anders, S. HTSeq–a Python framework to work with high-throughput sequencing data. Bioinformatics *31*, 166–9 (2015).

275. Fort, A. MBV: a method to solve sample mislabeling and detect technical bias in large combined genotype and sequencing assay datasets. Bioinformatics *33*, 1895–1897 (2017).

276. Jun, G. Detecting and estimating contamination of human DNA samples in sequencing and array-based genotype data. American Journal of Human Genetics *91*, 839–48 (2012).

277. Dobin, A. STAR: ultrafast universal RNA-seq aligner. Bioinformatics *29*, 15–21 (2013).

278. Van de Geijn, B. WASP: allele-specific software for robust molecular quantitative trait locus discovery. Nature Methods *12*, 1061–3 (2015).

279. Love, M. Moderated estimation of fold change and dispersion for RNA-seq data with DESeq2. Genome Biology *15*, 550 (2014).

280. Fang, H. XGR software for enhanced interpretation of genomic summary data, illustrated by application to immunological traits. Genome Medicine *8*, 129 (2016).

281. Bolotin, D. MiXCR: software for comprehensive adaptive immunity profiling. Nature Methods *12*, 380–1 (2015).

282. McCarthy, D. Scater: pre-processing, quality control, normalization and visualization of single-cell RNA-seq data in R. Bioinformatics *33*, 1179–1186 (2017).

283. Lun, A. A step-by-step workflow for low-level analysis of single-cell RNA-seq data with Bioconductor. F1000 Research *5*, 2122 (2016).

284. Stuart, T. Comprehensive Integration of Single-Cell Data. Cell *177*, 1888–1902.e21 (2019).

285. Zappia, L. Clustering trees: a visualization for evaluating clusterings at multiple resolutions. Gigascience *7*, giy083 (2018).

286. Aran, D. Reference-based analysis of lung single-cell sequencing reveals a transitional profibrotic macrophage. Nature Immunology *20*, 163–172 (2019).

287. Guo, X. Global characterization of T cells in non-small-cell lung cancer by single-cell sequencing. Nature Medicine *24*, 978–985 (2018).

288. Savas, P. Single-cell profiling of breast cancer T cells reveals a tissue-resident memory subset associated with improved prognosis. Nature Medicine *24*, 986–993 (2018).

289. Zhang, Y. A T cell resilience model associated with response to immunotherapy in multiple tumor types. Nature Medicine *28*, 1421–1431 (2022).

290. Lun, A. EmptyDrops: distinguishing cells from empty droplets in droplet-based single-cell RNA sequencing data. Genome Biology *20*, 63 (2019).

291. Wolock, S. Scrublet: Computational Identification of Cell Doublets in Single-Cell Transcriptomic Data. Cell Systems *8*, 281–291.e9 (2019).

292. Huang, Y. Vireo: Bayesian demultiplexing of pooled single-cell RNA-seq data without genotype reference. Genome Biology *20*, 273 (2019).

293. Young, M. SoupX removes ambient RNA contamination from droplet-based single-cell RNA sequencing data. Gigascience *9*, giaa151 (2020).

294. Hao, Y. Integrated analysis of multimodal single-cell data. Cell *184*, 3573–3587.e2 (2021).

295. Consortium, C. A blood atlas of COVID-19 defines hallmarks of disease severity and specificity. Cell *185*, 916–938.e58 (2022).

296. Al-Mossawi, H. Context-specific regulation of surface and soluble IL7R expression by an autoimmune risk allele. Nature Communications *10*, 4575 (2019).

297. Crinier, A. High-Dimensional Single-Cell Analysis Identifies Organ-Specific Signatures and Conserved NK Cell Subsets in Humans and Mice. Immunity *49*, 971–986.e5 (2018).

298. Vander Heiden, J. pRESTO: a toolkit for processing high-throughput sequencing raw reads of lymphocyte receptor repertoires. Bioinformatics *30*, 1930–1932 (2014).

299. Van Dijk, D. Recovering Gene Interactions from Single-Cell Data Using Data Diffusion. Cell *174*, 716–729.e27 (2018).

300. Efremova, M. CellPhoneDB: inferring cell-cell communication from combined expression of multi-subunit ligand-receptor complexes. Nature Protocols *15*, 1484–1506 (2020).

301. Conway, J. UpSetR: an R package for the visualization of intersecting sets and their properties. Bioinformatics *33*, 2938–2940 (2017).

302. Gu, Z. circlize implements and enhances circular visualization in R. Bioinformatics *30*, 2811–2 (2014).

303. Gu, Z. Complex heatmaps reveal patterns and correlations in multidimensional genomic data. Bioinformatics *32*, 2847–9 (2016).

304. Renkema, K. KLRG1+ Memory CD8 T Cells Combine Properties of Short-Lived Effectors and Long-Lived Memory. Journal of Immunology *205*, 1059–1069 (2020).

305. Peng, H. Metabolic Reprogramming and Reactive Oxygen Species in T Cell Immunity. Frontiers in Immunology *12* (2021).

306. Enamorado, M. Enhanced anti-tumour immunity requires the interplay between resident and circulating memory CD8+ T cells. Nature Communications *8* (2017).

307. Kim, K. The First-week Proliferative Response of Peripheral Blood PD-1+CD8+ T Cells Predicts the Response to Anti-PD-1 Therapy in Solid Tumors. Clinical Cancer Research *25*, 2144–2154 (2019).

308. Chronister, W. TCRMatch: Predicting T-Cell Receptor Specificity Based on Sequence Similarity to Previously Characterized Receptors. Frontiers in Immunology *12* (2021).

309. Huang, H. Analyzing the Mycobacterium tuberculosis immune response by T-cell receptor clustering with GLIPH2 and genome-wide antigen screening. Nature Biotechnology *38*, 1194–1202 (2020).

310. Theaker, S. T-cell libraries allow simple parallel generation of multiple peptide-specific human T-cell clones. Journal of Immunological Methods *430*, 43–50 (2016).

311. Szomolay, B. Identification of human viral protein-derived ligands recognized by individual MHCI-restricted T-cell receptors. Immunology and Cell Biology *94*, 573–82 (2016).

312. Yang, X. Autoimmunity-associated T cell receptors recognize HLA-B*27-bound peptides. Nature *612*, 771–777 (2022).

313. Diaz, L. VCAM-1 expression on CD8+ cells correlates with enhanced anti-HIV suppressing activity. Journal of Immunology *174*, 1574–9 (2005).

314. Kumari, S. T lymphocyte myosin IIA is required for maturation of the immunological synapse. Frontiers in Immunology *3* (2012).

315. Mąka, R. Rapid Rerouting of Myosin Traffic at the T Cell Immunological Synapse. bioRxiv (2022).

316. Gessner, A. Contribution of multidrug and toxin extrusion protein 1 (MATE1) to renal secretion of trimethylamine-N-oxide (TMAO). Scientific Reports *8* (2018).

317. Sauodi, A. Rho-GTPases as key regulators of T lymphocyte biology. Small GTPases *5* (2014).

318. Stetson, D. Type I interferons in host defense. Immunity *25*, 373–81 (2006).

319. Teijaro, J. Persistent LCMV infection is controlled by blockade of type I interferon signaling. Science *340*, 207–11 (2013).

320. Wang, B. The Significance of Type-I Interferons in the Pathogenesis and Therapy of Human Immunodeficiency Virus 1 Infection. Frontiers in Immunology *8* (2017).

321. Jacquelot, N. Sustained Type I interferon signaling as a mechanism of resistance to PD-1 blockade. Cell Research *29*, 846–861 (2019).

322. Boukhaled, G. Pre-encoded responsiveness to type I interferon in the peripheral immune system defines outcome of PD1 blockade therapy. Nature Immunology (2022).

323. Krieg, C. High-dimensional single-cell analysis predicts response to anti-PD-1 immunotherapy. Nature Medicine *24*, 144–153 (2018).

324. Huang, X. PD-1 expression by macrophages plays a pathologic role in altering microbial clearance and the innate inflammatory response to sepsis. PNAS *14*, 6303–8 (2009).

325. Li, T. SEMA6B Overexpression Predicts Poor Prognosis and Correlates With the Tumor Immunosuppressive Microenvironment in Colorectal Cancer. Frontiers in Molecular Bioscience *8* (2021).

326. Saric, A. SNX19 restricts endolysosome motility through contacts with the endoplasmic reticulum. Nature Communications *12* (2021).

327. Patel, N. OB-BP1/Siglec-6. a leptin- and sialic acid-binding protein of the immunoglobulin superfamily. Journal of Biological Chemistry *274*, 22729–38 (1999).

328. Gatto, M. Circulating Pentraxin3-Specific B Cells Are Decreased in Lupus Nephritis. Frontiers in Immunology *10* (2019).

329. Marks, E. Retinoic Acid Signaling in B Cells Is Required for the Generation of an Effective T-Independent Immune Response. Frontiers in Immunology *7* (2016).

330. Congy-Jolivet, N. Monocytes are the main source of STING-mediated IFN-α production. eBioMedicine *80* (2022).

331. Zemek, R. Temporally restricted activation of IFNβ signaling underlies response to immune checkpoint therapy in mice. Nature Communications *13* (2022).

332. Deo, S. Role played by Th2 type cytokines in IgE mediated allergy and asthma. Lung India *27*, 66–71 (2010).

333. Kawakami, A. Editorial: The role of monocytes/macrophages in autoimmunity and autoinflammation. Frontiers in Immunology *13* (2022).

334. Van Langelaar, J. B and T Cells Driving Multiple Sclerosis: Identity, Mechanisms and Potential Triggers. Frontiers in Immunology *11* (2020).

335. DeFuria, J. B cells promote inflammation in obesity and type 2 diabetes through regulation of T-cell function and an inflammatory cytokine profile. PNAS *110*, 5133–8 (2013).

336. Hemani, G. Orienting the causal relationship between imprecisely measured traits using GWAS summary data. PLoS Genetics *13* (2017).

337. McNerney, M. 2B4 (CD244) is a non-MHC binding receptor with multiple functions on natural killer cells and CD8+ T cells. Molecular Immunology *42*, 489–94 (2005).

338. Alderson, M. CD40 expression by human monocytes: regulation by cytokines and activation of monocytes by the ligand for CD40. Journal of Experimental Medicine *178*, 669–74 (1993).

339. Van de Sande, B. A scalable SCENIC workflow for single-cell gene regulatory network analysis. Nature Protocols *15*, 2247–2276 (2020).

340. Romano, E. Ipilimumab-dependent cell-mediated cytotoxicity of regulatory T cells ex vivo by nonclassical monocytes in melanoma patients. PNAS *112*, 6140–5 (2015).

341. Kirouac, D. Deconvolution of clinical variance in CAR-T cell pharmacology and response. Nature Biotechnology (2023).

342. Huang, A. A decade of checkpoint blockade immunotherapy in melanoma: understanding the molecular basis for immune sensitivity and resistance. Nature Immunology *23*, 660–670 (2022).

343. Moss, P. The T cell immune response against SARS-CoV-2. Nature Immunology *23*, 186–193 (2022).

344. Ghorani, E. The T cell differentiation landscape is shaped by tumour mutations in lung cancer. Nature Cancer *1*, 546–561 (2020).

345. Niknafs, N. Persistent mutation burden drives sustained anti-tumor immune responses. Nature Medicine *29*, 440–449 (2023).

346. Pan, L. T cell receptor convergence is an indicator of antigen-specific T cell response in cancer immunotherapies. eLife *11* (2022).

347. John Looney, T. TCR Convergence in Individuals Treated With Immune Checkpoint Inhibition for Cancer. Frontiers in Immunology *10* (2020).

348. Huutannin, J. Evolution and modulation of antigen-specific T cell responses in melanoma patients. Nature Communications *13* (2022).

349. Ubiparipovic, S. Antibody-mediated delivery of CRISPR-Cas9 ribonucleoproteins in human cells. Protein Engineering Design and Selection *35* (2022).

350. Borst, L. NKG2A is a late immune checkpoint on CD8 T cells and marks repeated stimulation and cell division. International Journal of Cancer *150*, 688–704 (2022).

351. Keegan, A. Plasma IL-6 changes correlate to PD-1 inhibitor responses in NSCLC. Journal of Immunotherapy for Cancer *8*, e000678 (2020).

352. Yuen, K. High systemic and tumor-associated IL-8 correlates with reduced clinical benefit of PD-L1 blockade. Nature Medicine *26*, 693–698 (2020).

353. Shive, C. Inflammation Perturbs the IL-7 Axis, Promoting Senescence and Exhaustion that Broadly Characterize Immune Failure in Treated HIV Infection. Journal of Acquired Immune Deficiency Syndrome *71*, 483–92 (2016).

354. Barras, D. Tumor Microenvironment Cellular Crosstalk Predicts Response to Adoptive TIL Therapy in Melanoma. bioRxiv (2022).

355. Singh, S. B Cells Are Required to Generate Optimal Anti-Melanoma Immunity in Response to Checkpoint Blockade. Frontiers in Immunology *13* (2022).

356. Giladi, A. Dissecting cellular crosstalk by sequencing physically interacting cells. Nature Biotechnology *38*, 629–637 (2020).

357. Kim, M. A long-acting interleukin-7, rhIL-7-hyFc, enhances CAR T cell expansion, persistence, and anti-tumor activity. Nature Communications *13* (2022).

358. Pellegrini, M. Adjuvant IL-7 antagonizes multiple cellular and molecular inhibitory networks to enhance immunotherapies. Nature Medicine *15*, 528–36 (2009).

359. Shen, L. Single-nucleotide polymorphisms can cause different structural folds of mRNA. PNAS *96*, 7871–6 (1999).

360. Beaudoin, J. 5′-UTR G-quadruplex structures acting as translational repressors. Nucleic Acids Research *38*, 7022–36 (2010).

361. Xu, H. Screening of Kozak-motif-located SNPs and analysis of their association with human diseases. Biochemical and Biophysical Research Communications *392*, 89–94 (2010).

362. Armata, I. Dopa-responsive dystonia: functional analysis of single nucleotide substitutions within the 5′ untranslated GCH1 region. Biochemical and Biophysical Research Communications *8* (2013).

363. Yazar, S. Single-cell eQTL mapping identifies cell type-specific genetic control of autoimmune disease. Science *376* (2022).

364. Nathan, A. Single-cell eQTL models reveal dynamic T cell state dependence of disease loci. Nature *606*, 120–128 (2022).

365. Ward, S. A method for conducting suppression assays using small numbers of tissue-isolated regulatory T cells. MethodsX *1*, 168–174 (2014).